

## Selection, processing, properties and applications of ultra-high temperature ceramic matrix composites, UHTCMCs – a review

Binner, Jon; Porter, Matthew; Baker, Benjamin; Zou, Ji; Venkatachalam, Vinu; Rubio Diaz, Virtudes; D'Angio', Andrea; Ramanujam, Prabhu; Zhang, Tailin; Tammana, S R C Murthy

DOI:

[10.1080/09506608.2019.1652006](https://doi.org/10.1080/09506608.2019.1652006)

License:

None: All rights reserved

*Document Version*

Peer reviewed version

*Citation for published version (Harvard):*

Binner, J, Porter, M, Baker, B, Zou, J, Venkatachalam, V, Rubio Diaz, V, D'Angio', A, Ramanujam, P, Zhang, T & Tammana, SRM 2019, 'Selection, processing, properties and applications of ultra-high temperature ceramic matrix composites, UHTCMCs – a review', *International Materials Reviews*.  
<https://doi.org/10.1080/09506608.2019.1652006>

[Link to publication on Research at Birmingham portal](#)

### **Publisher Rights Statement:**

Checked for eligibility: 19/09/2019

This is an Accepted Manuscript of an article published by Taylor & Francis in *International Materials Reviews* on 16/09/2019, available online: <http://www.tandfonline.com/10.1080/09506608.2019.1652006>

### **General rights**

Unless a licence is specified above, all rights (including copyright and moral rights) in this document are retained by the authors and/or the copyright holders. The express permission of the copyright holder must be obtained for any use of this material other than for purposes permitted by law.

- Users may freely distribute the URL that is used to identify this publication.
- Users may download and/or print one copy of the publication from the University of Birmingham research portal for the purpose of private study or non-commercial research.
- User may use extracts from the document in line with the concept of 'fair dealing' under the Copyright, Designs and Patents Act 1988 (?)
- Users may not further distribute the material nor use it for the purposes of commercial gain.

Where a licence is displayed above, please note the terms and conditions of the licence govern your use of this document.

When citing, please reference the published version.

### **Take down policy**

While the University of Birmingham exercises care and attention in making items available there are rare occasions when an item has been uploaded in error or has been deemed to be commercially or otherwise sensitive.

If you believe that this is the case for this document, please contact [UBIRA@lists.bham.ac.uk](mailto:UBIRA@lists.bham.ac.uk) providing details and we will remove access to the work immediately and investigate.

# Selection, Processing, Properties and Applications of Ultra-High Temperature Ceramic Matrix Composites, UHTCMCs – A Review

Jon Binner<sup>a,\*</sup>, Matt Porter<sup>a</sup>, Ben Baker<sup>a</sup>, Ji Zou<sup>a,\*</sup>, Vinothini

Venkatachalam<sup>a</sup>, Virtudes Rubio Diaz<sup>b</sup>, Andrea D'Angio<sup>b</sup>, Prabhu

Ramanujam<sup>c</sup>, Tailin Zhang<sup>a</sup> and Tammana S R C Murthy<sup>a,d,\*</sup>

<sup>a</sup> School of Metallurgy and Materials, University of Birmingham, B15 2SE, UK;

<sup>b</sup> National Composites Centre, NCC, Bristol & Bath Science Park, Emersons Green, Bristol, BS16 7FS;

<sup>c</sup> Wendt India Ltd, Hosur, India;

<sup>d</sup> Materials Group, Bhabha Atomic Research Centre, Mumbai 400085, India

\* Corresponding authors: [J.Binner@bham.ac.uk](mailto:J.Binner@bham.ac.uk) (Jon Binner), [murthi@iitkalumni.org](mailto:murthi@iitkalumni.org) (Tammana S.R.C. Murthy), [J.Zou@bham.ac.uk](mailto:J.Zou@bham.ac.uk) (Ji Zou)

## Short biographical notes of all contributors:

### *Jon Binner*

Jon is Professor of Ceramic Science & Engineering at the University of Birmingham, UK; until April 1<sup>st</sup> 2019 he was also the Deputy Head of the College of Engineering & Physical Sciences. He has been active in ceramics processing research since 1981 and has published ~220 refereed papers, as well as editing or contributing to 19 books and holding 7 patents with an 8<sup>th</sup> recently submitted. He has attracted 129 research grants to date, totalling ~£16.5M, this includes a current portfolio of about £1.9M. The focus of his research is the generation of both the necessary scientific understanding and the required engineering solutions for the design and development of materials and process routes that display technical and/or economic advantages over existing approaches. The range of products worked on ranges from nanostructured to traditional ceramics, interpenetrating composites to ultra-high temperature ceramic matrix composites. He has worked closely with industry to translate key developments, e.g. through the creation of a spin-out company to develop a ceramic sensor for measuring soil matric potential (1991), or via licensing, e.g. manufacturing routes for producing engineering ceramic foams (1995) and nanostructured ceramics (2012). He has supervised 35 Ph.D. students and 2 M.Phil. students to successful completion and 38 postdoctoral researchers. A further 7 Ph.D. students and 6 postdoctoral researchers are currently being supervised with more positions currently advertised. His research has received both national and international recognition; he has given ~65 keynotes, plenary and invited talks at international conferences, whilst the Institute of Materials, Minerals and Mining has awarded him the Holliday Prize (1995), Ivor Jenkins Medal (2007), Verulam Medal & Prize (2011) and Pfiel Award (2017). In March 2016 a research

1 programme that he was involved with funded by MBDA, a major European defence  
2 manufacturer, was presented an Innovation Award. He is a Fellow of the Institute of Materials,  
3 Minerals & Mining in the UK, the European Ceramic Society and the American Ceramic  
4 Society and in September 2017 he was voted to be one of only 5 Fellows worldwide of the  
5 Association for Microwave Power in Europe for Research and Education (AMPERE). In April  
6 2018 the EU Academy of Sciences invited him to become a Member. He is a Past-President of  
7 the Institute of Materials, Minerals & Mining and the current President of the European Ceramic  
8 Society, taking over as President in June 2019 for two years.  
9  
10  
11  
12

### 13 ***Matthew Porter***

14  
15  
16  
17 Matthew is currently a Ph.D. student in the School of Metallurgy & Materials at the University  
18 of Birmingham, UK, looking at the effectiveness of microwave energy for the densification of  
19 SiC/SiC CMCs using chemical vapour infiltration for aerospace applications, under the  
20 supervision of Prof Jon Binner. Matt obtained his B.Sc. from the University of Birmingham in  
21 Materials science in 2015, he then spent a short period at a textiles engineering firm who  
22 specialised in timing belt materials for the automotive industry before returning to Birmingham  
23 to undertake his Ph.D. in the Advanced Ceramics & Composites group. During this time Matt  
24 has been a visiting researcher at the Wright-Patterson Air Force Base, Ohio and Worcester  
25 Polytechnic Institute, Massachusetts. Matt has given two invited talks, presented at three  
26 international conferences and given a number of posters, of which he won the best poster at the  
27 3rd Global Congress on Microwave Energy Applications (2016). Matt is an active member of  
28 the American Ceramic Society where he is a chair on the President's Council of Student  
29 Advisors and on the committee for the UK Chapter of ACerS.  
30  
31  
32  
33  
34  
35  
36  
37  
38  
39

### 40 ***Benjamin Baker***

41  
42 Ben is currently a Ph.D. student in the School of Metallurgy & Materials at the University of  
43 Birmingham, UK, looking at the production and testing of ultra-high temperature ceramic  
44 matrix composites, UHTCMCs, with controlled heterogeneity, under the supervision of Prof Jon  
45 Binner. He graduated from the University of Durham with an M.Chem. in Chemistry in 2017.  
46 During this time, he completed industrial work with Infineum, a petrochemical additive  
47 company, in which he completed a research project into the electrostatic behaviours of additives  
48 in apolar media, a highly significant field in the understanding and processing of colloids and  
49 suspensions.  
50  
51  
52  
53  
54  
55  
56  
57  
58  
59  
60  
61  
62  
63  
64  
65

### ***Ji Zou***

1  
2  
3  
4  
5  
6  
7  
8  
9  
10  
11  
12  
13  
14  
15  
16  
17  
18  
19  
20  
21  
22  
23  
24  
25  
26  
27  
28  
29  
30  
31  
32  
33  
34  
35  
36  
37  
38  
39  
40  
41  
42  
43  
44  
45  
46  
47  
48  
49  
50  
51  
52  
53  
54  
55  
56  
57  
58  
59  
60  
61  
62  
63  
64  
65

Ji is currently a Research Fellow in the School of Metallurgy & Materials at the University of Birmingham, UK, looking at advanced materials for energy generation and transmission, under the supervision of Prof Jon Binner. Ji received his Ph.D. from the Shanghai Institute of Ceramics, Chinese Academic of Sciences. Before joining UoB, he worked as a postdoctoral researcher in KU Leuven (Belgium) and University of Stockholm (Sweden) for three years each. Ji has been active in the Processing-Structure-Property correlation of ceramics, especially for boride ceramics since 2007 and the additive manufacturing of ceramics and alloys since 2016. Ji has published 53 articles in peer-reviewed journals (including 4 in *Acta Materialia*, 9 in *Scripta Materialia*, 10 in the *Journal of the European Ceramic Society* and 8 in the *Journal of the American Ceramic Society*) with >800 citations. He serves as a member in the organizing committee of the International Conference on High-Performance Ceramics (CICC) series and an Editorial Board Member of the international journal, *Recent Patents in Materials Science*.

### ***Vinothini Venkatachalam***

26  
27  
28  
29  
30  
31  
32  
33  
34  
35  
36  
37  
38  
39  
40  
41  
42  
43  
44  
45  
46  
47  
48  
49  
50  
51  
52  
53  
54  
55  
56  
57  
58  
59  
60  
61  
62  
63  
64  
65

Vinothini is currently a Research Fellow in the School of Metallurgy & Materials at the University of Birmingham, UK, looking at the development of ultra-high temperature ceramic matrix composites (UHTCMCs) using radio frequency-enhanced chemical vapour infiltration for aerospace applications, under the supervision of Prof Jon Binner. Vinu worked as a Scientist at the National Aerospace Laboratory, India, on ternary carbides and joining of advanced materials for aerospace applications prior to obtaining her Ph.D. from the Department of Materials at Loughborough University, also under the supervision of Jon Binner. Then she moved to industrial R&D, working at Syfer Technology on developing a new range of capacitor devices, which received an outstanding innovative product of the year at the 10th Elektra European Electronics Industry Awards, 2012. She resumed her academic research, as a Research Fellow, at the Technical University of Denmark, working on high-temperature corrosion & protective coatings. Vinu has wide international experience of ceramic processing, from powders to the product, in both academia and industry. She has published 4 international journal papers, 4 peer-reviewed conference papers, presented in 13 international conferences and 8 national conferences.

### ***Virtudes Rubio Diaz***

55  
56  
57  
58  
59  
60  
61  
62  
63  
64  
65

Virtudes is currently an Advanced Research Engineer at the National Composites Centre in Bristol, UK, leading multiple CMC focused research initiatives with the overall aim of developing the UK's CMC capabilities by working both with academia and industry partners.

1 She obtained her Ph.D. from the Universidad Miguel Hernandex de Elche in 2012 and then  
2 worked on ultra-high temperature composites, first at Loughborough University and then as a  
3 senior research fellow at the University of Birmingham. During the latter, she researched the  
4 development of UHTCMCs on a programme involving the European defence company MBDA  
5 and DSTL in the UK and DGA in France. This work contributed significantly to the  
6 fundamental understanding of UHTCMC processing and thermo-ablative characterisation that  
7 underpins much of the current work at UoB. Her subsequent project, funded by the Horizon  
8 2020 programme of the European Commission, C3Harme, focused on the use of radio  
9 frequency as an alternative energy source for chemical vapour infiltration to densify UHTCMCs  
10 more rapidly. Virtu has delivered many research papers at international conferences, published  
11 3 papers and was involved in the research with funded by MBDA that was awarded an  
12 Innovation Award.  
13  
14  
15  
16  
17  
18  
19  
20

### 21 ***Andrea D'Angio***

22  
23 Andrea is Engineering Capability Lead of the Advanced Materials Team at the National  
24 Composites Centre in Bristol, UK, working on the manufacture and performance assessment of  
25 ceramic matrix composites. Andrea started his research in the field of UHTCs in 2013 as a  
26 Research Associate at The Institute of Science & Technology for Ceramics (CNR-ISTEC)  
27 where he worked on the development of dual architecture UHTCs. He graduated in 2017 from  
28 the University of Birmingham with a Doctorate of Philosophy in Material Science; his area of  
29 research, supervised by Prof Jon Binner, was the manufacture of SiC/SiC composites using  
30 microwave field-assisted chemical vapour infiltration. During this research, Andrea spent four  
31 months at the University of Missouri Science & Technology, Missouri, USA, working on the  
32 microstructure-property relationship of UHTCs. Andrea has delivered many presentations at  
33 international conferences and has 4 research papers.  
34  
35  
36  
37  
38  
39  
40  
41  
42

### 43 ***Prabhu Ramanujam***

44  
45 Prabhu is a Materials Specialist, R&D at Wendt India Ltd, Murugappa Group. Prior to that he  
46 worked as a Research Fellow at the University Of Birmingham and in Loughborough University  
47 on UHTCs and electroceramics. He received his PhD from Loughborough University, UK, from  
48 the Department of Materials under the supervision of Prof. Jon Binner and Prof. Bala  
49 Vaidhyanathan. His research interests are the synthesis & characterisation of nanoparticles,  
50 colloidal processing of ceramics and flash sintering of UHTC composites for hypersonic and  
51 super abrasives applications.  
52  
53  
54  
55  
56  
57  
58  
59  
60  
61  
62  
63  
64  
65

1  
2  
3  
4  
5  
6  
7  
8  
9  
10  
11  
12  
13  
14  
15  
16  
17  
18  
19  
20  
21  
22  
23  
24  
25  
26  
27  
28  
29  
30  
31  
32  
33  
34  
35  
36  
37  
38  
39  
40  
41  
42  
43  
44  
45  
46  
47  
48  
49  
50  
51  
52  
53  
54  
55  
56  
57  
58  
59  
60  
61  
62  
63  
64  
65

***Tailin Zhang***

Tailin Zhang is a Ph.D. student in the School of Metallurgy and Materials at the University of Birmingham, UK, working in the area of high entropy & ultra-high temperature ceramics. He obtained his B.Sc. from the Taiyuan University of Technology in Materials science and engineering in 2015, with an experience of additive manufacture of alloys, and he graduated from the University of Manchester with M.Sc. in materials in 2016.

***Tamma S.R.C. Murthy***

Murthy is currently a Senior Research Fellow in the School of Metallurgy & Materials, University Of Birmingham, UK and also a Scientific Officer (F) in the Materials Group in Bhabha Atomic Research Centre, Mumbai, India, 400085. Murthy has been active in the processing-structure-property correlation of non-oxide ceramics since 2002 and has published 70 articles for peer-reviewed journals and book chapters. His H-index in Scopus is 20 and in Google Scholar is 21. He has developed a process flow-sheet and infrastructure from the lab scale to pilot scale production of various borides and carbides for nuclear applications. He is recipient of Awards and Fellowships including Marie Curie Post-Doctoral Research Fellowship, 2018-2020; Distinguished Young Alumni Professional Achievement Award, 2017 (NIT-Warangal, India); Young Metallurgist of the Year Award - 2011 (Ministry of Steel, Govt. of India); Young Engineer Award, 2008; Group Achievement Awards in 2013 & 2014 (Department of Atomic Energy, India); All India Innovative Student Project Award in 2005 (Indian National Academy of Engineers) and Best /Merit Poster Awards at various conferences.

# Selection, Processing, Properties and Applications of Ultra-High Temperature Ceramic Matrix Composites, UHTCMCs - A Review

## Abstract

Composites are, in general, a rapidly evolving and growing technical field with a very wide range of applications across the aerospace, defence, energy, medical and transport sectors as a result of their superior mechanical and physical properties. Ultra-high temperature ceramic matrix composites, UHTCMCs, are a new subfield within the wider grouping of CMCs that offer applications in rocket and hypersonic vehicle components, particularly nozzles, leading edges and engine components. The design and development of structural materials for use in oxidizing and rapid heating environments at temperatures above 1600°C is therefore of both great scientific and engineering importance. UHTC materials are typically considered to be the carbides, nitrides, and borides of the transition metals, but the Group IV compounds (Zr, Hf & Ti) plus TaC are generally considered to be the main focus of research due to the superior melting temperatures and stable high-melting temperature oxide that forms in situ. The combination of properties makes these materials potential candidates for a variety of high-temperature structural applications, including engines, hypersonic vehicles, plasma arc electrodes, advanced nuclear fuels, fusion first walls and diverters, cutting tools, furnace elements and high-temperature shielding. This review presents on the selection, processing, properties, applications, outlook and future directions of UHTCMCs.

**Keywords:** Ultra high temperature ceramics; composites; review; matrix; fibre; chemical vapour infiltration; impregnation; oxidation; ablation; microstructure

## Introduction

As with everything in the 20th century, time was at a premium and no more so than in the aerospace industry during the 1960s [1]. During this period, the interest in ultra-high temperature ceramics (UHTCs) began; this group of materials were thought to have potential to withstand the severe aero-thermo-chemical environments of hypersonic flight, paving the foundations for flight speeds exceeding Mach 5. However, although research into UHTCs for this application still continues today these materials do not have sufficient thermal shock resistance and, hence interest began to focus on ultra-high temperature ceramic matrix composites, UHTCMCs, over the last decade.

The hypersonic regime, usually defined as speeds greater than Mach 5 (6173 km/h), continues to receive a great deal of attention from the scientific community. The potential benefits are numerous, military systems would become more effective [2], [3], whilst for potential future commercial travel it would translate into flight times between Europe and the US East Coast of around 1 – 1½ hours or to the Far East in under 3 hours.

Hypersonic speeds are generally associated with flight in the upper stratosphere where gas pressures can be very low but the presence of oxygen radicals is high [4]. There are numerous inhibiting physical factors to consider when travelling at these speeds inside the stratosphere, but the primary issue is the behaviour of air, which becomes very unstable as it no longer behaves as a perfect gas. Hypersonic flow behaviour is not governed by any one equation nor has a definitive definition been established as of yet [5], especially at high altitude. Coupled with the fact that at lower altitudes air is considered to be a continuum, but at near orbital travel the sparsity of molecules means special considerations must be made for the flow dynamics only adds to its unpredictability [6]. The non-linear nature of flow means that shock waves are curved and produce vorticity, which alters the flow field of over the aircraft body.

This is also a dependency on the shape of the leading edge; the shock wave of sharp leading edges propagate on the surface of the structure whereas for blunt edges the flow field propagates ahead, as shown in schematic Fig.1. Both induce frictional heating at the vehicle surface, though less so on the blunt edge, this becoming sufficiently intense they generate high enough thermal loads that alter the properties of



1 the surrounding gases, causing it to vibrate, dissociate, react, excite and eventually  
2 become fully ionizing, all whilst being surrounded by a corrosive plasma layer [7]–[9].  
3 Efforts have been made to combat this using a multitude of approaches including  
4 internal active cooling systems, heat shielding designs and aerodynamic engineering to  
5 increase or decrease drag of components to increase the conversion kinetic energy to  
6 thermal or vice versa. However, these methods work against the primary principle of  
7 aviation to keep mass to a minimum.  
8  
9  
10  
11  
12

13 With the primary issue being able to endure extreme heating profiles in corrosive  
14 environments under substantial and varying mechanical loads, the principle candidate  
15 materials were identified as being the highly refractory transitional metal carbides and  
16 borides. Collectively referred to as Ultra-High Temperature Ceramics, these non-oxides  
17 are able to operate at beyond 1800°C in air with the resulting oxide melting points being  
18 around 3000°C [10]. So far UHTCs have been investigated for potential use as sharp  
19 leading edges on sub-orbital and earth-to-orbital vehicles amongst other applications  
20 [1]. They have shown some potential in being able to facilitate manoeuvring during  
21 atmosphere exit and re-entry, whilst surviving shock wave loading and severe oxidation  
22 without significantly compromising their geometrical integrity[11], [12].  
23  
24  
25  
26  
27  
28  
29  
30  
31  
32

33 The relatively recent utilisation of these UHTCs means their definition is somewhat  
34 incomplete to distinguish them from advanced ceramics. They fit the widely regarded  
35 standard apophatic criteria of ceramics, in that they are inorganic, non-metallic solids  
36 and are defined by three other classifications as described by Fahrenholtz [13]. The  
37 most frequently used definition of UHTCs is that materials have a melting point greater  
38 than 3000°C. However, this definition has a large degree of uncertainty due to the  
39 difficulty associated with measuring temperatures experimentally in this region, with  
40 multiple studies regularly reporting melting points of UHTC's with approximately  
41 500°C difference [14], [15]. The second less commonly used criteria is the engineering  
42 definition determined by the application, where the ceramics highest operating  
43 temperature in air defines its classification as a UHTC. This has been set at ~2000°C [1]  
44 due to the temperatures experienced at hypersonic speed. The final method is a  
45 qualitative definition of UHTCs by their chemistry, which carbides, nitrides and borides  
46 of early transition metals are considered to possess the potential to be a UHTC. A  
47 combination of all three definitions currently best defines a UHTC.  
48  
49  
50  
51  
52  
53  
54  
55  
56  
57  
58  
59  
60  
61  
62  
63  
64  
65

1 UHTCs are severely limited as single phase monolithic components for structural  
2 applications since they have low fracture toughness. This makes them highly  
3 susceptible to thermal shock, hindering their short-term and long-term use as external  
4 thermal protection systems on leading edges and propulsion systems. This necessitates  
5 the addition of a secondary phase that enhances toughness but without degrading other  
6 properties. Attempts have been made to use addition of other ceramic phases to negate  
7 these effects, such as SiC and LaB<sub>6</sub>, but they have had limited success to date [16]. In  
8 spite of this, research effort continues to be focused on improving oxidation resistance  
9 and the thermomechanical properties, whilst, in parallel, effort is also being extended  
10 with respect to replicating the extreme conditions that components would experience in  
11 service [17] and during land-based tests [18]. This has led to the utilisation of  
12 reinforcing fibrous phases. The later are designed to symbiotically operate with the  
13 UHTC matrix to increase the toughness, whilst also permitting the tailoring of the  
14 mechanical and thermal properties towards specific applications. Fibre architecture,  
15 fibre type and the volume fractions of the different composite phases will all be  
16 described in more detail later in this review.

17  
18  
19  
20  
21  
22  
23  
24  
25  
26  
27  
28  
29  
30 The rapid expansion of carbon fibres into the commercial aerospace market [19] is a  
31 testament to this ability to be readily formed into a wide range of large complex shapes  
32 whilst not compromising on their excellent strength to weight ratio [17]. They exhibit  
33 many excellent advantages compared to other reinforcing fibres; high specific modulus,  
34 specific strength and stiffness, outstanding fatigue properties, a negative coefficient of  
35 longitudinal thermal expansion and low coefficient of thermal expansion. Carbon fibre  
36 also has relatively good temperature resistance under vacuum or inert gases, but is  
37 readily oxidised at ~500°C in air [10]. The literature has shown that this can be offset by  
38 the addition of borides or silicides as filler phases, coatings or dopants. At high or ultra-  
39 high temperatures, these additions help to protect the fibres from oxidation, enhancing  
40 the high-temperature performance of the composites [20].

41  
42  
43  
44  
45  
46  
47  
48  
49  
50  
51 Of the UHTCs, hafnium and zirconium diborides, with a continuous carbon fibre  
52 reinforcing phase, have emerged as candidate for use in hypersonic flight applications  
53 due to their desirable combination of high mechanical and good physical properties  
54 coupled with the ability to form refractory oxides that resist melting to temperatures  
55 >2500°C [21]. These materials also possess high thermal conductivity and a low  
56  
57  
58  
59  
60  
61  
62  
63  
64  
65

1 coefficient of thermal expansion, advantageous for dissipating heat and withstanding the  
2 high thermal gradients that are experienced in service. Their future success is hinged on  
3 understanding in detail the protection mechanisms offered by the formation of the  
4 oxides of the UTHCs during service.  
5  
6

7  
8 As indicated previously, the UHTC materials are typically considered to be the  
9 carbides, nitrides, and borides of the transition metals, but the Group IV compounds (Ti,  
10 Zr, Hf) plus TaC are generally considered to be the main focus of research due to their  
11 superior melting temperatures and stable high-melting temperature oxides that forms in  
12 situ. Though UHTCMCs are primarily considered for aerospace applications, their  
13 ability to offer a combination of properties useful for extreme environments make them  
14 potential candidates for a variety of other high-temperature, structural applications. This  
15 includes the nuclear energy industry as fuel rod cladding, neutron absorbers (due to the  
16 presence of B or Hf or Ta), fusion first walls and tokamak diverters due to their  
17 anticipated excellent neutronic properties [22]–[25]. Other applications include, but are  
18 not limited to, plasma facing materials, plasma arc electrodes, cutting tools, refractories  
19 in metal processing, for example thermowell tubes in the steel refinement process, and  
20 electrical devices such as heaters and igniters [13], [26], [27]. Concentrating solar  
21 power (CSP) is one of the most promising renewable energy technologies; sun radiation  
22 is collected and concentrated on a receiver, which makes the latter a key component.  
23 Recent studies have shown that some UHTCs offer good spectral selectivity and low  
24 emittance at high temperatures, enabling them to be considered for this application [28].  
25  
26  
27  
28  
29  
30  
31  
32  
33  
34  
35  
36  
37  
38  
39

40 A major focus of recent work is to combine the properties of the UHTC compounds  
41 with the concepts behind the design and manufacture of ceramic matrix composites, to  
42 form a new class of materials known as UHTCMCs. Whilst the type of reinforcement  
43 influences the mechanical properties, especially fracture toughness, it also affects  
44 processing. UHTCMCs are not easy to process; if sintered they require very high  
45 sintering temperatures ( $>2000^{\circ}\text{C}$ ). Whilst fine diameter continuous ceramic fibres offer  
46 superior mechanical properties, particularly fracture toughness, processing these  
47 materials without damaging the fibres or generating grain growth in the matrix is a  
48 major challenge for conventional sintering techniques such as hot pressing, which is  
49 commonly used for consolidation of particulate or chopped fibre reinforced composites.  
50 Techniques such as spark plasma sintering as well as non-sintering techniques including  
51  
52  
53  
54  
55  
56  
57  
58  
59  
60  
61  
62  
63  
64  
65

1  
2  
3  
4  
5  
6  
7  
8  
9  
10  
11  
12  
13  
14  
15  
16  
17  
18  
19  
20  
21  
22  
23  
24  
25  
26  
27  
28  
29  
30  
31  
32  
33  
34  
35  
36  
37  
38  
39  
40  
41  
42  
43  
44  
45  
46  
47  
48  
49  
50  
51  
52  
53  
54  
55  
56  
57  
58  
59  
60  
61  
62  
63  
64  
65

chemical vapour infiltration (CVI), reactive melt infiltration (RMI), and precursor infiltration and pyrolysis (PIP) are all being investigated.

Interest in UHTCMCs has increased significantly in recent years as it has increasingly become apparent that monolithic UHTCs do not have sufficient thermal shock resistance to provide thermal protection in a number of applications, including hypersonic vehicles [13]. A number of research groups around the world, including from Europe, the US, China, Japan, South Korea and India have now begun to research these materials.

This review will cover the selection, processing, properties, applications, outlook and future directions of UHTCMCs, with the greatest emphasis being given to the continuous fibre reinforced composites since these are likely to be the first materials to be commercialised, and the properties required of them.

## Materials selection

For any composite, selection of a matrix and second phase are very important in order to achieve the desired properties. This section covers the selection, properties and compatibility of matrix and second phase for UHTCMCs.

### Matrix selection

Materials chosen for UHTCMC matrices can be many and varied, dependent upon the intended applications. The latter may suit one specific set of material properties over another and comparisons, Fig. , [13], [29]–[35] between factors such as melting point, oxidation resistance, density, CTE and thermal conductivity can all affect the most appropriate choices [1], [12], [36], [37]. Given the extreme environments that these materials are used in, oxidation is inevitable during the lifecycles of the components. Therefore, if reusability is a criterion then materials that oxidise in a controlled manner to produce passivating oxidation products are beneficial. For other, less reusable UHT applications, such requirements are less applicable provided they survive the application environment.

Passivating oxidation products may be defined by their ability to retain particular thermomechanical properties and a level of resistance to further oxidation, all the while resisting ablation and denudation. Hence, the melting points and

1 microstructural properties of the oxide products of the materials used are critical. The  
2 high conductivities and melting points of TaC and TiB<sub>2</sub> are attractive qualities for  
3 potential components, but their oxidation products have an inappropriately low melting  
4 point. The borides, nitrides and carbides of Zr and Hf possess high melting temperature,  
5 hardness [38] oxidation resistance [39] and electrical and thermal conductivity [40],  
6 additionally boasting high oxide melting points. However, the specific oxidation  
7 resistances of each have ramifications on the stable oxidation products that form with  
8 regards to microstructure and protection capability. In a UHTCMC, protection of the  
9 reinforcement phase by the matrix from the aggressive external conditions is critical.  
10

11  
12  
13  
14  
15  
16  
17 The boride and carbide systems are generally the most frequently studied for  
18 aerospace and other applications as indicated in the previous section. Boride ceramics  
19 oxidise with the production of B<sub>2</sub>O<sub>3</sub>, which at relatively low temperatures becomes a  
20 liquid [29]. Nevertheless, even at ≤1000°C formation of an amorphous glassy or molten  
21 B<sub>2</sub>O<sub>3</sub> phase provides oxidation protection for the bulk boride beneath [41]. In higher  
22 temperature regimes, this liquid vaporises and this protection mechanism is lost. The  
23 group IV carbides benefit from incredibly high eutectic temperatures with a carbon /  
24 carbon (C / C) substrate [13] (3180 and 2910°C respectively for HfC and ZrC).  
25 However, studies have found that their oxidation resistance is lower than that of the  
26 borides [42] and that the formation of gases during oxidation produces non-protective  
27 scales up to 1500°C, which results in substantial denudation. Nitrides are the least well  
28 studied of the group IV UHTCs. Whilst they have comparably high melting points, they  
29 are reported to have equally poor oxidation protection and non-passivating oxidation  
30 products as the carbides [13], [43], [44]. Rather, they find many applications as coatings  
31 for cutting tools or in electronics applications due to their electrical properties [44].  
32  
33  
34  
35  
36  
37  
38  
39  
40  
41  
42  
43  
44

45 Additives can be included in the matrix to modify the oxidation / ablation  
46 behaviour [45]–[48]. SiC inclusions are known to increase the performance of UHTC  
47 materials at moderate temperatures by the formation of a silicate glass / molten silica  
48 layer from the oxidation of SiC to SiO<sub>2</sub>. This is supported by the UHTC-oxide solid  
49 scale to provide an effective barrier against oxygen ingress [45]. At higher  
50 temperatures, however, the oxidation mechanism of SiC shifts from ‘passive oxidation’,  
51 via a solid or liquid SiO<sub>2</sub> product, to ‘active oxidation’, where gaseous SiO is formed  
52 [46]. This is lost from the component, reducing or removing the efficacy of the  
53  
54  
55  
56  
57  
58  
59  
60  
61  
62  
63  
64  
65

1 protection. Equally, the oxidation of SiC produces a SiC-depleted region in the upper  
2 layers of UHTCs with an associated pore network. The latter, without a protective SiO<sub>2</sub>  
3 surface layer, provides a significant avenue for oxygen ingress and could lead to  
4 component failure [49]. The regime in which SiC provides enhanced oxidation  
5 protection is up to around 1650°C.  
6  
7  
8  
9

10 Other modifications to the matrix material can be made on the basis of  
11 manipulating the wetting and rheological characteristics of the surface oxides formed. A  
12 study using Zr / Ta boride ceramics [47] found that the glassy layer formed during  
13 plasma torch testing at 2900-3000°C provided a healing surface layer that filled matrix  
14 cracks and lowered the surface catalycity. Effects of other matrix dopants on the  
15 oxidation resistance of components will be discussed in detail in a later section, where it  
16 will be shown that the compatibility of dopants with the predominant matrix material is  
17 an influential selection criterion.  
18  
19  
20  
21  
22  
23  
24

25 In summary, the selection of the matrix phases used is highly dependent upon  
26 both the properties desired for a component with respect to its intended operability  
27 window and also the fabrication technique used. The latter directly affects the material  
28 quality, particularly maximum density achievable; these aspects are discussed in the  
29 subsequent sections.  
30  
31  
32  
33  
34  
35

## 36 **Second phase selection**

### 37 **Particulate, chopped fibre / whisker / CNT / graphene reinforcement**

38  
39 As mentioned earlier, despite their excellent high-temperature properties,  
40 UHTCs suffer, like other ceramics, from intrinsic brittleness, which restricts their  
41 engineering applications [50]. Hence, the toughening of UHTCs has been the focus of  
42 considerable research with particle dispersion toughening, chopped fibres, carbon  
43 nanotubes, graphite, graphene and whisker toughening all being examined [50].  
44  
45  
46  
47  
48  
49  
50  
51

52 A range of different types of particle reinforcement of UHTCs have been  
53 reported by various authors [51]–[71]. Use of sinter-additives has traditionally been one  
54 of the methods to improve the densification at lower temperatures, especially for  
55 difficult to sinter materials like UHTCs. Sinter-additives typically lead to liquid phase  
56 sintering by creating a liquid phase, whilst other additives can lead to solid state  
57  
58  
59  
60  
61  
62

1 reactions during sintering that can also be beneficial for the densification process [53],  
2 [69], [71]. Metallic additives such as Fe, Ni and Co melt at lower temperatures and wet  
3 the refractory boride / carbide / nitride particles, which lead to faster mass transport and  
4 particle rearrangement and concomitantly result in attaining better densification at lower  
5 temperatures and shorter times due to liquid phase sintering [53], [69], [71], [72].  
6  
7 However, the problem with using metallic additives is that at the ultra-high  
8  
9 temperatures, the metallic and intermetallics phases soften and melt, which degrades the  
10 mechanical properties and creep resistance significantly. Hence, the use of metallic  
11 sinter-additives are generally considered unsuitable for densification of UHTCs [53],  
12 [69], [71].  
13  
14  
15  
16  
17  
18

19 Liquid phase assisted sintering has also been observed with non-oxide sintering  
20 additives, especially Si-based such as SiC, MoSi<sub>2</sub>, ZrSi<sub>2</sub>, TiSi<sub>2</sub>, WSi<sub>2</sub> and TaSi<sub>2</sub> [22],  
21 [53], [69]–[80]. Such additions have led to improved densification and mechanical  
22 properties for most of the refractory borides as well as carbides [81]. The Si-based  
23 additives have also been reported to react with the surface oxide phases (such as B<sub>2</sub>O<sub>3</sub>)  
24 to form SiO<sub>2</sub>, which is a transient liquid above ~1850°C and enhances the densification.  
25 In fact, improvements to the mechanical, tribological properties and oxidation resistance  
26 on addition of the Si-based additives have been reported in the literature.  
27  
28  
29  
30  
31  
32  
33

34 In addition, nitrides such as AlN and ZrN and rare earth oxides / borides  
35 including La<sub>2</sub>O<sub>3</sub>, LaB<sub>6</sub>, NdB<sub>6</sub> and EuB<sub>6</sub> have also been explored as sintering additives  
36 for the borides to enhance both sinterability and the subsequent properties [22], [53],  
37 [71], [82], [83]. Removal of the B<sub>2</sub>O<sub>3</sub> surface oxide layer by the nitrides also prevents  
38 grain growth, which in turn aids densification. For the reasons mentioned above, the last  
39 two decades have witnessed extensive research activity related to exploring the use of  
40 particulate sinter-additives for attaining improved densification via solid-state sintering  
41 and concomitantly improved mechanical properties of the UHTCs. Even though  
42 sintering additives help in attaining better sinter densities for the UHTCs, it has been  
43 difficult to attain near theoretical densities by pressureless sintering routes. Hence, most  
44 UHTCs and their composites are densified using external pressure assisted sintering  
45 techniques such as hot pressing and spark plasma sintering. More details of the  
46 processing routes are described in the later sections, though there is still much room for  
47  
48  
49  
50  
51  
52  
53  
54  
55  
56  
57  
58  
59  
60  
61  
62  
63  
64  
65

1  
2  
3  
4  
5  
6  
7  
8  
9  
10  
11  
12  
13  
14  
15  
16  
17  
18  
19  
20  
21  
22  
23  
24  
25  
26  
27  
28  
29  
30  
31  
32  
33  
34  
35  
36  
37  
38  
39  
40  
41  
42  
43  
44  
45  
46  
47  
48  
49  
50  
51  
52  
53  
54  
55  
56  
57  
58  
59  
60  
61  
62  
63  
64  
65

improvement of the toughness, thermal properties, etc. for UHTCs by using a different type of reinforcements as discussed in the next section.

Hence, other researchers have explored the use of carbon nanotubes (CNTs), chopped fibres (carbon / SiC / ZrO<sub>2</sub>), non-oxide whiskers and graphene as reinforcement phases for UHTCs in the past few years. Table 1 [57], [84]–[121] summarises the results of various UHTCs consolidated through sintering processing routes, e.g. hot pressing or SPS, and using different forms of reinforcements. Improved fracture toughness and strength values were observed. Chopped fibres are particularly attractive, benefiting from excellent mechanical properties coupled with resistance to neutron irradiation, improved thermal conductivity and stability. Graphene has a high two-dimensional aspect ratio, which has also been shown to enhance the thermomechanical properties of UHTCs [86], [122]. Multi-walled carbon nanotube (MWCNT) reinforced UHTCs exhibited superior mechanical and transport properties, making them attractive candidates (at a reasonable cost) for nanoscale reinforcement of UHTCs. A maximum fracture toughness of 7.8 MPam<sup>1/2</sup>, with a strength of 894 MPa, was reported by incorporating multiwall CNTs in a HfB<sub>2</sub> matrix [87]. The major toughening mechanisms are reported to be one or more of the combination of reinforcement pull out, bridging, debonding, branching, stress-induced transformation and three dimensional crack deflection. Possible reactions between CNT or graphene with any oxide present in the UHTC during high temperature sintering might be a problem [87]. Homogenization of these additives in the UHTCs matrix is also challenging [87].

For fibre-toughened ceramics, the interfacial bonding plays an important role for load transfer and therefore affects the fracture toughness of the ceramics significantly. Thus, finding a method to optimize the fibre-matrix interfacial bonding strength is important when fabricating UHTCMCs with high fracture toughness [123]. The design parameters for the interface have been comprehensively reviewed by Faber [124] for conventional CMCs and include interface toughness and sliding resistance. These are related to the elastic properties of the fibre and matrix and are characteristic of the fibre / matrix interface. A brief discussion of these parameters has been included in the section covering the composites' microstructure.



1  
2  
3  
4  
5  
6  
7  
8  
9  
10  
11  
12  
13  
14  
15  
16  
17  
18  
19  
20  
21  
22  
23  
24  
25  
26  
27  
28  
29  
30  
31  
32  
33  
34  
35  
36  
37  
38  
39  
40  
41  
42  
43  
44  
45  
46  
47  
48  
49  
50  
51  
52  
53  
54  
55  
56  
57  
58  
59  
60  
61  
62  
63  
64  
65

Another challenge for these reinforcements (especially CNTs and graphene) is achieving uniform dispersion and minimising / avoiding agglomeration, which arises due to van der Waals interactions, in the matrix. A range of dispersion techniques have been used / reported to overcome the above issues, such as conventional ball-milling, colloidal processing, sol-gel processing and in-situ growth of CNTs within the UHTC particle by catalytic chemical vapour deposition and in situ thermal reduction of graphene oxide [88] and hetero-coagulation [84].

More recently, research has been focused on the use of continuous carbon / SiC fibres reinforced UHTC composites to improve the fracture toughness and strength. More details are discussed in the next section.

### **Continuous Fibre reinforcement**

In fibre reinforced ceramic matrix composites (FRCMCs), fibres are required to overcome the brittleness, low elongation to rupture and poor thermal shock resistance of the monolithic ceramics. Embedding fibres into a UHTC matrix implies that the associated fibres must also be able to withstand the extreme temperature and harsh environment in which long-term thermal and oxidation stability are priorities, however, it must be noted, that the deployment of UHTCMCs is also planned for non-reusable applications where the fibres need to withstand harsh environments only for a limited amount of time.

Organic polymer-based fibres cannot be used because of their low degradation temperature and, analogously, glass fibres are also excluded because they soften far below the operating temperatures of UHTCMCs. Inorganic fibres include those based on metals, carbon, oxides (e.g. alumina, mullite and zirconia) and non-oxide ceramics (e.g. Si-C-O, SiC, Si-C-N, Si-B-C-N, UHTCs). Oxide fibres exhibit relatively low temperature capabilities (up to 1200°C for short periods of time) and the low maturity of the commercial manufacture of Si-C-N and Si-B-N-C limit the options to carbon fibres, silicon carbide fibres and UHTC fibres. These are reviewed below.

#### Carbon fibres

Carbon fibres technically contain at least 92 wt.% carbon in the form of graphite. The anisotropic thermo-mechanical properties of the carbon fibres are due to

1 the strong covalent C - C bond of the graphite oriented along the axis of the fibre, whilst  
2 the properties are poor in the transverse direction since the interatomic forces between  
3 the basal planes are weak [125], [126]. Carbon fibres have a typical tensile strength  
4 ranging from 1.5 to 7 GPa and elastic modulus between 200-900 GPa [127]. The low  
5 density of carbon offers the highest specific modulus and highest specific strength of all  
6 reinforcing fibres. They are classified prevalently on the basis of their mechanical  
7 properties into four groups as shown in Fig. 3 [128]; super high strength (SHT),  
8 intermediate modulus / high strength (IM / HT), high modulus (HM) and ultra-high  
9 modulus (UHM). As a general trend, very high strength fibres are produced by drawing  
10 a high-carbon yield polymeric precursor such as polyacrylonitrile (PAN) [129], [130],  
11 [131]; such fibres account for ~90% of the total production. In contrast, very high  
12 modulus fibres are manufactured by the drawing of pitch, a tar-like mixture of branched  
13 hydrocarbons [132], [133] that is capable of forming a crystal-liquid mesophase during  
14 the manufacturing process [131]. The mechanical properties of carbon fibres obtained  
15 from both PAN and pitch are reported in Table 2 [128], [134]–[141].

16  
17  
18  
19  
20  
21  
22  
23  
24  
25  
26  
27  
28 It should be noted, however, that the development of carbon fibres has not been  
29 driven by the need to overcome their intrinsically low oxidation resistance (as low as  
30 400-500°C [10]), but rather from the mechanical performance required by different  
31 industry sectors and, of course, cost reduction. Some studies have shown that the choice  
32 of different carbon fibres in UHTC matrices does not affect key mechanical properties  
33 such as fracture toughness [113]. Similarly, the different thermal conductivities of PAN-  
34 and pitch-derived carbon fibres (being higher for the latter) is also not usually the  
35 determining factor in the choice of carbon fibres for UHTC applications. Rather, the  
36 primary factors that typically affect the choice between PAN- and pitch-derived fibres  
37 are the very high modulus of the latter, which makes weaving harder, in turn limiting  
38 preform architecture, and also their more limited availability.

### 49 Silicon carbide fibres

50  
51  
52 The early development of SiC fibres occurred in the 1970s [142]. Since then,  
53 they have been continuously developed and improved with the primary goal being to  
54 offer a better oxidation resistance than carbon fibres [143]. Other goals underpinning  
55 the development of the different generations of SiC fibres have been to improve the  
56 maximum operational temperature and provide a better thermal endurance. The  
57  
58  
59  
60  
61

1 schematic in Fig. 4 [144] shows the evolution of the microstructure and the properties of  
2 the commercially available SiC fibres over the three generations presented in Table 3  
3 [144]–[147].  
4  
5

6 Two different approaches are available commercially to prepare SiC fibres  
7 [146]: chemical vapour deposition on a core filament and the spinning of preceramic  
8 polymers.  
9

10 SiC fibres produced by CVD, such as the Tisics Sigma™ (Tisics Ltd.,  
11 Farnborough, UK) [148] and the SCS (Speciality Materials Inc., MA) [149] have a  
12 diameter above 100 µm. As a consequence, they have a high bending stiffness and  
13 therefore are difficult to weave. These fibres are generally used for intermediate  
14 temperatures in metal matrix composites as creep retardants and stiffeners [150].  
15  
16  
17  
18  
19  
20  
21  
22

23 The second manufacturing process is similar to that used for carbon fibres and is  
24 based on the melt or dry spinning of organic polymers. A polymer with a high  
25 molecular weight, adequate viscoelasticity and thermal stability enables a stable melt  
26 spinning process to be used without breaking the filament. Typical polymers used  
27 include polycarbosilanes or polycarbosilazanes. Subsequently, the green fibres are cured  
28 and then converted into ceramic fibres by pyrolysis [142], [151] in a controlled  
29 atmosphere and temperature from 1200°C to above 1700°C. The microstructural,  
30 mechanical and thermal properties are dependent on the precise production conditions  
31 [147]; the finer the microstructure, the higher the tensile strength whilst the creep,  
32 Young's modulus and thermal resistance are determined by the oxygen content and  
33 sintering aids [145]. The first generation of fibres (Nicalon, Tyranno S and Lox-M) had  
34 a high oxygen content due to the curing in air that lead to an amorphous Si-C-O matrix  
35 with an oxygen content of up to 20 wt.% Above 1200°C the glassy phase evaporates  
36 with a consequent degradation of the fibres and dramatic loss of strength. The low  
37 production temperature (around 1200°C) implies the formation of small crystallites (2-5  
38 nm) of β-SiC which, combined with an inter-granular amorphous phase, poorly resists  
39 creep at high temperature. Oxygen is also responsible for their low Young's modulus  
40 and thermal conductivity. This first generation of SiC fibres cannot be used for the  
41 fabrication of CMCs for long-term performance at 1100-1200°C [152], let alone in  
42 UHTCMCs.  
43  
44  
45  
46  
47  
48  
49  
50  
51  
52  
53  
54  
55  
56  
57  
58  
59  
60  
61  
62  
63  
64  
65

1 Oxygen reduction was the guideline for the development of the second  
2 generation of SiC fibres (Hi-Nicalon and Tyranno ZMI) [145]. New organometallic  
3 precursor (zirconium grafted in the polymeric chain of the polycarbosilane) for Tyranno  
4 ZMI and electron beam curing for the Hi-Nicalon allowed the oxygen content to be  
5 reduced below 10 and 1 wt.% respectively. Higher production temperatures were  
6 possible, with the formation of larger grains and, hence, reduced creep rates [146].  
7  
8  
9

10  
11 Further improvement led to the third generation of SiC fibres (Hi-Nicalon Type  
12 S, Tyranno SA3, Sylramic, Sylramic i-BN) [146]. They are characterized by an even  
13 lower oxygen content and near-stoichiometric composition. The creep rate has been  
14 drastically reduced with the presence of 200 nm  $\beta$ -SiC crystals, achieved due to the  
15 higher temperature production occurring at above 1700°C. In this generation of fibres,  
16 sintering aids like aluminium for Tyranno SA3 and boron for Sylramic are incorporated  
17 in the fibre structure to form a dense fibre [145], [146], [152]–[154]. Hi-Nicalon Type S  
18 fibres are the product of choice for the CMC components in Leap Engine and GE9X,  
19 where the operational temperatures can reach 1400°C with a lifetime >25,000 hours  
20 [155].  
21  
22  
23  
24  
25  
26  
27  
28  
29  
30

31 iBN-Sylramic silicon carbide fibres are an exclusive product developed by  
32 NASA Glenn Research Center (Ohio, USA) [147] and commercialised by COI  
33 Ceramics Inc. (San Diego, California, USA). These fibres are coated with boron nitride  
34 by modifying the gaseous atmosphere used during the curing process [146]; the BN  
35 coating enhances fibre pull-out [156]. Subsequent study at the NASA Glenn Research  
36 Centre [157] has led to the development of the Super Sylramic-iBN and -iC fibres, BN  
37 and C coated respectively. The creep rate in particular has been shown to decrease if the  
38 fibres have a larger and more homogeneous grain size (up to 500 nm) and the  
39 microstructure is also free from pores and impurities. These fibres are not yet  
40 commercially available, being still in the process of laboratory development, and  
41 therefore have not yet been trialled for UHTCMC applications.  
42  
43  
44  
45  
46  
47  
48  
49  
50  
51

52 As discussed in the section dedicated to oxidation, above 1600°C the oxidation  
53 of SiC in general turns from passive to active. This implies that in the UHTC range, SiC  
54 fibres offer little long term oxidation resistance. However, as already noted the same is  
55 also true for C fibres, thus SiC fibres are extensively studied as reinforcement for  
56  
57  
58  
59  
60  
61  
62  
63  
64  
65

1 UHTCMCs with other mechanisms being used to protect them. These are discussed  
2 elsewhere in this review.

### 3 UHTC fibres

4  
5  
6  
7 As already discussed C and SiC fibres can only partially fulfil all the  
8 requirements to withstand the extremely demanding environments that are required, for  
9 example, by re-entry vehicles in the hypersonic regime [1], [33], [38], [158]. At the  
10 laboratory scale, efforts have been made to prepare ZrC [159]–[163] and ZrB<sub>2</sub> [162]  
11 micro and nanofibers via electrospinning. Cui et al. [161] produced ZrC by  
12 electrospinning a solution of novolac phenolic resin and zirconium (IV) acetyl acetonate  
13 (following annealing). The fibres obtained had a diameter of ~300 nm. Electrospinning  
14 combined with a polymeric precursor was also used to produce ZrC nanofibres of  
15 similar diameters [164]. Li et al. [165] electrospun polyzirconoxane (PZO) as the  
16 zirconium source and polyacrylonitrile (PAN) as the spinning aid and primary carbon  
17 source. A larger, 20 μm, fibre of Zr-Si-C was obtained by the spinning of a sol-gel  
18 precursor made from zirconium tetra-kis(2,4-pentanedionate), novolac phenolic resin  
19 and tetraethoxysilane [163]. Chelich et al. [162] synthesised ZrB<sub>2</sub> nanofibres by  
20 electrospinning of a hybrid polymer solution of PVP / zirconium n-propoxide and boric  
21 acid. NbC and ZrC textiles were obtained by carbothermal reduction of electrospun  
22 niobia-complex and zirconia-complex fibre mats [166].  
23  
24  
25  
26  
27  
28  
29  
30  
31  
32  
33  
34  
35  
36

37  
38 At the pilot scale, Matech GSM (Matech Global Strategic Materials Inc.,  
39 California, USA) [167] has developed and patented [168] hafnium nitride and hafnium  
40 carbide fibres (e.g. HfC 2000-X) with potential applications for rocket nozzles and  
41 sharp leading edges; HfC is the highest known melting compound [168]–[170]. A  
42 hafnium-based preceramic polymer was produced through the reaction of hafnium  
43 chloride with amines or imines. Depending on the atmosphere of the heat treatment,  
44 HfN(C) or HfC fibres were obtained. The final density of the fibres was 7.0 g cm<sup>-3</sup> due  
45 to an excess of carbon, which acted as both a grain growth inhibitor and as a sintering  
46 aid. The fibres had a diameter of 5.0 μm, a Young's modulus of 500 GPa and tensile  
47 strength of 1.7 GPa. In 2009 Matech GSM transferred the HfC-preceramic polymer to a  
48 pilot production line capable of spinning multi-hundred filaments [171]. Matech GSM  
49 has also produced TaC fibres (TaC 1600-X) for aluminised propellant solid rocket  
50  
51  
52  
53  
54  
55  
56  
57  
58  
59  
60  
61  
62  
63  
64  
65

nozzles [172] and some mini-composites TaC<sub>f</sub>/ TaC<sub>m</sub> have been developed [171], [173].

As shown above, the manufacturing of UHTC fibres is still at the pilot scale at best. Although there is no data available in the literature with regard to the cost of future commercial HfC and TaC fibres, it is known that the cost of Hf and Ta-based preceramic polymers is higher than those used to produce SiC fibres and therefore it seems highly probable that the cost of the product will also be much higher. It is also not yet known whether these fibres will offer any advantages over C and SiC fibres since the authors are unaware of any research yet undertaken to investigate the potential that UHTC fibres offer to UHTCMCs.

### **Preform selection**

The fibre preform design is essential for achieving the composite performance required mechanical and thermal properties [174]–[176]. The ability to impregnate with a matrix is governed by the porosity (size and distribution) and hence the permeability of the preform to the matrix precursor, which can be in the form of solid, liquid or gas. This, in turn, is a function of the fibre orientation / architecture and fibre volume fraction [175]. Pre-existing technology from textile forming has been widely utilised for designing carbon / SiC fibre preforms using weaving, braiding, stitching, etc. The fibre orientation is very critical for both the in-plane and out-of-plane strength and life of the composites [177]–[180].

The fibre reinforcement architectures are classified (following the textile literature), first on the technologies used and then on the fibre topology, e.g., the number of fibre directions. When the fibres are oriented only in one direction they are referred to as unidirectional fibres and provide stiffness along the fibre direction but a lack of it in the orthogonal directions. Therefore, the fibres are commonly stacked in two directions (0° and 90°), yielding two dimensional (2D) preform structures. Various textile technologies has been utilised for manufacturing such preform structures, including weaving, braiding, knitting, stitching, etc. During weaving, two directional fibres (0° / 90°) are interlaced - warp and weft; in knitting, two directional fibres (0° / 90°) are drawn by loops of yarns over previous loops, whereas in braiding the fibres are typically limited to only one direction by intertwining. Most commonly used 2D

1 preform designs are classified as Plain [181], Twill, Satin [175] or Matt, the  
2 designations being based on the number of fibre tows used and the positions in which  
3 they are laid. Each preform design pattern, and the processing techniques used, offers  
4 different benefits and limitations, as outlined in Table 4.  
5  
6

7  
8 Nevertheless, in the 2D preforms, the fibres are oriented only in the plane of the  
9 laminate and are therefore vulnerable to delamination. Therefore through thickness fibre  
10 reinforcement has been included to develop three-dimensional (3D) fibre reinforced  
11 structures. Consequently, efforts have been carried out to modify the 2D preform  
12 structures for additional in plane support using simple techniques such as stitching and  
13 needling [182] and the results are referred as 2.5D preform structures [179], [183]–  
14 [185]. Extensive research developments and products have been carried out using 2.5D  
15 carbon fibre preforms from Surface Transforms, UK, in the past decade [17], [179],  
16 [186]–[189]. Fig. 5 shows the structure of their preform; it is made of PANOX fibres  
17 and very easy to fill with a UHTC powder matrix. In addition the filled 2.5D fibre  
18 architectures have shown some promising resistance to mechanical stresses [179] and  
19 thermoablative properties as well [18], [187].  
20  
21  
22  
23  
24  
25  
26  
27  
28  
29  
30

31 Further to the simple developments, complex 3D preform structures have also  
32 developed through advancements of computational analysis and robotic manufacturing  
33 technologies. Triaxial fibres of different orientation, referred to as 3D structures are  
34 made using various methods such as weaving, knitting and braiding. Based on the  
35 fibres' interlocking position, the 3D woven structures are further classified as layer to  
36 layer, angle and orthogonal interlock weave as shown in Table 4. The weaving design  
37 provides moderate properties and can be automated, but there are limits to the shape and  
38 drapability [190]. The 3D braided structure is suitable for complex shapes along with  
39 offering a good balance of in-plane and out-of-plane properties [191]. Some of the other  
40 techniques used for making 3D structure are like stitching, needling [192] and noobing.  
41  
42  
43  
44  
45  
46  
47  
48  
49

50 Noobed structures are defined by a new process of producing 3D structured by  
51 non-interlacing, orienting orthogonally the three sets of yarns and integrating the  
52 structured through binding [193]. It is a new 3D technology and is being explored with  
53 carbon, SiC and oxide ceramic fibres. The noobed structures can be uniaxial or  
54 multiaxial, which include an additional set of yarns placed in the  $\pm 0^\circ$  direction, as  
55  
56  
57  
58  
59  
60  
61  
62  
63  
64  
65

1 shown in Table 4 [193]. The main advantage of the noobed preform is that the fibres are  
2 uncrimped and their paths are nearly orthogonal to each other.  
3

4 Although the well-established 3D manufacturing methods have been  
5 demonstrated to produce near net-shape structures directly, control is essential to avoid  
6 damage occurring by the insertion of the through-thickness reinforcement, which will  
7 decrease the mechanical properties of the resulting 3D composites. Subsequently, in  
8 order to achieve the targeted outcome, the fibre preform design has to match with a  
9 suitable further matrix densification process to achieve the required performance, as  
10 detailed in the following sections.  
11

12 Selection of a suitable preform is based on the required properties for the intended  
13 application and compatibility for the chosen fabrication process. In addition, cost and  
14 availability in the required shapes, sizes & quantities also are important. Structure-  
15 texture and properties are correlated with each other, hence obtaining tailored structures  
16 and textures is very important when targeting demanding mechanical & thermal  
17 properties. Processing method, type and conditions all play a role in achieving this and  
18 hence the next section covers the different methods used to obtain the UHTCMCs.  
19

## 20 **Materials processing**

21 Various processing methods for UHTCMCs are reported in the literature and Fig. 6  
22 summarises the different approaches considered. Details of each method are discussed  
23 in the following sections, whilst their advantages and disadvantages are summarised in  
24 Table 5.  
25

## 26 **PIP process**

27 Precursor infiltration and pyrolysis (PIP) is a green-forming procedure, an  
28 overview of which is depicted in Fig. 7. A liquid chemical precursor is introduced to a  
29 reinforcement phase and subsequently pyrolysed at elevated temperatures. The  
30 pyrolysis reaction yields the required ceramic product, which is retained within the  
31 preform body. Due to the lower-than 100% efficiency of this process, the evolution of  
32 gaseous by-product and volume shrinkage from precursor to ceramic, this process must  
33 be performed iteratively many times, often a dozen or more, until a matrix of the desired  
34



or otherwise limiting density is achieved.

Optimisation of the process requires achieving a high ceramic density whilst limiting the number of energy-intensive pyrolysis steps. Hence, a high ceramic yield from precursors is important and the precursor choice is critical. There are many instances in the literature of precursors for ZrB<sub>2</sub>, ZrC, HfC and HfB<sub>2</sub> ceramics. Xie et al. [194] used a polymeric zirconium cyclopentadienyl / boron hydride species, Fig. [194], which led to a ceramic conversion yield of 65.5 wt% at 1200°C for 1 hour in inert conditions. The temperature of the pyrolysis was found to be critical with respect to ceramic product distribution. At 1200°C, a product ratio of 4 : 0 : 1 ZrB<sub>2</sub> : ZrC : ZrO<sub>2</sub> was obtained, which tended to 9 : 1 : 0 at 1800°C, though higher temperatures have, historically, been associated with graphitisation of carbon fibres [195]. The material possessed terminal vinyl groups to prevent excessive polymerisation of the precursor, thereby reducing precursor viscosity. In a previous study [196], an unmodified material lacking these groups showed a similar ceramic yield but poorer product ratio with respect to ZrB<sub>2</sub>. This highlights the significance that physical properties such as viscosity or polymer conformation may have on precursor efficacy.

Zhang et al. [197], Zhao et al. [198] and He et al. [199] all used an ‘organic zirconium-containing polymer’ sourced from the Institute of Process Engineering from the Chinese Academy of Sciences, which produced both ZrC and ZrB<sub>2</sub>. Zhang et al. [198] described a ceramic yield of around 30 wt%, whereas He et al. [199] reported a ceramic yield of 45 wt% at 1500°C and described the structure as a mixture of a polymeric zirconium complex of acetyl acetate and butoxide ligands, and an aminopolyborazine. The apparent range in ceramic yield is interesting and may reflect the pyrolysis temperature, given broadly as 1400 – 1600°C for 2 hours by Zhao et al. [198], but not given at all in the work of Zhang et al. [197].

Zhang et al. [200] produced 2D C / C-ZrB<sub>2</sub>-ZrC-SiC composites from a similar combination of organic zirconium polymer and a polyborazine. The zirconium polymer alone could generate a ZrC phase at a ceramic yield of 44 wt%, which improved to 60 wt% for the ZrB<sub>2</sub> when combined with the polyborazine. The mixed precursor had a very low viscosity ( $5 \times 10^{-3}$  Pa s) and the product ratio was seen to be controlled by both the pyrolysis temperature and the B : Zr molar ratio in the precursor mixture. Ratios of 1 : 1 generated both ZrB<sub>2</sub> and ZrN phases, whilst 2 : 1 was found to yield ZrB<sub>2</sub> in the

1  
2  
3  
4  
5  
6  
7  
8  
9  
10  
11  
12  
13  
14  
15  
16  
17  
18  
19  
20  
21  
22  
23  
24  
25  
26  
27  
28  
29  
30  
31  
32  
33  
34  
35  
36  
37  
38  
39  
40  
41  
42  
43  
44  
45  
46  
47  
48  
49  
50  
51  
52  
53  
54  
55  
56  
57  
58  
59  
60  
61  
62  
63  
64  
65

highest proportion. Ratios greater than this produced more complicated mixtures of ceramic phases, including boride, carbide, oxide and free carbon. 1650°C was the lowest pyrolysis temperature at which ZrB<sub>2</sub> was the thermodynamic product of the reaction, whereas at 1800°C it became the only major product. The mixed precursor required 16 PIP cycles to generate maximum density.

Mixed ceramic phases can be produced from some precursors, which in the case of ZrB<sub>2</sub>-SiC-based ceramics may be ideal for moderate temperature applications. Lv et al. [201] fabricated ZrC / ZrB<sub>2</sub>-SiC fibres from a mixed precursor of a zirconium cyclopentadienyl alkyl silane polymer with polyaminoborazine. The creation of both the UHTC phase with the self-healing SiC elements produced superior oxidation protection in temperature regimes up to 1650°C.

Whilst achieving mixed ceramic phases may be desirable in some applications, interpenetration of different ceramic phases of different crystal structures is difficult to control and may, in some cases, cause microstructural or application-based complications that detract from the overall usefulness of components. Producing pure phases of UHTC from PIP routes is, as has been described, complicated by the thermodynamic proclivity for the formation of other carbide, nitride and oxide phases due to the precursors frequently used. Li et al. [202] reported the production of ZrB<sub>2</sub> phase from polyzirconoxane ([ZrCl(OCH<sub>2</sub>CH<sub>2</sub>OH)(OH)<sub>2</sub>(H<sub>2</sub>O)]) [203], [204] boric acid and phenolic resin with pyrolysis at 1600°C; only small quantities of ZrC were present as an impurity.

Reports of the production of hafnium-based ceramics from PIP are fewer in number. Given the similarity of organozirconium and organohafnium chemistries, this is likely to be primarily due to material cost; hafnium-based chemicals tend to be much more expensive than zirconium-based chemicals though the resulting ceramic has much better oxidation and ablation resistance [33]. Nevertheless, the description of precursors for the HfC / HfB<sub>2</sub> systems are sparse [168]. Patra et al. [205] produced a hafnium/hydroxyquinone complex from hafnium tetrachloride for the production of HfC. Yan et al. [159] used an in-situ gelation method with an HfOCl<sub>2</sub>.8H<sub>2</sub>O salt, citric acid and ethylene glycol to produce a network where the glycol ester of citric acid complexes the Hf metal centres, this could then be pyrolysed to produce the HfC ceramic phase. This method has the potential of being industrially flexible in that the

1 precursor uses an aqueous solvent with environmentally benign gelling agents and the  
2 viscosity of the solution is tuneable based on the ethylene glycol: citric acid ratio. In  
3 contrast to the details provided by Yan et al. [159], however, many authors simply state  
4 the use of ‘an HfC precursor’ [206], [207]. The provision of greater detail in the  
5 composition and thermodynamics of developmental materials is beneficial to the growth  
6 of the area as a whole.  
7  
8  
9

10  
11 Issues with the PIP method centre around the microstructures produced,  
12 especially considering the numerous high temperature cycles required for densification  
13 and the frequent evolution of gaseous by-products. Many authors [182], [208] have  
14 reported that significant fibre degradation happens during the reaction of the carbon  
15 fibres with the precursor materials. This can result in either stronger bonding to fibres or  
16 loss of the structural integrity of the fibres, either causing a reduction in the degree of  
17 toughening achieved. The use of interphases coated onto the fibres to protect from this  
18 degradation [182], [209] has shown some improvements in mechanical properties.  
19 Having said that, the interphase coating, which is often PyC or SiC, can reduce the  
20 penetration of UHTC powders into the fibre tows. As a result, the in-situ UHTC content  
21 is low in close proximity to the fibres, which could result in poor oxidation protection.  
22 Pores are also generated during the volume shrinkage from precursor phase to ceramic  
23 [208], [210]–[212]. Pores and cracks generally form as the precursors shrink and any  
24 gaseous reaction products are evolved. Whilst these pathways allow pressure release  
25 from within the ceramic, they also allow oxygen ingress during testing or when in use.  
26  
27  
28  
29  
30  
31  
32  
33  
34  
35  
36  
37  
38  
39

40 Ziegler et al. [211] reported that the volume changes produce residual  
41 compressive stresses at the fibre / matrix interface, which resulted in the embrittlement  
42 of the CMC as density increased. It was observed that the direction of the shrinkage,  
43 towards or away from the fibres, was highly dependent upon local geometry. Reduction  
44 of the number of PIP cycles was clearly dependent upon the ceramic yield of the  
45 material [211]. King et al. [213] increased the ceramic yield of a SiC precursor by up to  
46 7% by heat-treatments of the liquid before pyrolysis, this removed the more volatile  
47 oligomeric precursors that limited the ceramic yield. Heat treatments can also improve  
48 the rheological properties of the precursor liquid; Ziegler et al. [211] observed that by  
49 choosing precursors capable of chemical cross-linking at lower temperatures allowed  
50 the precursor to solidify within the reinforcement, minimising losses due to evaporation  
51  
52  
53  
54  
55  
56  
57  
58  
59  
60  
61  
62  
63  
64  
65

1 or dripping as a result of gravity. Ziegler et al. [211] further suggested that precursors  
2 which underwent addition rather than condensation mechanisms were preferable in that  
3 mass loss and the creation of porous channels were both reduced. The wetting and  
4 rheological properties also need to be tuned whenever possible. The PIP process fills  
5 porosity by capillary pressure and Yan et al. [212] noted that high volumes of intertow  
6 porosity are apparent; superior interfacial energy balances between the substrate,  
7 precursor and atmosphere would result in superior coating and infiltration of the  
8 precursors.  
9  
10  
11  
12  
13  
14  
15  
16  
17

### 18 **Reactive melt infiltration**

19  
20  
21 Reactive melt infiltration (RMI) is the introduction of a molten metal, typically  
22 zirconium in the case of UHTCMC fabrication, into a porous fibrous preform in-situ  
23 where it reacts with either pre-matrix carbon or boron phase to form the UHTC phase  
24 with a high matrix density. This is not an iterative process, hence there must be a high  
25 ceramic yield with the correct molar and spatial balance of pre-matrix, typically  
26 deposited by CVI (see next section), and the reactive melt to form a dense homogeneous  
27 matrix [207] as shown in Fig. 9. This is the technique, for example, that has been  
28 pioneered for the mass production of SiC<sub>f</sub>/ SiC CMCs by General Electric [214] for  
29 their advanced civilian aerospace engine. These CMCs were the first to be used  
30 commercially in the civil aviation industry on General Electric's CFM LEAP engines  
31 [214] that were launched in 2016.  
32  
33  
34  
35  
36  
37  
38  
39  
40  
41

42 The reactive metal infiltration processes has several advantages[215], [216]: (i)  
43 it produces a near fully dense matrix; (ii) the processing time is shorter than for most  
44 ceramic matrix composite fabrication processes and is subsequently relatively cheap;  
45 (iii) the closed porosity at the surface can often eliminate the need for a final oxidation  
46 resistant coating and (iv) a reaction bonded UHTC matrix is effectively produced.  
47  
48  
49  
50  
51

52 The major disadvantages to this process are three-fold. For fibre composites the  
53 high temperatures required for reactive metal infiltration exposes the carbon fibres to  
54 very aggressive molten metals, often above 1400°C [217]. The exothermic nature of the  
55 reaction between constituents can also further increase the temperature locally, causing  
56 more damage [217]. The metal in this form is highly reactive and, if infiltration  
57  
58  
59  
60  
61  
62  
63  
64  
65

1 conditions are not strictly controlled, serious degradation of the carbon fibre preform  
2 [207], [218]–[220], Fig. 9a, will occur leading to deleterious consequences on the  
3 properties [216]. Often interface materials are needed to protect the fibres, as the CVI  
4 matrix is not sufficient to protect the fibres entirely [197], [218], such methods have met  
5 with limited success so far. The other major issue is the 5-10 vol% residual metallic  
6 phases [217], as shown in Fig. 9b [216], which have relatively low oxidation resistance  
7 and a lower melting point than the ceramic phases present. This metallic phase can lead  
8 to accelerated creep, crack propagation and further attack when the material is operating  
9 at high temperature [221], [222]. The final issue is due to the molten metal needing to  
10 react with the CVI matrix to form the UHTC in-situ; the reaction rate is limited by a  
11 number of factors, including: available surface area per volume, the molar volume of  
12 the UHTC produced, the thickness of the reaction barrier and the rate with which the  
13 fibre preforms becomes saturated [223]. One of the pivotal characteristics of the RMI  
14 process is the wettability of the transition metal alloy on the substrate. Table 6 [207],  
15 [220], [224]–[232] describes a number of alloying elements that have been successfully  
16 used to introduce zirconium into carbon fibre preforms to form ZrC and ZrB<sub>2</sub> in-situ.  
17 The literature is very limited in terms of hafnium infiltration and non-existent in terms  
18 of the production of hafnium diboride via this method to date. It is assumed that due to  
19 the proximity of hafnium and zirconium in the periodic table, the alloying elements  
20 needed to improve wetting characteristics will be somewhat similar as their effective  
21 nuclear charge is similar [233].  
22  
23  
24  
25  
26  
27  
28  
29  
30  
31  
32  
33  
34  
35  
36  
37  
38

39 The RMI process is attractive for fabricating high density, continuous fibre  
40 reinforced UHTC composites. However, the process has limitations such as the  
41 presence of residual metal phase, liquid metal corrosion of fibres, etc. as discussed more  
42 generally above [223]. Nevertheless, as stated it has already been commercialised for  
43 SiC<sub>f</sub>–SiC<sub>m</sub> composites [214].  
44  
45  
46  
47  
48

### 49 **Chemical vapour infiltration processing**

50  
51  
52

53 The use of chemical vapour infiltration (CVI) to deposit UHTC matrices is still  
54 very much a developing processing technique in the densification of UHTCMCs.  
55 However, there has been a relatively large body of research conducted on the deposition  
56 rather than infiltration of said matrices using chemical vapour deposition (CVD), a  
57  
58  
59  
60  
61  
62  
63  
64  
65

1 somewhat similar process. CVD works on the same basic principal of the thermal  
2 decomposition of a reactive gaseous mixture to form a solid product [234], in this case a  
3 UHTC layer or coating. It is proven that UHTC coatings deposited by CVD on C/C  
4 substrates can provide enhanced oxidation resistance and reduce ablation rate up to one  
5 order of magnitude [10], [235]. This is accompanied by the production of a number of  
6 chemical by-products, typically HCl and HF, which are exhausted out of the reaction  
7 chamber along with any unreacted precursor gases. It is a relatively low temperature  
8 and low-pressure densification route compared to other advanced manufacturing  
9 methods and can be very versatile since a wide range of material compositions can be  
10 produced, as shown in Table 7 [236], [237]. Fig. 10 presents a schematic of the growth  
11 of the ceramic deposit on the cross section of the fibres to the point of full densification  
12 by CVI.  
13  
14  
15  
16  
17  
18  
19  
20  
21

22 The resultant solid deposit is dense, fine grained (from a few to hundreds of  
23 nanometres) and potentially free from impurities if processing is controlled correctly  
24 [236], [237]. It is particularly suitable for the deposition of carbides and borides, which  
25 otherwise require high-temperature processing based on sintering techniques. Multiple  
26 compositions can also be infiltrated by alternating the gaseous precursors introduced  
27 into the reaction chamber [235], [238]–[241]; giving the ability to tailor microstructures,  
28 which can also be controlled by tuning the process parameters including temperature,  
29 chamber pressure and feed rate of the precursor. The main advantages and  
30 disadvantages of CVI are summarised in Table 5.  
31  
32  
33  
34  
35  
36  
37  
38  
39

40 Isothermal CVI, ICVI, is the most well-known and commonly used process by  
41 industry and although the benefits are evident, ICVI (Fig. 11a) suffers from a main  
42 drawback. The deposition occurs preferentially near the outer surface where the  
43 concentration of reactants, and often the temperature, is highest [237]. As a result,  
44 “crusting” occurs and seals the porosity at the surface of the preform prematurely, this  
45 requires the infiltration to be stopped and the porosity to be reopened by machining. In  
46 order to reduce the extent of crusting, the possibilities are to: i) decrease the process  
47 temperature, though this decreases the deposition rate and hence increases the process  
48 time, or ii) work at reduced pressure improving the gas diffusion in the preform.  
49 Nevertheless, as result of crusting, the processing time can be up to 2000 hours and  
50 hence the process is not cheap [242]–[244].  
51  
52  
53  
54  
55  
56  
57  
58  
59  
60  
61  
62  
63  
64  
65

1 Overall, the process is complex because it requires detailed awareness of the  
2 reaction chemistry, kinetics, temperature distribution, heat source, pressure and preform  
3 geometry [245], [246]. The final microstructure depends on all these variables and  
4 hence so do the thermo-mechanical properties. On this basis, a variety of CVI processes  
5 have been developed which can be classified by: i) temperature, ii) pressure and iii)  
6 heating method [247] as shown in the Table 8 [242]. For example, the deposition can be  
7 conducted in both hot-wall and cold-wall reactors, at chamber pressures as low as 100 -  
8  $10^{-1}$  Pa or at above-atmospheric pressure, with and without carrier gases, and at  
9 temperatures typically ranging from 200-1600°C. There are also a variety of enhanced  
10 CVI processes that involve the use of plasmas, lasers, hot filaments, or combustion  
11 reactions to increase deposition rates and/or lower deposition temperatures. A thermal  
12 gradient can be applied as shown in Fig. 11b, radiantly or inductively, to the fibre  
13 preform [242], [248]. This gradient causes the deposition to occur preferentially in the  
14 hot zone at a faster rate and the densification front then proceeds from the hotter zone  
15 toward the cooler region as the hot zone moves as a result of the changing thermal  
16 conductivity of the product. The gas phase flows into the cooler side of the preform so  
17 that the gas does not encounter a sealed region and can proceed unimpeded to the  
18 reaction zone. The advantage is a shorter infiltration time compared to isothermal CVI,  
19 typically only about 120 h. One preform can be densified per run, however, and  
20 controlling the deposition is difficult without very sophisticated and hence expensive  
21 temperature control systems [242].  
22  
23  
24  
25  
26  
27  
28  
29  
30  
31  
32  
33  
34  
35  
36  
37  
38

39 In terms of kinetics of the ceramic deposition from the gas phase, this is highly  
40 dependent on the processing variables and is gaseous species specific, though reaction  
41 rates have been described in a number of models [249]–[253]. In terms of the physical  
42 deposition rate, this is again reported for UHTC matrices in the CVD literature and can  
43 be somewhat translational in terms of the ceramic material deposited, though due to the  
44 diffusion times being slower in CVI rates are always lower [249].  
45  
46  
47  
48  
49  
50

51 In summary, the CVI process is very useful in that it enables the formation of  
52 reasonably dense, complex-shaped components at low processing temperatures that do  
53 not damage the fibres used for reinforcement. There is also the ability to create different  
54 matrix compositions and to achieve high purity whilst tailoring the microstructure.  
55 However, it is an intrinsically slow process and therefore the product can be expensive.  
56  
57  
58  
59  
60  
61  
62  
63  
64  
65

1  
2  
3  
4  
5  
6  
7  
8  
9  
10  
11  
12  
13  
14  
15  
16  
17  
18  
19  
20  
21  
22  
23  
24  
25  
26  
27  
28  
29  
30  
31  
32  
33  
34  
35  
36  
37  
38  
39  
40  
41  
42  
43  
44  
45  
46  
47  
48  
49  
50  
51  
52  
53  
54  
55  
56  
57  
58  
59  
60  
61  
62  
63  
64  
65

Amongst the different variations developed to overcome the limitations, one of the most promising currently is the use of microwave or radio frequency energy assisted CVI due to the ability to create an inverse thermal gradient profile, Fig. 11f, compared to conventional heating, Fig. 11a. This greatly reduces the process times, whilst retaining all of the advantages of the fundamental CVI process. However, it should be noted that this process is still limited to laboratory scale and so further work is needed before it can be commercialised. Currently there is no published literature showing fully dense UHTCMCs but such work is currently underway throughout the world [254].

### Slurry impregnation process

The slurry impregnation process (SIP) is perhaps the most common technique used to produce continuous fibre-reinforced ceramic composites. This process involves impregnating the fibres / woven fabrics by introducing a slurry made out of matrix powder. The slurry is generally prepared by ball milling the powder along with a binder and dispersant in a suitable solvent (aqueous or non-aqueous) using appropriate milling media that matches with the matrix material in terms of composition (to reduce deleterious impurities) and hardness [255]. After impregnation, the organics are removed in the drying stage and, if required because the powder is a precursor, the ‘green’ composite can be pyrolysed at elevated temperatures in a controlled atmosphere to avoid fibre degradation. The powder introduced via the slurry to create the matrix could have one of several different compositions or a mixture of them, including SiC, UHTCs, or their precursors.

Lange et al. [256], reported that the impregnation of a dry, porous medium with slurry typically occurs by capillary forces and / or applied pressure. The flow of liquid into a porous medium by differential pressure,  $\Delta P$ , is described by Darcy’s law:

$$h = (2K\Delta P/\eta)^{1/2} t^{1/2} \quad (1)$$

where  $h$  is the distance the liquid penetrates in a time period  $t$ ,  $K$  the permeability of the porous body and  $\eta$  is the viscosity of the slurry.

The permeability has been related with the pore size [257]:



$$K = \phi m^2 / k_0 \quad (2)$$

where  $\phi$  is the pore fraction,  $m$  the mean hydraulic radius (pore fraction divided by the wetted surface area) and  $k_0$  a constant.

Lange et al. [256] studied the factors influencing the infiltration of slurry into a porous structure, such as a fibrous preform, in detail and suggested that the particle-to-fibre diameter ratio plays a vital role in the packing density of the matrix powder around the fibres. The viscosity and the pore size of the preform are the key factors influencing the infiltration kinetics, which can be improved by increasing the capillarity and the external force applied. The latter can be achieved by either squeezing the fibres or preforms [18] or using pressure-assisted methods [10], [17], [258], but these techniques can open up undesirable voids between the fibres and/or deteriorate the homogeneity of the fibre orientations. To achieve a high enough densification level without risking damaging the structure of the porous body, several impregnation / pyrolysis sequences (typically 6 to 10 and sometimes even more) have therefore to be performed, which is time consuming and reduces the economics of the process.

When the required powder-to-fibre ratio is not met, the distribution of powder into the stacked fibres or preforms can fail to be sufficiently homogeneous across the sample; it is common for the powder to be concentrated in the first fabric layers at the surface. For example, Paul et al. [18] fabricated hybrid UHTC composites using 2.5D C-fibre preforms (containing 23 vol% fibres) using vacuum impregnation but only succeeded in getting ~7 mm of UHTC powder penetration into 17 mm thick samples, Fig. 12 [17], whilst Tang et al. [10] only obtained ~2 mm of penetration for 28 – 30 vol% fibre preforms, Fig. 13 [10]. Lee et al. [258] developed a modified infiltration technique using a mould with a deformable foil at the bottom, Fig. 14 [258]. When using conventional pressure casting, the relative density of the samples decreased with increasing slurry solids loading, a consequence of the incomplete infiltration of the slurry, but when the fabrics were subjected to deformation casting, the density increased even with increasing solid loading. Concentrated slurries with solids loading of up to 43 vol% have been successfully injected homogeneously into the fabrics [258].

A slurry injection method has been used by multiple authors to produce components of high ceramic homogeneity in fibre reinforcements characteristically

1  
2  
3  
4  
5  
6  
7  
8  
9  
10  
11  
12  
13  
14  
15  
16  
difficult to impregnate[61], [179], [186]. Very recently, Hu et al. [61] impregnated a 3D  
needle punched preform with an ethanol-based ZrC and SiC slurry to a green body  
relative density of 42% via this method, though the porosity distribution was not  
presented in detail, nor were the original fibre volume of the preforms reported.  
Extensive work done at the University of Birmingham[179], [186] has characterised the  
injection process for UHTCMCs, showing clearly with X-ray computed tomography  
(micro-CT) the development of the ceramic distribution via the injection method and  
the required parameters to maximise the extent of impregnation for HfB<sub>2</sub> slurries in  
2.5D C<sub>f</sub> preforms.

### 17 **Other methods**

18  
19  
20  
21  
22  
23  
24  
25  
26  
27  
28  
29  
30  
31  
32  
33  
34  
35  
36  
37  
38  
39  
40  
41  
42  
43  
44  
45  
The primary processing methods used, such as PIP, RMI, CVI and SIP, to create  
fine-grained UHTC matrices in continuous fibre preforms have been discussed in the  
previous sections. As indicated, each has its advantages and disadvantages. A number of  
other processes have been investigated, however, including: sputter deposition [259]–  
[261]; electroplating / electrophoretic deposition (EPD) [259], [261], [262]; electron  
beam irradiation [260], [263]; liquid precursor methods [260], [264], [265]; slurry  
coating [260], [266]; chemical liquid vapour deposition (CLVD) [267]; and pack  
cementation [260], [268], [269]. Each method offers specific advantages in terms of  
control of material composition, deposit thickness or cost, enabling the development of  
a wide range of microstructures and configurations. As just one example, EPD requires  
only simple equipment and low cost operating conditions [262], [270], [271].  
Nevertheless, these methods have not yet been explored extensively for UHTCMCs. A  
summary of the few available reports involving these techniques are briefly described  
below.

46  
47  
48  
49  
50  
51  
52  
53  
54  
55  
56  
57  
58  
59  
60  
61  
62  
63  
64  
65  
Pack cementation has been investigated by Li et al. [262], who incorporated a  
SiC nanowire – SiC – Si/SiC – ZrB<sub>2</sub> – ZrC matrix in a C/C composite via a three-step  
process involving pack cementation, EPD and a final pack cementation step. Meanwhile  
Tao et al. [272] prepared a ZrB<sub>2</sub> – SiC – Si/B-modified SiC coating on the surface of  
carbon/carbon composites by a two-step pack cementation process at 1900°C and Yao  
et al. [273] prepared a ZrB<sub>2</sub> – SiC coating on carbon/carbon composites also using a  
pack cementation process with Si, ZrB<sub>2</sub>, and B<sub>2</sub>O<sub>3</sub> powders at 1900–2200°C.

1 Corral et al. [274] developed UHTC coatings on C/C composites using  
2 inorganic–organic precursor solutions for infiltration and heat treatment at high  
3 temperatures (up to 2300°C) to convert them to borides and carbides. Zou et al. [230]  
4 infiltrated Zr melt into porous C/C to form ZrC coatings whilst Jayaseelan et al. [260]  
5 reported using a reactive infiltration process (RIP) to infiltrate porous carbon fibre  
6 reinforced carbon (C/C) composite hollow tubes with ZrB<sub>2</sub> particles by using inorganic–  
7 organic hybrid precursors of zirconium oxychloride (ZrOCl<sub>2</sub>·8H<sub>2</sub>O), boric acid and  
8 phenolic resin. He et al. [267] recently reported a CLVD process to prepare C/C – ZrC  
9 composites by using the precursors [(C<sub>4</sub>H<sub>8</sub>O)Zr<sub>2</sub>]<sub>n</sub> and liquid xylene (C<sub>8</sub>H<sub>10</sub>) in the  
10 temperature range of 800-1100°C and obtained a density of ~90% of theoretical.  
11  
12  
13  
14  
15  
16  
17  
18

19 Although these techniques enable the infiltration of nano-size particles and pure  
20 phase compounds, a major limitation is in achieving sufficient penetration of liquid  
21 precursors into preforms and hence the achievement of full densities. Many times,  
22 further densification has to be carried out by hot pressing, spark plasma sintering (SPS),  
23 CVI, etc. in order to obtain the required degree of densification. For example, Galizia et  
24 al. [275] produced C<sub>f</sub>/ZrB<sub>2</sub> UHTCMCs by electrophoretic deposition (EPD) of ZrB<sub>2</sub> on  
25 unidirectional carbon fibers followed by ZrB<sub>2</sub> infiltration and hot pressing. More details  
26 on densification of UHTCMCs by hot pressing (HP), SPS, pressureless sintering (PS)  
27 and hot isostatic pressing (HIP) are given in the next section.  
28  
29  
30  
31  
32  
33  
34  
35  
36  
37

## 38 **Sintering approaches**

### 39 **HP, SPS, HIP and pressureless**

40  
41  
42  
43  
44 As applied to UHTCMCs, the hot pressing (HP) technique comprises three main  
45 steps [221]:  
46

47  
48  
49 1) The continuous fibrous reinforcement is coated with interphase layers, typically  
50 pyrolytic carbon [276] or ceramic [275], [277] to enhance the fracture toughness of the  
51 composite and protect the fibres during pressing.  
52  
53

54  
55 2) The continuous fibres are impregnated with UHTC particles in the form of slurry  
56 and consolidated by vacuum bagging [276], [278]–[280], or cold compaction/lamination  
57 [276], [277]. If short fibres are used as reinforcement [92], [95], [113], [114], [118] a  
58  
59  
60  
61

1  
2 more traditional approach is the use of ball milling of the UHTC powders and short  
3 fibres as a slurry, followed by drying and uniaxial cold pressing.

4  
5 3) The assembly is sintered at high temperature (1600-2100°C) and pressure (~20-  
6 100 MPa) by HP, HP, SPS or PS.

7  
8  
9 As a result of the high refractoriness of UHTCs, the temperature and the pressure  
10 applied need to be much higher compared to other manufacturing processes, e.g. CVI  
11 and PIP. One advantage is that the matrix is sintered and thus can contribute to the  
12 structural properties and act as thermal barrier for the carbon fibres; another is that the  
13 fibre content can be up to 70 vol% [279]. A high relative density is usually achieved  
14 (>90%) [278], [281] leading to a high modulus and strength to rupture.

15  
16  
17  
18  
19  
20  
21 The process is typically fast, taking approximately one working day for the  
22 production of the green composite and a few hours for sintering [279]. The high  
23 temperature and pressure involved during the sintering stage, however, are reported to  
24 be responsible for fibre degradation and chemical interaction between the fibres and  
25 matrix, which leads to the formation of strong but brittle phases at the interfaces [92].  
26 As an example, the creation of carbides were ascribed to the carboreduction of the  
27 oxides impurities ( $ZrO_2$  and  $SiO_2$ ), naturally present in the UHTC powders, promoted  
28 by the carbon fibres [92], [95], [113] (see Fig. [113]). These phases dictate the  
29 mechanical behaviour of the UHTCMCs.

30  
31  
32  
33  
34  
35  
36  
37  
38  
39 As a result, one of the main efforts has been to reduce the sintering conditions by  
40 using sintering aids. The use of, for example, 5 vol% of  $Si_3N_4$  or 10 vol% of  $ZrSi_2$ ,  
41  $TaSi_2$  or  $MoSi_2$  has been investigated because of their proved efficacy in promoting  
42 densification and oxidation resistance [95], [113]. Sintering temperature onset was  
43 shown to lie in the range 1550-1580°C, compared to at least 1900°C for the  $ZrB_2$  [33].  
44 Despite the reduction of the sintering temperature, the formation of SiC and ZrC  
45 surrounding the fibres was still observed. However, as discussed by Zoli et al. [281],  
46 despite the formation of brittle phases, pull-out still occurs because of the onion-like  
47 structure of the carbon fibres. It has also been reported that other mechanisms of  
48 toughening are activated, either crack deflection [275] or, in weak matrix composites  
49 such as porous  $C_f-ZrB_2$  [279], with a fracture mechanism similar to that which occurs in  
50 oxide-oxide CMCs [282]. Table 9 [275], [276], [278], [279], [281], [283] summarises  
51  
52  
53  
54  
55  
56  
57  
58  
59  
60  
61

1 the thermomechanical behaviour achieved by hot pressed UHTCMCs, including  
2 microstructural and physical properties.  
3

4 The sintering stage has also been carried out by spark plasma sintering (SPS) [110],  
5 [284], [285]. This enables the sintering of ceramics in a short time because of the high  
6 heating ramp rate ( $\sim 1000^{\circ}\text{C}/\text{min}$ ) and reduced dwell time (a few minutes), potentially  
7 diminishing the interaction time of the fibre with the matrix [110]. The relative density  
8 of 96.7% achieved for samples of  $\text{ZrB}_2 - \text{C}_f$  sintered at  $1900^{\circ}\text{C}$  was significantly higher  
9 than for analogous specimens produced by conventional hot pressing, which achieved  
10 only 85% of their theoretical density. Lee et al. [284] investigated the effect of  
11 temperature on the integrity of composites made of SiC fibres (Hi-Nicalon Type S with  
12 200 nm of BN coating) in a matrix of  $\text{ZrB}_2$  with  $\text{MoSi}_2$ ,  $\text{B}_4\text{C}$  and carbon additives.  
13 Brittleness of the composite was observed when sintering occurred above  $1600^{\circ}\text{C}$ ; it  
14 was ascribed to fibre degradation, growth of the  $\text{ZrB}_2$  grains into the rather soft BN and  
15 the decomposition of BN due to the reaction with  $\text{ZrO}_2$ ,  $\text{B}_4\text{C}$  and C.  
16  
17  
18  
19  
20  
21  
22  
23  
24  
25  
26

27 Relatively little work has been done on hot isostatic pressing, HIP, and pressureless  
28 sintering: temperatures as high as  $2000^{\circ}\text{C}$  have been employed for  $\text{C}_f\text{-ZrB}_2$  with 20  
29 vol% of SiC and a pressure of 105 MPa for  $\text{C}_f\text{-TaC}$  sintered by HIP [277]. Nasiri et al.  
30 [117] used pressureless sintering for  $\text{C}_f\text{-ZrB}_2$  composites but using temperatures in  
31 excess of  $2100^{\circ}\text{C}$ . Tallon has also used pressureless sintering for porous UHTCs [286],  
32 though these are not composites and hence will not be discussed further here.  
33  
34  
35  
36  
37  
38  
39

40 In summary, hot pressing is the most common route for the processing of  
41 UHTCMCs and it both reduces the processing times and allows high densities to be  
42 achieved. However, the high pressure and temperature involved are detrimental for the  
43 integrity of the reinforcement. Use of sintering aids alleviate the sintering conditions,  
44 but they are often responsible of the formation of brittle phases at the interface fibre-  
45 matrix and, hence, only a marginal increase in the fracture toughness of the material is  
46 observed when they are used. SPS promotes densification at lower temperatures and in  
47 shorter times, but additives, external pressure and high temperatures (if compared to  
48 other manufacturing process such as RMI and CVI) are still required. Relatively few  
49 projects have explored the use of pressureless sintering and HIP for UHTCMCs  
50 although they have the advantage of manufacturing near-net shape components.  
51  
52  
53  
54  
55  
56  
57  
58  
59  
60  
61  
62  
63  
64  
65

## Material characterisation

The quality of the fabricated UHTCMCs can be determined by microstructural characterisation and the evaluation of mechanical and thermal properties. The influences of various methods of fabrication and the type of matrix and second phase on these properties are described in this section.

### Microstructural characterisation

No matter which shaping approach is adopted, composites with fine grains and well distributed secondary phases are generally desired for the particulate / chopped fibre reinforced UHTCs [33]. The elimination of large agglomerates is helpful to reduce the size of the critical flaws and therefore improve the strength and reliability of the ceramics [287]. However, in practice, microstructures of UHTCMCs can be inhomogeneous and are highly dependent on the processing methods and preform used. For example, typical defects in the as-sintered 1D -  $C_f/ZrB_2$  composite (stacked cross - ply 0 – 90°, Fig. 16) include lenticular-shaped voids and vertical cracks in the ceramic layer, Fig. 16a [279]. Further investigation indicated that micro- and macro-cracks generated by the TEC mismatch between the fibre and matrix could be reduced if the  $C_f$  bundles were aligned unidirectionally at the adjacent layers, Fig. 16b [281]. Moreover, the elimination of such defects could be realized by optimizing the green forming approach, although no details have been reported [288].

For the  $C_f$  - UHTC powder composites prepared by SIP technology (see section on SIP), the distribution of UHTC powder was related to the porosity in the preform, the direction of infiltration and the rheological properties of the slurry [10], [18], [179], [289]. Taking 2.5D -  $C_f$  preforms as an example, UHTCs powders were found to concentrate at the regions near the surface where the slurry infiltration occurred, Fig. 13a [10]. The as-infiltrated green body was subsequently subjected to an isothermal CVI process and the pyrolytic carbon (PyC) deposited on the fibre could be clearly seen, as shown in Fig. 17 [10]. The PyC was infiltrated into the voids between the carbon fibres and the UHTC particles, integrating the particles into the composites, Fig. 17. It worth noting that the powders prefer concentrating into the area near the surface and the random layers in the preform, Fig. 18 [18], during SIP, the random layer with larger

1 pore size and higher porosity was generated as result of the Surface Transform's  
2 needling process.  
3

4 Typical microstructures for UHTCMCs prepared by PIP (see section on PIP) are  
5 similar to those of composites made using SIP. However, much finer UHTC particles  
6 (down to  $\sim 1 \mu\text{m}$ ) could be seen in the sample produced by PIP due to the nature of the  
7 process; PIP involves pyrolysis of precursors [290], [291]. Taking a C/C–ZrB<sub>2</sub>–ZrC–  
8 SiC composite as an example, submicron-sized ZrB<sub>2</sub>, SiC and ZrC particles were found  
9 to pack loosely in the voids between the carbon fibre bundles, Fig. 19a [290]. Large  
10 agglomeration with a core (ZrB<sub>2</sub>) - shell (ZrC-SiC) structure can also be seen in this  
11 sample, Fig. 19b [290]. Since the viscosity of the precursor is lower than that of typical  
12 powder-based slurries, the particles infiltrated deeper during PIP processing.  
13  
14  
15  
16  
17  
18  
19  
20  
21

22 As described in section on sintering, HP & SPS are normally used to further  
23 densify green bodies prepared by SIP or PIP to reduce the porosity in the UHTCMCs.  
24 Fig. 20 [289] shows a typical interface in C<sub>f</sub>/ZrB<sub>2</sub>–SiC composites densified by SIP and  
25 HIP. Elemental mappings indicate that, apart from limited ZrO<sub>2</sub> particles, no other  
26 phase from the reaction between fibre and matrix were observed, Fig. 20 [289]. The  
27 interfacial reaction was avoided by impregnation of the slurry prepared from nano-sized  
28 ZrB<sub>2</sub> into the C<sub>f</sub> preform. Benefiting from the better sinterability of nano-sized powders,  
29 the post - sintering temperature for such composites was reduced to 1400°C [292].  
30  
31  
32  
33  
34  
35  
36  
37

38 Although reports of ZrC and ZrB<sub>2</sub> CVD coatings on the C<sub>f</sub> preforms exist [293],  
39 investigations into the use of CVI to deposit a UHTC matrix in fibre preforms are rather  
40 limited.[249]. The most widely infiltrated substances during CVI are C and SiC. The  
41 effect of the interface with the carbon fibre and its influence on ZrC powder infiltration  
42 and the subsequent SiC - CVI process was investigated by Wang et al. [294]. The  
43 resulting images with different interfaces are compared in Fig. 21 [294]. Carbon  
44 deposition (or C - SiC deposition) on the carbon filaments facilitated the connection of  
45 the fibres, which retarded the further infiltration of ZrC particles into the wrapped  
46 carbon bundle. Therefore, a higher ZrC percentage was realized in the composite  
47 without a carbon interface, Fig. 21a.  
48  
49  
50  
51  
52  
53  
54  
55  
56

57 Typical microstructures of UHTCMCs densified by RMI are compared in Fig.  
58 22 [295]–[297]. Firstly, as indicated previously, RMI normally results in a high relative  
59  
60  
61  
62  
63  
64  
65

1 density for the UHTCMC, hence, as expected, limited porosity can be observed in either  
2 the C<sub>f</sub>/ZrC [295] or C<sub>f</sub>/ZrC-SiC [296] composites. Secondly, according to the different  
3 reactions during RMI, trace amount of unreacted materials with lower melting  
4 temperature are typically found as the residual phase in the final samples, e.g. α - Zr in  
5 C<sub>f</sub>/Zr, Fig. 22a, and ZrSi<sub>2</sub> in C<sub>f</sub>/ZrB<sub>2</sub>-SiC-ZrC, Fig. 22c & d. In a recent study [297],  
6 (Ti, Zr)C formed from a metal melt of Ti<sub>0.8</sub>Zr<sub>0.2</sub> and PyC during RMI could be further  
7 converted into Zr<sub>0.8</sub>Ti<sub>0.2</sub>C<sub>0.74</sub>B<sub>0.26</sub>. The microstructure of this novel composite was  
8 composed of a surface Ti-Zr-B-C coating and C<sub>f</sub>/Ti-Zr-B-C-SiC matrix, as shown in  
9 Fig. 22e. PIP could also be combined with both RMI and CVI in order to achieve better  
10 microstructures for improved desired properties [294]. C<sub>f</sub>/ZrC-SiC composites were  
11 fabricated via RMI of Si into C<sub>f</sub>/ZrC-C preforms [296]. The protective PyC coating on  
12 the C<sub>f</sub> was generated by CVI, whilst the slurry infiltrated ZrC particles consumed the  
13 molten Si during the RMI process, which resulted in forming ZrSi<sub>2</sub> and SiC products  
14 and a much denser and finer microstructure was obtained, Fig. 22c & d.  
15  
16  
17  
18  
19  
20  
21  
22  
23  
24  
25

26 In summary, as expected, the microstructure obtained depends very strongly on  
27 the process route used to prepare the UHTCMCs and the microstructure, as well as the  
28 composition, directly affects the resultant properties. Hence it is essential to design the  
29 microstructure and then select the best processing route to achieve it if the targeted  
30 properties are to be obtained. To achieve this with UHTCMCs, a combination of two or  
31 more techniques, yielding a hybrid process route, may be the best route forward [249].  
32  
33  
34  
35  
36  
37

## 38 **Mechanical Properties**

39  
40  
41  
42 As a baseline material for UHTCs, the strength, fracture toughness and hardness  
43 of ZrB<sub>2</sub>-SiC particle reinforced composites (ZS<sub>p</sub>) have been the most investigated [33].  
44 Results have shown that the fracture strength of ZS<sub>p</sub> at room temperature has more  
45 relied on the grain size of the SiC rather than that of the ZrB<sub>2</sub>; when the SiC particle  
46 size increased in ZrB<sub>2</sub>-SiC systems, both the strength and toughness of the ceramics  
47 decreased accordingly [298]. The high temperature strength of UHTCs has been found  
48 to be related to the grain boundary phase; the softening of these phases causes the  
49 strength degradation at elevated temperatures [188], [299]–[302]. By removing the  
50 oxide impurities via adding WC in ZrB<sub>2</sub>-SiC, strong ZrB<sub>2</sub>-SiC-WC ceramics without  
51 strength degradation up to 2000°C have been successfully developed [303]–[305]. The  
52  
53  
54  
55  
56  
57  
58  
59  
60  
61  
62  
63  
64  
65



1  
2  
3  
4  
5  
6  
7  
8  
9  
10  
11  
12  
13  
14  
15  
16  
17  
18  
19  
20  
21  
22  
23  
24  
25  
26  
27  
28  
29  
30  
31  
32  
33  
34  
35  
36  
37  
38  
39  
40  
41  
42  
43  
44  
45  
46  
47  
48  
49  
50  
51  
52  
53  
54  
55  
56  
57  
58  
59  
60  
61  
62  
63  
64  
65

mechanical properties of monolithic and particulate reinforced UHTCs have been well reviewed; interested readers can find more information from [33]. This chapter will therefore focus mainly on the mechanical properties of UHTCMCs.

The flexural strength and elastic modulus of selected UHTCMCs are compared in Table 10 [179], [192], [227], [279], [281], [294]–[296], [306]–[308], together with the open porosity. It can be seen that samples produced using RMI result in lower open porosity, typically <10% [191], [227], [296], [306]. When an additional and subsequent hot-pressing stage was utilised, even lower open porosity, <5%, was observed [281]. The pore / filler size and its distribution in the porous preforms are also very important for reducing the voids in composites, since they are related to the capillary pressure driving force for the melt during RMI. It is worth noting, however, that lower open porosity doesn't always mean higher flexural strength. In fact, the flexural strength values of many UHTCMCs, especially those produced by RMI, are typically less than 200 MPa. Low strengths have also been observed for samples made by hot pressing (HP) stacked 1D or 2D fabrics [279]; detailed investigations showed that defects such as cracks and voids were readily observed in these samples [191], [227], [279], [295], [307]. For both the RMI and HP, the low strengths probably result from the presence of residual stresses, which, in turn, will arise during cooling after densification as a result of CTE mismatch between the matrix, fibre and / or unreacted alloy. Defects are most likely to occur in the dense samples where there is no free space to release the stress, reinforcing the reason why the strengths are typically lower for composites made by RMI and HP compared to materials formed by a combination of PIP and CVI [294]. A detailed discussion about the effects of residual stresses on thermal damage accumulation in  $C_f$  reinforced UHTCs can be found elsewhere [309].

Interestingly,  $C_f/ZrC-SiC$  samples obtained by a modified RMI route (infiltration of Si into nano-porous  $C_f/ZrC-C$  preforms prepared by colloidal processing) show a much higher strength of ~380 MPa [296]. The authors argued that the excellent mechanical performance could be attributed to a denser microstructure, limited Si or C residue, no interphase degradation and some reinforced elements in the matrix. By carefully reducing the volume of large defects, UHTCMCs densified by post-HP have also been shown to exhibit excellent mechanical properties and non-brittle behaviour during flexure up to 1500°C [281].

1 For C<sub>f</sub>-UHTC composites in which densification was achieved using CVI to  
2 deposit a carbon matrix within carbon fibre preforms containing impregnated (and  
3 unsintered) UHTC powder, a comprehensive understanding of the mechanical  
4 performance has been provided by Rubio et al. [179]. Whether under bending,  
5 compression or shear test, C<sub>f</sub> plies with 0° orientation exhibited higher resistance to the  
6 stress than the 90° plies and the random orientation layers. Also, no tensile strength  
7 degradation was found for these composites up to 1000°C.  
8  
9  
10  
11  
12

13 Although the fractural toughness is important for monolithic ceramics, its value  
14 hasn't been reported for UHTCMCs very often, especially for composites not densified  
15 by sintering. It should be noted that K<sub>IC</sub> refers to the critical value of the Mode I stress  
16 intensity factor that is measured when the plane strain condition is satisfied at the crack  
17 tip [310]. However, due to the different fibre arrangements, the existence of interfaces  
18 and the fracture of the fibre & matrix, different fracture modes for cracks, including but  
19 not limited to mode I, mixed I / II and mode II, might coexist during a fracture  
20 toughness test [311], [312]. Therefore, in UHTCMCs, the definition of K<sub>IC</sub> has  
21 generally not been strictly followed, nevertheless, the limited results available show that  
22 the incorporations of continuous fibres into UHTCs do significantly improves K<sub>IC</sub>. For  
23 example, the fracture toughness (determined by the chevron notched beam method) for  
24 2D-C<sub>f</sub>/ZrB<sub>2</sub> – SiC – Si<sub>3</sub>N<sub>4</sub> fabricated by slurry infiltration and hot-pressing reached 9.6  
25 ± 0.7 MPa m<sup>1/2</sup> [281], a much higher value than that for ZrB<sub>2</sub>-SiC ceramics hot-pressed  
26 under similar conditions (3 – 5 MPa m<sup>1/2</sup>) [313], [314]. Even the K<sub>IC</sub> of 1D-C<sub>f</sub>/ZrB<sub>2</sub> –  
27 SiC composites [288] varied from 4.75 to 8.35 MPa m<sup>1/2</sup>. The load-displacement curves  
28 of all the samples during the toughness measurements displayed quasi-brittle fracture  
29 behaviour and significant fibre bundle pull-out, whilst individual fibre pull-out was  
30 observed for samples with a higher K<sub>IC</sub> and weaker fibre / matrix interface. This work,  
31 however, is mainly focused on toughness arising from crack initiation resistance, which  
32 can be regarded as rather simplistic. Compared to the particulate reinforced composites,  
33 fibre reinforced composites are expected to exhibit significant extrinsic toughening  
34 resulting from the pull-out of fibre with the crack propagation. Hence, initiation  
35 toughness may not be very useful as a design parameter. Unfortunately, the crack  
36 resistance curve, or R curve (material resistance as a function of crack extension [315],  
37 hasn't been well explored in the field of UHTCMCs. Limited results from fibre-glass  
38 composites [316] show that the crack resistance is dominated by frictional dissipation  
39  
40  
41  
42  
43  
44  
45  
46  
47  
48  
49  
50  
51  
52  
53  
54  
55  
56  
57  
58  
59  
60  
61  
62  
63  
64  
65

upon the pull-out of fibres, which fracture in the wake of the crack plane. Even when the initial toughness was at a similar level, a significant increase in crack resistance was observed in the composite when fibre pull-out was extensive. This suggests that, as for other composites, both the crack initiation and crack propagation resistance of UHTCMCs can be further improved by optimising the interface between the fibre and the matrix. A thorough analysis of the crack resistance curve for UHTCMCs is necessary to develop the understanding of their fracture toughness.

According to the above discussion, it is clear that controlling the fibre pull-out in a fibre-reinforced material is crucial to maximizing their mechanical performance. The latter occurs when crack deflection along a fibre/matrix interface becomes easier than its penetration through the fibre. He & Hutchison [317], [318] found that this competition was reliant on the ratio of the fracture energy of the interface ( $G_c^i$ ) and the fibre ( $G_c$ ), as illustrated in Fig. 23 [124]. The Dundurs' parameter ( $\alpha$ ) in the x - axis could be calculated based on the plane strain modulus for the fibre and matrix, according to Eq. (3-5).

$$\alpha = \frac{\overline{E}_f - \overline{E}_m}{\overline{E}_f + \overline{E}_m} \quad (3)$$

$$\overline{E}_f = E_f (1 - \nu_f^2) \quad (4)$$

$$\overline{E}_m = E_m (1 - \nu_m^2) \quad (5)$$

Here, subscripts  $f$  and  $m$  refer to the fibre and the matrix, respectively.  $\overline{E}$  is the plane strain modulus for the phase  $x$ ;  $E_x$  and  $\nu_x$  are the elastic moduli and Poisson's ratio for the fibre and matrix.

According to Fig. 23, when the fibre modulus is significantly larger than that of the matrix, crack deflection along an interface is favourable for a wide range of  $G_c^i/G_c$  values and so the relative strength of the interface is not critical. Porous UHTCMCs can be classified in this way, since the modulus of the porous matrix (porosity up to about 50 – 60 vol%) is likely to be lower than that of the carbon fibre. However, if the modulus of the fibre is similar to or smaller than that of the matrix, the ratio  $G_c^i/G_c$  must

1  
2  
3  
4  
5  
6  
7  
8  
9  
10  
11  
12  
13  
14  
15  
16  
17  
18  
19  
20  
21  
22  
23  
24  
25  
26  
27  
28  
29  
30  
31  
32  
33  
34  
35  
36  
37  
38  
39  
40  
41  
42  
43  
44  
45  
46  
47  
48  
49  
50  
51  
52  
53  
54  
55  
56  
57  
58  
59  
60  
61  
62  
63  
64  
65

be small enough (on the order of 0.25-0.5) in order to facilitate fibre pull-out [124]. Pressure-sintered UHTCMCs and composites densified by RMI usually have a denser matrix and hence a higher modulus (e.g., the modulus of TORAYCA® T700 C<sub>f</sub> and dense ZrB<sub>2</sub>-SiC ceramics are 230 and ~450 GPa, respectively) and thus belong to this category. Therefore, a weak interface must be created between the fibre and matrix to reduce the G<sub>ic</sub>, this is usually achieved using either amorphous carbon or *h*-BN [124]. Such an interface engineering strategy has been well developed for the processing of CMCs [124] and has recently also been applied in the field of UHTCMCs. Silvestroni *et al.* [319] found using Si doped BN-coatings on Hi-Nicalon fibres within 25 vol% continuous SiC<sub>f</sub> reinforced 65 vol% ZrB<sub>2</sub>- 10 vol% ZrSi<sub>2</sub> composites results in a much higher inelastic work of fracture (108 ±21 J/m<sup>2</sup>) compared to their counterparts without the coating (30±8 J/m<sup>2</sup>). Hu *et al.* [320] also found that C<sub>f</sub>/ZrC-SiC composites with a PyC coating on the C<sub>f</sub> exhibited a much higher work of fracture and fracture toughness at room temperature compared to the same composites without the coating although the existence of such a soft interphase slightly lowered the fracture strength of the composite [319], [320]. In addition, it is essential to avoid any possible reactions between the fibre and matrix during post-processing and the service of the composites since this can undo any benefits gained by controlling the fibre / matrix interface strength. In both of Silvestroni's [319] and Hu's [320] work, the interfaces, either in the form of BN or PyC, were found to effectively hinder the fibre degradation during processing by reducing the reactions between the fibre and the matrix.

Residual stresses and their distribution within the composite can also affect fibre pull-out and the degree of toughening achieved. Residual stresses can accumulate in any ceramic matrix composites during cooling from the processing temperature as a result of the thermal expansion mismatch between the fibres and the matrix. In pressure-sintered UHTCMCs that have achieved high density, residual stresses can occur both in the direction normal and parallel to the fibre. In order to facilitate the pull-out of the fibre, tensile stresses in the radial direction should exist at the fibre-matrix interface; such condition can be met when the thermal contraction of the fibers is higher than that of the matrix. Unfortunately, C<sub>f</sub> has a negative coefficient of longitudinal thermal expansion. Its axial CTE values depend on the modulus, e.g. CTE values of carbon fibre with moduli of 200-300 GPa and 700-900 GPa are 0.4-0.8×10<sup>-6</sup>/°C and 1.6×10<sup>-6</sup>/°C, respectively [321]. Such values are much smaller than those for the UHTC matrix, e.g.

1  
2  
3  
4  
5  
6  
7  
8  
9  
10  
11  
12  
13  
14  
15  
16  
17  
18  
19  
20  
21  
22  
23  
24  
25  
26  
27  
28  
29  
30  
31  
32  
33  
34  
35  
36  
37  
38  
39  
40  
41  
42  
43  
44  
45  
46  
47  
48  
49  
50  
51  
52  
53  
54  
55  
56  
57  
58  
59  
60  
61  
62  
63  
64  
65

$6.8 \times 10^{-6}/^{\circ}\text{C}$  for  $\text{ZrB}_2$  [322]. Therefore, an interface layer must be coated onto the fibres to alter the compressive radial stresses developed in them.

Understanding the mechanical properties of UHTCMCs at elevated temperatures is essential for understanding their performance in the service environment. Although very limited results have been reported to date, some have been very encouraging [281], [323]. For example, Zoli et al. [281] found the flexural strength of  $\text{C}_f/\text{ZrB}_2\text{-SiC-Si}_3\text{N}_4$  increased from 360 MPa at RT to 550 MPa at 1500°C, this composite also exhibited excellent thermal shock resistance. Very recently, Ding et al. [323] reported that the interphase between fibre and matrix played an important role on the high temperature strength of  $\text{C}_f/\text{SiBCN}$ . A SiC / PyC coating on the fibre effectively avoided the degradation of the interphase and enhanced the load transfer between the fibre and matrix, therefore the strength of  $\text{C}_f/\text{Si-B-C-N}$  was maintained to 1600°C. The importance of interphase on the mechanical properties of UHTCMCs has also been highlighted elsewhere [294].

The long-time-service properties of materials subjected to cyclic (fatigue) and constant (creep) loading are critical for certain applications of CMCs, for example  $\text{SiC}_f/\text{SiC}$  composites [324], though no results have been found to date for UHTCMCs. The reason for the latter may be because much of the focus of the present work is on applications that only need short service lives, typically seconds to a few minutes [18], [183], [325]. As applications are considered that require much longer service lives, it is likely that more attention will be given to these properties. It is assumed that, as for other CMCs, these properties are likely to be highly reliant on the performance of the fibre, the crack initiation resistance of the matrix and the sliding resistance between the fibre and the matrix [33].

### **Thermal and electrical properties**

Properties such as thermal conductivity, specific heat capacity ( $C_p$ ), coefficient of thermal expansion (CTE) and electrical conductivity are important for many high temperature applications and these can be significantly influenced by the presence of second phases. In addition, continuous fibre reinforced composites often exhibit anisotropy, especially in their thermal conductivity and CTE, and the thermal and electrical properties can be significantly affected by the level of residual porosity

1 present. Thus, for many applications where the thermal and electrical properties are  
2 critical, the chemical composition, fibre preform structure and the densification route of  
3 the UHTCMCs will all need to be strictly controlled. Details on a range of properties  
4 are given in Table 11 [38], [58], [98], [116], [118], [205], [210], [221], [322], [326]–  
5 [343].  
6  
7  
8  
9

#### 10 Coefficient of Thermal Expansion (CTE)

11  
12 In general, UHTCs and UHTCMCs are need to have a small coefficient of thermal  
13 expansion (CTE) because a large value can cause instability on the local surface at high  
14 temperature as a result of an imbalance in internal thermal stresses. Comparing the data  
15 in Table 11, the CTE of each UHTC fluctuates near  $7 \times 10^{-6} \text{ K}^{-1}$ , the variation with  
16 temperature being relatively small and the difference between transition metal carbides  
17 and borides not very large. From the energy point of view, generally stronger bonds  
18 between atoms can result in lower CTE. The CTE of the monolithic UHTCs can be  
19 affected by the presence of doped second phases such as  $\text{MoSi}_2$ ,  $\text{TaSi}_2$ ,  $\text{ZrSi}_2$  and  $\text{SiC}$ .  
20 Pienti et al. [98], [333] found that doping with  $\text{SiC}$  significantly reduced the CTE of  
21  $\text{HfC}$  and  $\text{TaC}$  because of the lower CTE of  $\text{SiC}$ ; whilst doping with  $\text{TaSi}_2$  or  $\text{MoSi}_2$   
22 caused only a minor change in value. It was also observed that residual porosity  
23 increased the CTE, so achieving a denser UHTC reduced the CTE. Zimmermann et al.  
24 [322] also reported that the addition of 30 vol%  $\text{SiC}$  to  $\text{ZrB}_2$  resulted in a decrease in  
25 CTE, however only at higher temperatures (1300 – 1675 K), whilst at lower  
26 temperatures (300 – 1300 K) this effect was not observed.  
27  
28  
29  
30  
31  
32  
33  
34  
35  
36  
37  
38  
39  
40  
41

42 The CTE of UHTCMCs is significantly lower than that for the corresponding  
43 UHTCs due to the much lower CTE of the carbon fibres ( $C_f$ ), Table 11. The presence of  
44  $C_f$  can also cause anisotropy; Paul et al. [183] showed that in the plane of the  $C_f$ , the  
45 CTE reflects the value for  $C_f$  whilst perpendicular to the  $C_f$  the CTE depends more on  
46 the matrix and the presence of porosity and cracks. The large difference in CTE  
47 between carbon fibre and UHTC matrix can also yield residual stresses, as discussed in  
48 the mechanical properties section above.  
49  
50  
51  
52  
53  
54  
55

#### 56 Thermal Conductivity ( $k_{\text{TH}}$ )

1  
2  
3  
4  
5  
6  
7  
8  
9  
10  
11  
12  
13  
14  
15  
16  
17  
18  
19  
20  
21  
22  
23  
24  
25  
26  
27  
28  
29  
30  
31  
32  
33  
34  
35  
36  
37  
38  
39  
40  
41  
42  
43  
44  
45  
46  
47  
48  
49  
50  
51  
52  
53  
54  
55  
56  
57  
58  
59  
60  
61  
62  
63  
64  
65

At present, obtaining values for the thermal conductivity of UHTCs or UHTCMCs mainly relies on experimental determination since there is no theoretical equation with sufficient accuracy. It can be seen from Table 11 that the  $K_{TH}$  of the borides is higher than that of the carbides, this is due to the lower atomic weight yielding a higher Debye temperature. However, the  $K_{TH}$  of the two types of UHTC are inversely related to the temperature; increasing temperature causes the  $K_{TH}$  of borides to decrease whilst that of carbides increases. Like CTE, the  $K_{TH}$  of the materials can be modified by addition of second phases. For example, Guo et al. [339] indicated that introducing  $MoSi_2$  into  $ZrB_2$  leads to a decrease in  $K_{TH}$ , whilst 5-30 vol% SiC increases  $K_{TH}$ , a result also found by Mallik et al. [334], [344].

A range of reports [333], [340], [343], [345], [346] have indicated that the presence of defects, such as porosity, can significantly reduce  $K_{TH}$ . This is partly because the  $K_{TH}$  of gases is close to zero and partly due to phonon scattering, thus denser materials, as expected, have higher  $K_{TH}$  values.

### Specific Heat Capacity ( $C_p$ )

It is well known that the specific heat capacity ( $C_p$ ) is one of the basic properties of matter, depending on the composition of the material. Since carbon atoms are larger and heavier than boron atoms, the  $C_p$  of borides is larger than for the corresponding carbides at the same temperature. Addition of second phases with higher  $C_p$  values also therefore increases the  $C_p$  for UHTCs and UHTCMCs. For example, both Guo et al. [339] and Tian et al. [346] showed that introducing SiC raises the  $C_p$  of UHTCs.

### **Electrical conductivity**

Carbon fibres are considered to be a medium electrical conductor with electrical conductivities in the order of  $10^{-3} \Omega \text{ cm}$  [347] and many studies have focused on improving the electrical properties of composite materials; however, this is currently not a major research direction for UHTCMCs. Temperature and doping level are two parameters that can significantly affect the electrical properties of the materials. For UHTCs and UHTCMCs, the most effective way to increase electrical conductivity is doping and literature values are given in Table 12 [339], [348]–[350]. Guo et al. [339] studied the introduction of different proportions of  $MoSi_2$  and SiC into  $ZrB_2$  and found

1 that the electrical conductivity decreased with an increase in MoSi<sub>2</sub> or SiC content,  
2 which was due to the lower intrinsic electrical conductivities of the dopants. Similar  
3 studies by Mallik et al. [334] and Zhang et al. [348] on ZrB<sub>2</sub>-SiC and HfB<sub>2</sub>-SiC also  
4 reported that the resistivity of composites increased with increasing volume content of  
5 SiC across the range 5 – 40 vol%.  
6  
7  
8  
9

10 From a structural point of view, a denser and less defective material can achieve  
11 higher electrical conductivity since defects such as porosity, cracks and interfaces all  
12 reduce the conduction path, a result confirmed by Guo. et al. [328]. The electrical  
13 conductivity of UHTCMCs is also likely to be anisotropic due to the use of C<sub>f</sub>; the  
14 conductivity is higher in the plane of the C<sub>f</sub> tows for 2D and 2.5D-based composites.  
15  
16  
17  
18  
19

## 20 **Emissivity**

21  
22

23 The modification of the emissivity of the material is a method for actively  
24 increasing the heat transfer rate of the surface of the material. Current doping studies for  
25 UHTCs focus on two major directions, one of them is the use of rare earth doping [351],  
26 [352] whilst the other branch involves using transition metal silicides [353]–[356]. The  
27 work to date, however, has only focused on the modification of UHTCs rather than  
28 UHTCMCs. Nevertheless, the same principles will apply and hence there is the  
29 possibility to change the overall emissivity of the composites by changing the ceramic  
30 phase composition or using a high emissivity coating [353].  
31  
32  
33  
34  
35  
36  
37  
38

39 For UHTCs, Tan et al. [351], [352] have indicated that samarium doping can  
40 increase the emissivity of ZrB<sub>2</sub> – 20 vol% SiC, although the trend varied with  
41 temperature. Doping with 5 mol% Sm(NO<sub>3</sub>)<sub>3</sub> yielded the highest emissivity ( $\epsilon=0.91$ )  
42 though the results should be treated with caution since they were obtained from UHTCs  
43 subject to oxidation and ablation and hence a change of surface topography. Balat-  
44 Pichelin et al. [353] pointed out that doping with 5% Si<sub>3</sub>N<sub>4</sub> can be beneficial to  
45 increasing the emissivity of the base material ZrB<sub>2</sub> – 15% SiC<sub>f</sub> and the emissivity  
46 increased with temperature (~0.75 at 1200 K and ~0.90 at 1750 K). Du et al.'s [354]  
47 research on TaSi<sub>2</sub>-based and MoSi<sub>2</sub>-based coatings showed that increasing material  
48 density is beneficial with respect to increasing the emissivity and that it is necessary to  
49 prevent the oxidation of the coating to maintain the emissivity. Shao et al. [356] had  
50 similar results from research on WSi<sub>2</sub> – MoSi<sub>2</sub> – Si – SiB<sub>6</sub>-borosilicate glass coatings.  
51  
52  
53  
54  
55  
56  
57  
58  
59  
60  
61



## Ablation and Oxidation

### Testing methods and ablation

Table 13 [18], [109], [181], [182], [187], [197], [198], [207], [209], [210], [222], [227], [229], [357]–[371] summarises the methods used for testing UHTCs and their composites under conditions simulating launch and re-entry environments to different degrees. Typical re-entry conditions can include: heat flux enthalpies of  $20 \text{ MJ kg}^{-1}$ , speeds of Mach 7 to 9, mass flow rates of  $75 \text{ g s}^{-1}$  [45], combined with plasmonic and dissociating environments. The goal is to understand the underpinning thermal ablation mechanisms so that improved materials can be developed. Different test methods include: laser ablation methods [372], [373], arc jet [45], [374], [375], scramjet [376], high velocity oxyflame (HVOF) [109] and oxyacetylene torch (OAT) testing [17]. Amongst the test methods, HVOF and OAT are the relatively cost-effective screening techniques, whilst the others are costlier and available only in a few select locations in a handful of countries. It is extremely difficult to simulate the exact re-entry / hypersonic conditions at ground level, in a single method. Scramjet and arc jet methods are the closest to real use, but are extremely expensive tests to run. Oxyacetylene (OAT) and oxypropane (OPT) testing can reach similar temperatures and heat fluxes but the gas velocities are an order of magnitude too slow. They do form fast, cheap test methods though, that can be used for initial screening.

Laser ablation testing has been used to evaluate the ablation resistance of UHTCs in rapid tests that vaporise the UHTCs in a controlled atmosphere. The approach uses both continuous [372] and pulsed lasers [227] as a heat source and is able to test the materials at extreme heat fluxes of around  $100 \text{ MW m}^{-2}$  [377], enabling temperatures of about  $3200^\circ\text{C}$  to be achieved very rapidly. Whilst laser ablation can create extreme heat fluxes, the gas chemistries and high flow velocities of real applications are much more difficult to add in during testing, which is a significant disadvantage.

In HVOF testing, whilst the flame can reach supersonic velocities, e.g. Mach 2.5, which can induce useful mechanical stresses [109], the gas composition and heat fluxes do not approach those of real applications; e.g. a heat flux of only  $2.5 \text{ MW m}^{-2}$  was achieved. The required large sample dimensions are also a limiting factor.

1 Free-jet facilities have been used for high temperature testing in a sublimation  
2 regime [378]. It is an integrated testing system comprised of a hypersonic wind tunnel  
3 and arc / plasma heater [379] and is primarily designed to evaluate gas intake and  
4 engine performance in a supersonic / hypersonic flow. In this method, a conical nozzle  
5 is used to expand the preheated gas from where it is passed into a test section where the  
6 samples are mounted tangentially. The surface temperatures are measured using  
7 pyrometers; a stagnation temperature of 2400°C has been measured [380] and a heat  
8 flux of 4 – 6 MW m<sup>-2</sup> achieved [381]. The main disadvantage is the requirement of  
9 large, and expensive, test facility.  
10

11  
12  
13  
14  
15  
16  
17 Similar to the free-jet method, the arc jet and scram jet tests are the best ground-  
18 based techniques, both of which simulate re-entry conditions reasonably well. The  
19 scram jet reproduces aerothermal conditions similar to actual flight, however, the gas  
20 chemistries are different from the atmosphere, since the temperature is not enough for  
21 the dissociation of gases to occur. It uses natural gases as the source in a combustion  
22 heater and the supersonic nozzle accelerates the test gas to a maximum speed of Mach  
23 7. It provides opportunities to test both oxidation behaviour and the thermal stresses  
24 under extreme conditions, reaching test velocities of Mach 5 – 7 at heat fluxes of up to  
25 12 MW m<sup>-2</sup>. Arc jet testing simulates the most aggressive conditions to study the  
26 response of materials suitable for thermal protection systems, it also accounts for high  
27 fluid velocities and catalytic recombination effects [376]. It uses a plasma torch of  
28 typically 20 – 80 kW with inert gases (N<sub>2</sub> and Ar); the atmospheric air composition is  
29 simulated by adding O<sub>2</sub> into the test chamber. When the stream of plasma containing  
30 N<sub>2</sub>/Ar enters the chamber at Mach 3, with an enthalpy of 20 MJ kg<sup>-1</sup>, it reacts with O<sub>2</sub> to  
31 form disassociated mixtures of NO, N<sub>2</sub> and O at a low pressure of between 100 – 500  
32 Pa. This allows the test samples to experience something close to the re-entry conditions  
33 of around 2000°C with a heat flux of 16 MW m<sup>-2</sup>. However, the facilities are very  
34 expensive and not widely available.  
35  
36  
37  
38  
39  
40  
41  
42  
43  
44  
45  
46  
47  
48  
49

50  
51 OAT and OPT testing has therefore been developed, to determine the oxidation  
52 and erosion behaviour of UHTC materials. OAT testing can reach temperatures up to  
53 3000°C and heat fluxes up to 17 MW m<sup>-2</sup> [187], whilst the equivalent figures for the  
54 OPT test are 2500°C and 6 MW m<sup>-2</sup> [187]. Interestingly, the gas velocity for both  
55 systems, which has been directly measured [382], were very similar at Mach ~0.6. The  
56  
57  
58  
59  
60  
61  
62  
63  
64  
65

1 flames involved can also be manipulated by varying the gas chemistry to be either  
2 oxidising, reducing or neutral and the distance between the flame and the sample and  
3 the angle the flame makes on contact with the sample can all be varied. As indicated,  
4 the disadvantages of this method are the absence of a plasma environment and  
5 hypersonic flow velocities, but measurements can be done very rapidly and at very low  
6 cost.  
7  
8  
9

## 10 **Oxidation**

11  
12  
13  
14  
15 Most ultra-high temperature applications also involve exposure to oxidizing and  
16 corrosive environments, which demands resistance to oxidation, ablation and corrosion  
17 [53], [383]. The oxidation behaviour of non-oxide ceramics depends highly on the  
18 properties of the oxidation product and on the combination of physical and chemical  
19 processes taking place on the surface exposed to the oxygen containing atmosphere. In  
20 general, the chemical composition, structure and texture of an oxidized surface define  
21 the oxidation stability of a ceramic material [1]. However, the rapid oxidation of borides  
22 and carbides at  $\sim 600^\circ\text{C}$  results in the formation of  $\text{B}_2\text{O}_3$ , which evaporates at  $\sim 1000^\circ\text{C}$ ,  
23 or  $\text{CO}/\text{CO}_2$  [11], [53], [316]. It is reported that  $\text{ZrB}_2$  is more protective compared to  $\text{ZrC}$   
24 with respect to oxidation at up to  $1200^\circ\text{C}$  due to the formation of  $\text{ZrO}_2$  containing a  
25 molten layer of boron oxide, whereas only porous  $\text{ZrO}_2$  forms for  $\text{ZrC}$ , which is not  
26 protective to further ingress of oxygen [42]. A history of studies on the oxidation of  
27 diborides has been presented by Opeka et al. and others [30].  
28  
29  
30  
31  
32  
33  
34  
35  
36  
37  
38  
39

40 Over the past decade, researchers across the globe have investigated the  
41 oxidation behaviour of UHTCs ( $\text{ZrB}_2$ ,  $\text{HfB}_2$ ,  $\text{ZrC}$ ,  $\text{HfC}$ , etc.) [22], [77], [386]–[390].  
42 Modification of the chemical composition of the oxide surface layer, leading to  
43 decreased inward diffusion of oxygen, is one of the ways of controlling oxidation  
44 resistance of non-oxide ceramics. This modification can be accomplished by changing  
45 the bulk composition, or applying suitable coatings [1].  
46  
47  
48  
49  
50  
51

52 The poor oxidation resistance of  $\text{ZrC}$  is considered as a great restriction in  
53 applications at high temperatures in the presence of oxygen. Numerous studies [391]–  
54 [396] have been reported on the oxidation behaviour of  $\text{ZrC}$  and  $\text{HfC}$  with respect to the  
55 effect of temperature, time, oxygen partial pressures and sintering aids (type and its  
56 quantity). In general, the oxidation of  $\text{ZrC}$  is diffusion controlled as for other UHTCs  
57  
58  
59  
60  
61  
62  
63  
64  
65

1 and oxidation appears preferentially along grain boundaries in sintered compounds  
2 [395]. It has been reported that the starting temperature of oxidation should be at 300°C  
3 for stoichiometric or nearly stoichiometric ZrC, independent of oxygen pressures [392].  
4 Before the formation of zirconia, a thin intermediate layer of oxycarbide is believed to  
5 form owing to oxygen diffusion [391], [397]. At elevated temperatures, the crystalline  
6 oxycarbide layer can become amorphous, from which the cubic / tetragonal zirconia  
7 nanocrystals will subsequently form. The cubic ZrO-like oxide was also reported to  
8 form after low-temperature oxidation, as confirmed by measurements involving  
9 photoelectron spectroscopy [396], [398]. It is known that additions of higher valence  
10 metals into the ZrO<sub>2</sub> lattice will reduce oxygen vacancy concentration and diffusion,  
11 which reduce oxygen transport through the skeleton phase and so this may improve the  
12 oxidation / ablation resistance as well [1].  
13  
14  
15  
16  
17  
18  
19  
20  
21  
22

23 Relatively little research has been undertaken into the oxidation performance of  
24 UHTCMCs compared to UHTCs, mainly because UHTCMCs are still relatively new  
25 materials. There has been some work on the oxidation / thermoablation behaviour of  
26 UHTCMCs [254] and one of the primary goals has been to protect the fibres, and hence  
27 the fibre / matrix interfaces, from the oxidative environment since fracture toughness is  
28 one of the main properties of UHTCMCs. Fibre interface coatings can serve as reaction  
29 and diffusion barriers in aggressive operating conditions, protecting the underlying  
30 fibres from the oxidation [123], [399]. It is critically important that all the fibres are  
31 uniformly coated since poorly or uncoated fibres can bond to the matrix, increasing the  
32 fibre / matrix interface strength and hence reducing the likelihood of the crack deviating  
33 along the interface as discussed earlier. Oxidation of the fibre surfaces will also degrade  
34 the fibre properties leading to losses in fibre and hence composite strength [399].  
35  
36  
37  
38  
39  
40  
41  
42  
43  
44

45 A multi-layer SiC – Si – ZrB<sub>2</sub> coating, deposited by pack cementation on C/C  
46 composites [273], was reported to offer excellent oxidation resistance at 1500°C for  
47 more than 386 h due to the formation of an integrated layer of SiO<sub>2</sub>-ZrSiO<sub>4</sub>. The  
48 retention of 84% of the flexural strength after 20 thermal shocks between 1500°C and  
49 room temperature was also reported. A SiC nanowire – SiC – Si/SiC – ZrB<sub>2</sub> – ZrC  
50 coating was also deposited on C/C composites by a combination process of pack  
51 cementation and EPD [262] with a view to improving the oxidation resistance.  
52 Compared to a SiC – ZrB<sub>2</sub> – ZrC coating without nanowires, the EPD-SiC nanowire-  
53  
54  
55  
56  
57  
58  
59  
60  
61  
62

1 toughened coating showed a remarkably improved resistance for oxidation and thermal  
2 shock, which was ascribed to the smaller size of cracks that were formed. It was  
3 believed that the latter occurred by the nanowires helping to alleviate the thermal  
4 stresses developed and increasing the coating toughness [262]. A combination of ZrB<sub>2</sub>  
5 or HfB<sub>2</sub> and SiC coated by CVD onto C/C composites exhibited protection against  
6 oxidation, even in wet air [266].  
7  
8  
9

10  
11 Since the role of the second phase on oxidation behaviour remains  
12 fundamentally the same irrespective of whether the material is a UHTC or a UHTCMC,  
13 the majority of the discussion below is based on reports of the oxidation behaviour of  
14 UHTCs.  
15  
16  
17  
18  
19

20 The addition of silica formers or rare earth elements, notably silicides, SiC,  
21 Si<sub>3</sub>N<sub>4</sub>, Ti<sub>3</sub>SiC<sub>2</sub>, Y, La, Eu, Ce and Yb, can reduce the oxidation rate through the  
22 formation of a more stable borosilicate glass / rare earth (RE) oxides up to ~1600°C (for  
23 Si formers) and >2000°C (for RE oxides) [67], [210], [221], [292], [300], [301], [314],  
24 [316]–[318], [323]–[331]. Several groups have studied the effects of SiC additions on  
25 the behaviour of Zr and Hf diborides or carbides when exposed to air at elevated  
26 temperatures [325], [389], [390], [400]–[403]. The isothermal oxidised surface of the  
27 ZrB<sub>2</sub>-SiC-ZrC ceramic was oxidized to a white ZrO<sub>2</sub> phase, which was partially covered  
28 with a thin SiO<sub>2</sub>-rich layer at 1600 ± 15°C in 2 min. The thickness of the oxide layer  
29 increased as the oxidation time increased to 40 min, with an accompanying increase of  
30 the quantity of pores in the oxide layer [404]. Shaffer [405] and Pastor and Meyer [406]  
31 evaluated the oxidation resistance of ZrB<sub>2</sub> with additions of the silicides of Ta, Nb, W,  
32 Cr, Mo, Zr, Mo<sub>0.5</sub>Ta<sub>0.5</sub> and Mo<sub>0.8</sub>Ta<sub>0.2</sub>. Oxidation experiments with varying proportions  
33 of MoSi<sub>2</sub> (1 to 20 mol%) were studied at 1950°C and the reported optimum composition  
34 was 10 mol% for ZrB<sub>2</sub>. The ZrB<sub>2</sub> + 10 mol% MoSi<sub>2</sub> composition was marketed by the  
35 company Carborundum, USA, under the Trade name “Boride Z” [1], [405]. ZrB<sub>2</sub> + 15  
36 wt% CrSi<sub>2</sub> composition was reported to be the most oxidation resistant by Pastor and  
37 Meyer [406]. The flexural strength of the ZrB<sub>2</sub>-SiC-ZrC **ceramics** oxidised specimens at  
38 1400°C for 30 min were measured as 660 MPa, which is higher than that of the room  
39 temperature value of 580 MPa [407]. The formation of the oxide layers resulted in: (i)  
40 healing of the surface flaws, (ii) an increase in flexural strength, (iii) the formation of a  
41 compressive stress zone beneath the surface oxide layers, (iv) a decrease in thermal  
42  
43  
44  
45  
46  
47  
48  
49  
50  
51  
52  
53  
54  
55  
56  
57  
58  
59  
60  
61  
62  
63  
64  
65

1 stress and (v) the consumption of thermal stress. These five aspects improved the  
2 thermal shock resistance of ZrB<sub>2</sub>-SiC-ZrC ceramics. Thus the thin oxide layer formed  
3 acted as a passivation layer and prevented further oxidation, also healing defects and  
4 flaws [407].  
5  
6

7  
8 One of the key findings based on Zr and Hf borides and carbides with Si-based  
9 additives up to temperatures of 1500°C are the formation of different grades of oxide  
10 layer, including: (1) a SiO<sub>2</sub>-rich glassy layer on the surface (top layer), (2) a thin  
11 Zr/HfO<sub>2</sub>-SiO<sub>2</sub> layer (intermediate layer) and (3) a Si-depleted matrix phase (beneath the  
12 above layer) and (4) the unaffected matrix phase [390], [401], [403], [404], [408]–[413].  
13 The oxidation behaviour of TaC- and HfC-based composites was investigated with the  
14 addition of 15 vol% short SiC Tyranno SA3 fibres [98]. Several oxidation studies have  
15 been reported on continuous / chopped carbon / SiC fibre-reinforced UHTC composites  
16 with the additions of Si-based additives such as SiC, silicides [221], [274], [278], [279],  
17 [283], [414]–[426]. The oxidation behaviour of continuous carbon fibre reinforced  
18 ZrB<sub>2</sub>-SiC ceramic composites was reported to reveal that above 15 vol% SiC content  
19 was required to form an homogeneous protective borosilicate glass that covered the  
20 entire sample and minimized fibre burnout [427]. A dense UHTC matrix ZrB<sub>2</sub>  
21 accompanied by a relatively strong C<sub>f</sub> interface and SiC was reported to provide good  
22 oxidation protection [283]. The presence of 8 mol% W in ZrB<sub>2</sub> formed a WO<sub>3</sub> / B<sub>2</sub>O<sub>3</sub>  
23 interface oxide layer that enhanced the ZrO<sub>2</sub> oxide scale adhesion to the composite  
24 [428]. Talmy et al. [429] reported that TaB<sub>2</sub> additions to ZrB<sub>2</sub>-20 vol% SiC were more  
25 effective in improving oxidation resistance at temperatures between 1200 and 1400°C  
26 than additions of other group IV–VI transition metal borides, including Cr, Nb, Ti and  
27 V.  
28  
29  
30  
31  
32  
33  
34  
35  
36  
37  
38  
39  
40  
41  
42  
43  
44  
45

46 Similarly, addition of rare earths in the form of its borides (NdB<sub>6</sub>, LaB<sub>6</sub>, EuB<sub>6</sub>)  
47 to ZrB<sub>2</sub> are also reported to improve the oxidation resistance compared to monolithic  
48 ZrB<sub>2</sub> [48], [82]. LaB<sub>6</sub> was also identified as a beneficial additive to ZrB<sub>2</sub>-SiC based on  
49 its ability to act as a modifier for the ZrO<sub>2</sub>, which stabilised the formation of the  
50 tetragonal phase [48], [389]. The oxidation behaviour of directly solidified eutectic  
51 LaB<sub>6</sub>-ZrB<sub>2</sub> in situ composites was studied by Chen et al. [430], who reported the  
52 parabolic rate constant (kp) to be  $9.71 \times 10^{-3} \exp(-31000/RT) \text{ mg}^2 \text{ cm}^{-4} \text{ min}^{-1}$  in the range  
53 912-1094°C. Above 1094°C, rapid oxidation kinetics were observed with formation of  
54  
55  
56  
57  
58  
59  
60  
61  
62  
63  
64  
65

1 enriched  $\text{La}_2\text{O}_3$  and  $\text{B}_2\text{O}_3$  constituent with  $\text{ZrO}_2$  deficiency in the outer scale [431],  
2 [432]. The pyrochlore phases associated with  $\text{ZrO}_2$  and rare earth oxides are also known  
3 to exhibit significantly lower oxygen diffusion than  $\text{ZrO}_2$  [1], [433].  
4  
5

6 It is well known that texture influences the mechanical properties and it is also  
7 reported that texture plays an important role in oxidation resistance. For example, Ni et  
8 al. [434] reported that a textured  $\text{HfB}_2$ -based material exhibited much better oxidation  
9 resistance by forming a rich  $\text{SiO}_2$  glassy layer on the particular-oriented matrix. Similar  
10 observations were not seen in  $\text{ZrB}_2$ - $\text{SiC}$  composites, however [434]. Further work is  
11 required in this area if the underpinning mechanisms are to be understood and hence the  
12 effect of texture elucidated, allowing the design of composite structures to be optimised.  
13  
14  
15  
16  
17  
18  
19

20 The oxidation behaviour of  $\text{HfB}_2$  with the addition of  $\text{SiC}$  and other silicides has  
21 also been reported in the literature [435]–[438]. The oxidation behaviour of  $\text{HfB}_2$ - $\text{TaSi}_2$   
22 is similar to that of diborides with  $\text{MoSi}_2$  additions for temperatures up to  $1900^\circ\text{C}$  [374].  
23 Although additions of  $\text{SiB}_6$  (10 and 20 vol%) to  $\text{HfB}_2$  were found to increase oxidation  
24 resistance, they were no better than  $\text{SiC}$  additions [1]. Oxidation of the modifying  
25 diborides resulted in the formation of the corresponding oxides in the surface  
26 borosilicate glass.  $\text{TaB}_2$ -doped  $\text{HfB}_2$  was synthesized by a boro/carbothermal reduction  
27 reaction, with an initial co-precipitation route to promote mixing [439]. It was believed  
28 that the Ta atom from the dopants substituted for the Hf atom in the  $\text{HfB}_2$  lattice to form  
29 a solid solution of  $(\text{Hf}, \text{Ta})\text{B}_2$ , which played a key role in stabilising the oxidation  
30 products of  $\text{HfB}_2$  in the tetragonal phase. The results of static furnace oxidation testing  
31 at  $1400$ - $1600^\circ\text{C}$  showed that the addition of the Ta dopants inhibited the formation of  
32 monoclinic  $\text{HfB}_2$  and almost fully stabilized the oxide scale of  $\text{HfB}_2$  in the tetragonal  
33 phase. This meant that the volume change due to the tetragonal to monoclinic  $\text{HfO}_2$   
34 phase transformation was avoided, resulting in a denser oxide layer.  
35  
36  
37  
38  
39  
40  
41  
42  
43  
44  
45  
46  
47

48 It is known from the literature that borate and silicate glasses containing  
49 transition / rare earth metal oxides show a strong tendency to phase separate as a result  
50 of immiscibility in the phase diagram [440]. Systems exhibiting such immiscibility are  
51 characterized by steeply rising liquidus temperatures and increased viscosity. As  
52 demonstrated by the Stokes–Einstein relationship [441], the latter decreases the oxygen  
53 diffusion rate through the oxide surface scale, since the diffusivity is inversely  
54 proportional to viscosity. Another potential benefit of increased viscosity, as well as  
55  
56  
57  
58  
59  
60  
61

1 increased liquidus temperature, is the suppression of boron evaporation from the glass  
2 [1]. A survey of oxidation resistance of the diborides of Hf, Zr, Ti, Ta, and Nb from  
3 1200 to 2200°C using inductively heated samples in flowing He-O<sub>2</sub> mixtures, revealed  
4 that HfB<sub>2</sub> was the most oxidation resistant, followed by ZrB<sub>2</sub> [1], [442] and then the  
5 other diborides such as TiB<sub>2</sub>, TaB<sub>2</sub> and NbB<sub>2</sub> [389], [443]. Opila et al. [1] also reported  
6 that the addition of 20 vol% TaSi<sub>2</sub> improved the oxidation behaviour of ZrB<sub>2</sub>-SiC up to  
7 1627°C in air, however, its addition did not show any improvement in the HfB<sub>2</sub>-SiC  
8 system. When WC and WB containing HfB<sub>2</sub>-SiC samples were oxidized at 1600 and  
9 1800°C, the resulting oxide scales were reported to be the same thickness as the base  
10 materials, suggesting that the oxidation resistance was not modified. However, when the  
11 samples were oxidized at 2000°C, a 30% reduction in scale thickness was reported due  
12 to the formation of a more viscous phase-separated glass in the outermost regions of the  
13 scale and a denser inner HfO<sub>2</sub> that restricted oxygen penetration to the sample [436].  
14 Similar observations of improved oxidation resistance with the addition of W-based  
15 compounds were reported for ZrB<sub>2</sub> also by Zhang et.al [428], [444]. In-situ formed SiC  
16 whiskers (SiC<sub>w</sub>) have been shown to improve the oxidation resistance of HfB<sub>2</sub>-based  
17 composites [445], while HfB<sub>2</sub>-SiC-Si / SiC coatings deposited by CVD on C / C  
18 composites improved the oxidation resistance and alleviated the thermal stresses  
19 present. Finally, the use of nitride additives has been shown to lead to rupture of the  
20 oxide scale and loss of protective behaviour at temperatures as low as 1400°C [389],  
21 [410].

22  
23  
24  
25  
26  
27  
28  
29  
30  
31  
32  
33  
34  
35  
36  
37  
38  
39 In summary, the oxidation resistance of UHTCMCs can be significantly  
40 enhanced by compositional design leading to the formation of a surface layer of  
41 immiscible, multicomponent glass. The resulting increased liquidus temperatures and  
42 viscosities, as well as decreased oxygen diffusivities, in the immiscible glasses are  
43 considered responsible for the observed improvement in the oxidation resistance of the  
44 composites. It is beneficial to optimise the type and quantity of glass-forming elements  
45 in the form of additives in the UHTCMCs to obtain superior oxidation & ablation  
46 resistance for ultrahigh temperature applications. Although addition of second phases  
47 may improve the oxidation resistance, there is also a need to optimise the type and  
48 quantity of the second phase in order to optimise and balance the components' inherent  
49 properties (mechanical, physical, thermal) to best suit the end user application.  
50  
51  
52  
53  
54  
55  
56  
57  
58  
59  
60  
61  
62  
63  
64  
65



1  
2  
3  
4  
5  
6  
7  
8  
9  
10  
11  
12  
13  
14  
15  
16  
17  
18  
19  
20  
21  
22  
23  
24  
25  
26  
27  
28  
29  
30  
31  
32  
33  
34  
35  
36  
37  
38  
39  
40  
41  
42  
43  
44  
45  
46  
47  
48  
49  
50  
51  
52  
53  
54  
55  
56  
57  
58  
59  
60  
61  
62  
63  
64  
65

However, there is limited information available on the texture effects of oxidation resistance of UHTCMCs.

## Summary and Outlook

Composites are, in general, a rapidly evolving and growing technical field with a very wide range of applications across the aerospace, defence, energy, medical and transport sectors as a result of their superior mechanical and physical properties. Ultra-high temperature ceramic matrix composites, UHTCMCs, are a new subfield within the wider grouping of CMCs that offer applications in rocket and hypersonic vehicle components, particularly nozzles, leading edges and engine components [2], [17].

Whilst UHTCs have some excellent properties as single phase monolithic components in structural applications, they are severely limited by their low fracture toughness, which makes them highly susceptible to thermal shock, hindering both their short-term and long-term use as external thermal protection systems on leading edges and propulsion systems. This has led to the utilisation of reinforcement, most typically in the form of a continuous fibrous phase. Reinforcing fibres symbiotically operate with the UHTC matrix to increase the toughness of the monolithic phase, whilst they are, in turn, protected by the matrix. Their addition permits the tailoring of the mechanical and thermal properties for use in different end use components via consideration of fibre architecture, fibre type and volume fractions of phases in the composite, in addition to choosing the most suitable processing method to obtain the desired microstructure [13], [183]. Techniques such as chemical vapour infiltration (CVI), reactive melt infiltration (RMI) and precursor infiltration and pyrolysis (PIP) are all being investigated, together with the more conventional slurry impregnation (SIP) followed by sintering, typically involving the pressure-based approaches of hot pressing or spark plasma sintering.

The selection of the matrix phases used is highly dependent upon both the properties desired for a component with respect to its intended operability window, but also on the fabrication techniques at the fabricator's disposal. This latter will set limits on the material quality, maximum density achievable and the process routes possible.

Although particulate second phases can improve the sinterability of UHTCs and enhance fracture toughness by up to around 100% compared to the baseline monolithic,

1 the absolute values of fracture toughness are still only  $\leq 5 \text{ MPa m}^{1/2}$ ; values that are still  
2 very low compared to most structural engineering materials [56], [62]. Researchers have  
3 also explored other types of second phase reinforcement, including carbon nanotubes,  
4 graphene, a range of chopped fibres and whiskers. However, these types of additives  
5 still only improve the toughness to  $\sim 8 \text{ MPa m}^{1/2}$  and failure is still predominantly  
6 catastrophic [99], [111]. Continuous fibre reinforcement using a range of different  
7 fibres, including C, SiC and even UHTC fibres, can improve the fracture toughness and  
8 strength to the point where they begin to meet the structural requirements.  
9

10  
11  
12  
13  
14  
15  
16 Structure-texture and properties are all correlated with each other, hence learning  
17 how to obtain tailored structures and textures is crucial if the required mechanical &  
18 thermal properties are to be achieved. The processing method and process conditions all  
19 play a role and the required control needs to be identified and learnt. Precursor  
20 infiltration and pyrolysis (PIP) [195], [196] and slurry impregnation process (SIP) [255],  
21 [256] are green-forming procedures used to produce continuous fibre-reinforced  
22 ceramic composites. Hot pressing & spark plasma sintering can reduce the processing  
23 times and enable high densities to be achieved. However, the high pressure and  
24 temperature involved are detrimental for the integrity of the reinforcement. Use of  
25 sintering aids reduce the sintering conditions, but they can be responsible of the  
26 formation of brittle phases at the fibre-matrix interface, which, in turn, reduce the  
27 benefits to be gained in terms of the fracture toughness. The reactive melt infiltration  
28 (RMI) process is attractive for fabricating continuous fibre reinforced UHTC  
29 composites without the fibres being too significantly damaged, whilst still being able to  
30 obtain high densities [215], [217]. However, this process also has limitations including  
31 the presence of residual metal phases and liquid metal corrosion of fibres, amongst  
32 others. The use of chemical vapour infiltration (CVI) to deposit UHTC matrices is still  
33 very much a developing processing technique in the densification of UHTCMCs. It is  
34 useful in that it yields reasonably dense, complex-shaped components at low processing  
35 temperatures that do not damage the fibres used for reinforcement [189], [246].  
36  
37 However, it is an intrinsically slow process and therefore the product can be expensive.  
38  
39 Amongst the different variations developed to overcome the limitations, one of the most  
40 promising currently is the use of microwave or radio frequency energy assisted CVI due  
41 to the ability to create an inverse thermal gradient profile, compared to conventional  
42 heating. This greatly reduces the process times, from  $\sim 2000$  hours down to  $< 100$ , whilst  
43  
44  
45  
46  
47  
48  
49  
50  
51  
52  
53  
54  
55  
56  
57  
58  
59  
60  
61  
62  
63  
64  
65

1 retaining all of the advantages of the fundamental CVI process. However, it should be  
2 noted that this process is still limited to the laboratory scale, but further work is ongoing  
3 that will hopefully lead to it being commercialised.  
4

5  
6 The soundness of the fabricated UHTCMCs can be determined by  
7 microstructural characterisation and evaluation of mechanical and thermal properties,  
8 the latter including oxidation & ablation. As indicated, the microstructural features of  
9 the UHTCMCs are highly reliant on the processing method used and hence it is  
10 essential to select the correct process in order to achieve the required microstructure,  
11 which will, in turn, yield the targeted properties of the composites. To achieve this with  
12 UHTCMCs, the possibility of combining of two or more technologies from among CVI,  
13 SIP, RMI, PIP, HP and SPS becomes an interesting concept, allowing the whole process  
14 – microstructure – property relationship to be designed. Furthermore, the advanced  
15 characterization of UHTCMCs, with ability for atomic scale resolution, especially at the  
16 matrix and fibre interface, is also critical to developing an understanding of the  
17 toughening mechanisms in UHTCMCs in depth.  
18  
19  
20  
21  
22  
23  
24  
25  
26  
27  
28

29 The flexural strength values of many UHTCMCs, especially those produced by  
30 RMI and HP, are typically less than 200 MPa [179], [191]. For both the RMI and HP  
31 processes, the low strengths probably result from the presence of residual stresses,  
32 which, in turn, arise during cooling after densification as a result of CTE mismatch  
33 between the matrix, fibre and/or unreacted alloy. UHTCMCs densified by post-HP  
34 exhibit excellent mechanical properties and non-brittle behaviour during flexure up to  
35 1500°C. Although the fractural toughness is important for monolithic ceramics, its  
36 value hasn't been reported for UHTCMCs very often, especially for composites not  
37 densified by sintering. Understanding the mechanical properties of UHTCMCs at  
38 elevated temperatures is essential for understanding their performance in the service  
39 environment. Unfortunately, very limited results have been reported to date.  
40  
41  
42  
43  
44  
45  
46  
47  
48  
49

50 Amongst the thermal ablation methods, arc jet and scram jet testing are the best  
51 ground-based techniques since they simulate actual re-entry conditions the closest. The  
52 oxidation resistance of UHTCMCs can be significantly enhanced by compositional  
53 design leading to the formation of a surface layer of immiscible multicomponent glass.  
54 The resulting increased liquidus temperatures and viscosities, as well as decreased  
55 oxygen diffusivities, in the immiscible glasses are considered responsible for the  
56  
57  
58  
59  
60  
61

1  
2  
3  
4  
5  
6  
7  
8  
9  
10  
11  
12  
13  
14  
15  
16  
17  
18  
19  
20  
21  
22  
23  
24  
25  
26  
27  
28  
29  
30  
31  
32  
33  
34  
35  
36  
37  
38  
39  
40  
41  
42  
43  
44  
45  
46  
47  
48  
49  
50  
51  
52  
53  
54  
55  
56  
57  
58  
59  
60  
61  
62  
63  
64  
65

observed improvement in the oxidation resistance of the composites. It is beneficial to optimise the type and quantity of glass-forming elements in the form of additives in the UHTCMCs to obtain superior oxidation & ablation resistance for ultrahigh temperature applications. Although addition of second phases may improve the oxidation resistance, there is also a need to optimise the type and quantity of the second phase in order to optimise / balance the components inherent properties (mechanical, physical, thermal) to best suit the end user application [206], [357]. Moreover, there is limited information available on the texture effects of oxidation resistance of the UHTCMCs.

As is well known, the development of new materials offers tremendous opportunities for realizing many of the new advanced technologies that are required by mankind to meet our global demands. UHTCMCs will undoubtedly play a useful role in some of these technologies, including aerospace and energy, the latter including solar power, fission and fusion [446], since the factor that they have in common is that they generate fairly extreme environments. Meeting such aggressive requirements will necessitate the design of components with a suitable matrix, fibre reinforcement and interphase coating(s) and the development and exploitation of micro- and macrostructure control with increasing complexity at multiple length scales. The technically and economically successful manufacturing of components from these materials is currently a challenge and therefore provides fertile ground for innovation [446].

The main interest in fibre reinforced ceramic matrix composites in general arises from their non-brittle mechanical behaviour and improved reliability compared to their unreinforced counterparts [123], [124], [245]. However, this non-brittle character is observed only for well-processed materials, i.e. when i) the fibres are not damaged (etched, corroded, degraded, eroded, etc.) during processing [123]; ii) the fibres are weakly bonded to the matrix as a result of interfacial engineering by adopting techniques as shown in Fig. 6; [123], [246] and iii) both the fibres and interphases are protected against environmental effects, e.g. by use of coatings [123], [246], [447] or doping the UHTC matrix [18], [183], [448]. Each of these helps to ensure that the toughening mechanism(s) provided by the fibres is not degraded and so helps to maximise the properties of the composite.

1  
2  
3  
4  
5  
6  
7  
8  
9  
10  
11  
12  
13  
14  
15  
16  
17  
18  
19  
20  
21  
22  
23  
24  
25  
26  
27  
28  
29  
30  
31  
32  
33  
34  
35  
36  
37  
38  
39  
40  
41  
42  
43  
44  
45  
46  
47  
48  
49  
50  
51  
52  
53  
54  
55  
56  
57  
58  
59  
60  
61  
62  
63  
64  
65

Composition, micro- and macrostructures all need to be *designed* to yield the required properties and then sophisticated processing techniques need to be explored further in order to make viable components. This includes learning how to densify the materials at temperatures low enough to avoid damaging the fibres, whilst fast enough to keep costs down and without generating any brittle reaction products at the matrix / fibre interface. The solution might be the creation of ‘hybrid’ processes that combine elements of two – or more – existing process routes. Strength, toughness and oxidation / ablation resistance can also be tailored by introducing carefully selected fillers into the composites. For real applications, it is also essential to be able to join these new materials, so reliable and user-friendly joining methods are required to allow the assembly of potentially complex structures that can withstand the extreme environments required by the end applications. Relatively little work has been done in this area to date.

Multiscale modelling is going to be essential, both of the individual parts of the materials and processes and the creation of models that link across between processing and properties and that can be validated through extensive experimental work and characterisation. This integrated selection–design–modelling–experiment–manufacturing approach, spanning the ceramics–ensembles–component–system hierarchy, embraces the integrated computational materials engineering and the materials genome initiative paradigms [446]. Although not easy or low cost to create, in the longer term they will significantly reduce the costs of manufacturing new materials that offer the required combination of properties. In addition, new and ever-more realistic testing is required – though it also can’t afford to be too expensive or new materials will not be developed at a fast enough pace. So tests that can be done rapidly and at low cost but which provide excellent guidance on the performance of the materials and components under real environmental conditions are needed. Finally, we need to ensure that we have a new generation of scientists and engineers with the required skills – the ‘people pipeline’ is a key necessity for all new and expanding research areas. Research organisations, universities and industry must all work together to ensure that this happens smoothly and collaboration is the key; our planet is shrinking by the day in terms of the ability to interact across borders and exchange workers and best practice. We need to ensure that the development of skilled individuals remains at the forefront of our thinking. UHTCMCs are poised to shape the future of aerospace

1 applications, but paradigm and culture shifts will be needed to accelerate their  
2 development and take advantage of their full potential [446].  
3  
4  
5  
6  
7

## 8 **Acknowledgements** 9

10  
11 This work has been supported by a number of different research grants,  
12 including:  
13  
14

15  
16 *Materials systems for extreme environments (XMat)*, EPSRC research grant agreement  
17 number EP/K008749/1-2 (2013-18).  
18  
19

20  
21 *Ultra-high temperature ceramic materials*, MCM-ITP research grant agreement number  
22 4700003222 (2014-16).  
23  
24

25  
26 *Next generation ceramic composites for combustion harsh environments and space*  
27 (*C3Harme*), EU Horizon 2020 research grant agreement number GA 685594 (2016-20).  
28  
29

30  
31 *Effect of rare-earth doping elements on the mechanical and oxidation resistance*  
32 *performance of SiC coated C fibre / ZrC composites for high temperature applications*  
33 (*EREMOZ*), EU Horizon 2020 research grant agreement number 748568 (2018-20).  
34  
35

36  
37 *UK's Engineering and Physical Science Research Council entitled 'Materials Systems*  
38 *for Extreme Environments'*, grant number EP/K008749/2 and *'Multiscale tuning of*  
39 *interfaces and surfaces for energy applications'*, grant number EP/P007821/1  
40  
41  
42  
43  
44  
45  
46  
47  
48  
49  
50  
51  
52  
53  
54  
55  
56  
57  
58  
59  
60  
61  
62  
63  
64  
65

## List of Figures

- 1  
2  
3 Fig. 1 Schematic on the effect of the shape of the leading edge on the shock wave  
4 propagation on the surface of the structure.  
5
- 6 Fig. 2 Some summary data for common UHTCs ubiquitous in literature; HfB<sub>2</sub>, ZrB<sub>2</sub>,  
7 ZrC, HfC, TaC, TiB<sub>2</sub>, SiC is provided for contrast, due to its frequent inclusion  
8 as a secondary matrix component [13], [29]–[35].  
9
- 10 Fig. 3 a) Classification of the carbon fibres (value based on available commercial  
11 fibres of Table 2 and their use, b) different applications and properties [128],  
12 [134]–[141].  
13  
14
- 15 Fig. 4 Microstructural features of three generations of SiC fibres: reprinted with  
16 permission from John Wiley and Sons, Macromolecular Materials and  
17 Engineering, 297(6), Fig.16 in p. 512 [144].  
18  
19
- 20 Fig. 5 Structure of the 2.5 D carbon fibre preform bought from Surface Transforms,  
21 UK  
22
- 23 Fig. 6 Process flow sheet summarises the different methods of process for obtaining  
24 the UHTCMCs (CVI-chemical vapour infiltration, CVD-chemical vapour  
25 deposition, ED-Electro deposition, EPD- Electrophoretic deposition, PIP-  
26 precursor infiltration and pyrolysis, RMI - reactive melt infiltration, SIP -  
27 slurry impregnation process, HP – hot pressing, PS- pressureless sintering, SPS  
28 – spark plasma sintering, HIP – hot isostatic pressing)  
29  
30
- 31 Fig. 7 The steps involved in the production of a composite via PIP. (a) A liquid  
32 precursor impregnated fabric dries, leaving residual porosity; (b) pyrolysis  
33 begins, resulting in an evolution of gaseous by-products and volume shrinkage  
34 from the polymer-ceramic transition; (c) a porous microstructure, with  
35 microcracks and pores shown in the matrix phases.  
36  
37
- 38 Fig. 8 The precursor used by Xie et al for a ZrB<sub>2</sub> / ZrC matrix: reprinted with  
39 permission from Elsevier, Ceramics International, 2015, 41[5], Eq. 1 in p. 6228  
40 [194].  
41  
42
- 43 Fig. 9 (a) The reactive melt infiltration process and (b) residual free metal phase:  
44 reprinted with permission from Jeff Crompton,  
45 [https://uk.comsol.com/blogs/multiphysics-analysis-advanced-materials-  
46 ceramic-matrix-composites/](https://uk.comsol.com/blogs/multiphysics-analysis-advanced-materials-ceramic-matrix-composites/) [216].  
47  
48  
49  
50  
51  
52  
53  
54  
55  
56  
57  
58  
59  
60  
61  
62  
63  
64  
65

- 1  
2  
3  
4  
5  
6  
7  
8  
9  
10  
11  
12  
13  
14  
15  
16  
17  
18  
19  
20  
21  
22  
23  
24  
25  
26  
27  
28  
29  
30  
31  
32  
33  
34  
35  
36  
37  
38  
39  
40  
41  
42  
43  
44  
45  
46  
47  
48  
49  
50  
51  
52  
53  
54  
55  
56  
57  
58  
59  
60  
61  
62  
63  
64  
65
- Fig. 10 Schematic showing the growth of ceramic deposit on the cross section of the fibres to the point of full densification by CVI method.
- Fig. 11 a) Isothermal chemical vapour infiltration (ICVI), b) Thermal gradient (TGCVI), c) Isothermal forced flow CVI (FFCVI), d) Forced Flow Thermal Gradient CVI, e) Laser Chemical Vapour Infiltration (LCVI), f) Thermal gradient of Microwave and Radio Frequency CVI (MCVI and RFCVI) and g) pulse pressure CVI (PCVI).
- Fig. 12 3D micro-CT cross section of a UHTC composite prepared by squeeze impregnation showing powder penetration: reprinted with permission from *Am. Ceram. Soc. Bull.* 91, (2012), Fig.11 in p. 26 [17].
- Fig. 13 Backscattered electron images of particles distribution in C / C-UHTC composites: (a) C / C - ZrB<sub>2</sub>, (b) C / C - 4ZrB<sub>2</sub> - 1SiC, and (c) C / C - 1ZrB<sub>2</sub> - 2SiC - 2HfC: reprinted with permission from Elsevier, *Mater. Sci. Eng. A* 465, (2007) Fig.1 in p. 3 [10].
- Fig. 14 Schematics of moulds for conventional vacuum-assisted pressure casting and a new deformation process. (a, b) The conventional fixture of a firm mould. Woven fabric suppresses the infiltration of slurry. (c) Mould with a deformable foil during initial infiltration. The fabrics are pressed by the difference of pressure ( $\Delta P$ ) inside and outside of the mould. (d) The onset of outward deformation of the foil by the slurry. (e) Completion of the full deformation and infiltration of the slurry. (f) Removal of excess slurry by squeezing the mould: reprinted with permission from John Wiley and Sons, *J. Am. Ceram. Soc.* 90, (2007) Fig.1 in p. 2658 [258].
- Fig. 15 a) Cross section of C<sub>f</sub>-ZrB<sub>2</sub> composite using ZrSi<sub>2</sub> as a sintering aid. b) and c) Details of the fibre / matrix interface show the formation of brittle phases of SiC and ZrC: reprinted with permission from Elsevier, *Journal of the European Ceramic Society* 36 (2016) Fig.3 in p. 19 [113].
- Fig.16 (a) Cross section of C<sub>f</sub> - ZrB<sub>2</sub> composites produced by vacuum bagging followed by hot pressing at 1700°C for 20 mins: reprinted with permission from Elsevier, *Materials & Design* 85 (2015) Fig.3d in p. 130 [279]. (b) Cross section of C<sub>f</sub> - ZrB<sub>2</sub> composites, which was prepared by the infiltrate of ZrB<sub>2</sub> into unidirectional fabrics that were stacked in 0 - 0° configuration. The



sample was densified at 1800 - 1900°C for 30 – 40 mins: reprinted with permission from iStec, Scientific Reports 8[9148] (2018) Fig.2a in p. 3[281].

- 1  
2  
3  
4  
5  
6  
7  
8  
9  
10  
11  
12  
13  
14  
15  
16  
17  
18  
19  
20  
21  
22  
23  
24  
25  
26  
27  
28  
29  
30  
31  
32  
33  
34  
35  
36  
37  
38  
39  
40  
41  
42  
43  
44  
45  
46  
47  
48  
49  
50  
51  
52  
53  
54  
55  
56  
57  
58  
59  
60  
61  
62  
63  
64  
65
- Fig. 17 The local microstructure of (Fig. 12a) after a carbon CVI at a higher magnification: reprinted with permission from Elsevier, Materials Science and Engineering: A 465 (2007) Fig.2 in p. 3 [281].
- Fig. 18 Powder distribution of a UHTC composite produced by slurry infiltration (a) The detailed microstructure of the top (b) and bottom of the composite (c): reprinted with permission from Elsevier, J. Eur. Ceram. Soc., 33[2], Fig.2 in p. 425 [288].
- Fig. 19 BSE images (a) (b) on the cross section of the C/C–ZrB<sub>2</sub>–ZrC–SiC composites prepared by PIP at different magnifications: reprinted with permission from Elsevier, Corros. Sci., 98, Fig. 4 in p. 554 [290].
- Fig. 20 A tight and clean interface on the C<sub>f</sub>/ZrB<sub>2</sub>-SiC composite prepared by SIP and hot pressing, and corresponding elemental distributions: reprinted with permission from Elsevier, Journal of the European Ceramic Society, 39 (2019), Fig. 6 in p. 802 [289].
- Fig. 21 The polished surface of C<sub>f</sub>/ZrC-SiC produced by PIP+CVI with different interfaces (a) none; (b) PyC; (c) PyC+SiC: reprinted with permission from John Wiley and Sons, J. Am. Ceram. Soc., **91[10]**, Fig.1 in p. 3435 [294].
- Fig. 22 The microstructure of C<sub>f</sub>/ZrC (a,b): reprinted with permission from John Wiley and Sons, Int. J. Appl. Ceram. Technol., vol. 8, no. 2, Fig.6a & Fig.7b in p. 324 & 335 [295]; C<sub>f</sub>/ZrC-SiC(c,d): reprinted with permission from John Wiley and Sons, J. Am. Ceram. Soc., vol. 101, no. 8, Fig.1B and Fig.3A in p. 3255 & 3256 [296]; C<sub>f</sub>/Zr-Ti-B-C (e) composite densified by RMI: reprinted with permission from Author, Nat. Commun., vol. 8, 15836, Fig.4a in p.4 [297].
- Fig. 23 Debonding map showing crack penetration and crack deflection regimes as a function of Dundurs's parameter [124].

## List of Tables

- 1  
2 Table 1 UHTCMCs reinforced with Chopped fibre / whisker / CNT / graphene  
3 reinforcement [57], [84]–[121].  
4  
5 Table 2 Mechanical properties of carbon fibres produced by PAN and Pitch precursor  
6 [128].  
7  
8 Table 3 Physical, mechanical and thermal properties of the commercially available  
9 SiC fibres [144]–[147].  
10  
11 Table 4 Different preform types, manufacturing techniques, advantages and  
12 disadvantages. [193] – reference for one last figure  
13  
14 Table 5 Summary of the advantages and disadvantages of various densification /  
15 consolidation methods  
16  
17 Table 6 Literature reported data on RMI of UHTCMCs [207], [220], [224]–[232].  
18  
19 Table 7 Precursors and the conditions needed for the deposition of oxide / non-oxide  
20 ceramics [236], [237].  
21  
22 Table 8 Chemical vapour infiltration variants w.r.t. temperature, pressure, heating  
23 [242].  
24  
25 Table 9 Mechanical properties, density achieved and sintering conditions of  
26 UHTCMCs processed by hot pressing [275], [276], [278], [279], [281], [283]  
27  
28 Table 10 Properties of carbon fibre reinforced ultra-high temperature ceramic matrix  
29 composites prepared by different approaches [179], [192], [227], [279], [281],  
30 [294]–[296], [306]–[308].  
31  
32 Table 11 Thermal properties (melting point, CTE, thermal conductivity, diffusivity,  
33 Cp) of UHTCs and UHTCMCs [38], [58], [98], [116], [118], [205], [210],  
34 [221], [322], [326]–[343].  
35  
36 Table 12 Electrical properties of UHTCMCs reported in the literature [339], [348]–  
37 [350].  
38  
39 Table 13 Thermal ablative methods and properties of various UHTCMCs [18], [109],  
40 [181], [182], [187], [197], [198], [207], [209], [210], [222], [227], [229],  
41 [357]–[371]  
42  
43  
44  
45  
46  
47  
48  
49  
50  
51  
52  
53  
54  
55  
56  
57  
58  
59  
60  
61  
62  
63  
64  
65

## References

- [1] M. M. Opeka, I. G. Talmy, and J. A. Zaykoski, "Oxidation-based materials selection for 2000°C + hypersonic aerosurfaces: Theoretical considerations and historical experience," *J. Mater. Sci.*, vol. 39, no. 19, pp. 5887–5904, Oct. 2004.
- [2] P. L. Moses, V. L. Rausch, L. T. Nguyen, and J. R. Hill, "NASA hypersonic flight demonstrators—overview, status, and future plans," *Acta Astronaut.*, vol. 55, no. 3–9, pp. 619–630, Aug. 2004.
- [3] N. R. Council, *Evaluation of the National Aerospace Initiative*. Washington, D.C.: National Academies Press, 2004.
- [4] M. Holden, "A review of aerothermal problems associated with hypersonic flight," in *24th Aerospace Sciences Meeting*, 1986.
- [5] M.L. Rasmussen, *Hypersonic Flow*. New York: John Wiley and Sons Ltd, 1994.
- [6] John D. Anderson Jr., *Hypersonic and High-Temperature Gas Dynamics, Second Edition*, Second. Virginia: American Institute of Aeronautics and Astronautics, Inc., 2006.
- [7] J. L. Stollery, "Hypersonic viscous interaction on curved surfaces," *J. Fluid Mech.*, vol. 43, no. 3, pp. 497–511, Sep. 1970.
- [8] J. L. Stollery, "Hypersonic Flight," *Nature*, vol. 240, no. 5377, pp. 133–135, Nov. 1972.
- [9] R. Courant and K. O. Friedrichs, *Supersonic flow and shock waves*. Springer-Verlag, 1976.
- [10] S. Tang, J. Deng, S. Wang, W. Liu, and K. Yang, "Ablation behaviors of ultra-high temperature ceramic composites," *Mater. Sci. Eng. A*, vol. 465, no. 1–2, pp. 1–7, Sep. 2007.
- [11] T. A. Parthasarathy, R. A. Rapp, M. Opeka, and R. J. Kerans, "A model for the oxidation of ZrB<sub>2</sub>, HfB<sub>2</sub> and TiB<sub>2</sub>," *Acta Mater.*, vol. 55, no. 17, pp. 5999–6010, Oct. 2007.
- [12] R. Savino, M. De Stefano Fumo, D. Paterna, and M. Serpico, "Aerothermodynamic study of UHTC-based thermal protection systems," *Aerosp. Sci. Technol.*, vol. 9, no. 2, pp. 151–160, Mar. 2005.
- [13] W. G. Fahrenholtz, E. J. Wuchina, W. E. Lee, Y. Zhou, and G. Geiger, *Ultra-High Temperature Ceramics*. Hoboken, NJ: John Wiley & Sons, Inc, 2014.
- [14] P. Rogl and P. E. Potter, "A critical review and thermodynamic calculation of the binary system: Zirconium-boron," *Calphad*, vol. 12, no. 2, pp. 191–204, Apr. 1988.
- [15] F. W. Glaser and B. Post, "System Zirconium-Boron," *JOM*, vol. 5, no. 9, pp. 1117–1118, Sep. 1953.
- [16] J. Han, P. Hu, X. Zhang, S. Meng, and W. Han, "Oxidation-resistant ZrB<sub>2</sub>-SiC composites at 2200°C," *Compos. Sci. Technol.*, vol. 68, no. 3–4, pp. 799–806, Mar. 2008.
- [17] P. Paul, A., Venugopal, S., Binner, J., Vaidhyanathan, B., Jayaseelan, D.D., Zapata-Solvas, E., Lee, W.E., Heaton, A., Brown, "UHTC composites for hypersonic applications," *Am. Ceram. Soc. Bull.*, vol. 91, no. 1, pp. 22–28, Oct. 2012.
- [18] A. Paul, S. Venugopal, J. G. P. Binner, B. Vaidhyanathan, A. C. J. Heaton, and P. M. Brown, "UHTC-carbon fibre composites: Preparation, oxyacetylene torch testing and characterisation," *J. Eur. Ceram. Soc.*, vol. 33, no. 2, pp. 423–432, Feb. 2013.
- [19] Tim Bowler, "Carbon fibre planes: Lighter and stronger by design - BBC News,"

- 1  
2  
3  
4  
5  
6  
7  
8  
9  
10  
11  
12  
13  
14  
15  
16  
17  
18  
19  
20  
21  
22  
23  
24  
25  
26  
27  
28  
29  
30  
31  
32  
33  
34  
35  
36  
37  
38  
39  
40  
41  
42  
43  
44  
45  
46  
47  
48  
49  
50  
51  
52  
53  
54  
55  
56  
57  
58  
59  
60  
61  
62  
63  
64  
65
- BBC*, 2014. [Online]. Available: <https://www.bbc.co.uk/news/business-25833264>. [Accessed: 04-Jan-2019].
- [20] J. M. Quenisset, "Carbon combinations. Carbon/Carbon composites," *Adv. Mater.*, vol. 6, no. 2, pp. 176–177, Feb. 1994.
- [21] T. S. Reinhart, F. H. Froes, and Society for the Advancement of Material and Process Engineering., "Stability Characterization of diboride Composites Under High-Velocity Atmospheric Flight Conditions," in *Advanced materials : meeting the economic challenge : 24th International SAMPE Technical Conference : Westin Harbour Castle Hotel, Toronto, Canada, October 20-22, 1992*, 1992, p. 718.
- [22] T. S. R. C. Murthy, J. K. Sonber, K. Sairam, R. D. Bedse, and J. K. Chakarvartty, "Development of Refractory and Rare Earth Metal Borides & Carbides for High Temperature Applications," *Mater. Today Proc.*, vol. 3, no. 9, pp. 3104–3113, 2016.
- [23] A. Bhattacharya *et al.*, "Nano-scale microstructure damage by neutron irradiations in a novel Boron-11 enriched TiB<sub>2</sub> ultra-high temperature ceramic," *Acta Mater.*, vol. 165, pp. 26–39, Feb. 2019.
- [24] S. C. Middleburgh, D. C. Parfitt, P. R. Blair, and R. W. Grimes, "Atomic Scale Modeling of Point Defects in Zirconium Diboride," *J. Am. Ceram. Soc.*, vol. 94, no. 7, pp. 2225–2229, Jul. 2011.
- [25] G. Gutierrez *et al.*, "Thermal behaviour of xenon in zirconium carbide at high temperature: Role of residual zirconia and free carbon," *J. Nucl. Mater.*, vol. 416, no. 1–2, pp. 94–98, Sep. 2011.
- [26] E. Wuchina *et al.*, "UHTCs: Ultra-High Temperature Ceramic Materials for Extreme Environment Applications," *Electrochem. Soc. Interface*, vol. 16, no. 4, pp. 30–36, 2007.
- [27] C. Mroz, "Minerals Review: Zirconium Diboride," *Am. Ceram. Soc. Bull.*, vol. 74, no. 6, pp. 164–165, 1995.
- [28] E. Sani, L. Mercatelli, M. Meucci, A. Balbo, L. Silvestroni, and D. Sciti, "Compositional dependence of optical properties of zirconium, hafnium and tantalum carbides for solar absorber applications," *Sol. Energy*, vol. 131, pp. 199–207, Jun. 2016.
- [29] K. Gürçan and E. Ayas, "In-situ synthesis and densification of HfB<sub>2</sub> ceramics by the spark plasma sintering technique," *Ceram. Int.*, vol. 43, no. 4, pp. 3547–3555, 2017.
- [30] M. M. Opeka, I. G. Talmy, E. J. Wuchina, J. A. Zaykoski, and S. J. Causey, "Mechanical, Thermal, and Oxidation Properties of Refractory Hafnium and zirconium Compounds," *J. Eur. Ceram. Soc.*, vol. 19, no. 13–14, pp. 2405–2414, Oct. 1999.
- [31] Netschz, "Thermal Properties of Ceramics." Netschz, 2012.
- [32] A. L. Chamberlain, W. G. Fahrenholtz, G. E. Hilmas, and D. T. Ellerby, "High-Strength Zirconium Diboride-Based Ceramics," *J. Am. Ceram. Soc.*, vol. 87, no. 6, pp. 1170–1172, Jun. 2004.
- [33] W. G. Fahrenholtz, G. E. Hilmas, I. G. Talmy, and J. A. Zaykoski, "Refractory Diborides of Zirconium and Hafnium," *J. Am. Ceram. Soc.*, vol. 90, no. 5, pp. 1347–1364, May 2007.
- [34] P. Schwarzkopf and R. Kieffer, *Refractory Hard Metals: Borides, Carbides, Nitrides and Silicides*. New York: Macmillan Company, 1953.
- [35] H. S. Hong and K. S. Lee, "Thermodynamic evaluation of the Ta–O system from pure tantalum to tantalum pentoxide," *J. Alloys Compd.*, vol. 360, no. 1, pp. 198–

204, 2003.

- [36] R. Wang and W. Li, "Characterization models for thermal shock resistance and fracture strength of ultra-high temperature ceramics at high temperatures," *Theor. Appl. Fract. Mech.*, vol. 90, pp. 1–13, 2017.
- [37] M. W. D. Van, J. D. G. Drewry, D. E. King, and C. M. Hudson, "The hypersonic environment: Required operating conditions and design challenges," *J. Mater. Sci.*, vol. 39, no. 19, pp. 5915–5924, Oct. 2004.
- [38] E. Wuchina *et al.*, "Designing for ultrahigh-temperature applications: The mechanical and thermal properties of  $\text{HfB}_2$ ,  $\text{HfC}_x$ ,  $\text{HfN}_x$  and  $\text{Hf(N)}$ ," *J. Mater. Sci.*, vol. 39, no. 19, pp. 5939–5949, Oct. 2004.
- [39] R. J. Irving and I. G. Worsley, "The oxidation of titanium diboride and zirconium diboride at high temperatures," *J. Less Common Met.*, vol. 16, no. 2, pp. 103–112, 1968.
- [40] L. G.-Q. Han Ke-Chang Dong Chuang, Tai Kai-Ping, "Influence of Nitrogen Vacancy Concentration on Mechanical and Electrical Properties of Rocksalt Zirconium Nitride Films," *Acta Metall. Sin. Lett.*, vol. 30, no. 11, pp. 1100–1108, 2017.
- [41] L. Silvestroni, S. Failla, I. Neshpor, and O. Grigoriev, "Method to improve the oxidation resistance of  $\text{ZrB}_2$ -based ceramics for reusable space systems," *J. Eur. Ceram. Soc.*, vol. 38, no. 6, pp. 2467–2476, 2018.
- [42] A. K. Kuriakose and J. L. Margrave, "The Oxidation Kinetics of Zirconium Diboride and Zirconium Carbide at High Temperatures," *J. Electrochem. Soc.*, vol. 111, no. 7, p. 827, 1964.
- [43] M. Desmaison Brut, J. Montintin, F. Valin, and M. Boncoeur, "Mechanical properties and oxidation behaviour of HIPed hafnium nitride ceramics," *J. Eur. Ceram. Soc.*, vol. 13, no. 4, pp. 379–386, Jan. 1994.
- [44] P. Patsalas *et al.*, "Conductive nitrides: Growth principles, optical and electronic properties, and their perspectives in photonics and plasmonics," *Mater. Sci. Eng. R Reports*, vol. 123, pp. 1–55, 2018.
- [45] R. Savino, M. De Stefano Fumo, D. Paterna, A. Di Maso, and F. Monteverde, "Arc-jet testing of ultra-high-temperature-ceramics," *Aerosp. Sci. Technol.*, vol. 14, no. 3, pp. 178–187, Apr. 2010.
- [46] D. L. Poerschke, M. D. Novak, N. Abdul-Jabbar, S. Krämer, and C. G. Levi, "Selective active oxidation in hafnium boride-silicon carbide composites above 2000°C," *J. Eur. Ceram. Soc.*, vol. 36, no. 15, pp. 3697–3707, 2016.
- [47] V. V Kurbatkina, E. I. Patsera, E. A. Levashov, and A. N. Timofeev, "Self-propagating high-temperature synthesis of refractory boride ceramics  $(\text{Zr,Ta})\text{B}_2$  with superior properties," *J. Eur. Ceram. Soc.*, vol. 38, no. 4, pp. 1118–1127, 2018.
- [48] X. Zhang, P. Hu, J. Han, L. Xu, and S. Meng, "The addition of lanthanum hexaboride to zirconium diboride for improved oxidation resistance," *Scr. Mater.*, vol. 57, no. 11, pp. 1036–1039, Dec. 2007.
- [49] C. Carney *et al.*, "Oxidation response of a  $\text{SiC}_t/\text{SiC}$  CMC with a  $\text{HfB}_2$ -based coating in an arc jet test," *Adv. Appl. Ceram.*, vol. 117, no. sup1, pp. s19–s25, Oct. 2018.
- [50] P. Hu *et al.*, "Rolling compacted fabrication of carbon fiber reinforced ultra-high temperature ceramics with highly oriented architectures and exceptional mechanical feedback," *Ceram. Int.*, vol. 44, no. 12, pp. 14907–14912, Aug. 2018.
- [51] I. Akin, M. Hotta, F. C. Sahin, O. Yucel, G. Goller, and T. Goto, "Microstructure and densification of  $\text{ZrB}_2$ - $\text{SiC}$  composites prepared by spark plasma sintering,"

- J. Eur. Ceram. Soc.*, vol. 29, no. 11, pp. 2379–2385, Aug. 2009.
- [52] Muksin, D.-H. Yoon, and K. Raju, “Effects of Sc<sub>2</sub>O<sub>3</sub> sintering aid for the densification and mechanical properties of SiC–ZrB<sub>2</sub> composites,” *Ceram. Int.*, vol. 42, no. 6, pp. 7300–7308, May 2016.
- [53] I.-M. M. Low, Y. (Yoshio) Sakka, and C. F. (Chunfeng) Hu, *MAX Phases and Ultra-High Temperature Ceramics for Extreme Environments*. IGI Global, 2013.
- [54] V. Rubio, P. Ramanujam, and J. Binner, “Ultra-high temperature ceramic composite,” *Adv. Appl. Ceram.*, vol. 117, no. sup1, pp. 56–61, Oct. 2018.
- [55] A. Purwar and B. Basu, “Thermo-structural design of ZrB<sub>2</sub>-SiC-based thermal protection system for hypersonic space vehicles,” *J. Am. Ceram. Soc.*, vol. 100, no. 4, pp. 1618–1633, Apr. 2017.
- [56] J. K. Sonber, T. S. R. C. Murthy, K. Sairam, A. Nagaraj, S. Majumdar, and V. Kain, “ZrB<sub>2</sub> based novel composite with NiAl as reinforcement phase,” *Int. J. Refract. Met. Hard Mater.*, vol. 70, no. August 2017, pp. 56–65, Jan. 2018.
- [57] M. Shahedi Asl, B. Nayebi, and M. Shokouhimehr, “TEM characterization of spark plasma sintered ZrB<sub>2</sub>-SiC-graphene nanocomposite,” *Ceram. Int.*, vol. 44, no. 13, pp. 15269–15273, Sep. 2018.
- [58] R. Tu *et al.*, “Mechanical, electrical and thermal properties of ZrC-ZrB<sub>2</sub>-SiC ternary eutectic composites prepared by arc melting,” *J. Eur. Ceram. Soc.*, vol. 38, no. 11, pp. 3759–3766, Sep. 2018.
- [59] B. Xie *et al.*, “Influence of SiC on phase and microstructure of ZrB<sub>2</sub> powders synthesized via carbothermal reduction at different temperatures,” *Ceram. Int.*, vol. 44, no. 8, pp. 8795–8799, Jun. 2018.
- [60] V. Guérineau and A. Julian-Jankowiak, “Oxidation mechanisms under water vapour conditions of ZrB<sub>2</sub>-SiC and HfB<sub>2</sub>-SiC based materials up to 2400°C,” *J. Eur. Ceram. Soc.*, vol. 38, no. 2, pp. 421–432, Feb. 2018.
- [61] P. Hu *et al.*, “Architectural engineering inspired method of preparing C<sub>2</sub>/ZrC-SiC with graceful mechanical responses,” *J. Am. Ceram. Soc.*, vol. 102, no. 1, pp. 70–78, Jan. 2019.
- [62] J. Ren, Y. Zhang, Y. Fu, P. Zhang, S. Tian, and L. Zhang, “Effects of the second phase on the microstructure and ablation resistance of HfC coating on C/C composites,” *Surf. Coatings Technol.*, vol. 344, pp. 250–258, Jun. 2018.
- [63] Y. Jing, H. Yuan, and Z. Lian, “Microstructure and Mechanical Properties of ZrB<sub>2</sub>-HfC Ceramics Influenced by HfC Addition,” *Materials (Basel)*, vol. 11, no. 10, p. 2046, Oct. 2018.
- [64] J. K. Sonber *et al.*, “Friction and wear properties of zirconium diboride in sliding against WC ball,” *Int. J. Refract. Met. Hard Mater.*, vol. 76, no. 0, pp. 41–48, Nov. 2018.
- [65] E. Castle, T. Csanádi, S. Grasso, J. Dusza, and M. Reece, “Processing and Properties of High-Entropy Ultra-High Temperature Carbides,” *Sci. Rep.*, vol. 8, no. 1, pp. 1–12, 2018.
- [66] A. Vinci, L. Zoli, D. Sciti, J. Watts, G. E. Hilmas, and W. G. Fahrenholtz, “Mechanical behaviour of carbon fibre reinforced TaC/SiC and ZrC/SiC composites up to 2100°C,” *J. Eur. Ceram. Soc.*, vol. 39, no. 4, pp. 780–787, Apr. 2019.
- [67] D. Wu, G. Huangfu, D. Wang, B. Wei, Y. Wang, and Y. Zhou, “Microstructure and mechanical properties of ZrC-TaC composite fabricated by displacive compensation of porosity at 1300 °C,” *Ceram. Int.*, vol. 44, no. 1, pp. 246–253, Jan. 2018.
- [68] J. K. Sonber, “Studies on synthesis, densification and oxidation of zirconium

- diboride based materials,” PhD thesis Homi Bhabha National Institute, 2015.
- [69] J. K. Sonber and A. K. Suri, “Synthesis and consolidation of zirconium diboride: review,” *Adv. Appl. Ceram.*, vol. 110, no. 6, pp. 321–334, Aug. 2011.
- [70] T S R C Murthy, “Effect of Sinter Additives on the Consolidation and Properties of Titanium Diboride Composites,” PhD thesis, Homi Bhabha National Institute, 2012.
- [71] A. Mukhopadhyay, G. B. Raju, and B. Basu, “Ultra High Temperature Ceramics,” in *MAX Phases and Ultra-High Temperature Ceramics for Extreme Environments*, IGI Global, 2013, pp. 49–99.
- [72] E. Ghasali and M. Shahedi Asl, “Microstructural development during spark plasma sintering of ZrB<sub>2</sub>–SiC–Ti composite,” *Ceram. Int.*, vol. 44, no. 15, pp. 18078–18083, Oct. 2018.
- [73] M. T. S. R. Ch., B. Basu, R. Balasubramaniam, A. K. Suri, C. Subramanian, and R. K. Fotedar, “Processing and Properties of TiB<sub>2</sub> with MoSi<sub>2</sub> Sinter-additive: A First Report,” *J. Am. Ceram. Soc.*, vol. 89, no. 1, pp. 131–138, Jan. 2006.
- [74] T. S. R. C. Murthy, B. Basu, A. Srivastava, R. Balasubramaniam, and A. K. Suri, “Tribological properties of TiB<sub>2</sub> and TiB<sub>2</sub>–MoSi<sub>2</sub> ceramic composites,” *J. Eur. Ceram. Soc.*, vol. 26, no. 7, pp. 1293–1300, Jan. 2006.
- [75] T. S. R. C. Murthy *et al.*, “Preparation and property evaluation of TiB<sub>2</sub>+TiSi<sub>2</sub> composite,” *Int. J. Refract. Met. Hard Mater.*, vol. 27, no. 3, pp. 629–636, May 2009.
- [76] T. S. R. C. Murthy *et al.*, “A new TiB<sub>2</sub>+CrSi<sub>2</sub> composite – Densification, characterization and oxidation studies,” *Int. J. Refract. Met. Hard Mater.*, vol. 28, no. 4, pp. 529–540, Jul. 2010.
- [77] J. K. Sonber, T. S. R. C. Murthy, C. Subramanian, R. C. Hubli, R. K. Fotedar, and A. K. Suri, “Effect of WSi<sub>2</sub> addition on densification and properties of ZrB<sub>2</sub>,” *Adv. Appl. Ceram.*, vol. 113, no. 2, pp. 114–119, Feb. 2014.
- [78] V. Reddy *et al.*, “Densification and mechanical properties of CrB<sub>2</sub>+MoSi<sub>2</sub> based novel composites,” *Ceram. Int.*, vol. 41, no. 6, pp. 7611–7617, Jul. 2015.
- [79] T. S. R. C. Murthy, J. K. Sonber, K. Sairam, and R. D. Bedse, “Development and Characterization of (Ti,Cr)B<sub>2</sub> based Composites,” *BARC Newsl.*, vol. January-Fe, no. February, pp. 1–10, 2016.
- [80] E. P. Simonenko, N. P. Simonenko, E. K. Papynov, E. A. Gridasova, V. G. Sevastyanov, and N. T. Kuznetsov, “Production of HfB<sub>2</sub>–SiC (10–65 vol % SiC) Ultra-High-Temperature Ceramics by Hot Pressing of HfB<sub>2</sub>–(SiO<sub>2</sub>–C) Composite Powder Synthesized by the Sol–Gel Method,” *Russ. J. Inorg. Chem.*, vol. 63, no. 1, pp. 1–15, Jan. 2018.
- [81] S. Guo, “High-temperature mechanical behavior of ZrB<sub>2</sub>-based composites with micrometer- and nano-sized SiC particles,” *J. Am. Ceram. Soc.*, vol. 101, no. 7, pp. 2707–2711, 2018.
- [82] J. K. Sonber, “Effect of NdB<sub>6</sub> addition on Densification and Properties Of ZrB<sub>2</sub>,” *Ceram. - Silikaty*, vol. 60, no. 1, pp. 41–47, Mar. 2016.
- [83] E. Zapata Solvas, D. Gómez García, A. Domínguez Rodríguez, and W. E. Lee, “High temperature creep of 20 vol%. SiC–HfB<sub>2</sub> UHTCs up to 2000°C and the effect of La<sub>2</sub>O<sub>3</sub> addition,” *J. Eur. Ceram. Soc.*, vol. 38, no. 1, pp. 47–56, Jan. 2018.
- [84] W.-W. Wu, M. Estili, G.-J. Zhang, and Y. Sakka, “Dispersion and structural evolution of multi-walled carbon nanotubes in ZrB<sub>2</sub> matrix,” *Ceram. Int.*, vol. 43, no. 13, pp. 10533–10539, Sep. 2017.
- [85] S. Zhou, Z. Wang, and W. Zhang, “Effect of graphite flake orientation on

- microstructure and mechanical properties of ZrB<sub>2</sub>-SiC-graphite composite,” *J. Alloys Compd.*, vol. 485, no. 1–2, pp. 181–185, Oct. 2009.
- [86] G. B. Yadukulakrishnan, S. Karumuri, A. Rahman, R. P. Singh, A. Kaan Kalkan, and S. P. Harimkar, “Spark plasma sintering of graphene reinforced zirconium diboride ultra-high temperature ceramic composites,” *Ceram. Int.*, vol. 39, no. 6, pp. 6637–6646, Aug. 2013.
- [87] H. Jin, S. Meng, W. Xie, C. Xu, and J. Niu, “HfB<sub>2</sub>-CNTs composites with enhanced mechanical properties prepared by spark plasma sintering,” *Ceram. Int.*, vol. 43, no. 2, pp. 2170–2173, 2017.
- [88] X. Zhang, Y. An, J. Han, W. Han, G. Zhao, and X. Jin, “Graphene nanosheet reinforced ZrB<sub>2</sub>-SiC ceramic composite by thermal reduction of graphene oxide,” *RSC Adv.*, vol. 5, no. 58, pp. 47060–47065, 2015.
- [89] M. Shahedi Asl and M. Ghassemi Kakroudi, “Characterization of hot-pressed graphene reinforced ZrB<sub>2</sub>-SiC composite,” *Mater. Sci. Eng. A*, vol. 625, pp. 385–392, 2015.
- [90] Y. Cheng, P. Hu, S. Zhou, X. Zhang, and W. Han, “Using macroporous graphene networks to toughen ZrC-SiC ceramic,” *J. Eur. Ceram. Soc.*, vol. 38, no. 11, pp. 3752–3758, Sep. 2018.
- [91] I. Akin and G. Goller, “Spark Plasma Sintering of Zirconia-Toughened Alumina Composites and Ultra-High Temperature Ceramics Reinforced with Carbon Nanotubes,” in *Research and Innovation in Carbon Nanotube-Based Composites*, no. December, D. B. Attaf, Ed. Hong Kong: The World Academic Publishing Co. Ltd., 2015, pp. 85–101.
- [92] D. Sciti and L. Silvestroni, “Processing, sintering and oxidation behavior of SiC fibers reinforced ZrB<sub>2</sub> composites,” *J. Eur. Ceram. Soc.*, vol. 32, no. 9, pp. 1933–1940, Jul. 2012.
- [93] L. Silvestroni, D. D. Fabbriche, and D. Sciti, “Tyranno SA3 fiber-ZrB<sub>2</sub> composites. Part I: Microstructure and densification,” *Mater. Des.*, vol. 65, pp. 1253–1263, Jan. 2015.
- [94] L. Pienti, D. Sciti, L. Silvestroni, and S. Guicciardi, “Effect of milling on the mechanical properties of chopped SiC fiber-reinforced ZrB<sub>2</sub>,” *Materials (Basel)*, vol. 6, no. 5, pp. 1980–1993, 2013.
- [95] F. Yang, X. Zhang, J. Han, and S. Du, “Characterization of hot-pressed short carbon fiber reinforced ZrB<sub>2</sub>-SiC ultra-high temperature ceramic composites,” *J. Alloys Compd.*, vol. 472, no. 1–2, pp. 395–399, Mar. 2009.
- [96] D. Sciti, S. Guicciardi, and L. Silvestroni, “SiC chopped fibers reinforced ZrB<sub>2</sub>: Effect of the sintering aid,” *Scr. Mater.*, vol. 64, no. 8, pp. 769–772, Apr. 2011.
- [97] L. Silvestroni, S. Guicciardi, M. Nygren, C. Melandri, and D. Sciti, “Effect of the Sintering Additive on Microstructure and Mechanical Properties of Hi-Nicalon TM SiC Fibers in a HfB<sub>2</sub> Matrix,” *J. Am. Ceram. Soc.*, vol. 96, no. 2, pp. 643–650, Oct. 2012.
- [98] L. Pienti, L. Silvestroni, E. Landi, C. Melandri, and D. Sciti, “Microstructure, mechanical properties and oxidation behavior of TaC- and HfC-based materials containing short SiC fiber,” *Ceram. Int.*, vol. 41, no. 1, pp. 1367–1377, Jan. 2015.
- [99] S. R. Bakshi *et al.*, “Spark plasma sintered tantalum carbide-carbon nanotube composite: Effect of pressure, carbon nanotube length and dispersion technique on microstructure and mechanical properties,” *Mater. Sci. Eng. A*, vol. 528, no. 6, pp. 2538–2547, Mar. 2011.
- [100] Y. Wang, M. Zhu, L. Cheng, and L. Zhang, “Fabrication of SiCw reinforced



- ZrB<sub>v</sub>-based ceramics,” *Ceram. Int.*, vol. 36, no. 6, pp. 1787–1790, Aug. 2010.
- [101] L. Jia, Z. Xinghong, W. Zhi, and H. Wenbo, “Microstructure and mechanical properties of ZrB<sub>2</sub>-SiC-ZrO<sub>2f</sub> ceramic,” *Scr. Mater.*, vol. 64, no. 9, pp. 872–875, May 2011.
- [102] M. Shahedi Asl, I. Farahbakhsh, and B. Nayebi, “Characteristics of multi-walled carbon nanotube toughened ZrB<sub>2</sub>-SiC ceramic composite prepared by hot pressing,” *Ceram. Int.*, vol. 42, no. 1, pp. 1950–1958, 2016.
- [103] F. Y. Yang, “Preparation and Properties of ZrB<sub>2</sub>-SiC Ceramic Composites Reinforced by Carbon Nanotubes,” *J. Inorg. Mater.*, vol. 23, no. 5, pp. 950–954, Oct. 2008.
- [104] J. Lin, Y. Huang, H. Zhang, Y. Yang, and N. Li, “Microstructure and mechanical properties of spark plasma sintered ZrB<sub>2</sub>-SiC-MWCNT composites,” *Ceram. Int.*, vol. 41, no. 10, pp. 15261–15265, Dec. 2015.
- [105] G. B. Yadhukulakrishnan *et al.*, “Spark plasma sintering of silicon carbide and multi-walled carbon nanotube reinforced zirconium diboride ceramic composite,” *Mater. Sci. Eng. A*, vol. 552, pp. 125–133, Aug. 2012.
- [106] M. Shahedi Asl, F. Golmohammadi, M. Ghassemi Kakroudi, and M. Shokouhimehr, “Synergetic effects of SiC and Csf in ZrB<sub>2</sub>-based ceramic composites. Part I: Densification behavior,” *Ceram. Int.*, vol. 42, no. 3, pp. 4498–4506, Feb. 2016.
- [107] R. B. Acicbe and G. Goller, “Densification behavior and mechanical properties of spark plasma-sintered ZrC-TiC and ZrC-TiC-CNT composites,” *J. Mater. Sci.*, vol. 48, no. 6, pp. 2388–2393, Mar. 2013.
- [108] G. Sagdic, S. Goller, “Densification behavior and mechanical properties of spark plasma sintered ZrC-SiC and ZrC-SiC-CNT composites,” *J. Aust. Ceram. Soc.*, vol. 50, no. 2, pp. 76–82, 2014.
- [109] D. Sciti, L. Zoli, L. Silvestroni, A. Cecere, G. D. Di Martino, and R. Savino, “Design, fabrication and high velocity oxy-fuel torch tests of a C<sub>f</sub>-ZrB<sub>2</sub> - fiber nozzle to evaluate its potential in rocket motors,” *Mater. Des.*, vol. 109, pp. 709–717, Nov. 2016.
- [110] L. Zoli, A. Vinci, L. Silvestroni, D. Sciti, M. Reece, and S. Grasso, “Rapid spark plasma sintering to produce dense UHTCs reinforced with undamaged carbon fibres,” *Mater. Des.*, vol. 130, no. May, pp. 1–7, Sep. 2017.
- [111] J. Sha, J. Li, S. H. Wang, Y. Wang, Z. Zhang, and J. Dai, “Toughening effect of short carbon fibers in the ZrB<sub>2</sub>-ZrSi<sub>2</sub> ceramic composites,” *Mater. Des.*, vol. 75, pp. 160–165, Jun. 2015.
- [112] J. J. Sha *et al.*, “ZrB<sub>2</sub>-based composites toughened by as-received and heat-treated short carbon fibers,” *J. Eur. Ceram. Soc.*, vol. 37, no. 2, pp. 549–558, Feb. 2017.
- [113] L. Silvestroni, D. Dalle Fabbriche, C. Melandri, and D. Sciti, “Relationships between carbon fiber type and interfacial domain in ZrB<sub>2</sub> -based ceramics,” *J. Eur. Ceram. Soc.*, vol. 36, no. 1, pp. 17–24, Jan. 2016.
- [114] F. Yang, X. Zhang, J. Han, and S. Du, “Mechanical properties of short carbon fiber reinforced ZrB<sub>2</sub>-SiC ceramic matrix composites,” *Mater. Lett.*, vol. 62, no. 17–18, pp. 2925–2927, Jun. 2008.
- [115] L. Silvestroni, D. Sciti, C. Melandri, and S. Guicciardi, “Tyranno SA3 fiber-ZrB<sub>2</sub> composites. Part II: Mechanical properties,” *Mater. Des.*, vol. 65, pp. 1264–1273, Jan. 2015.
- [116] W.-B. Tian, Y.-M. Kan, G.-J. Zhang, and P.-L. Wang, “Effect of carbon nanotubes on the properties of ZrB<sub>2</sub>-SiC ceramics,” *Mater. Sci. Eng. A*, vol. 487,

- no. 1–2, pp. 568–573, Jul. 2008.
- [117] Z. Nasiri, M. Mashhadi, and A. Abdollahi, “Effect of short carbon fiber addition on pressureless densification and mechanical properties of ZrB<sub>2</sub>–SiC–Csf nanocomposite,” *Int. J. Refract. Met. Hard Mater.*, vol. 51, pp. 216–223, Jul. 2015.
- [118] S. Guo, K. Naito, and Y. Kagawa, “Mechanical and physical behaviors of short pitch-based carbon fiber-reinforced HfB<sub>2</sub>–SiC matrix composites,” *Ceram. Int.*, vol. 39, no. 2, pp. 1567–1574, Mar. 2013.
- [119] M. Shahedi Asl, M. Ghassemi Kakroudi, R. Abedi Kondolaji, and H. Nasiri, “Influence of graphite nano-flakes on densification and mechanical properties of hot-pressed ZrB<sub>2</sub>–SiC composite,” *Ceram. Int.*, vol. 41, no. 4, pp. 5843–5851, May 2015.
- [120] X. Zhang, Z. Wang, X. Sun, W. Han, and C. Hong, “Effect of graphite flake on the mechanical properties of hot pressed ZrB<sub>2</sub>–SiC ceramics,” *Mater. Lett.*, vol. 62, no. 28, pp. 4360–4362, Nov. 2008.
- [121] Z. Wang, C. Hong, X. Zhang, X. Sun, and J. Han, “Microstructure and thermal shock behavior of ZrB<sub>2</sub>–SiC–graphite composite,” *Mater. Chem. Phys.*, vol. 113, no. 1, pp. 338–341, Jan. 2009.
- [122] R. Alexander *et al.*, “Effect of graphene nano-platelet reinforcement on the mechanical properties of hot pressed boron carbide based composite,” *Ceram. Int.*, vol. 44, no. 8, pp. 9830–9838, Jun. 2018.
- [123] J. D. Kiser, R. Andrulonis, K. E. David, and C. Davies, *Composite Materials Handbook Volume 5 - Revision A*, vol. 5. SAE International, 2017.
- [124] K. T. Faber, “Ceramic Composite Interfaces: Properties and Design,” *Annu. Rev. Mater. Sci.*, vol. 27, no. 1, pp. 499–524, Aug. 1997.
- [125] J. Buckley, “Carbon-Carbon, An Overview,” *Am. Ceram. Soc. Bull.*, vol. 67, no. 2, pp. 364–368, 1988.
- [126] B. T. B. T. Kelly, *Physics of graphite*. Applied Science, 1981.
- [127] X. Huang, “Fabrication and Properties of Carbon Fibers,” *Materials (Basel)*, vol. 2, no. 4, pp. 2369–2403, Dec. 2009.
- [128] S. J. Park, *Carbon Fibers*, vol. 210. Dordrecht: Springer Netherlands, 2015.
- [129] E. Fitzer, “Pan-based carbon fibers—present state and trend of the technology from the viewpoint of possibilities and limits to influence and to control the fiber properties by the process parameters,” *Carbon N. Y.*, vol. 27, no. 5, pp. 621–645, Jan. 1989.
- [130] Akio Shindo, “Process for the preparation of carbon fibers,” US3529934A, 04-Jan-1968.
- [131] W. N. Reynolds and J. V. Sharp, “Crystal shear limit to carbon fibre strength,” *Carbon N. Y.*, vol. 12, no. 2, pp. 103–110, Apr. 1974.
- [132] X. Huang, “Fabrication and Properties of Carbon Fibers,” *Materials (Basel)*, vol. 2, no. 4, pp. 2369–2403, Dec. 2009.
- [133] P. Morgan, *Carbon fibers and their composites*. Taylor & Francis, 2005.
- [134] “Teijin Carbon – Tenax® Filament Yarn.” [Online]. Available: <https://www.tejincarbon.com/products/tenaxr-carbon-fiber/tenaxr-filament-yarn>. [Accessed: 24-Jan-2019].
- [135] “TORAYCA ® yarn | TORAYCA® | TORAY.” [Online]. Available: [http://www.torayca.com/en/lineup/product/pro\\_001\\_01.html](http://www.torayca.com/en/lineup/product/pro_001_01.html). [Accessed: 24-Jan-2019].
- [136] “PAN Fiber - Mitsubishi Chemical Carbon Fiber Composites.” [Online]. Available: <http://mccfc.com/pan-fiber/>. [Accessed: 24-Jan-2019].

- 1 [137] “Carbon Fiber DataSheet | Hexcel.” [Online]. Available:  
2 <https://www.hexcel.com/Resources/DataSheets/Carbon-Fiber>. [Accessed: 24-Jan-  
3 2019].
- 4 [138] “Search | Solvay.” [Online]. Available:  
5 <https://www.solvay.com/en/search?f%5B0%5D=fsection%3AProducts>.  
6 [Accessed: 24-Jan-2019].
- 7 [139] “Carbon Fiber.” [Online]. Available: [http://www.formosa.co.kr/products/carbon-  
8 fiber/#collapse-1-12662](http://www.formosa.co.kr/products/carbon-fiber/#collapse-1-12662). [Accessed: 24-Jan-2019].
- 9 [140] “SIGRAFIL C PAN-based Carbon Fiber SGL CARBON.” [Online]. Available:  
10 [https://www.sglgroup.com/cms/international/products/product-groups/cf/carbon-  
11 fiber-continuous-tow/index.html?\\_\\_locale=en](https://www.sglgroup.com/cms/international/products/product-groups/cf/carbon-fiber-continuous-tow/index.html?__locale=en). [Accessed: 24-Jan-2019].
- 12 [141] “GRANOC Yarn | Nippon Graphite Fiber Corporation | Unique properties of  
13 GRANOC contribute to the development of advanced technology.” [Online].  
14 Available: [http://www.ngfworld.com/en/en\\_product/en\\_yarn.html](http://www.ngfworld.com/en/en_product/en_yarn.html). [Accessed:  
15 24-Jan-2019].
- 16 [142] S. Yajima, Y. Hasegawa, K. Okamura, and T. Matsuzawa, “Development of high  
17 tensile strength silicon carbide fibre using an organosilicon polymer precursor,”  
18 *Nature*, vol. 273, no. 5663, pp. 525–527, Jun. 1978.
- 19 [143] W. Caputo, AJ (Caputo, Aj); Lackey, WJ (Lackey, “Continued Development of  
20 the Fabrication of Ceramic Fiber-Reinforced Ceramic Composites,” *Am. Ceram.*  
21 *Soc. Bull.*, vol. 63, no. 12, pp. 1477–1477, 1984.
- 22 [144] D. Schawaller, B. Clauß, and M. R. Buchmeiser, “Ceramic Filament Fibers - A  
23 Review,” *Macromol. Mater. Eng.*, vol. 297, no. 6, pp. 502–522, Jun. 2012.
- 24 [145] A. R. Bunsell and A. Piant, “A review of the development of three generations of  
25 small diameter silicon carbide fibres,” *J. Mater. Sci.*, vol. 41, no. 3, pp. 823–839,  
26 Feb. 2006.
- 27 [146] O. Flores, R. K. Bordia, D. Nestler, W. Krenkel, and G. Motz, “Ceramic Fibers  
28 Based on SiC and SiCN Systems: Current Research, Development, and  
29 Commercial Status,” *Adv. Eng. Mater.*, vol. 16, no. 6, pp. 621–636, Jun. 2014.
- 30 [147] J. A. DiCarlo and H.-M. Yun, “Non-oxide (Silicon Carbide) Fibers,” in  
31 *Handbook of Ceramic Composites*, Springer, Boston, MA, 2005, pp. 33–52.
- 32 [148] “Silicon Carbide Fibre| TISICS Ltd.” [Online]. Available:  
33 <https://www.tisics.co.uk/Silicon-Carbide-Fibre>. [Accessed: 06-Jan-2019].
- 34 [149] “Specialty Materials, Inc. - Boron Fiber, SCS Silicon Carbide Fibers and Boron  
35 Nanopowder.” [Online]. Available: <http://specmaterials.com/>. [Accessed: 06-Jan-  
36 2019].
- 37 [150] R. Leucht and H. J. Dudek, “Properties of SiC-fibre reinforced titanium alloys  
38 processed by fibre coating and hot isostatic pressing,” *Mater. Sci. Eng. A*, vol.  
39 188, no. 1–2, pp. 201–210, Nov. 1994.
- 40 [151] S. Yajima, Y. Hasegawa, J. Hayashi, and M. Imura, “Synthesis of continuous  
41 silicon carbide fibre with high tensile strength and high Young’s modulus,” *J.*  
42 *Mater. Sci.*, vol. 13, no. 12, pp. 2569–2576, Dec. 1978.
- 43 [152] N. P. Bansal, *Handbook of Ceramic Composites*. Springer US, 2005.
- 44 [153] Y. Lipowitz, J., Rabe, J. A., Zangvil, A. & Xu, “Structure and Properties of  
45 Sylramic™ Silicon Carbide Fiber—A Polycrystalline, Stoichiometric  $\beta$ - Sic  
46 Composition,” in *Proceedings of the 21 st Annual Conference on Composites,*  
47 *Advanced Ceramics, Materials, and Structures-A*, 1997, vol. January 12-16, pp.  
48 147–157.
- 49 [154] J. DiCarlo, *Advances in SiC/SiC Composites for Aero-Propulsion in Ceramic*  
50 *matrix composites : materials, modeling and technology*. 2015.

- 1 [155] “GE Aviation is fired up about CMCs! | The GE Aviation Blog | Aerospace  
2 & Flight News,” 2015. [Online]. Available:  
3 <https://blog.geaviation.com/manufacturing/ge-aviation-fired-up-about-cmcs/>.  
4 [Accessed: 30-Apr-2019].
- 5 [156] R. Naslain *et al.*, “Boron Nitride Interphase in Ceramic-Matrix Composites,” *J.*  
6 *Am. Ceram. Soc.*, vol. 74, no. 10, pp. 2482–2488, Oct. 1991.
- 7 [157] J. A. Dever, M. V. Nathal, and J. A. DiCarlo, “Research on High-Temperature  
8 Aerospace Materials at NASA Glenn Research Center,” *J. Aerosp. Eng.*, vol. 26,  
9 no. 2, pp. 500–514, Apr. 2013.
- 10 [158] S. Johnson and M. Gasch, “Assessment of the State of the Art of Ultra High  
11 Temperature Ceramics,” Moffett Field, 2009.
- 12 [159] C. Yan, R. Liu, C. Zhang, and Y. Cao, “Zirconium carbide, hafnium carbide and  
13 their ternary carbide nanoparticles by an in situ polymerization route,” *RSC Adv.*,  
14 vol. 5, no. 46, pp. 36520–36529, 2015.
- 15 [160] K. Nakane, S. Matsuoka, S. Gao, S. Yonezawa, J. H. Kim, and N. Ogata,  
16 “Formation of inorganic nanofibers by heat-treatment of poly(vinyl alcohol)-  
17 zirconium compound hybrid nanofibers,” *J. Min. Metall. Sect. B Metall.*, vol. 49,  
18 no. 1, pp. 77–82, 2013.
- 19 [161] X. M. Cui, Y. S. Nam, J. Y. Lee, and W. H. Park, “Fabrication of zirconium  
20 carbide (ZrC) ultra-thin fibers by electrospinning,” *Mater. Lett.*, vol. 62, no. 12–  
21 13, pp. 1961–1964, Apr. 2008.
- 22 [162] R. Ghelich, R. Mehdinavaz Aghdam, F. S. Torknik, M. R. Jahannama, and M.  
23 Keyanpour-Rad, “Carbothermal reduction synthesis of ZrB<sub>2</sub> nanofibers via pre-  
24 oxidized electrospun zirconium n-propoxide,” *Ceram. Int.*, vol. 41, no. 5, pp.  
25 6905–6911, Jun. 2015.
- 26 [163] I. Hasegawa, Y. Fukuda, and M. Kajiwara, “Inorganic–organic hybrid route to  
27 synthesis of ZrC and Si–Zr–C fibres,” *Ceram. Int.*, vol. 25, no. 6, pp. 523–527,  
28 Aug. 1999.
- 29 [164] X. Tao *et al.*, “A facile method to prepare ZrC nanofibers by electrospinning and  
30 pyrolysis of polymeric precursors,” *Ceram. Int.*, vol. 43, no. 4, pp. 3910–3914,  
31 Mar. 2017.
- 32 [165] F. Li, Z. Kang, X. Huang, and G.-J. Zhang, “Fabrication of zirconium carbide  
33 nanofibers by electrospinning,” *Ceram. Int.*, vol. 40, no. 7, pp. 10137–10141,  
34 Aug. 2014.
- 35 [166] J. S. Atchison, M. Zeiger, A. Tolosa, L. M. Funke, N. Jäckel, and V. Presser,  
36 “Electrospinning of ultrafine metal oxide/carbon and metal carbide/carbon  
37 nanocomposite fibers,” *RSC Adv.*, vol. 5, no. 45, pp. 35683–35692, 2015.
- 38 [167] “MATECH | Military Advanced Technology.” [Online]. Available:  
39 <http://www.matech.net/>. [Accessed: 06-Jan-2019].
- 40 [168] K. Pope, E.J.A. and Kratsch and Pope E.J.A and Kratsch K.M, “Pre-ceramic  
41 polymers to hafnium carbide and hafnium nitride ceramic fibers and matrices,”  
42 10/058,808, 2002.
- 43 [169] E. J. A. Pope, “Ultra-High-Temperature Refractory Metal Carbide CMC’s.,” in  
44 *29th Annual Conference on Composites, Materials and Structures (U.S. Only/ITAR restricted)* (2005), 2005.
- 45 [170] E. J. A. Pope, “Pre-ceramic Polymers to Hafnium Carbide Fibres and Matrices.,”  
46 in *National Space and Missile Materials Symposium (U.S. Only/ITAR restricted)*  
47 (2004), 2004.
- 48 [171] E. J. A. . Kratsch *et al.*, “High Temperature and Ultra-High temperature Ceramic  
49 Fibre Development and Applications.,” in *(AFRL, 2009)*, 2009.
- 50  
51  
52  
53  
54  
55  
56  
57  
58  
59  
60  
61  
62  
63  
64  
65

- 1 [172] G. Metcalfe, E. N., W. B., and M. Opeka, "Oxidation Above 3300°C of  
2 Refractory Materials in an Aluminized Flame," in *4th, International Symposium*  
3 *on High Temperature Corrosion and Materials Chemistry Proceedings-*  
4 *Electrochemical Society Pv;*, 2003, pp. 420–430.
- 5 [173] E. J. A. Pope, "TaC<sub>f</sub>/TaC CMCs for Ultra-High-Temperature Applications.," in  
6 *29th Annual Conference on Composites, Materials and Composites (2005).*,  
7 2005.
- 8 [174] K. A. W. Maurice James Evans, "Manufacture of carbon fibre preform Page,"  
9 GB 2234989 A, 1999.
- 10 [175] L. M. Manocha and O. P. Bahl, "Influence of carbon fiber type and weave pattern  
11 on the development of 2D carbon-carbon composites," *Carbon N. Y.*, vol. 26, no.  
12 1, pp. 13–21, 1988.
- 13 [176] C. C. M. Ma;, N. H. Tai;, W. C. Change;, and Y. P. Tsai, "Morphologies,  
14 Microstructure and Mechanical Properties of 2D Carbon/Carbon Composites  
15 during the CVI Densification Process," *Carbon N. Y.*, vol. 34, no. 10, pp. 1175–  
16 1179, 1996.
- 17 [177] S. Berthon and G. Malé, "Infiltration of zirconium diboride by ICVI in porous  
18 materials," *Compos. Sci. Technol.*, vol. 57, no. 2, pp. 217–227, Jan. 1997.
- 19 [178] U. Beier, F. Fischer, J. K. W. Sandler, V. Altstädt, C. Weimer, and W. Buchs,  
20 "Mechanical performance of carbon fibre-reinforced composites based on  
21 stitched preforms," *Compos. Part A Appl. Sci. Manuf.*, vol. 38, no. 7, pp. 1655–  
22 1663, Jul. 2007.
- 23 [179] V. Rubio *et al.*, "Materials characterisation and mechanical properties of C<sub>f</sub>-  
24 UHTC powder composites," *J. Eur. Ceram. Soc.*, vol. 39, no. 4, pp. 813–824,  
25 Apr. 2019.
- 26 [180] P. M. Ajayan, L. S. Schadler, C. Giannaris, and A. Rubio, "Single-Walled  
27 Carbon Nanotube-Polymer Composites: Strength and Weakness," *Adv. Mater.*,  
28 vol. 12, no. 10, pp. 750–753, May 2000.
- 29 [181] Y. Wang, W. Liu, L. Cheng, and L. Zhang, "Preparation and properties of 2D  
30 C/ZrB<sub>2</sub>-SiC ultra high temperature ceramic composites," *Mater. Sci. Eng. A*, vol.  
31 524, no. 1–2, pp. 129–133, Oct. 2009.
- 32 [182] J. Xie, K. Li, H. Li, Q. Fu, and L. Guo, "Ablation behavior and mechanism of  
33 C/C–ZrC–SiC composites under an oxyacetylene torch at 3000°C," *Ceram. Int.*,  
34 vol. 39, no. 4, pp. 4171–4178, May 2013.
- 35 [183] A. Paul, V. Rubio, J. Binner, B. Vaidhyanathan, A. Heaton, and P. Brown,  
36 "Evaluation of the high temperature performance of HfB<sub>2</sub> UHTC particulate  
37 filled C<sub>f</sub>/C composites," *Int. J. Appl. Ceram. Technol.*, vol. 14, no. 3, pp. 344–  
38 353, May 2017.
- 39 [184] J. P. Ai, S. S. Luo, W. K. Li, S. W. Wang, and G. H. Zhou, "Mechanical  
40 Properties and Microstructure of 2.5D C/ZrO<sub>2</sub> Composites Prepared by Precursor  
41 Infiltration and Pyrolysis," *Key Eng. Mater.*, vol. 697, pp. 639–643, Jul. 2016.
- 42 [185] G. Boitier, J. Vicens, and J. . Chermant, "Understanding the creep behavior of a  
43 2.5D C<sub>f</sub>-SiC composite-I. Morphology and microstructure of the as-received  
44 material," *Mater. Sci. Eng. A*, vol. 279, no. 1–2, pp. 73–80, Feb. 2000.
- 45 [186] I. D. B. Baker, V. Rubio, P. Ramanujam, J. Binner, A. Hussain, T. Ackerman, P.  
46 Brown, "Development of a slurry injection technique for continuous fibre ultra-  
47 high temperature ceramic matrix composites (UHTCMCs)," *J. Eur. Ceram. Soc.*,  
48 vol. Under revi, 2019.
- 49 [187] A. Paul, J. G. P. Binner, B. Vaidhyanathan, A. C. J. Heaton, and P. M. Brown,  
50 "Heat flux mapping of oxyacetylene flames and their use to characterise C<sub>f</sub>-HfB<sub>2</sub>  
51  
52  
53  
54  
55  
56  
57  
58  
59  
60  
61  
62  
63  
64  
65

- composites,” *Adv. Appl. Ceram.*, vol. 115, no. 3, pp. 158–165, Apr. 2016.
- [188] A. D’Angio, J. Zou, J. Binner, H. Ma, G. E. Hilmas, and W. G. Fahrenholtz, “Mechanical properties and grain orientation evolution of zirconium diboride-zirconium carbide ceramics,” *J. Eur. Ceram. Soc.*, vol. 38, no. 2, pp. 391–402, Feb. 2018.
- [189] L. A. Timms, W. Westby, C. Prentice, D. Jaglin, R. A. Shatwell, and J. G. P. Binner, “Reducing chemical vapour infiltration time for ceramic matrix composites,” *J. Microsc.*, vol. 201, no. 2, pp. 316–323, Feb. 2001.
- [190] X. Chen, S. Dong, Y. Kan, H. Zhou, J. Hu, and D. Wang, “3D C<sub>f</sub>/SiC-ZrC-ZrB<sub>2</sub> composites fabricated via sol-gel process combined with reactive melt infiltration,” *J. Eur. Ceram. Soc.*, vol. 36, no. 15, pp. 3607–3613, Nov. 2016.
- [191] J. Jiang, S. Wang, W. Li, Z. Chen, and Y. Zhu, “Preparation of 3D C<sub>f</sub>/ZrC–SiC composites by joint processes of PIP and RMI,” *Mater. Sci. Eng. A*, vol. 607, pp. 334–340, Jun. 2014.
- [192] Q. Li *et al.*, “Fabrication and Properties of 3-D C<sub>f</sub>/SiC-ZrC Composites, Using ZrC Precursor and Polycarbosilane,” *J. Am. Ceram. Soc.*, vol. 95, no. 4, pp. 1216–1219, Apr. 2012.
- [193] B. S. Sugun; and R. Sundaram, “3D Composites: Opportunities & Challenges,” *J. Indian Inst. Sci.*, vol. 95:3, no. Jul.–Sep., pp. 1–13, 2016.
- [194] Z. Xie, T. Zhou, and Y. Gou, “Synthesis and characterization of zirconium diboride ceramic precursor,” *Ceram. Int.*, vol. 41, no. 5, Part A, pp. 6226–6231, 2015.
- [195] A. Gao, C. Zhao, S. Luo, Y. Tong, and L. Xu, “Correlation between graphite crystallite distribution morphology and the mechanical properties of carbon fiber during heat treatment,” *Mater. Lett.*, vol. 65, no. 23, pp. 3444–3446, 2011.
- [196] Z. Xie, X. Deng, X. Suo, T. Zhou, and Y. Gou, “Synthesis and characterization of zirconium diboride precursor based on polycentric bridge bonds,” *Mater. Chem. Phys.*, vol. 159, pp. 178–184, 2015.
- [197] M. Zhang, K. zhi Li, X. hong Shi, and W. long Tan, “Effects of SiC interphase on the mechanical and ablation properties of C/C-ZrC-ZrB<sub>2</sub>-SiC composites prepared by precursor infiltration and pyrolysis,” *Mater. Des.*, vol. 122, pp. 322–329, 2017.
- [198] X. Zhao, Y. Wang, L. Duan, L. Luo, and Y. Lu, “Improved ablation resistance of C/SiC-ZrB<sub>2</sub> composites via polymer precursor impregnation and pyrolysis,” *Ceram. Int.*, vol. 43, no. 15, pp. 12480–12489, 2017.
- [199] J. He, Y. Gao, Y. Wang, J. Fang, and L. An, “Synthesis of ZrB<sub>2</sub>-SiC nanocomposite powder via polymeric precursor route,” *Ceram. Int.*, vol. 43, no. 1, pp. 1602–1607, Jan. 2017.
- [200] W. Zhang, C. Xie, M. Ge, and X. Wei, “C/C-ZrB<sub>2</sub>-ZrC-SiC Composites Derived from Polymeric Precursor Infiltration and Pyrolysis Part I,” in *MAX Phases and Ultra-High Temperature Ceramics for Extreme Environments*, C. F. H. Low, I. M., Y. Sakka, Ed. United States of America: IGI Global, 2013, pp. 413–434.
- [201] X. Lv, S. Yu, M. Ge, Y. Tian, and W. Zhang, “Synthesis and microstructure of continuous composite ceramic fibres of ZrC/ZrB<sub>2</sub>-SiC derived from polymeric precursors,” *Ceram. Int.*, vol. 42, no. 7, pp. 9299–9303, May 2016.
- [202] Y. Li, X. Tao, W. Qiu, J. Zhao, and T. Zhao, “Preparation of powdered zirconium diboride by a solution precursor conversion method,” *J. Beijing Univ. Chem. Technol. (Natural Sci. Ed.)*, vol. 37, no. 4, pp. 78–82, 2010.
- [203] G. Takahiro, Y. Hiroshi, H. Takaaki, B. K. Kyoko, and A. Yoshimoto, “Preparation of polyzirconoxane from zirconium oxychloride octahydrate and

- ethylene glycol as a precursor for zirconia ceramics,” *Appl. Organomet. Chem.*, vol. 14, no. 2, pp. 119–126, 2000.
- [204] Y. Abe, T. Kudo, H. Tomioka, T. Gunji, Y. Nagao, and Y. Abe, “Preparation of continuous zirconia fibres from polyzirconoxane synthesized by the facile one-pot reaction,” *J. Mater. Sci.*, vol. 33, no. 7, pp. 1863–1870, Apr. 1998.
- [205] N. Patra, N. Al Nasiri, D. D. Jayaseelan, and W. E. Lee, “Thermal properties of C<sub>f</sub>/HfC and C<sub>f</sub>/HfC-SiC composites prepared by precursor infiltration and pyrolysis,” *J. Eur. Ceram. Soc.*, vol. 38, no. 5, pp. 2297–2303, May 2018.
- [206] M. Yan, H. Li, Q. Fu, J. Xie, L. Liu, and B. Feng, “Ablative Property of C/C–SiC–HfC Composites Prepared via Precursor Infiltration and Pyrolysis under 3,000°C Oxyacetylene Torch,” *Acta Metall. Sin. (English Lett.)*, vol. 27, no. 6, pp. 981–987, Dec. 2014.
- [207] L. Duan, X. Zhao, and Y. Wang, “Comparative ablation behaviors of C/SiC–HfC composites prepared by reactive melt infiltration and precursor infiltration and pyrolysis routes,” *Ceram. Int.*, vol. 43, no. 18, pp. 16114–16120, Dec. 2017.
- [208] D. Huang, M. Zhang, Q. Huang, L. Wang, and K. Tong, “Mechanical Property, Oxidation and Ablation Resistance of C/C–ZrB<sub>2</sub>–ZrC–SiC Composite Fabricated by Polymer Infiltration and Pyrolysis with Preform of C<sub>f</sub>/ZrB<sub>2</sub>,” *J. Mater. Sci. Technol.*, vol. 33, no. 5, pp. 481–486, 2017.
- [209] Q. Li, S. Dong, Z. Wang, and G. Shi, “Fabrication and properties of 3-D C<sub>f</sub>/ZrB<sub>2</sub>–ZrC–SiC composites via polymer infiltration and pyrolysis,” *Ceram. Int.*, vol. 39, no. 5, pp. 5937–5941, Jul. 2013.
- [210] L. Zhuang, Q.-G. Fu, and T.-Y. Liu, “Ablation resistance of wedge-shaped C/C–ZrB<sub>2</sub>–ZrC–SiC composites exposed to an oxyacetylene torch,” *Corros. Sci.*, vol. 112, pp. 462–470, Nov. 2016.
- [211] G. Ziegler, I. Richter, and D. Suttor, “Fiber-reinforced composites with polymer-derived matrix: processing, matrix formation and properties,” *Compos. Part A Appl. Sci. Manuf.*, vol. 30, no. 4, pp. 411–417, 1999.
- [212] C. Yan, R. Liu, C. Zhang, Y. Cao, and X. Long, “Mechanical behaviour and microstructure of C<sub>f</sub>/ZrC, C<sub>f</sub>/SiC and C<sub>f</sub>/ZrC – SiC composites,” *Adv. Appl. Ceram.*, vol. 115, no. 7, pp. 391–395, 2016.
- [213] D. King, Z. Apostolov, T. Key, C. Carney, and M. Cinibulk, “Novel processing approach to polymer-derived ceramic matrix composites,” *Int. J. Appl. Ceram. Technol.*, vol. 15, no. 2, pp. 399–408, 2018.
- [214] “GE Aviation fired up on CMCs.” General Electric, Delaware, US, 2015.
- [215] W. B. Hillig *et al.*, “Fabrication of Ceramic Matrix Composites by Liquid Silicon Infiltration (LSI),” *Ceram. Int.*, vol. 38, no. 2, pp. 191–196, 2012.
- [216] Jeff Crompton and J. Compton, “Multiphysics Analysis of Advanced Materials: Ceramic Matrix Composites | COMSOL Blog,” *COMSOL BLOG*, 2014. [Online]. Available: <https://uk.comsol.com/blogs/multiphysics-analysis-advanced-materials-ceramic-matrix-composites/>. [Accessed: 04-Jan-2019].
- [217] E. O. Einset, “Analysis of reactive melt infiltration in the processing of ceramics and ceramic composites,” *Chem. Eng. Sci.*, vol. 53, no. 5, pp. 1027–1039, Feb. 1998.
- [218] L. Zhang, S. Dong, H. Zhou, Y. Kan, F. Zhou, and Z. Wang, “3D C<sub>f</sub>/ZrC–SiC composites fabricated with ZrC nanoparticles and ZrSi<sub>2</sub> alloy,” *Ceram. Int.*, vol. 40, no. 8, Part A, pp. 11795–11801, 2014.
- [219] X. Chen *et al.*, “Interphase degradation of three-dimensional C<sub>f</sub>/SiC–ZrC–ZrB<sub>2</sub> composites fabricated via reactive melt infiltration,” *J. Am. Ceram. Soc.*, vol. 100, no. 10, pp. 4816–4826, Oct. 2017.

- 1 [220] M. Küttemeyer, L. Schomer, T. Helmreich, S. Rosiwal, and D. Koch, "Fabrication  
2 of ultra high temperature ceramic matrix composites using a reactive melt  
3 infiltration process," *J. Eur. Ceram. Soc.*, vol. 36, no. 15, pp. 3647–3655, Nov.  
4 2016.
- 5 [221] S. Tang and C. Hu, "Design, Preparation and Properties of Carbon Fiber  
6 Reinforced Ultra-High Temperature Ceramic Composites for Aerospace  
7 Applications: A Review," *J. Mater. Sci. Technol.*, vol. 33, no. 2, pp. 117–130,  
8 Feb. 2017.
- 9 [222] Y. Liu, Q. Fu, J. Zhang, L. Li, and L. Zhuang, "Erosion resistance of C/C-SiC-  
10 ZrB<sub>2</sub> composites exposed to oxyacetylene torch," *J. Eur. Ceram. Soc.*, vol. 36,  
11 no. 15, pp. 3815–3821, Nov. 2016.
- 12 [223] W. B. Hillig, "Melt Infiltration Approach to Ceramic Matrix Composites," *J. Am.*  
13 *Ceram. Soc.*, vol. 71, no. 2, p. C- 96-C- 99, 1988.
- 14 [224] Y. Tong, S. Bai, Y. Ye, H. Zhang, and Z. Yang, "Reactive melt infiltration of a  
15 ZrB<sub>2</sub> modified C/ZrC composite by a eutectic Zr–B alloy," *Mater. Lett.*, vol. 138,  
16 pp. 208–211, 2015.
- 17 [225] S. Chen, C. Zhang, Y. Zhang, and H. Hu, "Preparation and properties of carbon  
18 fiber reinforced ZrC–ZrB<sub>2</sub> based composites via reactive melt infiltration,"  
19 *Compos. Part B Eng.*, vol. 60, pp. 222–226, Apr. 2014.
- 20 [226] M. Kutemeyer Helmreich, T., Koch, D., Rosiwal, S., "Influence of Zirconium-  
21 Based Alloys on Manufacturing and Mechanical-Properties of Ultra High  
22 Temperature Ceramic Matrix Composites," *Adv. Appl. Ceram. Struct. Funct.*  
23 *Bioceram.*, vol. Submitted, 2018.
- 24 [227] Y. Tong, S. Bai, and K. Chen, "C/C–ZrC composite prepared by chemical vapor  
25 infiltration combined with alloyed reactive melt infiltration," *Ceram. Int.*, vol. 38,  
26 no. 7, pp. 5723–5730, 2012.
- 27 [228] Z. Li, H. Li, S. Zhang, J. Wang, W. Li, and F. Sun, "Effect of reaction melt  
28 infiltration temperature on the ablation properties of 2D C/C–SiC–ZrC  
29 composites," *Corros. Sci.*, vol. 58, pp. 12–19, 2012.
- 30 [229] Y. Wang, X. Zhu, L. Zhang, and L. Cheng, "Reaction kinetics and ablation  
31 properties of C/C–ZrC composites fabricated by reactive melt infiltration,"  
32 *Ceram. Int.*, vol. 37, no. 4, pp. 1277–1283, 2011.
- 33 [230] L. Zou, N. Wali, J.-M. Yang, and N. P. Bansal, "Microstructural development of  
34 a C<sub>f</sub>/ZrC composite manufactured by reactive melt infiltration," *J. Eur. Ceram.*  
35 *Soc.*, vol. 30, no. 6, pp. 1527–1535, 2010.
- 36 [231] H. Pi, S. Fan, and Y. Wang, "C/SiC–ZrB<sub>2</sub>–ZrC composites fabricated by reactive  
37 melt infiltration with ZrSi<sub>2</sub> alloy," *Ceram. Int.*, vol. 38, no. 8, pp. 6541–6548,  
38 2012.
- 39 [232] X. Chen *et al.*, "Reaction mechanism and microstructure development of ZrSi<sub>2</sub>  
40 melt-infiltrated Cf/SiC-ZrC-ZrB<sub>2</sub> composites: The influence of preform pore  
41 structures," *J. Mater.*, vol. 4, no. 3, pp. 266–275, Sep. 2018.
- 42 [233] M. . Muolo, E. Ferrera, R. Novakovic, and A. Passerone, "Wettability of  
43 zirconium diboride ceramics by Ag, Cu and their alloys with Zr," *Scr. Mater.*,  
44 vol. 48, no. 2, pp. 191–196, Jan. 2003.
- 45 [234] Y. Wang, Q. Liu, J. Liu, L. Zhang, and L. Cheng, "Deposition Mechanism for  
46 Chemical Vapor Deposition of Zirconium Carbide Coatings," *J. Am. Ceram.*  
47 *Soc.*, vol. 91, no. 4, pp. 1249–1252, Apr. 2008.
- 48 [235] A. Allemand *et al.*, "Protection against Oxydation by CVD or SPS Coatings of  
49 Hafnium Carbide and Silicon Carbide on Carbon/Carbon Composites," *Adv.*  
50 *Ceram. Coatings Mater. Extrem. Environ. II*, pp. 161-169., 2013.
- 51  
52  
53  
54  
55  
56  
57  
58  
59  
60  
61  
62  
63  
64  
65



- 1 [236] H. O. Pierson, *Handbook of refractory carbides and nitrides: Properties,*  
2 *characteristics, processing and applications.* Noyes Publication, New York, NY  
3 (United States), 1997.
- 4 [237] H. Pierson, *Handbook of Chemical Vapour Deposition: Principles, Technology*  
5 *and Applications.* New York: William Andrew Publishing, 1999.
- 6 [238] J. Arnold, J. O., Y.K. Chen, T. Squire, D. Srivastava, G. Allen and E. V. and M.  
7 P. L. M. Stackpoole, H. E. Goldstein, “Nanostructured Thermal Protection  
8 Systems for Space Exploration Missions,” 2004.
- 9 [239] V. Wunder et al., “Multilayer coatings on CFC composites for high-temperature  
10 applications,” *Surf. Coatings Technol.*, vol. 100, pp. 329-332., 1998.
- 11 [240] C. Subramanian and K. N. Strafford, “Review of multicomponent and multilayer  
12 coatings for tribological applications,” *Wear*, vol. 165, no. 1, pp. 85–95, 1993.
- 13 [241] F. Smeacetto *et al.*, “Protective coatings for carbon bonded carbon fibre  
14 composites,” *Ceram. Int.*, 2008.
- 15 [242] I. Golecki, “Rapid vapor-phase densification of refractory composites.,” *Mater.*  
16 *Sci. Eng. R-Reports*, vol. 20, no. 2, pp. 37-124., 1997.
- 17 [243] J. Y. Ofori; and S. V Sotirchos, “Optimal pressures and temperatures for isobaric,  
18 isothermal chemical vapor infiltration,” *Aiche J.*, vol. 42, no. 10, pp. 2828-2840.,  
19 1996.
- 20 [244] X. Ma Yin, X., Cao, X., Chen, L., Cheng, L., and Zhang, L., “Effect of heat  
21 treatment on the mechanical properties of SiC<sub>f</sub>/BN/SiC fabricated by CVI,”  
22 *Ceram. Int.*, vol. 42, no. 2, pp. 3652-3658., 2016.
- 23 [245] R. Naslain Hannache, H., Heraud, L., Christin, F., Rossignol, J.Y., and Colmet,  
24 R., “Advanced Ceramic-Ceramic Composite-Materials from the CVI Process,”  
25 *Am. Ceram. Soc. Bull.*, vol. 62, no. 11, 1983.
- 26 [246] R. Naslain, F. Langlais, and R. Fedou, “The Cvi-Processing of Ceramic Matrix  
27 Composites,” *Le J. Phys. Colloq.*, vol. 50, no. C5, pp. 191–207, May 1989.
- 28 [247] K. Yee, “Protective coatings for metals by chemical vapour deposition,” *Int. Met.*  
29 *Rev.*, vol. 23, no. 1, pp. 19-42., 1978.
- 30 [248] H.-J. Li, H. Xue, Y.-J. Wang, Q.-G. Fu, and D.-J. Yao, “A MoSi<sub>2</sub>–SiC–Si  
31 oxidation protective coating for carbon/carbon composites,” *Surf. Coatings*  
32 *Technol.*, vol. 201, no. 24, pp. 9444–9447, Oct. 2007.
- 33 [249] A. Lazzeri, “CVI Processing of Ceramic Matrix Composites,” in *Ceramics and*  
34 *Composites Processing Methods*, Hoboken, NJ, USA: John Wiley & Sons, Inc.,  
35 2012, pp. 313–349.
- 36 [250] G. Q. Lu, “Modelling the densification of porous structures in CVI ceramic  
37 composites processing,” *J. Mater. Process. Technol.*, vol. 37, no. 1–4, pp. 487–  
38 498, Feb. 1993.
- 39 [251] J. M. Rosas, J. Bedia-Matamoros, J. Rodríguez-Mirasol, and T. Cordero,  
40 “Kinetics of pyrolytic carbon infiltration for the preparation of ceramic/carbon  
41 and carbon/carbon composites,” *Carbon N. Y.*, vol. 42, no. 7, pp. 1285–1290,  
42 Jan. 2004.
- 43 [252] Y. S. Lin and A. J. Burggraaf, “Modelling and analysis of CVD processes in  
44 porous media for ceramic composite preparation,” *Chem. Eng. Sci.*, vol. 46, no.  
45 12, pp. 3067–3080, Jan. 1991.
- 46 [253] J. P. Dekker, R. Moene, and J. Schoonman, “The influence of surface kinetics in  
47 modelling chemical vapour deposition processes in porous preforms,” *J. Mater.*  
48 *Sci.*, vol. 31, pp. 3021–3033, 1996.
- 49 [254] D. Sciti, L. Silvestroni, F. Monteverde, A. Vinci, and L. Zoli, “Introduction to  
50 H2020 project C 3 HARME – next generation ceramic composites for  
51  
52  
53  
54  
55  
56  
57  
58  
59  
60  
61  
62  
63  
64  
65

- combustion harsh environment and space,” *Adv. Appl. Ceram.*, vol. 117, no. sup1, pp. 70–75, Oct. 2018.
- [255] M. Balasubramanian, *Composite Materials and Processing*. CRC Press, 2013.
- [256] F. F. Lange, W. C. Tu, and A. G. Evans, “Processing of damage-tolerant, oxidation-resistant ceramic matrix composites by a precursor infiltration and pyrolysis method,” *Mater. Sci. Eng. A*, vol. 195, pp. 145–150, Jun. 1995.
- [257] J. S. Reed, “Liquid Permeability of Packed Particles: Why Perpetuate the Carmen-Kozeny Model?,” *J. Am. Ceram. Soc.*, vol. 76, no. 2, pp. 547–548, Feb. 1993.
- [258] S.-H. Lee, M. Weinmann, and F. Aldinger, “Fabrication of Fiber-Reinforced Ceramic Composites by the Modified Slurry Infiltration Technique,” *J. Am. Ceram. Soc.*, vol. 90, no. 8, pp. 2657–2660, Aug. 2007.
- [259] A. V. Vasin *et al.*, “Amorphous  $\text{SiO}_x\text{C}_y$  (:Er) films deposited by RF-magnetron sputtering on  $\text{ZrB}_2$ –SiC ceramics: Antioxidation and strengthening effects,” *Surf. Coatings Technol.*, vol. 343, pp. 11–16, Jun. 2018.
- [260] D. D. Jayaseelan, R. G. de Sá, P. Brown, and W. E. Lee, “Reactive infiltration processing (RIP) of ultra high temperature ceramics (UHTC) into porous C/C composite tubes,” *J. Eur. Ceram. Soc.*, vol. 31, no. 3, pp. 361–368, Mar. 2011.
- [261] J. D. Buckley and D. D. (Dan D. Edie, *Carbon-carbon materials and composites*. Noyes Publications, 1993.
- [262] L. Li, H. Li, Y. Li, X. Yin, Q. Shen, and Q. Fu, “A SiC– $\text{ZrB}_2$ –ZrC coating toughened by electrophoretically-deposited SiC nanowires to protect C/C composites against thermal shock and oxidation,” *Appl. Surf. Sci.*, vol. 349, pp. 465–471, Sep. 2015.
- [263] M. D. Alvey and P. M. George, “ $\text{ZrPt}_3$  as a high-temperature, reflective, oxidation-resistant coating for carbon-carbon composites,” *Carbon N. Y.*, vol. 29, no. 4–5, pp. 523–530, Jan. 1991.
- [264] Y. Yan, Z. Huang, S. Dong, and D. Jiang, “New Route to Synthesize Ultra-Fine Zirconium Diboride Powders Using Inorganic/Organic Hybrid Precursors,” *J. Am. Ceram. Soc.*, vol. 89, no. 11, pp. 3585–3588, Nov. 2006.
- [265] J. A. Jensen, J. E. Gozum, D. M. Pollina, and G. S. Girolami, “Titanium, zirconium, and hafnium tetrahydroborates as ‘tailored’ CVD precursors for metal diboride thin films,” *J. Am. Chem. Soc.*, vol. 110, no. 5, pp. 1643–1644, Mar. 1988.
- [266] D. W. McKee, “Oxidation behavior and protection of carbon/carbon composites,” *Carbon N. Y.*, vol. 25, no. 4, pp. 551–557, Jan. 1987.
- [267] Q. He, H. Li, C. Wang, S. Chen, and J. Lu, “Densification behavior and ablation property of C/C–ZrC composites prepared by chemical liquid vapor deposition process at temperatures from 800 to 1100 °C,” *Ceram. Int.*, vol. 44, no. 7, pp. 7991–8004, May 2018.
- [268] J. Pourasad, N. Ehsani, and Z. Valefi, “Oxidation resistance of a SiC– $\text{ZrB}_2$  coating prepared by a novel pack cementation on SiC-coated graphite,” *J. Mater. Sci.*, vol. 52, no. 3, pp. 1639–1646, Feb. 2017.
- [269] J. Prakash, M. Gade, B. Paul, and K. Dasgupta, “A facile route for graded conversion of carbon fabric to silicon carbide fabric and its oxidation kinetics study in atmospheric high-temperature environment,” *Bull. Mater. Sci.*, vol. 41, no. 4, p. 108, Aug. 2018.
- [270] H. Mei, Q. Bai, T. Ji, H. Li, and L. Cheng, “Effect of carbon nanotubes electrophoretically-deposited on reinforcing carbon fibers on the strength and toughness of C/SiC composites,” *Compos. Sci. Technol.*, vol. 103, pp. 94–99,

Oct. 2014.

- 1 [271] J. Guo and C. Lu, "Continuous preparation of multiscale reinforcement by  
2 electrophoretic deposition of carbon nanotubes onto carbon fiber tows," *Carbon*  
3 *N. Y.*, vol. 50, no. 8, pp. 3101–3103, Jul. 2012.
- 4 [272] T. Feng, H.-J. Li, X.-H. Shi, X. Yang, and S.-L. Wang, "Oxidation and ablation  
5 resistance of ZrB<sub>2</sub>–SiC–Si/B-modified SiC coating for carbon/carbon  
6 composites," *Corros. Sci.*, vol. 67, pp. 292–297, Feb. 2013.
- 7 [273] X. Yao, H. Li, Y. Zhang, H. Wu, and X. Qiang, "A SiC–Si–ZrB<sub>2</sub> multiphase  
8 oxidation protective ceramic coating for SiC-coated carbon/carbon composites,"  
9 *Ceram. Int.*, vol. 38, no. 3, pp. 2095–2100, Apr. 2012.
- 10 [274] E. L. Corral and R. E. Loehman, "Ultra-High-Temperature Ceramic Coatings for  
11 Oxidation Protection of Carbon–Carbon Composites," *J. Am. Ceram. Soc.*, vol.  
12 91, no. 5, pp. 1495–1502, May 2008.
- 13 [275] P. Galizia, S. Failla, L. Zoli, and D. Sciti, "Tough salami-inspired C<sub>f</sub>/ZrB<sub>2</sub>  
14 UHTCMCs produced by electrophoretic deposition," *J. Eur. Ceram. Soc.*, vol.  
15 38, no. 2, pp. 403–409, Feb. 2018.
- 16 [276] K. Xiao, Q. Guo, Z. Liu, S. Zhao, and Y. Zhao, "Influence of fiber coating  
17 thickness on microstructure and mechanical properties of carbon fiber-reinforced  
18 zirconium diboride based composites," *Ceram. Int.*, vol. 40, no. 1, pp. 1539–  
19 1544, Jan. 2014.
- 20 [277] C. Kim, D. S. Grummon, and G. Gottstein, "Processing and interface  
21 characteristics of graphite fiber reinforced tantalum carbide matrix composites,"  
22 *Scr. Metall. Mater.*, vol. 25, no. 10, pp. 2351–2356, Oct. 1991.
- 23 [278] L. Zoli, V. Medri, C. Melandri, and D. Sciti, "Continuous SiC fibers–ZrB<sub>2</sub>  
24 composites," *J. Eur. Ceram. Soc.*, vol. 35, no. 16, pp. 4371–4376, Dec. 2015.
- 25 [279] D. Sciti, A. Natali Murri, V. Medri, and L. Zoli, "Continuous C fibre composites  
26 with a porous ZrB<sub>2</sub> Matrix," *Mater. Des.*, vol. 85, pp. 127–134, Nov. 2015.
- 27 [280] D. Sciti, L. Pienti, A. Natali Murri, E. Landi, V. Medri, and L. Zoli, "From  
28 random chopped to oriented continuous SiC fibers–ZrB<sub>2</sub> composites," *Mater.*  
29 *Des.*, vol. 63, pp. 464–470, Nov. 2014.
- 30 [281] L. Zoli, A. Vinci, P. Galizia, C. Melandri, and Di. Sciti, "On the thermal shock  
31 resistance and mechanical properties of novel unidirectional UHTCMCs for  
32 extreme environments," *Sci. Rep.*, vol. 8, no. 1, p. 9148, Dec. 2018.
- 33 [282] R. Naslain and W. Krenkel, *Ceramic Matrix Composites*, vol. 22-26 June, no. 13.  
34 Weinheim, Germany: Wiley-VCH Verlag GmbH & Co. KGaA, 2008.
- 35 [283] L. Zoli and D. Sciti, "Efficacy of a ZrB<sub>2</sub>–SiC matrix in protecting C fibres from  
36 oxidation in novel UHTCMC materials," *Mater. Des.*, vol. 113, pp. 207–213,  
37 Jan. 2017.
- 38 [284] S. H. Lee, H. D. Kim, and Y. Kagawa, "SiC–ZrB<sub>2</sub> Fiber-Reinforced Composites  
39 Prepared by Spark Plasma Sintering," in *ICCM17 proceedings*, 2017, pp. 1–10.
- 40 [285] L. Silvestroni, M. Nygren, and D. Sciti, "Study of the interactions between HfB<sub>2</sub>  
41 and Hi-Nicalon™ fiber," *J. Eur. Ceram. Soc.*, vol. 33, no. 15–16, pp. 2879–2888,  
42 Dec. 2013.
- 43 [286] V. Rubio, J. Binner, A. T Ackerman, S. Cousinet, N. Pommepuy, and X.  
44 Bertrand, "Ultra high temperature ceramic composite materials," in *ECI*  
45 *Symposium Series*, (2017), 2017.
- 46 [287] J. Zou *et al.*, "A top-down approach to densify ZrB<sub>2</sub>–SiC–BN composites with  
47 deeper homogeneity and improved reliability," *Chem. Eng. J.*, vol. 249, pp. 93–  
48 101, Aug. 2014.
- 49 [288] A. Vinci, L. Zoli, D. Sciti, C. Melandri, and S. Guicciardi, "Understanding the  
50  
51  
52  
53  
54  
55  
56  
57  
58  
59  
60  
61  
62  
63  
64  
65

- mechanical properties of novel UHTCMCs through random forest and regression tree analysis,” *Mater. Des.*, vol. 145, pp. 97–107, May 2018.
- [289] P. Hu, D. Zhang, S. Dong, Q. Qu, and X. Zhang, “A novel vibration-assisted slurry impregnation to fabricate  $C_f/ZrB_2$ -SiC composite with enhanced mechanical properties,” *J. Eur. Ceram. Soc.*, vol. 39, no. 4, pp. 798–805, Apr. 2019.
- [290] D. Huang *et al.*, “Ablation mechanism of C/C– $ZrB_2$ –ZrC–SiC composite fabricated by polymer infiltration and pyrolysis with preform of  $C_f/ZrB_2$ ,” *Corros. Sci.*, vol. 98, pp. 551–559, Sep. 2015.
- [291] D. Liu, W.-F. Qiu, T. Cai, Y. Sun, A.-J. Zhao, and T. Zhao, “Synthesis, Characterization, and Microstructure of ZrC/SiC Composite Ceramics via Liquid Precursor Conversion Method,” *J. Am. Ceram. Soc.*, vol. 97, no. 4, pp. 1242–1247, Apr. 2014.
- [292] P. Hu, K. Gui, W. Hong, X. Zhang, and S. Dong, “High-performance  $ZrB_2$ -SiC- $C_f$  composite prepared by low-temperature hot pressing using nanosized  $ZrB_2$  powder,” *J. Eur. Ceram. Soc.*, vol. 37, no. 6, pp. 2317–2324, Jun. 2017.
- [293] Y. Zhu, L. Cheng, M. Li, B. Ma, Y. Liu, and L. Zhang, “The synthesis and characterization of CVD  $ZrB_2$  coating from  $ZrCl_4$ - $BCl_3$ - $H_2$ -Ar system,” *Ceram. Int.*, vol. 44, no. 2, pp. 2002–2010, Feb. 2018.
- [294] Z. Wang *et al.*, “Fabrication and Properties of  $C_f$ /SiC-ZrC Composites,” *J. Am. Ceram. Soc.*, vol. 91, no. 10, pp. 3434–3436, Oct. 2008.
- [295] L. Zou, N. Wali, J.-M. Yang, N. P. Bansal, and D. Yan, “Microstructural Characterization of a  $C_f$ /ZrC Composite Manufactured by Reactive Melt Infiltration,” *Int. J. Appl. Ceram. Technol.*, vol. 8, no. 2, pp. 329–341, Mar. 2011.
- [296] D.-W. Ni *et al.*, “Fabrication and properties of  $C_f$ /ZrC-SiC-based composites by an improved reactive melt infiltration,” *J. Am. Ceram. Soc.*, vol. 101, no. 8, pp. 3253–3258, Aug. 2018.
- [297] Y. Zeng *et al.*, “Ablation-resistant carbide  $Zr_{0.8}Ti_{0.2}C_{0.74}B_{0.26}$  for oxidizing environments up to 3,000 °C,” *Nat. Commun.*, vol. 8, p. 15836, Jun. 2017.
- [298] A. Rezaie, W. G. Fahrenholtz, and G. E. Hilmas, “Effect of hot pressing time and temperature on the microstructure and mechanical properties of  $ZrB_2$ -SiC,” *J. Mater. Sci.*, vol. 42, no. 8, pp. 2735–2744, Apr. 2007.
- [299] J. Zou *et al.*, “High-temperature bending strength, internal friction and stiffness of  $ZrB_2$ -20vol% SiC ceramics,” *J. Eur. Ceram. Soc.*, vol. 32, no. 10, pp. 2519–2527, Aug. 2012.
- [300] E. W. Neuman, G. E. Hilmas, and W. G. Fahrenholtz, “Mechanical behavior of zirconium diboride–silicon carbide–boron carbide ceramics up to 2200°C,” *J. Eur. Ceram. Soc.*, vol. 35, no. 2, pp. 463–476, Feb. 2015.
- [301] J. Zou, G.-J. Zhang, J. Vleugels, and O. Van der Biest, “High temperature strength of hot pressed  $ZrB_2$ -20vol% SiC ceramics based on  $ZrB_2$  starting powders prepared by different carbo/boro-thermal reduction routes,” *J. Eur. Ceram. Soc.*, vol. 33, no. 10, pp. 1609–1614, Sep. 2013.
- [302] P. Hu and Z. Wang, “Flexural strength and fracture behavior of  $ZrB_2$ -SiC ultra-high temperature ceramic composites at 1800°C,” *J. Eur. Ceram. Soc.*, vol. 30, no. 4, pp. 1021–1026, Mar. 2010.
- [303] J. Zou, H.-B. Ma, A. D’Angio, and G.-J. Zhang, “Tungsten carbide: A versatile additive to get trace alkaline-earth oxide impurities out of  $ZrB_2$  based ceramics,” *Scr. Mater.*, vol. 147, pp. 40–44, Apr. 2018.
- [304] L. Silvestroni, H.-J. Kleebe, W. G. Fahrenholtz, and J. Watts, “Super-strong materials for temperatures exceeding 2000°C,” *Sci. Rep.*, vol. 7, no. 1, p. 40730,

Feb. 2017.

- 1 [305] J. Zou *et al.*, “Strong ZrB<sub>2</sub>-SiC-WC Ceramics at 1600°C,” *J. Am. Ceram. Soc.*,  
2 vol. 95, no. 3, pp. 874–878, Feb. 2012.
- 3 [306] X. Chen *et al.*, “Microstructure and mechanical properties of three dimensional  
4 C<sub>f</sub>/SiC-ZrC-ZrB<sub>2</sub> composites prepared by reactive melt infiltration method,” *J.*  
5 *Eur. Ceram. Soc.*, vol. 36, no. 16, pp. 3969–3976, Dec. 2016.
- 6 [307] D. Wang, Y. Wang, J. Rao, J. Ouyang, Y. Zhou, and G. Song, “Influence of  
7 reactive melt infiltration parameters on microstructure and properties of low  
8 temperature derived Cf/ZrC composites,” *Mater. Sci. Eng. A*, vol. 568, pp. 25–  
9 32, Apr. 2013.
- 10 [308] D. Zhao, C. Zhang, H. Hu, and Y. Zhang, “Preparation and characterization of  
11 three-dimensional carbon fiber reinforced zirconium carbide composite by  
12 precursor infiltration and pyrolysis process,” *Ceram. Int.*, vol. 37, no. 7, pp.  
13 2089–2093, Sep. 2011.
- 14 [309] P. Galizia, L. Zoli, and D. Sciti, “Impact of residual stress on thermal damage  
15 accumulation, and Young’s modulus of fiber-reinforced ultra-high temperature  
16 ceramics,” *Mater. Des.*, vol. 160, pp. 803–809, Dec. 2018.
- 17 [310] Marc Meyers; and K. Chawla, *Mechanical Behaviour of Materials*, Second edi.  
18 Cambridge: Cambridge university press, 2008.
- 19 [311] S. V. Nair, T.-J. Gwo, N. M. Narbut, J. G. Kohl, and G. J. Sundberg,  
20 “Mechanical Behavior of a Continuous-SiC-Fiber-Reinforced RBSN-Matrix  
21 Composite,” *J. Am. Ceram. Soc.*, vol. 74, no. 10, pp. 2551–2558, Oct. 1991.
- 22 [312] N. M. Narbut, “Mechanical Behavior of a Continuous Fiber Reinforced  
23 SiC/RBSN Ceramic Composite,” University of Massachusetts Amherst, 1992.
- 24 [313] J. Zou, G.-J. Zhang, Y.-M. Kan, and P.-L. Wang, “Hot-Pressed ZrB<sub>2</sub>- SiC  
25 Ceramics with VC Addition: Chemical Reactions, Microstructures, and  
26 Mechanical Properties,” *J. Am. Ceram. Soc.*, vol. 92, no. 12, pp. 2838–2846, Dec.  
27 2009.
- 28 [314] J. Zou, G.-J. Zhang, H. Zhang, Z.-R. Huang, J. Vleugels, and O. Van der Biest,  
29 “Improving high temperature properties of hot pressed ZrB<sub>2</sub>-20vol% SiC  
30 ceramic using high purity powders,” *Ceram. Int.*, vol. 39, no. 1, pp. 871–876,  
31 Jan. 2013.
- 32 [315] D. Munz, “What Can We Learn from R-Curve Measurements?,” *J. Am. Ceram.*  
33 *Soc.*, vol. 90, no. 1, pp. 1–15, Jan. 2007.
- 34 [316] F. Zok, O. Sbaizero, C. L. Hom, and A. G. Evans, “Mode I Fracture Resistance  
35 of a Laminated Fiber-Reinforced Ceramic,” *J. Am. Ceram. Soc.*, vol. 74, no. 1,  
36 pp. 187–193, Jan. 1991.
- 37 [317] H. Ming Yuan and J. W. Hutchinson, “Crack deflection at an interface between  
38 dissimilar elastic materials,” *Int. J. Solids Struct.*, vol. 25, no. 9, pp. 1053–1067,  
39 1989.
- 40 [318] M. Y. He and J. W. Hutchinson, “Kinking of a Crack Out of an Interface,” *J.*  
41 *Appl. Mech.*, vol. 56, no. 2, p. 270, 1989.
- 42 [319] L. Silvestroni, D. Sciti, G. E. Hilmas, W. G. Fahrenholtz, and J. Watts, “Effect of  
43 a weak fiber interface coating in ZrB<sub>2</sub> reinforced with long SiC fibers,” *Mater.*  
44 *Des.*, vol. 88, pp. 610–618, Dec. 2015.
- 45 [320] P. Hu *et al.*, “Damage mechanism analysis to the carbon fiber and fiber-ceramic  
46 interface tailoring of C<sub>f</sub>/ZrC-SiC using PyC coating,” *Ceram. Int.*, vol. 44, no. 15,  
47 pp. 19038–19043, Oct. 2018.
- 48 [321] M. MInus and S. Kumar, “The processing, properties, and structure of carbon  
49 fibers,” *JOM*, vol. 57, no. 2, pp. 52–58, Feb. 2005.
- 50  
51  
52  
53  
54  
55  
56  
57  
58  
59  
60  
61  
62  
63  
64  
65

- 1 [322] J. W. Zimmermann, G. E. Hilmas, W. G. Fahrenholtz, R. B. Dinwiddie, W. D.  
2 Porter, and H. Wang, "Thermophysical Properties of ZrB<sub>2</sub> and ZrB<sub>2</sub>-SiC  
3 Ceramics," *J. Am. Ceram. Soc.*, vol. 91, no. 5, pp. 1405–1411, May 2008.
- 4 [323] Q. Ding *et al.*, "Mechanical properties and microstructure evolution of 3D C<sub>f</sub>  
5 /SiBCN composites at elevated temperatures," *J. Am. Ceram. Soc.*, vol. 101, no.  
6 10, pp. 4699–4707, Oct. 2018.
- 7 [324] A. Raffray *et al.*, "Design and material issues for high performance SiC<sub>f</sub>/SiC-  
8 based fusion power cores," *Fusion Eng. Des.*, vol. 55, no. 1, pp. 55–95, May  
9 2001.
- 10 [325] R. Loehman, E. Corral, H. P. Dumm, P. Kotula, and R. Tandon, "Ultra High  
11 Temperature Ceramics for Hypersonic Vehicle Applications," 2006.
- 12 [326] Q. Fu, J. Jing, B. Tan, R. Yuan, L. Zhuang, and L. Li, "Nanowire-toughened  
13 transition layer to improve the oxidation resistance of SiC–MoSi<sub>2</sub>–ZrB<sub>2</sub> coating  
14 for C/C composites," *Corros. Sci.*, vol. 111, pp. 259–266, Oct. 2016.
- 15 [327] S. Tang, J. Deng, S. Wang, and W. Liu, "Comparison of thermal and ablation  
16 behaviors of C/SiC composites and C/ZrB<sub>2</sub>-SiC composites," *Corros. Sci.*, vol.  
17 51, no. 1, pp. 54–61, Jan. 2009.
- 18 [328] S. Guo, "Thermal and electrical properties of hot-pressed short pitch-based  
19 carbon fiber-reinforced ZrB<sub>2</sub>-SiC matrix composites," *Ceram. Int.*, vol. 39, no. 5,  
20 pp. 5733–5740, Jul. 2013.
- 21 [329] C. Hu, S. Pang, S. Tang, Y. Wang, and H.-M. Cheng, "An integrated composite  
22 with a porous C<sub>f</sub>/C-ZrB<sub>2</sub>-SiC core between two compact outer layers of C<sub>f</sub>/C-  
23 ZrB<sub>2</sub>-SiC and C<sub>f</sub>/C-SiC," *J. Eur. Ceram. Soc.*, vol. 35, no. 3, pp. 1113–1117,  
24 Mar. 2015.
- 25 [330] R. Inoue, Y. Arai, Y. Kubota, K. Goto, and Y. Kogo, "Development of short- and  
26 continuous carbon fiber-reinforced ZrB<sub>2</sub>-SiC-ZrC matrix composites for thermal  
27 protection systems," *Ceram. Int.*, vol. 44, no. 13, pp. 15859–15867, Sep. 2018.
- 28 [331] L. F. He, Y. W. Bao, J. Y. Wang, M. S. Li, and Y. C. Zhou, "Microstructure and  
29 mechanical and thermal properties of ternary carbides in Hf–Al–C system," *Acta*  
30 *Mater.*, vol. 57, no. 9, pp. 2765–2774, May 2009.
- 31 [332] O. Cedillos-Barraza, S. Grasso, N. Al Nasiri, D. D. Jayaseelan, M. J. Reece, and  
32 W. E. Lee, "Sintering behaviour, solid solution formation and characterisation of  
33 TaC, HfC and TaC–HfC fabricated by spark plasma sintering," *J. Eur. Ceram.*  
34 *Soc.*, vol. 36, no. 7, pp. 1539–1548, Jun. 2016.
- 35 [333] L. Pienti, D. Sciti, L. Silvestroni, A. Cecere, and R. Savino, "Ablation tests on  
36 HfC- and TaC-based ceramics for aeropropulsive applications," *J. Eur. Ceram.*  
37 *Soc.*, vol. 35, no. 5, pp. 1401–1411, May 2015.
- 38 [334] M. Mallik, A. J. Kailath, K. K. Ray, and R. Mitra, "Electrical and thermophysical  
39 properties of ZrB<sub>2</sub> and HfB<sub>2</sub> based composites," *J. Eur. Ceram. Soc.*, vol. 32, no.  
40 10, pp. 2545–2555, Aug. 2012.
- 41 [335] G. Shao *et al.*, "High emissivity MoSi<sub>2</sub>-TaSi<sub>2</sub>-borosilicate glass porous coating  
42 for fibrous ZrO<sub>2</sub> ceramic by a rapid sintering method," *J. Alloys Compd.*, vol.  
43 690, pp. 63–71, Jan. 2017.
- 44 [336] J. Kulczyk-Malecka *et al.*, "Thermo – mechanical properties of SPS produced  
45 self-healing thermal barrier coatings containing pure and alloyed MoSi<sub>2</sub>  
46 particles," *J. Eur. Ceram. Soc.*, vol. 38, no. 12, pp. 4268–4275, Sep. 2018.
- 47 [337] S.-Q. Guo, Y. Kagawa, T. Nishimura, D. Chung, and J.-M. Yang, "Mechanical  
48 and physical behavior of spark plasma sintered ZrC–ZrB<sub>2</sub>-SiC composites," *J.*  
49 *Eur. Ceram. Soc.*, vol. 28, no. 6, pp. 1279–1285, Jan. 2008.
- 50 [338] R. W. Harrison and W. E. Lee, "Processing and properties of ZrC, ZrN and ZrCN  
51  
52  
53  
54  
55  
56  
57  
58  
59  
60  
61  
62  
63  
64  
65

- ceramics: a review,” *Adv. Appl. Ceram.*, 2016.
- [339] S. Guo, Y. Kagawa, T. Nishimura, and H. Tanaka, “Thermal and Electric Properties in Hot-Pressed ZrB<sub>2</sub>- MoSi<sub>2</sub> -SiC Composites,” *J. Am. Ceram. Soc.*, vol. 90, no. 7, pp. 2255–2258, Jul. 2007.
- [340] C. Li, K. Li, H. Li, H. Ouyang, Y. Zhang, and L. Guo, “Mechanical and thermophysical properties of carbon/carbon composites with hafnium carbide,” *Ceram. Int.*, vol. 39, no. 6, pp. 6769–6776, Aug. 2013.
- [341] J. Ren, Y. Zhang, P. Zhang, T. Li, J. Li, and Y. Yang, “Ablation resistance of HfC coating reinforced by HfC nanowires in cyclic ablation environment,” *J. Eur. Ceram. Soc.*, vol. 37, no. 8, pp. 2759–2768, Jul. 2017.
- [342] J. F. Justin and A. Jankowiak, “Ultra High Temperature Ceramics: Densification, Properties and Thermal Stability,” 2011.
- [343] D. Mikociak, A. Rudawski, and S. Blazewicz, “Mechanical and thermal properties of C/C composites modified with SiC nanofiller,” *Mater. Sci. Eng. A*, vol. 716, pp. 220–227, Feb. 2018.
- [344] M. Mallik, S. Roy, K. K. Ray, and R. Mitra, “Effect of SiC content, additives and process parameters on densification and structure-property relations of pressureless sintered ZrB<sub>2</sub>-SiC composites,” *Ceram. Int.*, vol. 39, no. 3, pp. 2915–2932, 2013.
- [345] C. Pradere and C. Sauder, “Transverse and longitudinal coefficient of thermal expansion of carbon fibers at high temperatures (300–2500K),” *Carbon N. Y.*, vol. 46, no. 14, pp. 1874–1884, Nov. 2008.
- [346] R. Luo, T. Liu, J. Li, H. Zhang, Z. Chen, and G. Tian, “Thermophysical properties of carbon/carbon composites and physical mechanism of thermal expansion and thermal conductivity,” *Carbon N. Y.*, vol. 42, no. 14, pp. 2887–2895, Jan. 2004.
- [347] W. E. Org, S. Rebouillat, and M. E. G. Lyons, “Measuring the Electrical Conductivity of Single Fibres,” *Int. J. Electrochem. Sci*, vol. 6, pp. 5731–5740, 2011.
- [348] L. Zhang, D. A. Pejaković, J. Marschall, and M. Gasch, “Thermal and Electrical Transport Properties of Spark Plasma-Sintered HfB<sub>2</sub> and ZrB<sub>2</sub> Ceramics,” *J. Am. Ceram. Soc.*, vol. 94, no. 8, pp. 2562–2570, Aug. 2011.
- [349] M. Mallik, A. J. Kailath, K. K. Ray, and R. Mitra, “Effect of SiC content on electrical, thermal and ablative properties of pressureless sintered ZrB<sub>2</sub> -based ultrahigh temperature ceramic composites,” *J. Eur. Ceram. Soc.*, vol. 37, no. 2, pp. 559–572, Feb. 2017.
- [350] C. Hu *et al.*, “Microstructure and properties of ZrB<sub>2</sub>-SiC and HfB<sub>2</sub>-SiC composites fabricated by spark plasma sintering (SPS) using TaSi<sub>2</sub> as sintering aid,” *J. Ceram. Soc. Japan*, vol. 118, no. 1383, pp. 997–1001, Nov. 2010.
- [351] W. Tan, C. A. Petorak, and R. W. Trice, “Rare-earth modified zirconium diboride high emissivity coatings for hypersonic applications,” *J. Eur. Ceram. Soc.*, vol. 34, no. 1, pp. 1–11, Jan. 2014.
- [352] W. Tan, M. Adducci, C. Petorak, B. Thompson, A. E. Brenner, and R. W. Trice, “Effect of rare-earth dopant (Sm) concentration on total hemispherical emissivity and ablation resistance of ZrB<sub>2</sub> /SiC coatings,” *J. Eur. Ceram. Soc.*, vol. 36, no. 16, pp. 3833–3841, Dec. 2016.
- [353] M. Balat-Pichelin, E. Bêche, D. Sciti, and D. Alfano, “Emissivity, catalycity and microstructural characterization of ZrB<sub>2</sub>-SiC fiber based UHTC at high temperature in a non-equilibrium air plasma flow,” *Ceram. Int.*, vol. 40, no. 7, pp. 9731–9742, Aug. 2014.

- 1 [354] B. Du, S. Zhou, X. Zhang, C. Hong, and Q. Qu, "Preparation of a high spectral  
2 emissivity TaSi<sub>2</sub>-based hybrid coating on SiOC-modified carbon-bonded carbon  
3 fiber composite by a flash sintering method," *Surf. Coatings Technol.*, vol. 350,  
4 pp. 146–153, Sep. 2018.
- 5 [355] X. Tao *et al.*, "Effect of TaSi<sub>2</sub> content on the structure and properties of TaSi<sub>2</sub> -  
6 MoSi<sub>2</sub> -borosilicate glass coating on fibrous insulations for enhanced surficial  
7 thermal radiation," *Surf. Coatings Technol.*, vol. 316, pp. 122–130, Apr. 2017.
- 8 [356] G. Shao, Y. Lu, D. A. H. Hanaor, S. Cui, J. Jiao, and X. Shen, "Improved  
9 oxidation resistance of high emissivity coatings on fibrous ceramic for reusable  
10 space systems," *Corros. Sci.*, vol. 146, pp. 233–246, Jan. 2019.
- 11 [357] L. Luo, Y. Wang, L. Duan, L. Liu, and G. Wang, "Ablation behavior of C/SiC-  
12 HfC composites in the plasma wind tunnel," *J. Eur. Ceram. Soc.*, vol. 36, no. 15,  
13 pp. 3801–3807, Nov. 2016.
- 14 [358] Q. Feng *et al.*, "Microstructure analysis of C<sub>f</sub>/SiC–ZrC composites in both  
15 fabrication and plasma wind tunnel testing processes," *Ceram. Int.*, vol. 40, no. 1,  
16 pp. 1199–1204, Jan. 2014.
- 17 [359] J. Li *et al.*, "Effect of ZrC–SiC content on microstructure and ablation properties  
18 of C/C composites," *Trans. Nonferrous Met. Soc. China*, vol. 26, no. 10, pp.  
19 2653–2664, Oct. 2016.
- 20 [360] S. Wang *et al.*, "Microstructure and ablation mechanism of C/C-ZrC-SiC  
21 composites in a plasma flame," *Ceram. Int.*, vol. 43, no. 14, pp. 10661–10667,  
22 Oct. 2017.
- 23 [361] D. Zhao, C. Zhang, H. Hu, and Y. Zhang, "Ablation behavior and mechanism of  
24 3D C/ZrC composite in oxyacetylene torch environment," *Compos. Sci. Technol.*,  
25 vol. 71, no. 11, pp. 1392–1396, Jul. 2011.
- 26 [362] Y. Liu, Q. Fu, Y. Guan, B. Wang, and Q. Shen, "Ablation behavior of sharp-  
27 shape C/C-SiC-ZrB<sub>2</sub> composites under oxyacetylene flame," *J. Alloys Compd.*,  
28 vol. 713, pp. 19–27, Aug. 2017.
- 29 [363] L. Zhuang *et al.*, "Ablation behaviour of C/C and C/C–ZrC–SiC composites with  
30 cone-shaped holes under an oxyacetylene flame," *Corros. Sci.*, vol. 102, pp. 84–  
31 92, Jan. 2016.
- 32 [364] J. Lu *et al.*, "Ablation resistance of SiC–HfC–ZrC multiphase modified  
33 carbon/carbon composites," *Corros. Sci.*, vol. 103, pp. 1–9, Feb. 2016.
- 34 [365] B. Feng, H. Li, Y. Zhang, L. Liu, and M. Yan, "Effect of SiC/ZrC ratio on the  
35 mechanical and ablation properties of C/C–SiC–ZrC composites," *Corros. Sci.*,  
36 vol. 82, pp. 27–35, May 2014.
- 37 [366] Y. Jia, X. Yao, J. Sun, and H. Li, "Effect of ZrC particle size on the ablation  
38 resistance of C/C-ZrC-SiC composites," *Mater. Des.*, vol. 129, pp. 15–25, Sep.  
39 2017.
- 40 [367] C. Yan, R. Liu, B. Zha, and C. Zhang, "Fabrication and properties of 3-  
41 dimensional 4-directional C<sub>f</sub>/HfC-SiC composites by precursor impregnation and  
42 pyrolysis process," *J. Alloys Compd.*, vol. 739, pp. 955–960, Mar. 2018.
- 43 [368] S. Chen, G. Li, H. Hu, Y. Li, and M. Mei, "Microstructure and properties of  
44 ablative C/ZrC–SiC composites prepared by reactive melt infiltration of  
45 zirconium and vapour silicon infiltration," *Ceram. Int.*, vol. 43, no. 3, pp. 3439–  
46 3442, Feb. 2017.
- 47 [369] J. P. Zhang, Q. G. Fu, and L. Wang, "Preparation, ablation behavior and thermal  
48 retardant ability of C/C-HfB<sub>2</sub> -SiC composites," *Mater. Des.*, vol. 132, pp. 552–  
49 558, Oct. 2017.
- 50 [370] L. Li, Y. Wang, L. Cheng, and L. Zhang, "Preparation and properties of 2D  
51  
52  
53  
54  
55  
56  
57  
58  
59  
60  
61  
62  
63  
64  
65



- C/SiC–ZrB<sub>2</sub>–TaC composites,” *Ceram. Int.*, vol. 37, no. 3, pp. 891–896, Apr. 2011.
- [371] Y. Liu, Q. Fu, B. Wang, T. Liu, and J. Sun, “The ablation behavior and mechanical property of C/C–SiC–ZrB<sub>2</sub> composites fabricated by reactive melt infiltration,” *Ceram. Int.*, vol. 43, no. 8, pp. 6138–6147, Jun. 2017.
- [372] X. Luan *et al.*, “Laser ablation behavior of Cf/SiHfBCN ceramic matrix composites,” *J. Eur. Ceram. Soc.*, vol. 36, no. 15, pp. 3761–3768, Nov. 2016.
- [373] L. Larrimbe *et al.*, “High Heat Flux Laser Testing of HfB<sub>2</sub> Cylinders,” *J. Am. Ceram. Soc.*, vol. 100, no. 1, pp. 293–303, Jan. 2017.
- [374] D. Sciti, V. Medri, and L. Silvestroni, “Oxidation behaviour of HfB<sub>2</sub>–15 vol.% TaSi<sub>2</sub> at low, intermediate and high temperatures,” *Scr. Mater.*, vol. 63, no. 6, pp. 601–604, Sep. 2010.
- [375] X. Zhang, P. Hu, J. Han, and S. Meng, “Ablation behavior of ZrB<sub>2</sub>–SiC ultra high temperature ceramics under simulated atmospheric re-entry conditions,” *Compos. Sci. Technol.*, vol. 68, no. 7–8, pp. 1718–1726, Jun. 2008.
- [376] T. A. Parthasarathy, M. D. Petry, G. Jefferson, M. K. Cinibulk, T. Mathur, and M. R. Gruber, “Development of a Test to Evaluate Aerothermal Response of Materials to Hypersonic Flow Using a Scramjet Wind Tunnel,” *Int. J. Appl. Ceram. Technol.*, vol. 8, no. 4, pp. 832–847, Jul. 2011.
- [377] L. Larrimbe *et al.*, “High Heat Flux Laser Testing of HfB<sub>2</sub> Cylinders,” *J. Am. Ceram. Soc.*, vol. 100, no. 1, pp. 293–303, Jan. 2017.
- [378] N. S. Diaconis, M. J. Engel, and J. W. Metzger, “Oxidation and sublimation of graphite in simulated re-entry environments,” *AIAA J.*, vol. 5, no. 3, pp. 451–460, Mar. 1967.
- [379] M. Funatsu, M. Ozawa, H. Shirai, and F. Takakusagi, “Experimental Study of Ablation Processes of SiC-based Materials in Air Plasma Freejets,” *Trans. Japan Soc. Aeronaut. Sp. Sci. Aerosp. Technol. Japan*, vol. 8, no. ists27, p. Pe\_41–Pe\_46, 2010.
- [380] E. R. Smart Michael, “Free-jet testing of a rest scramjet at off-design conditions,” in *25th AIAA Aerodynamic Measurement Technology and Ground Testing Conference*, 2006.
- [381] M. Funatsu, K. Konishi, M. Kawada, M. Ozawa, and F. Takakusagi, “Visualizations of SiC Ablations in Air Plasma Freejets,” *Trans. Japan Soc. Aeronaut. Sp. Sci. Aerosp. Technol. Japan*, vol. 12, no. 29, pp. 45–50, 2014.
- [382] B. J. R. V, and Presser S, “Measurement of the velocity of oxyacetylene and oxypropane torches for UHTC composite testing,” *to be Publ.*, 2019.
- [383] J. K. Sonber, T. S. R. Ch. Murthy, C. Subramanian, R. C. Hubli, and A. K. Suri, “Processing Methods for Ultra High Temperature Ceramics,” in *MAX Phases and Ultra-High Temperature Ceramics for Extreme Environments*, IGI Global, 2013, pp. 180–202.
- [384] J. B. Berkowitz-Mattuck, “High-Temperature Oxidation,” *J. Electrochem. Soc.*, vol. 113, no. 9, p. 908, Sep. 1966.
- [385] T. A. Parthasarathy, R. A. Rapp, M. Opeka, and R. J. Kerans, “A model for the oxidation of ZrB<sub>2</sub>, HfB<sub>2</sub> and TiB<sub>2</sub>,” *Acta Mater.*, vol. 55, no. 17, pp. 5999–6010, Oct. 2007.
- [386] D. Sciti, A. Balbo, and A. Bellosi, “Oxidation behaviour of a pressureless sintered HfB<sub>2</sub>–MoSi<sub>2</sub> composite,” *J. Eur. Ceram. Soc.*, vol. 29, no. 9, pp. 1809–1815, Jun. 2009.
- [387] C.-M. Chen, L. T. Zhang, W. C. Zhou, and M. Q. Li, “High temperature oxidation of LaB<sub>6</sub>–ZrB<sub>2</sub> eutectic in situ composite,” *Acta Mater.*, vol. 47, no. 6,

- pp. 1945–1952, Apr. 1999.
- [388] F. Monteverde and A. Bellosi, “Oxidation of ZrB<sub>2</sub> - Based Ceramics in Dry Air,” *J. Electrochem. Soc.*, vol. 150, no. 11, p. B552, 2003.
- [389] W. G. Fahrenholtz and G. E. Hilmas, “Oxidation of ultra-high temperature transition metal diboride ceramics,” *Int. Mater. Rev.*, vol. 57, no. 1, pp. 61–72, Jan. 2012.
- [390] W. G. Fahrenholtz, “Thermodynamic Analysis of ZrB<sub>2</sub> /SiC Oxidation: Formation of a SiC-Depleted Region,” *J. Am. Ceram. Soc.*, vol. 90, no. 1, pp. 143–148, Jan. 2007.
- [391] S. Shimada, M. Inagaki, and M. Suzuki, “Microstructural observation of the ZrC/ZrO<sub>2</sub> interface formed by oxidation of ZrC,” *J. Mater. Res.*, vol. 11, no. 10, pp. 2594–2597, Oct. 1996.
- [392] S. Shimada and T. Ishil, “Oxidation Kinetics of Zirconium Carbide at Relatively Low Temperatures,” *J. Am. Ceram. Soc.*, vol. 73, no. 10, pp. 2804–2808, Oct. 1990.
- [393] S. Shimada, M. Nishisako, M. Inagaki, and K. Yamamoto, “Formation and Microstructure of Carbon-Containing Oxide Scales by Oxidation of Single Crystals of Zirconium Carbide,” *J. Am. Ceram. Soc.*, vol. 78, no. 1, pp. 41–48, Jan. 1995.
- [394] A. Bellucci, D. Gozzi, T. Kimura, T. Noda, and S. Otani, “Zirconia growth on zirconium carbide single crystals by oxidation,” *Surf. Coatings Technol.*, vol. 197, no. 2–3, pp. 294–302, Jul. 2005.
- [395] G. A. Rama Rao and V. Venugopal, “Kinetics and mechanism of the oxidation of ZrC,” *J. Alloys Compd.*, vol. 206, no. 2, pp. 237–242, May 1994.
- [396] W. Hu, Y. Tian, and Z. Liu, “Carbon Vacancy Ordered Non-Stoichiometric ZrC<sub>0.6</sub>,” in *MAX Phases and Ultra-High Temperature Ceramics for Extreme Environments*, IGI Global, 2013, pp. 478–508.
- [397] S. Shimada, “Oxidation and Mechanism of Single Crystal Carbides with Formation of Carbon,” *J. Ceram. Soc. Japan*, vol. 109, no. 1267, pp. S33–S42, 2001.
- [398] K. Edamoto, T. Nagayama, K. Ozawa, and S. Otani, “Angle-resolved and resonant photoemission study of the ZrO-like film on ZrC(100),” *Surf. Sci.*, vol. 601, no. 21, pp. 5077–5082, Nov. 2007.
- [399] L. Casas and J. M. Martínez-Esnaola, “Modelling the effect of oxidation on the creep behaviour of fibre-reinforced ceramic matrix composites,” *Acta Mater.*, vol. 51, no. 13, pp. 3745–3757, Aug. 2003.
- [400] W. C. Tripp, H. H. Davis, and H. C. Graham, “Effect of an SiC addition on the oxidation of ZrB<sub>2</sub>,” *Amer. Ceram. Soc. Bull.*, vol. 52, no. 8, pp. 612–616, 1973.
- [401] A. Rezaie, W. G. Fahrenholtz, and G. E. Hilmas, “Evolution of structure during the oxidation of zirconium diboride–silicon carbide in air up to 1500°C,” *J. Eur. Ceram. Soc.*, vol. 27, no. 6, pp. 2495–2501, Jan. 2007.
- [402] K. Shugart, W. Jennings, and E. Opila, “Initial Stages of ZrB<sub>2</sub> -30 vol% SiC Oxidation at 1500°C,” *J. Am. Ceram. Soc.*, vol. 97, no. 5, pp. 1645–1651, May 2014.
- [403] S. N. Karlsdottir and J. W. Halloran, “Rapid Oxidation Characterization of Ultra-High Temperature Ceramics,” *J. Am. Ceram. Soc.*, vol. 90, no. 10, pp. 3233–3238, Oct. 2007.
- [404] Z. Wang and Z. Wu, “Fabrication, Microstructure, and Properties of Zirconium Diboride Matrix Ceramic,” in *MAX Phases and Ultra-High Temperature Ceramics for Extreme Environments*, IGI Global, 2013, pp. 354–412.

- 1  
2  
3  
4  
5  
6  
7  
8  
9  
10  
11  
12  
13  
14  
15  
16  
17  
18  
19  
20  
21  
22  
23  
24  
25  
26  
27  
28  
29  
30  
31  
32  
33  
34  
35  
36  
37  
38  
39  
40  
41  
42  
43  
44  
45  
46  
47  
48  
49  
50  
51  
52  
53  
54  
55  
56  
57  
58  
59  
60  
61  
62  
63  
64  
65
- [405] S. P.T.B, "An Oxidation Resistant Boride Composition," *J. Name Am. Ceram. Soc. Bull. (U.S.)*, vol. 41, 1962.
- [406] R. Pastor, H.; Meyer, "An investigation of the effect of additions of metal silicides on titanium and zirconium borides from the point of view of their sintering behaviour and their resistance to oxidation at high temperature," *Rev. Int. Htes Temp. Refract. II*, vol. 11, no. 1, pp. 41–54, 1974.
- [407] Z. Wu, Z. Wang, G. Shi, and J. Sheng, "Effect of surface oxidation on thermal shock resistance of the ZrB<sub>2</sub>-SiC-ZrC ceramic," *Compos. Sci. Technol.*, vol. 71, no. 12, pp. 1501–1506, Aug. 2011.
- [408] F. Monteverde and A. Bellosi, "Microstructure and Properties of an HfB<sub>2</sub>-SiC Composite for Ultra High Temperature Applications," *Adv. Eng. Mater.*, vol. 6, no. 5, pp. 331–336, May 2004.
- [409] J. W. Hinze, "The High-Temperature Oxidation Behavior of a HfB<sub>2</sub> + 20 vol% SiC Composite," *J. Electrochem. Soc.*, vol. 122, no. 9, p. 1249, Sep. 1975.
- [410] F. Monteverde, "The thermal stability in air of hot-pressed diboride matrix composites for uses at ultra-high temperatures," *Corros. Sci.*, vol. 47, no. 8, pp. 2020–2033, Aug. 2005.
- [411] M. Gasch, "Processing, Properties, and Arc Jet Oxidation of Hafnium Diboride/Silican Carbide Ultra-High Temperature Ceramics," vol. 39, no. 17, pp. 5925–5937, 2004.
- [412] E. J. Opila and M. C. Halbig, "Oxidation of ZrB<sub>2</sub>-SiC," in *25th Annual Conference on Composites, Advanced Ceramics, Materials, and Structures: A Ceramic Engineering and Science Proceedings, Volume 22, Issue 3*, Hoboken, NJ, USA: John Wiley & Sons, Inc., 2008, pp. 221–228.
- [413] X. W. Yin, L. F. Cheng, L. T. Zhang, N. Travitzky, and P. Greil, "Fibre-reinforced multifunctional SiC matrix composite materials," *Int. Mater. Rev.*, vol. 62, no. 3, pp. 117–172, Apr. 2017.
- [414] L. S. Walker and E. L. Corral, "Self-Generating High-Temperature Oxidation-Resistant Glass-Ceramic Coatings for C-C Composites Using UHTCs," *J. Am. Ceram. Soc.*, vol. 97, no. 9, pp. 3004–3011, Sep. 2014.
- [415] W. Lu, F. Qian-gang, and Z. Feng-ling, "A novel gradient SiC-ZrB<sub>2</sub>-MoSi<sub>2</sub> coating for SiC coated C/C composites by supersonic plasma spraying," *Surf. Coatings Technol.*, vol. 313, pp. 63–72, Mar. 2017.
- [416] Y. L. Zhang, J. Ren, S. Tian, H. Li, X. Ren, and Z. Hu, "HfC nanowire-toughened TaSi<sub>2</sub>-TaC-SiC-Si multiphase coating for C/C composites against oxidation," *Corros. Sci.*, vol. 90, pp. 554–561, Jan. 2015.
- [417] X. Ren, H. Li, K. Li, and Q. Fu, "Preparation of oxidation protective Hf<sub>0.2</sub>Ta<sub>0.8</sub>B<sub>2-x</sub>-SiC coating by in-situ reaction method on SiC-coated carbon/carbon composites," *J. Alloys Compd.*, vol. 618, pp. 390–395, Jan. 2015.
- [418] T. Feng, H. Li, M. Hu, H. Lin, and L. Li, "Oxidation and ablation resistance of the ZrB<sub>2</sub>-CrSi<sub>2</sub>-Si/SiC coating for C/C composites at high temperature," *J. Alloys Compd.*, vol. 662, pp. 302–307, Mar. 2016.
- [419] X. Ren, H. Li, Y. Chu, Q. Fu, and K. Li, "Ultra-High-Temperature Ceramic HfB<sub>2</sub>-SiC Coating for Oxidation Protection of SiC-Coated Carbon/Carbon Composites," *Int. J. Appl. Ceram. Technol.*, vol. 12, no. 3, pp. 560–567, May 2015.
- [420] M. Pavese, P. Fino, C. Badini, A. Ortona, and G. Marino, "HfB<sub>2</sub>/SiC as a protective coating for 2D C<sub>f</sub>/SiC composites: Effect of high temperature oxidation on mechanical properties," *Surf. Coatings Technol.*, vol. 202, no. 10, pp. 2059–2067, Feb. 2008.

- [421] D. Sciti, L. Silvestroni, G. Saccone, and D. Alfano, "Effect of different sintering aids on thermo-mechanical properties and oxidation of SiC fibers – Reinforced ZrB<sub>2</sub> composites," *Mater. Chem. Phys.*, vol. 137, no. 3, pp. 834–842, Jan. 2013.
- [422] L. Silvestroni and D. Sciti, "Oxidation of ZrB<sub>2</sub> Ceramics Containing SiC as Particles, Whiskers, or Short Fibers," *J. Am. Ceram. Soc.*, vol. 94, no. 9, pp. 2796–2799, Sep. 2011.
- [423] W. Z. Zhang, Y. Zeng, L. Gbologah, X. Xiong, and B. Y. Huang, "Preparation and oxidation property of ZrB<sub>2</sub>-MoSi<sub>2</sub>/SiC coating on carbon/carbon composites," *Trans. Nonferrous Met. Soc. China*, vol. 21, no. 7, pp. 1538–1544, Jul. 2011.
- [424] S. M. Johnson, "Ultra High Temperature Ceramics Application: Issues and Prospects," 2011.
- [425] A. Vinci, L. Zoli, E. Landi, and D. Sciti, "Oxidation behaviour of a continuous carbon fibre reinforced ZrB<sub>2</sub>-SiC composite," *Corros. Sci.*, vol. 123, no. November 2016, pp. 129–138, Jul. 2017.
- [426] O. Haibo *et al.*, "Self-healing ZrB<sub>2</sub>-SiO<sub>2</sub> oxidation resistance coating for SiC coated carbon/carbon composites," *Corros. Sci.*, vol. 110, pp. 265–272, Sep. 2016.
- [427] A. Vinci, L. Zoli, and D. Sciti, "Influence of SiC content on the oxidation of carbon fibre reinforced ZrB<sub>2</sub>/SiC composites at 1500 and 1650°C in air," *J. Eur. Ceram. Soc.*, vol. 38, no. 11, pp. 3767–3776, Sep. 2018.
- [428] S. C. Zhang, G. E. Hilmas, and W. G. Fahrenholtz, "Improved Oxidation Resistance of Zirconium Diboride by Tungsten Carbide Additions," *J. Am. Ceram. Soc.*, vol. 91, no. 11, pp. 3530–3535, Nov. 2008.
- [429] I. Talmy, J. Zaykoski, M. Opeka, and S. Dallek, "High temperature corrosion and materials chemistry III : proceedings of the International Symposium," in *High Temperature Corrosion and Materials Chemistry III*, M. McNallan, E. J. Opila, Electrochemical Society. High Temperature Materials Division., Electrochemical Society. Corrosion Division., and D. C. . Electrochemical Society. Meeting (199th : 2001 : Washington, Eds. Pennington, NJ, 2001: Electrochemical Society, 2001, p. 144.
- [430] C.-M. Chen, L. T. Zhang, W. C. Zhou, Z. Z. Hao, Y. J. Jiang, and S. L. Yang, "Microstructure, mechanical performance and oxidation mechanism of boride in situ composites," *Compos. Sci. Technol.*, vol. 61, no. 7, pp. 971–975, May 2001.
- [431] I. Bogomol and P. Loboda, "Directionally Solidified Ceramic Eutectics for High-Temperature Applications," in *MAX Phases and Ultra-High Temperature Ceramics for Extreme Environments*, C. I. M. Low (Curtin University, Perth, Australia); Y. Sakka (National Institute for Materials Science (NIMS), Japan); C. F. Hu (Chinese Academy of Sciences, Ed. Hershey, PA 17033-1240: IGI Global, 2013, pp. 303–322.
- [432] I. Bogomol, T. Nishimura, Y. Nesterenko, O. Vasylykiv, Y. Sakka, and P. Loboda, "The bending strength temperature dependence of the directionally solidified eutectic LaB<sub>6</sub>-ZrB<sub>2</sub> composite," *J. Alloys Compd.*, vol. 509, no. 20, pp. 6123–6129, May 2011.
- [433] E. L. Courtright, H. C. Graham, A. P. Katz, and R. J. Kerans, "Ultrahigh Temperature Assessment Study: Ceramic Matrix Composites," 1992.
- [434] D.-W. Ni, G.-J. Zhang, Y.-M. Kan, and Y. Sakka, "Textured HfB<sub>2</sub>-based ultrahigh-temperature ceramics with anisotropic oxidation behavior," *Scr. Mater.*, vol. 60, no. 10, pp. 913–916, May 2009.
- [435] C. M. Carney, P. Mogilvesky, and T. A. Parthasarathy, "Oxidation Behavior of

- Zirconium Diboride Silicon Carbide Produced by the Spark Plasma Sintering Method,” *J. Am. Ceram. Soc.*, vol. 92, no. 9, pp. 2046–2052, Sep. 2009.
- [436] C. M. Carney, T. A. Parthasarathy, and M. K. Cinibulk, “Oxidation Resistance of Hafnium Diboride Ceramics with Additions of Silicon Carbide and Tungsten Boride or Tungsten Carbide,” *J. Am. Ceram. Soc.*, vol. 94, no. 8, pp. 2600–2607, Aug. 2011.
- [437] C. M. Carney and T. S. Key, “Comparison of the oxidation protection of HfB<sub>2</sub> based ultra-high temperature ceramics by the addition of SiC or MoSi<sub>2</sub>,” in *Ceramic Engineering and Science Proceedings*, 2014, pp. 261–273.
- [438] F. Monteverde, “Ultra-high temperature HfB<sub>2</sub>-SiC ceramics consolidated by hot-pressing and spark plasma sintering,” *J. Alloys Compd.*, vol. 428, no. 1–2, pp. 197–205, 2007.
- [439] P. Zheng, B. Vaidhyanathan, S. Grasso, C. Carney, and J. Binner, “Synthesis, Sintering and Oxidation Testing of Ta-Doped HfB<sub>2</sub> Powders,” *Prep.*
- [440] W. Vogel, *Glass Chemistry*. Springer Berlin Heidelberg, 1994.
- [441] P. W. Atkins, *Physical Chemistry*. Oxford University Press, 1978.
- [442] L. Kaufman; and E. Clougherty, “Technical Report RTD-TDR-63-4096,” 1963.
- [443] M. J. Gasch, D. T. Ellerby, and S. M. Johnson, “Ultra High Temperature Ceramic Composites,” in *Handbook of Ceramic Composites*, Springer US, 2005, pp. 197–224.
- [444] S. C. Zhang, W. G. Fahrenholtz, and G. E. Hilmas, “Oxidation of ZrB<sub>2</sub> and ZrB<sub>2</sub>-SiC Ceramics with Tungsten Additions,” in *ECS Transactions*, 2009, vol. 16, no. 44, pp. 137–145.
- [445] T. Wang and R. Luo, “Oxidation protection and mechanism of the HfB<sub>2</sub>- SiC-Si/SiC coatings modified by in-situ strengthening of SiC whiskers for C/C composites,” *Ceram. Int.*, vol. 44, no. 11, pp. 12370–12380, Aug. 2018.
- [446] N. P. Padture, “Advanced structural ceramics in aerospace propulsion,” *Nat. Mater.*, vol. 15, no. 8, pp. 804–809, Aug. 2016.
- [447] S. Chand, “Review Carbon fibers for composites,” *J. Mater. Sci.*, vol. 35, no. 6, pp. 1303–1313, 2000.
- [448] A. Paul, J. Binner, and B. Vaidhyanathan, “UHTC Composites for Hypersonic Applications,” in *Ultra-High Temperature Ceramics*, W. G. Fahrenholtz, E. J. Wuchina, W. E. Lee, and Y. Zhou, Eds. Hoboken, NJ: John Wiley & Sons, Inc, 2014, pp. 144–166.

# Design, Selection, Processing, Properties and Applications of Ultra-High Temperature Ceramic Matrix Composites, UHTCMCs - A Review

Total 23 figures

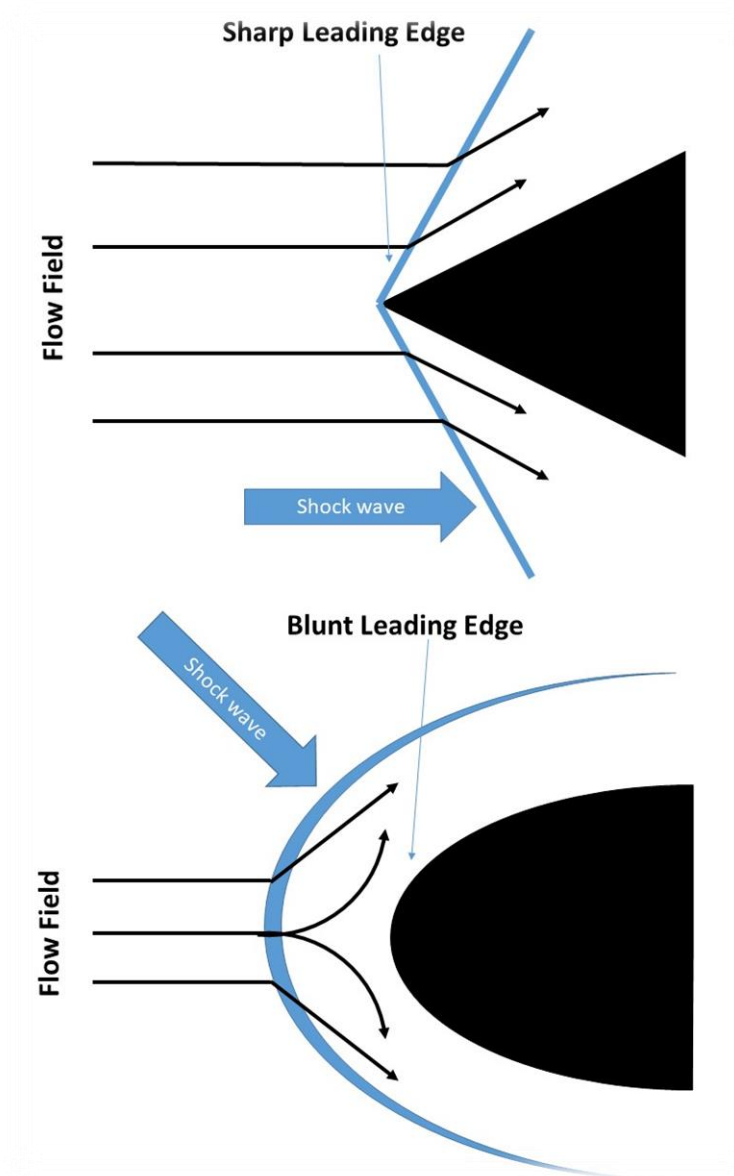


**Fig. 1** Schematic on the effect of shape of leading edge on the shock wave propagation on the surface of the structure.

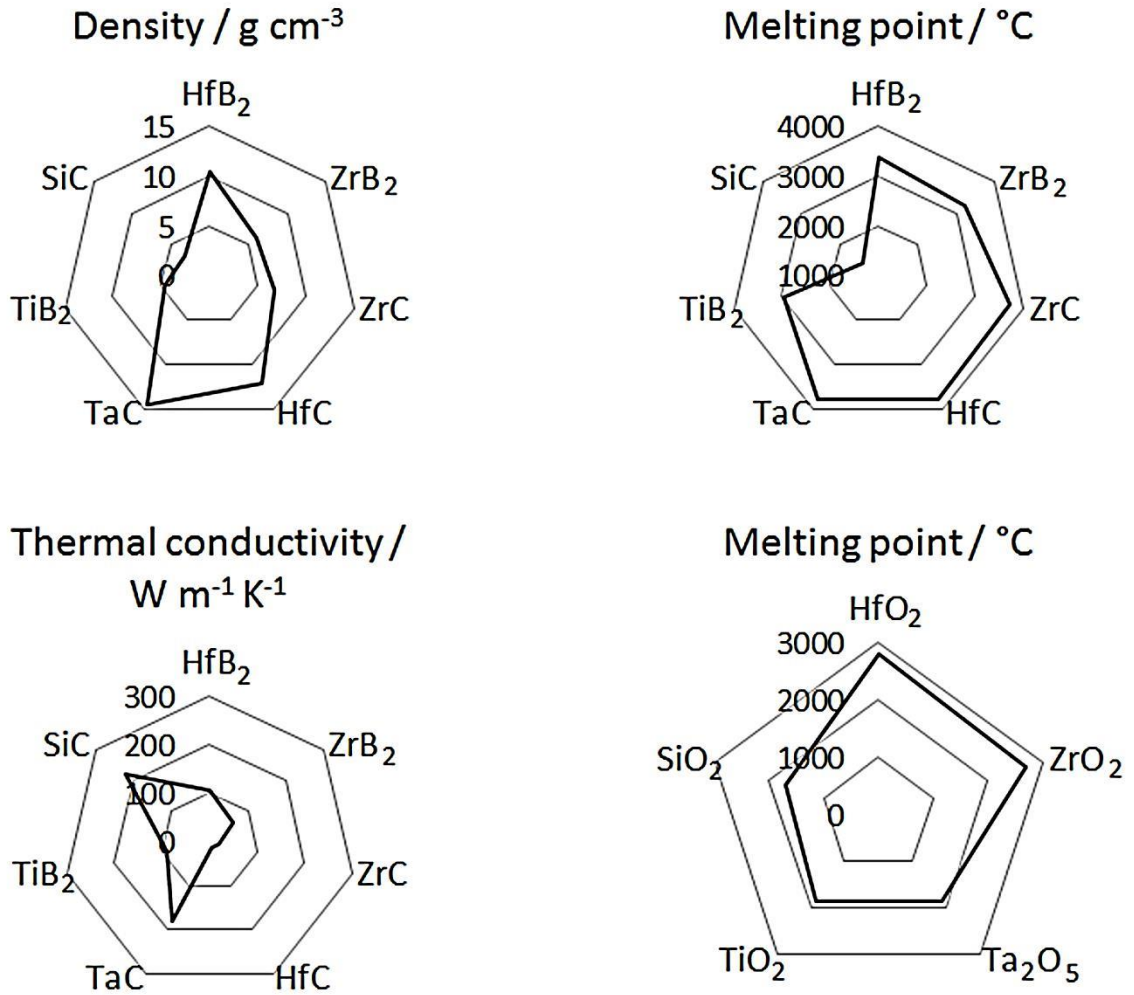


**Fig. 2** Some summary data for common UHTCs ubiquitous in literature; HfB<sub>2</sub>, ZrB<sub>2</sub>, ZrC, HfC, TaC, TiB<sub>2</sub>, SiC is provided for contrast, due to its frequent inclusion as a secondary matrix component [13], [29]–[35].

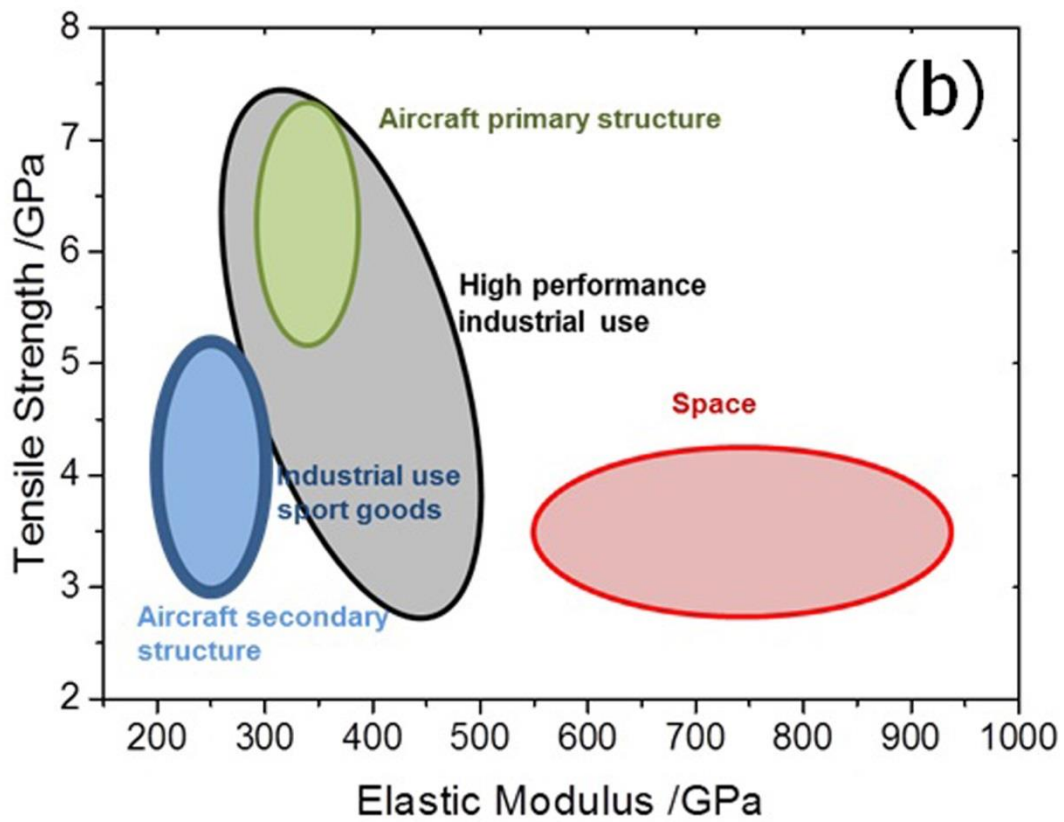
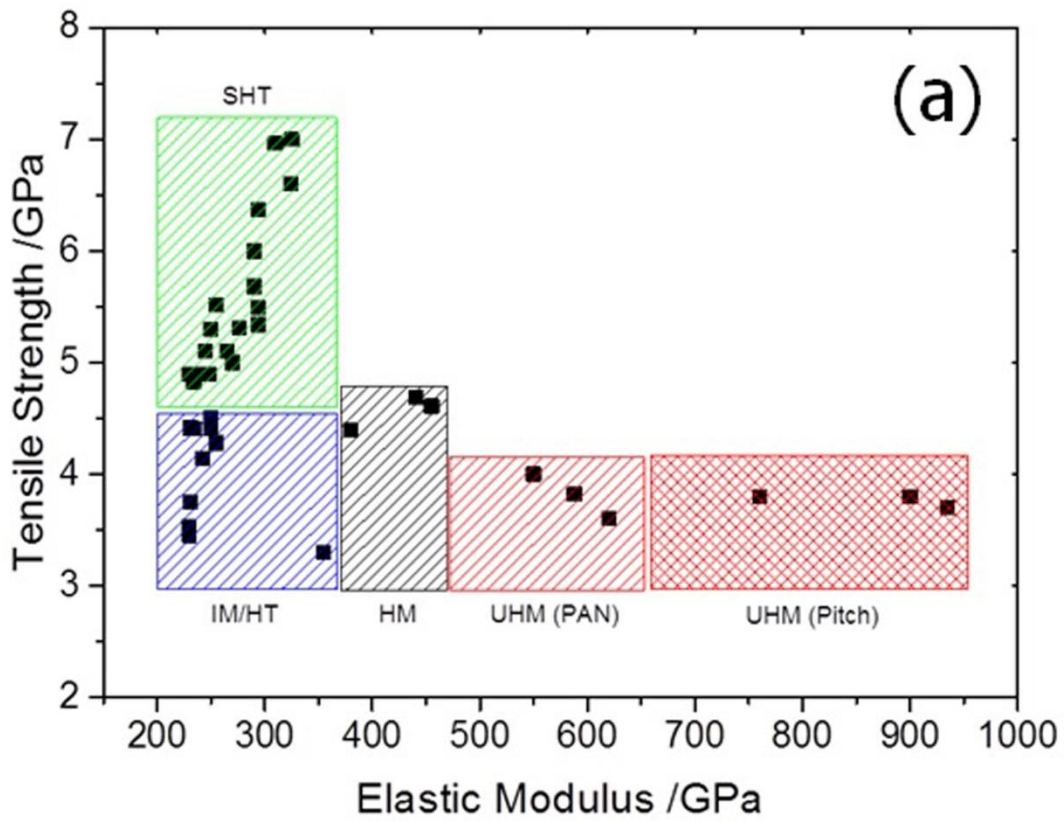


**Fig. 3. a) Classification of the carbon fibres (value based on available commercial fibres of Error! Reference source not found. and their use, b) different applications with required properties range [128]**



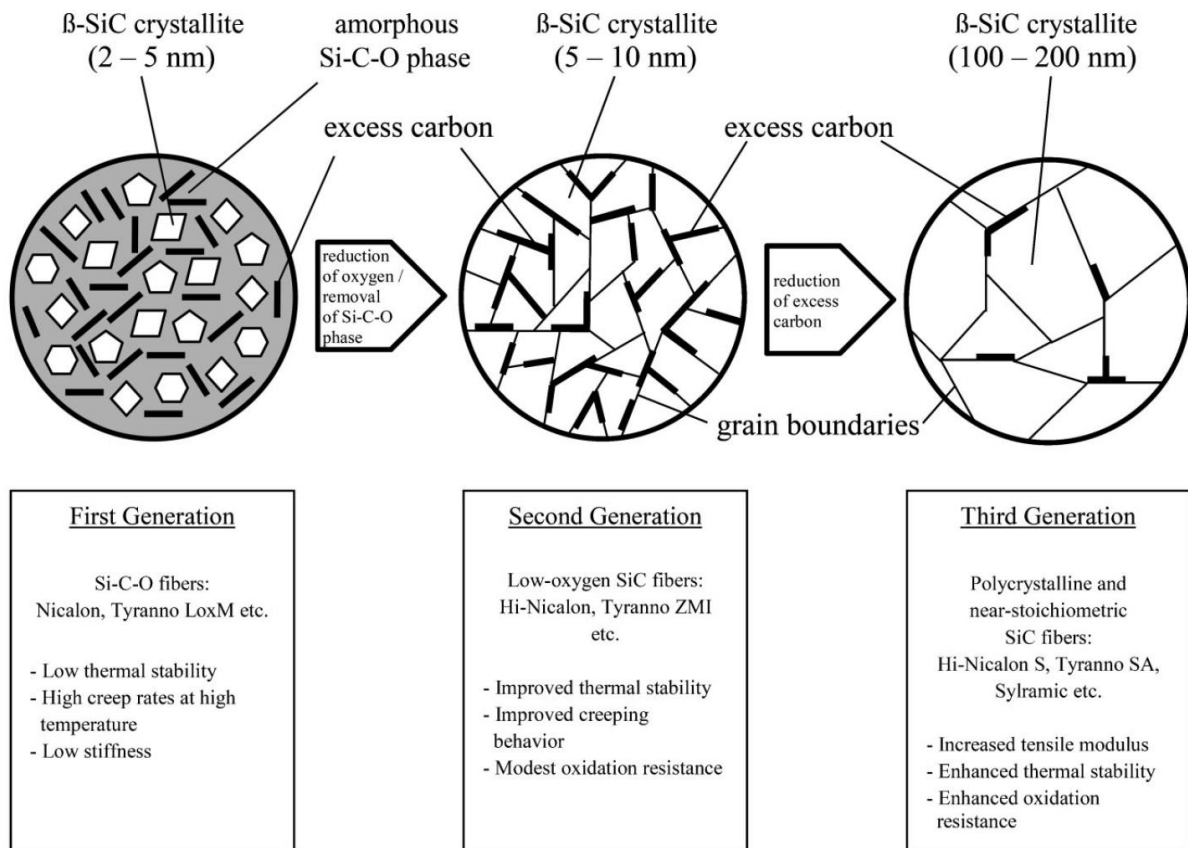


**Fig. 4 Microstructural of the three generations of SiC fibres: reprinted with permission from John Wiley and Sons, Macromolecular Materials and Engineering, 297(6), Fig.16 in p. 512 [144].**

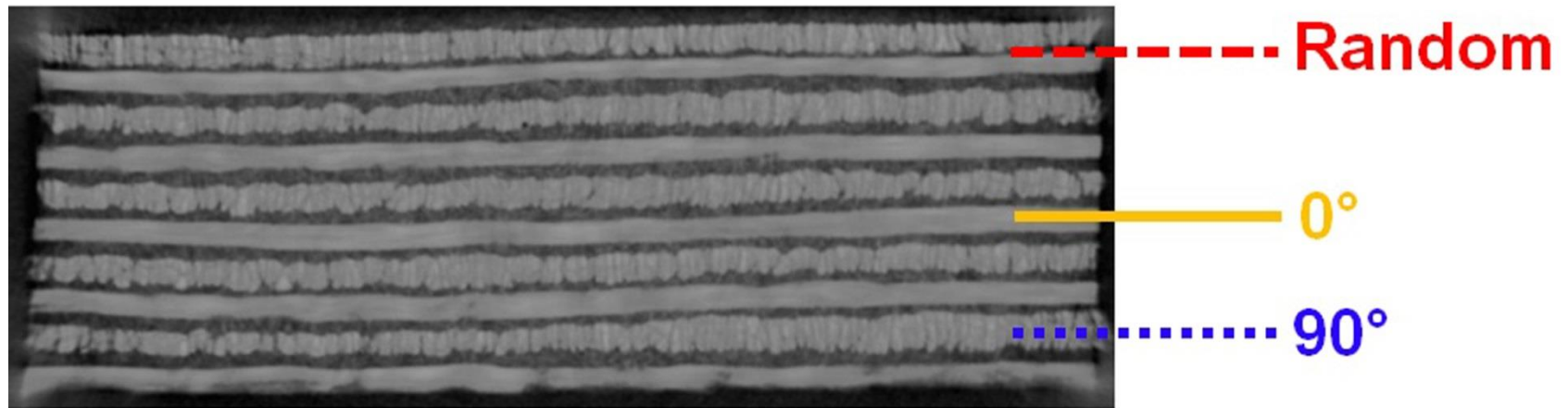


**Fig. 5 Structure of the 2.5 D carbon fibre preform bought from Surface Transforms, UK (Structure: RO/90°/RO/0°/RO, 23% fibre, 77% porosity, bulk density: 0.36 g/cc, Random oriented (RO) arises from the needling process)**

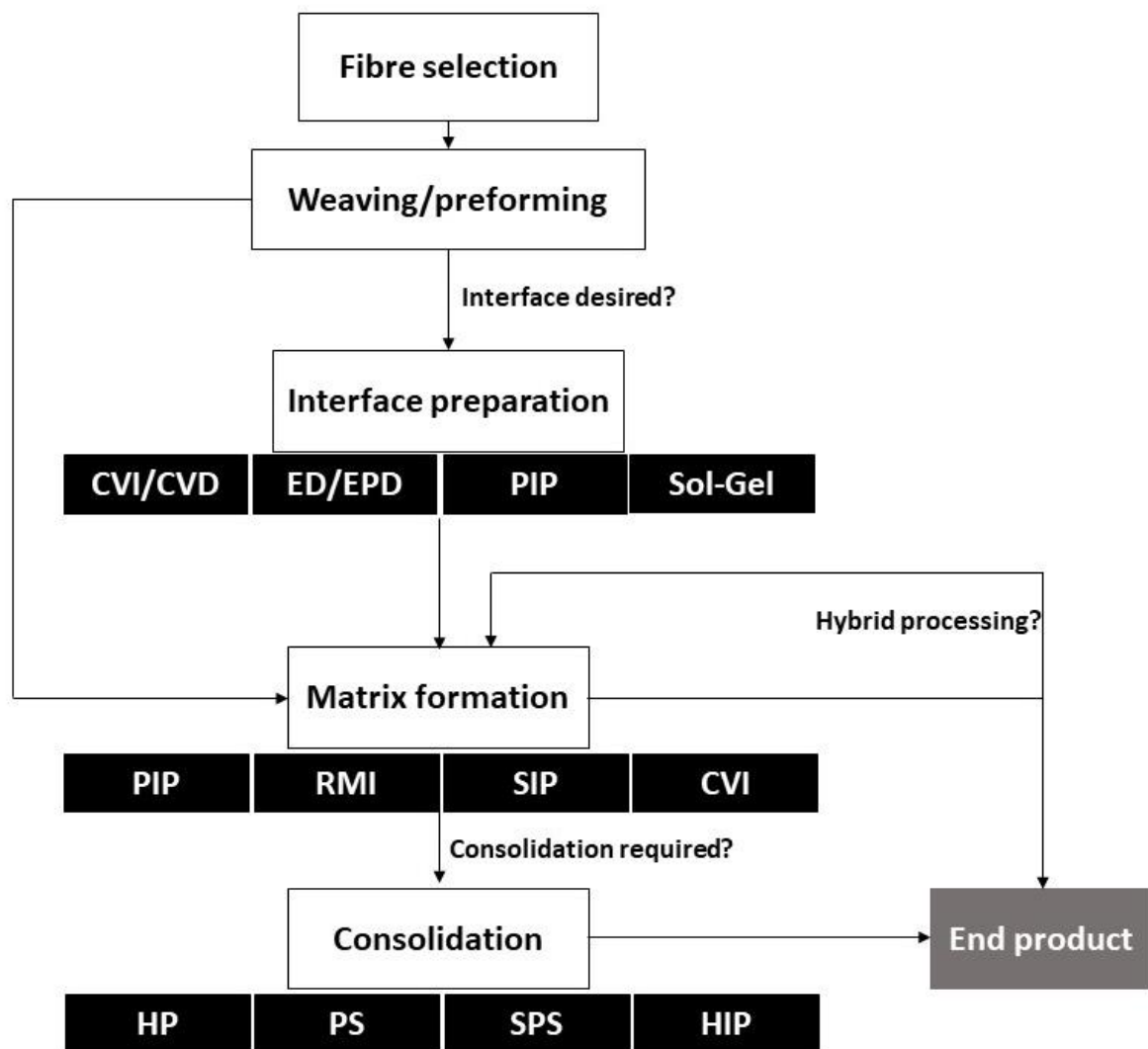


**Fig. 6** Process flow sheet summarises the different methods of process for obtaining the UHTCMCs (CVI-chemical vapour infiltration, CVD-chemical vapour deposition, ED-Electro deposition, EPD- Electrophoretic deposition, PIP- precursor infiltration and pyrolysis, RMI - reactive melt infiltration, SIP - slurry impregnation process, HP – hot pressing, PS- pressureless sintering, SPS – spark plasma sintering, HIP – hot isostatic pressing)

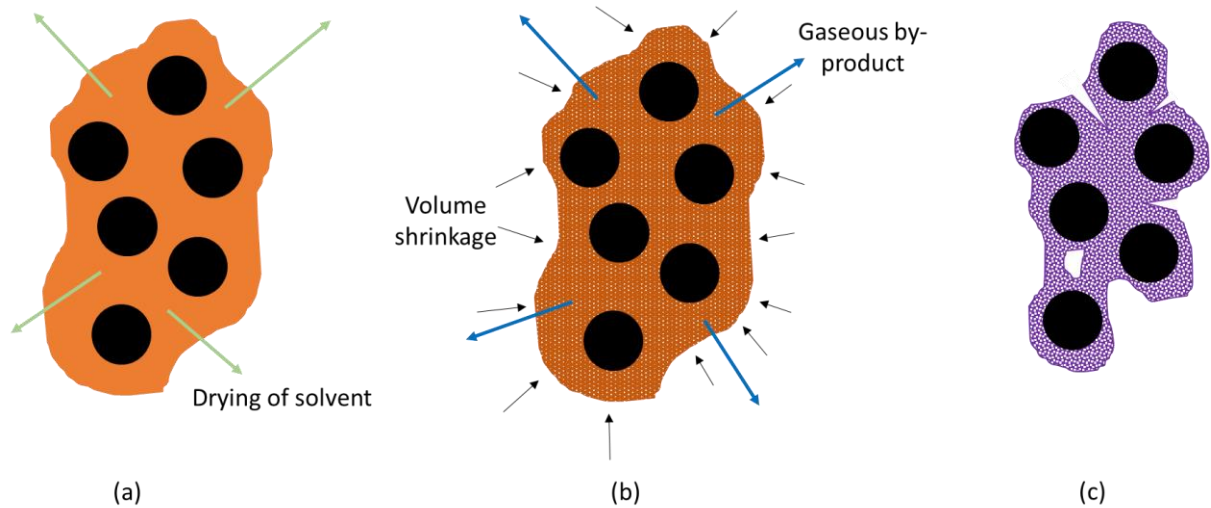


**Fig. 7 The steps involved in production of a composite via PIP. (a) A liquid precursor impregnated fabric dries, leaving residual porosity; (b) pyrolysis begins, resulting in evolution of gaseous by-products and volume shrinkage from the polymer-ceramic transition; (c) a porous microstructure, with microcracks and pores shown in the matrix phases.**

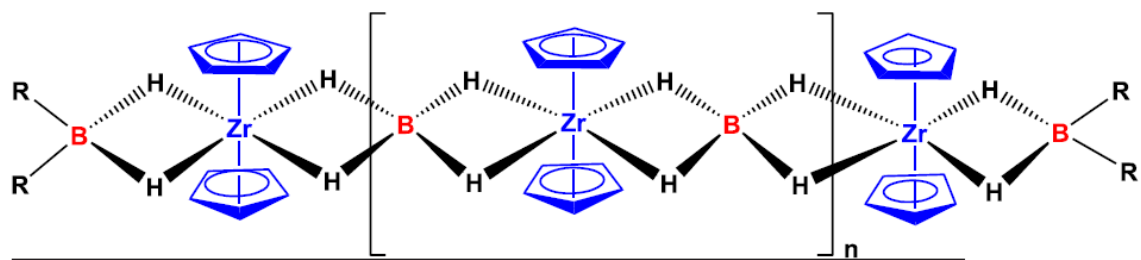


**Fig. 8** The precursor used by Xie et al for a ZrB<sub>2</sub>/ZrC matrix: reprinted with permission from Elsevier, *Ceramics International*, 2015, 41[5], Eq. 1 in p. 6228 [194].

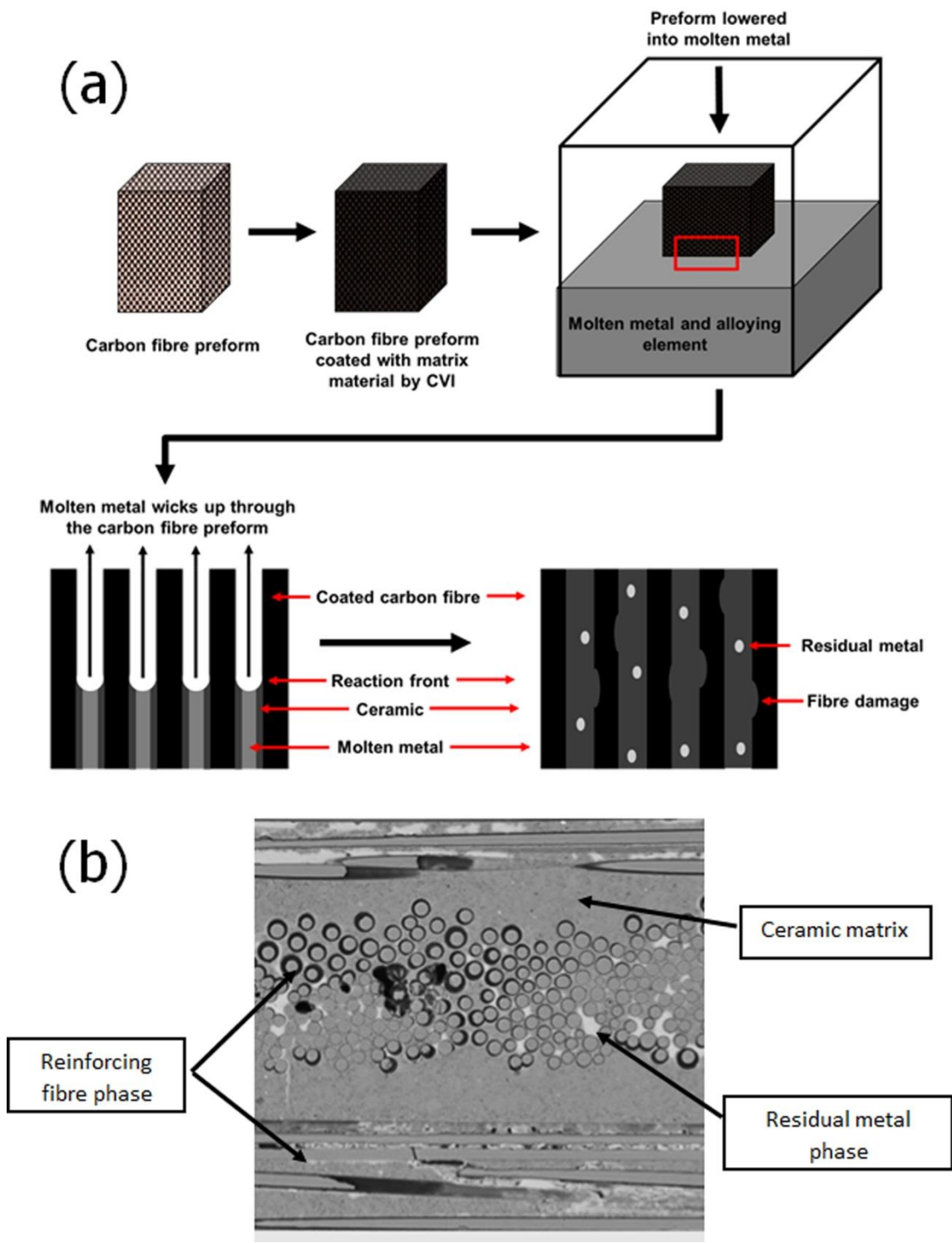


**Fig. 9 (a) The reactive melt infiltration process and (b) residual free metal phase:** reprinted with permission from Jeff Crompton, <https://uk.comsol.com/blogs/multiphysics-analysis-advanced-materials-ceramic-matrix-composites/> [216].

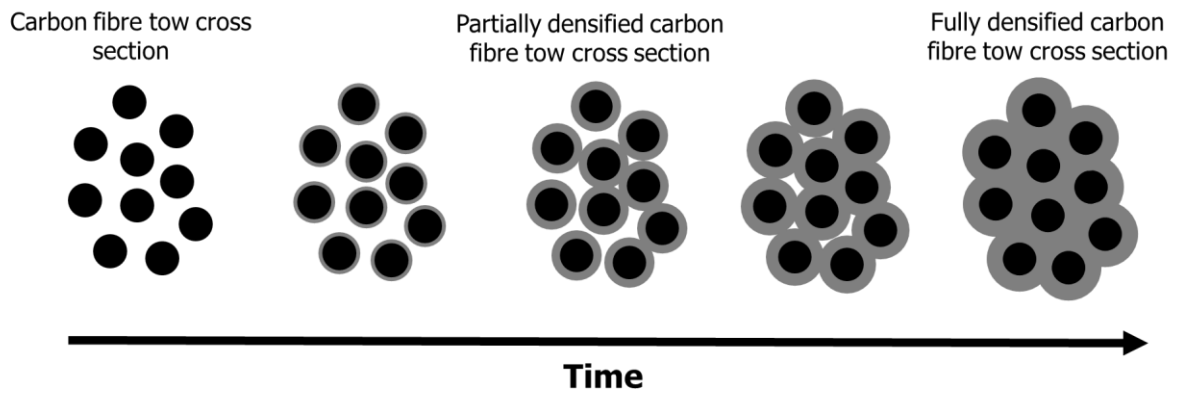


**Fig. 10** Schematic showing the growth of ceramic deposit on the cross section of the fibres to the point of full densification by CVI method.

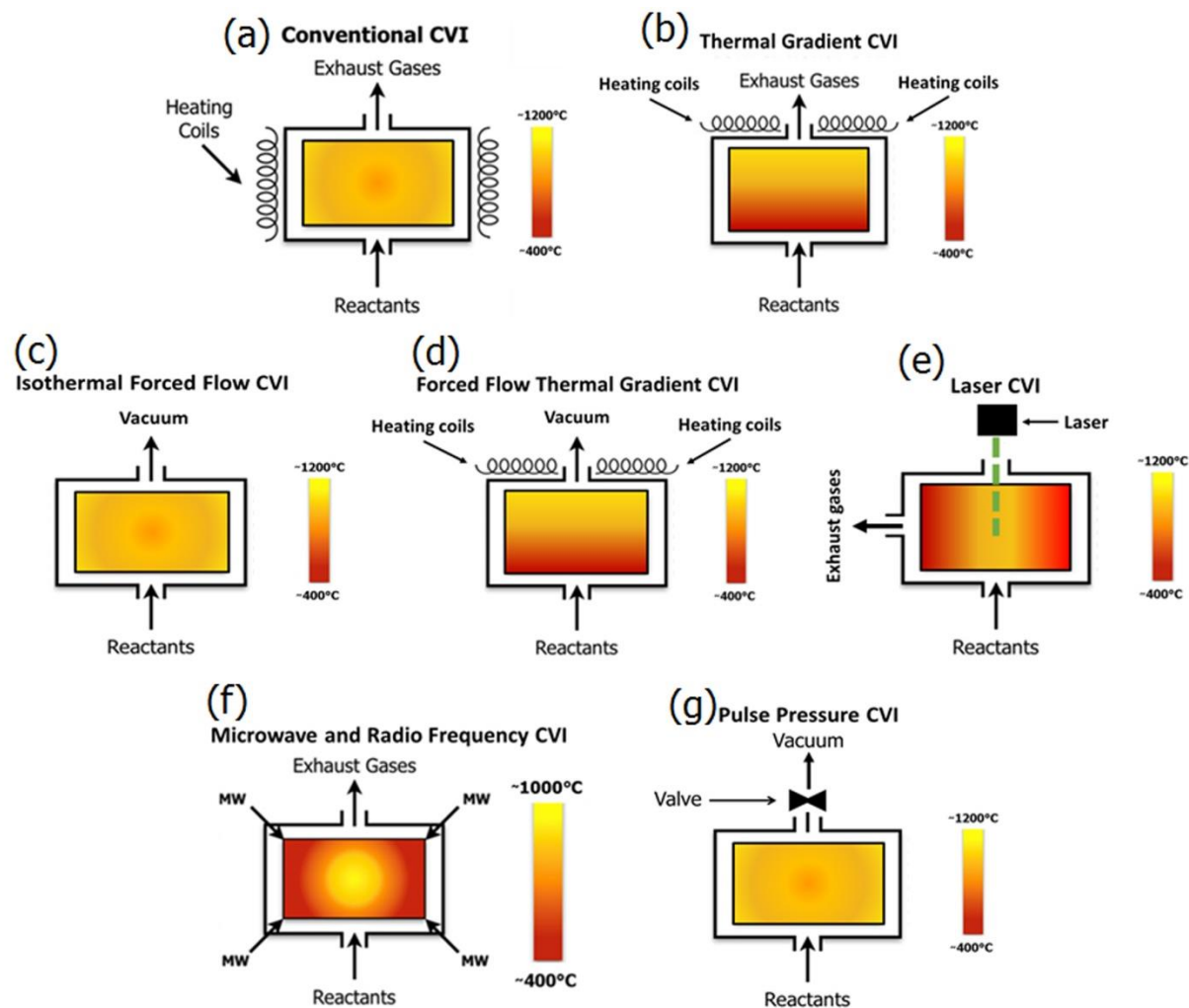


**Fig. 11 a) Isothermal chemical vapour infiltration (ICVI), b) Thermal gradient (TGCVI), c) Isothermal forced flow CVI (FFCVI), d) Forced Flow Thermal Gradient CVI, e) Laser Chemical Vapour Infiltration (LCVI), f) Thermal gradient of Microwave and Radio Frequency CVI (MCVI and RFCVI) and g) pulse pressure CVI (PCVI).**



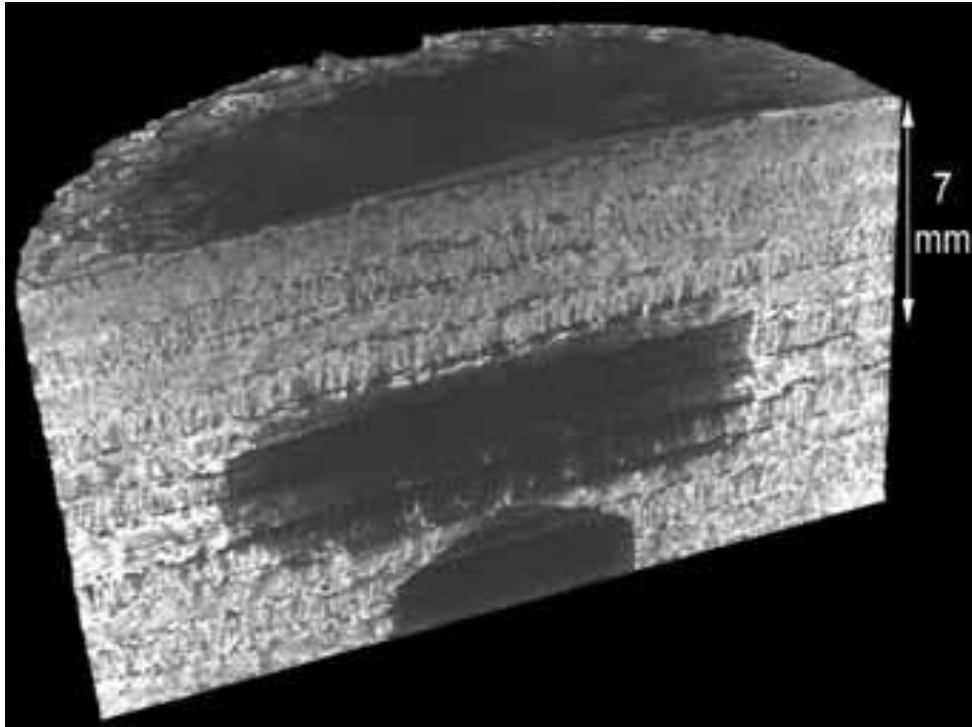


**Fig. 12 3D micro-CT cross section of a UHTC composite prepared by squeeze impregnation showing powder penetration: reprinted with permission from Am. Ceram. Soc. Bull. 91, (2012), Fig.11 in p. 26 [17].**

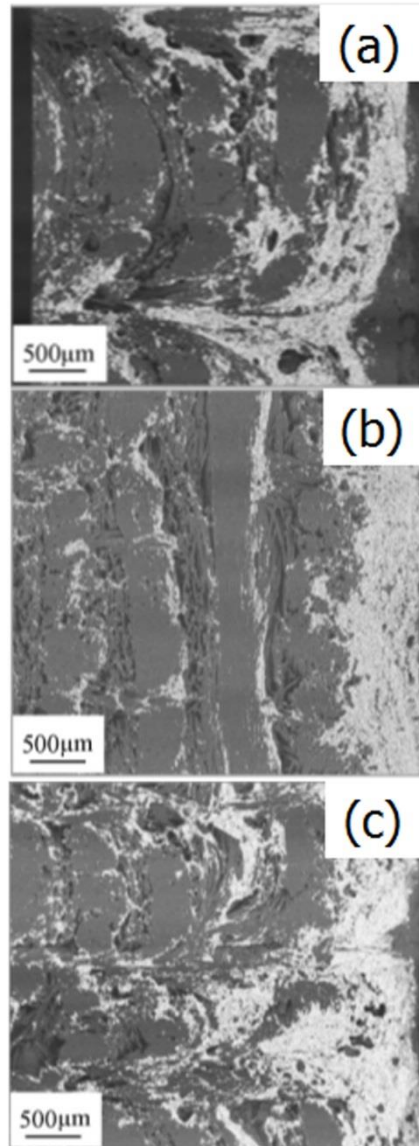


**Fig. 13 Backscattered electron images of particles distribution in C / C-UHTC composites: (a) C / C - ZrB<sub>2</sub>, (b) C / C - 4ZrB<sub>2</sub> - 1SiC, and (c) C / C - 1ZrB<sub>2</sub> - 2SiC - 2HfC: reprinted with permission from Elsevier, Mater. Sci. Eng. A 465, (2007) Fig.1 in p. 3 [10].**

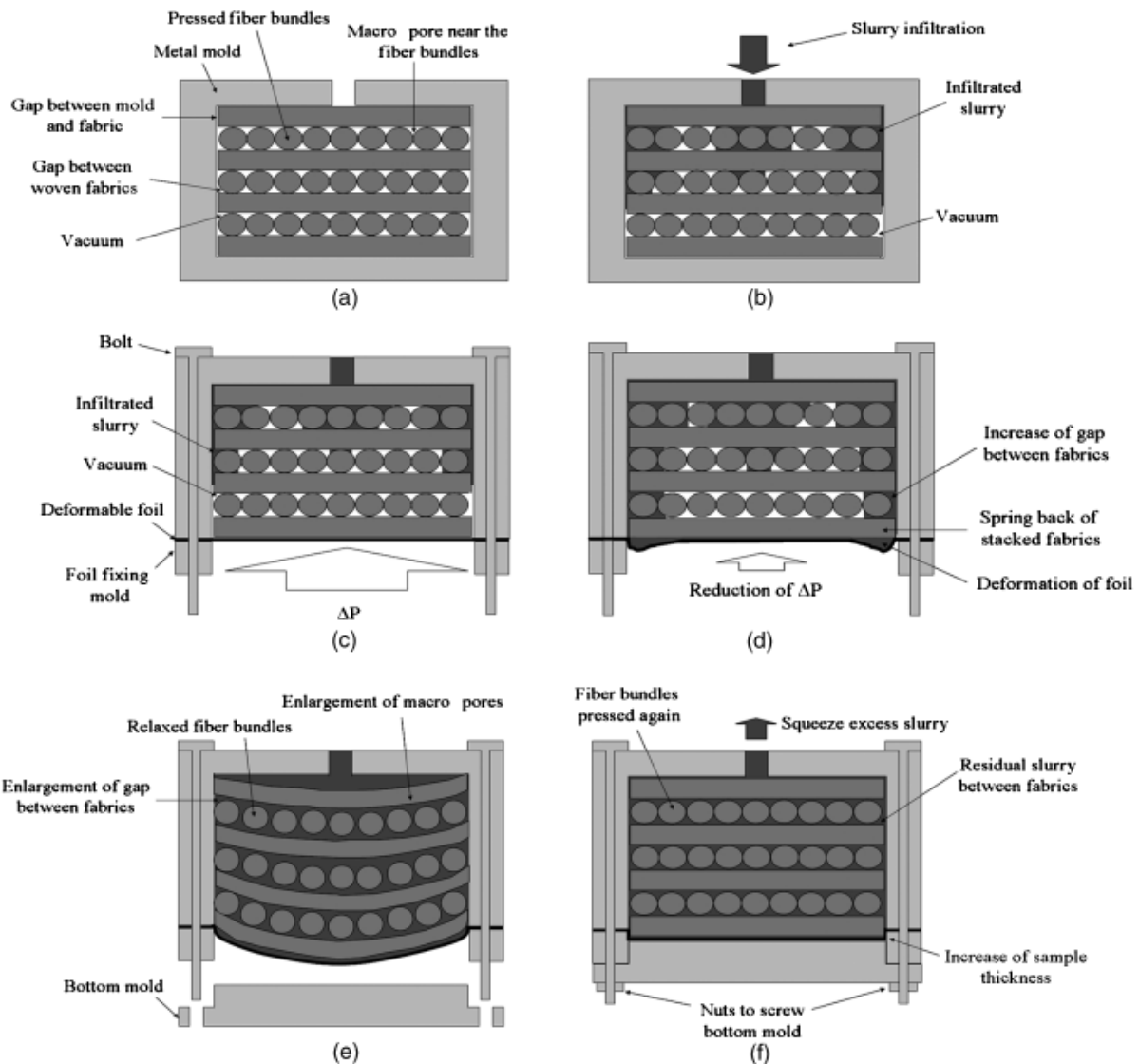


**Fig. 14 Schematics of moulds for conventional vacuum-assisted pressure casting and a new deformation process. (a, b) Conventional fixture of a firm mould. Woven fabric suppress the infiltration of slurry. (c) Mould with a deformable foil during initial infiltration. The fabrics are pressed by the difference of pressure ( $\Delta P$ ) inside and outside of the mould. (d) Onset of outward deformation of the foil by the slurry. (e) Completion of the full deformation and infiltration of the slurry. (f) Removal of excess slurry by squeezing the mould: reprinted with permission from John Wiley and Sons, *J. Am. Ceram. Soc.* 90, (2007) Fig.1 in p. 2658 [258].**

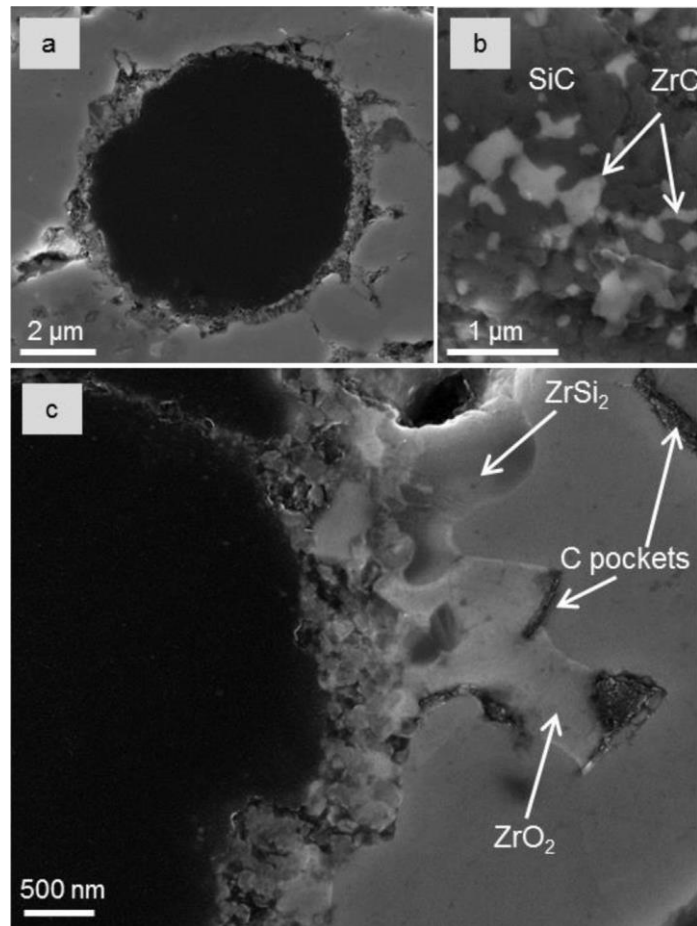


**Fig. 15 a) Cross section of Cf-ZrB<sub>2</sub> composite using ZrSi<sub>2</sub> as sintering aid. b) and c) Details of the fibre / matrix interface show the formation of brittle phases of SiC and ZrC: reprinted with permission from Elsevier, Journal of the European Ceramic Society 36 (2016) Fig.3 in p. 19 [113].**

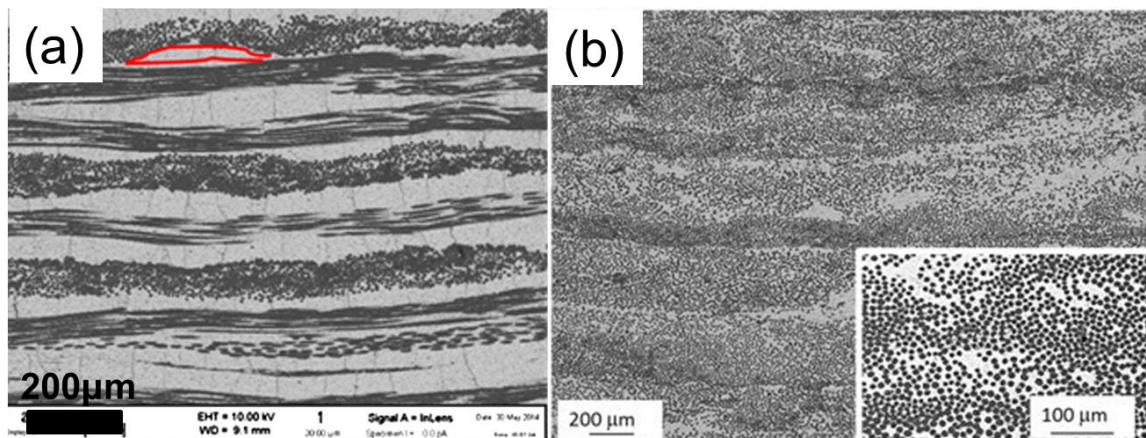


**Fig.16 (a) Cross section of  $C_f - ZrB_2$  composites produced by vacuum bagging followed by hot pressing at  $1700^\circ C$  for 20 mins: reprinted with permission from Elsevier, *Materials & Design* 85 (2015) Fig.3d in p. 130 [279]. (b) Cross section of  $C_f - ZrB_2$  composites, which was prepared by the infiltrate of  $ZrB_2$  into unidirectional fabrics that were stacked in  $0 - 0^\circ$  configuration. The sample was densified at  $1800 - 1900^\circ C$  for 30 – 40 mins: reprinted with permission from ISTE, *Scientific Reports* 8[9148] (2018) Fig.2a in p. 3 [281].**

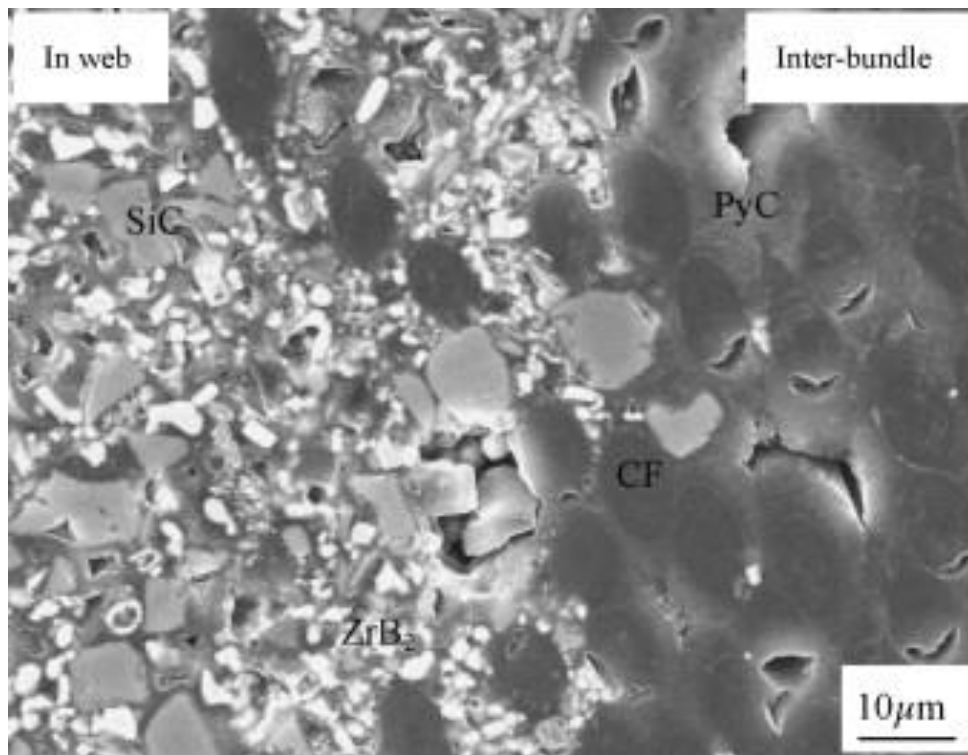


**Fig. 17** The local microstructure of (Fig. 12a) after a carbon CVI at a higher magnification: reprinted with permission from Elsevier, *Materials Science and Engineering: A* 465 (2007) Fig.2 in p. 3 [281].

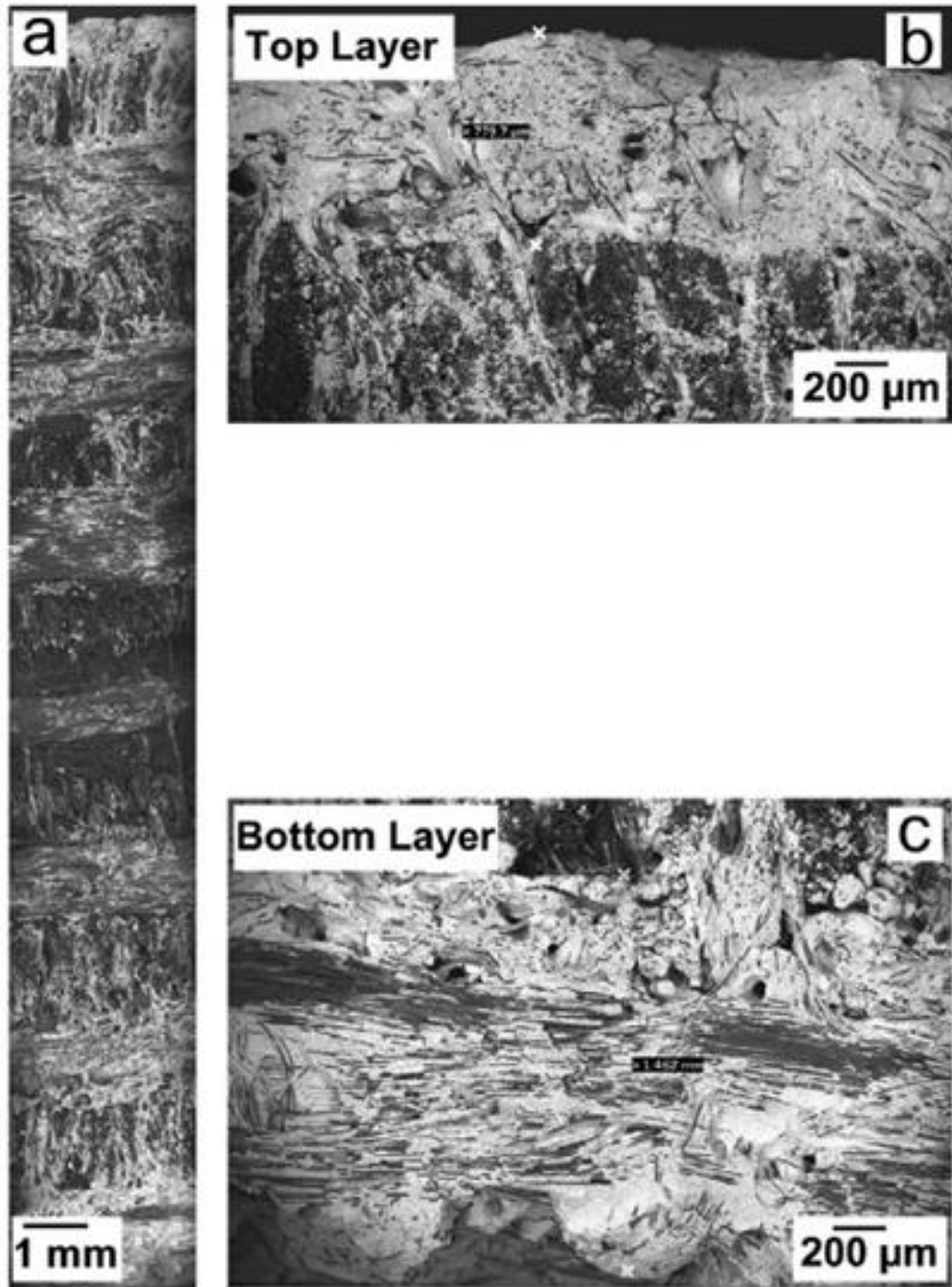


**Fig. 18 Powder distribution of a UHTC composite produced by slurry infiltration (a) The detailed microstructure of the top (b) and bottom of the composite (c): reprinted with permission from Elsevier, J. Eur. Ceram. Soc., 33[2], Fig.2 in p. 425 [288].**

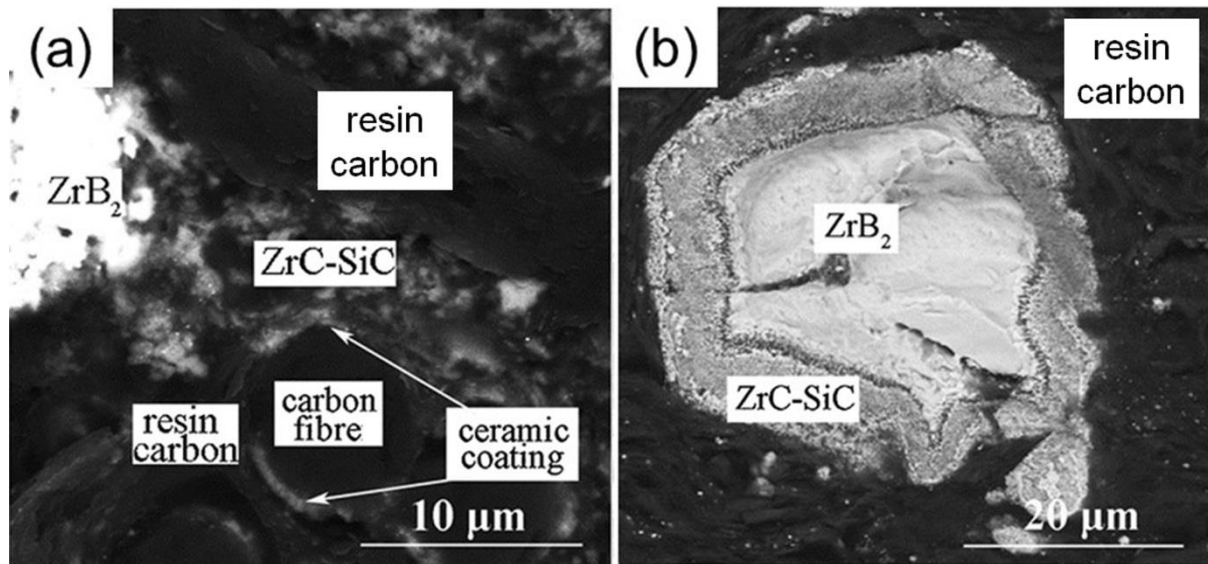


**Fig. 19** BSE images (a) (b) on the cross section of the C/C-ZrB<sub>2</sub>-ZrC-SiC composites prepared by PIP at different magnifications): reprinted with permission from Elsevier, Corros. Sci., 98 (2015), Fig. 4 in p. 554 [290].



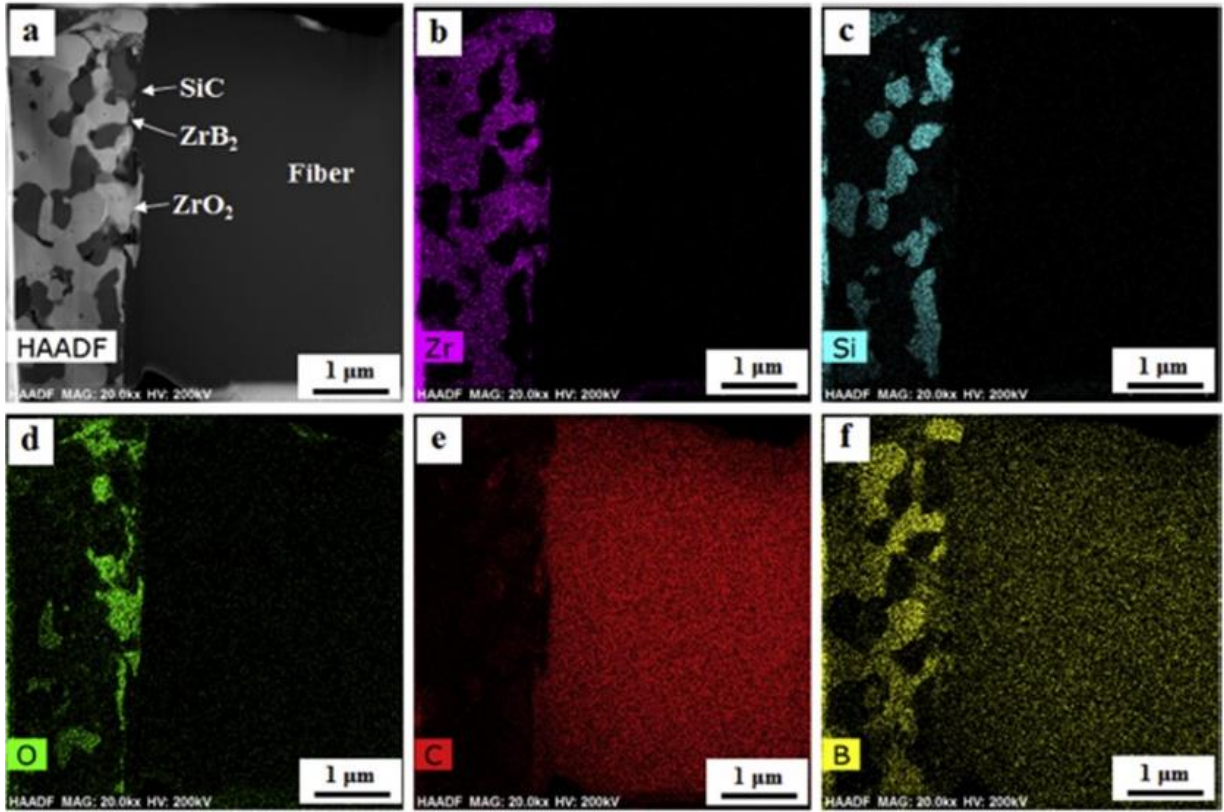


**Fig. 20** A tight and clean interface on the  $C_f/ZrB_2-SiC$  composite prepared by SIP and hot pressing, and corresponding elemental distributions: reprinted with permission from Elsevier, *Journal of the European Ceramic Society*, 39 (2019), Fig. 6 in p. 802 [289].

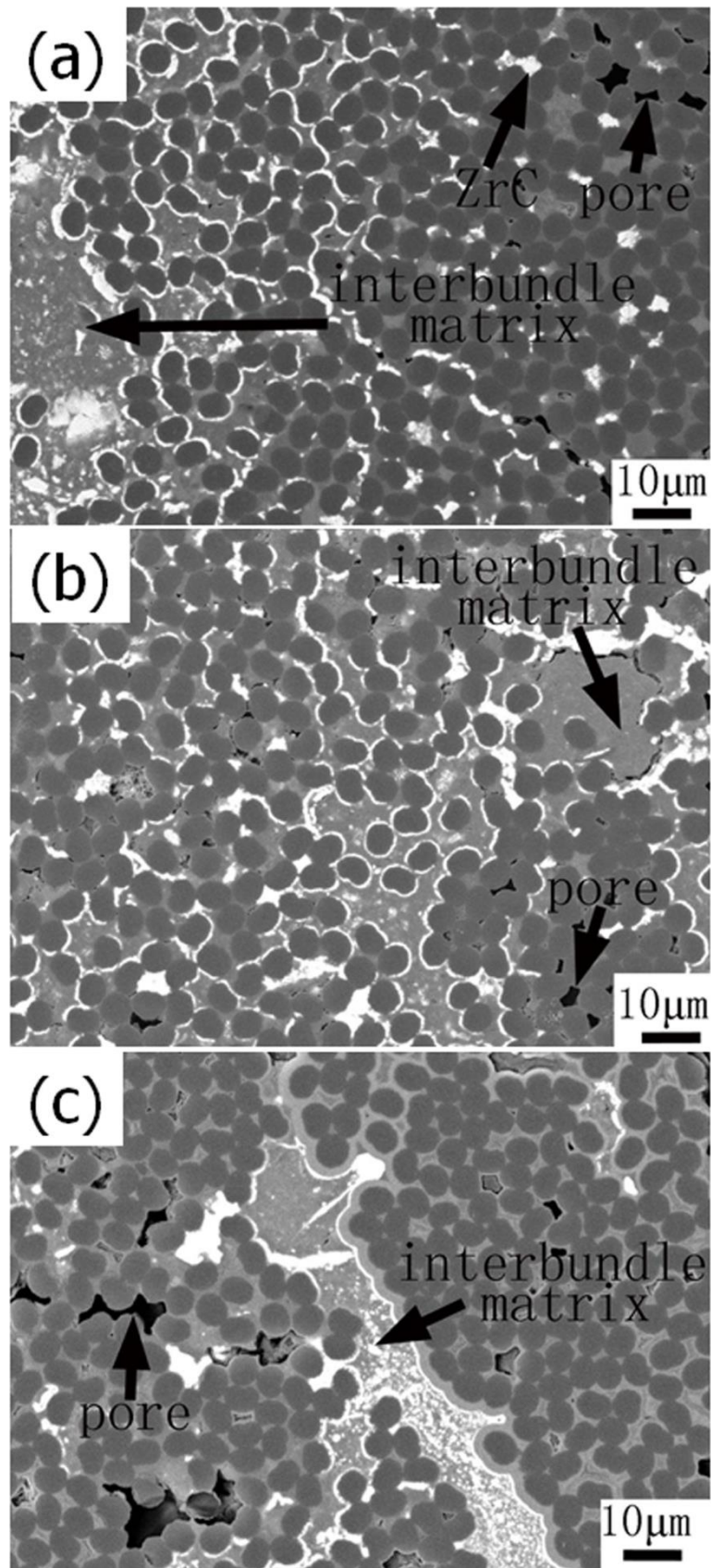


**Fig. 21** The polished surface of  $C_i/ZrC-SiC$  produced by PIP+CVI with different interface (a) none; (b) PyC; (c) PyC+SiC: reprinted with permission from John Wiley and Sons, *J. Am. Ceram. Soc.*, 91[10], Fig.1 in p. 3435 [294].

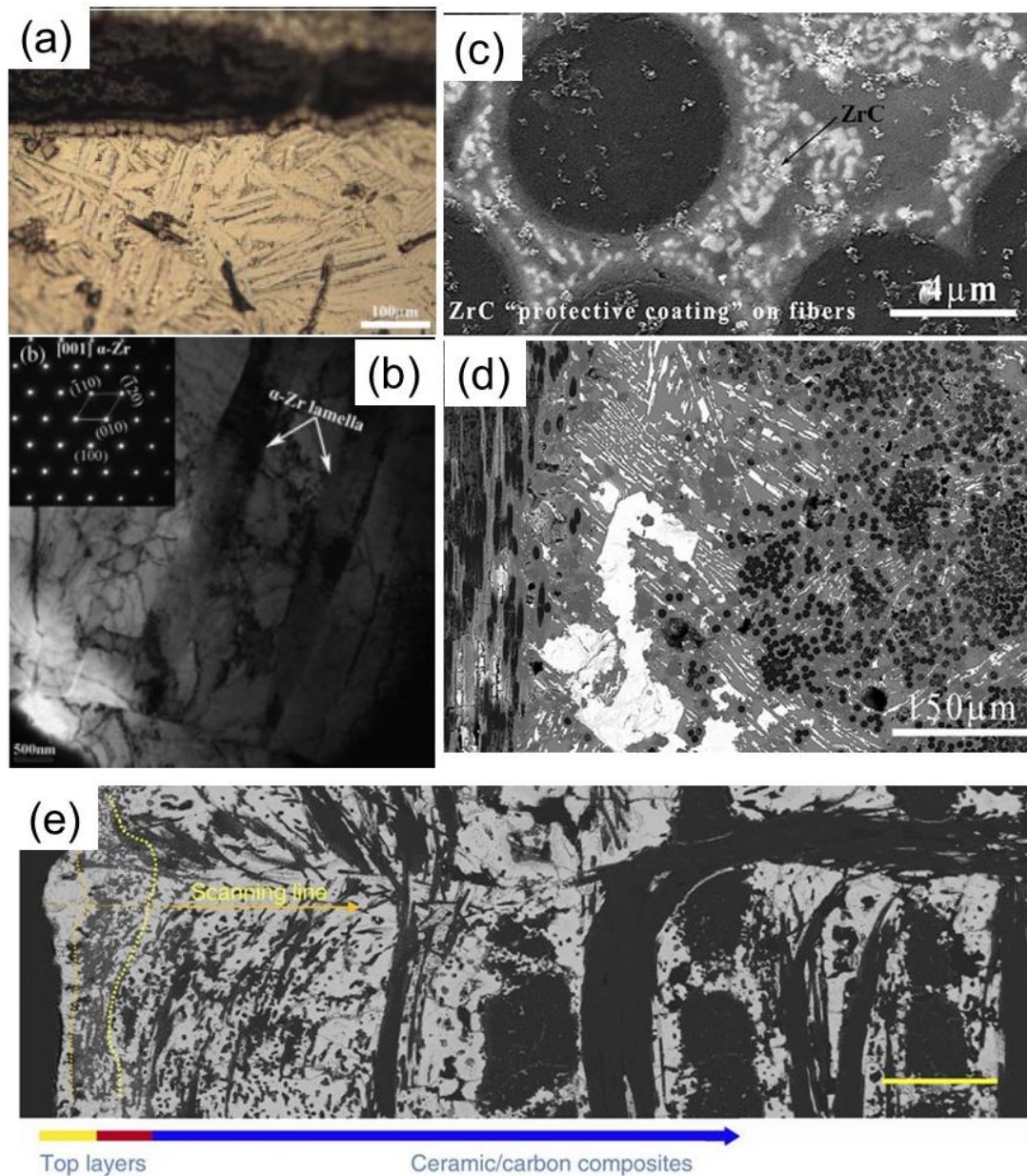


**Fig. 22** The microstructure of  $C_f/ZrC$  (a,b): reprinted with permission from John Wiley and Sons, *Int. J. Appl. Ceram. Technol.*, 8[2], Fig.6a & Fig.7b in p. 324 & 335 [295];  $C_f/ZrC-SiC$  (c,d): reprinted with permission from John Wiley and Sons, *J. Am. Ceram. Soc.*, 101[8], Fig.1B and Fig.3A in p. 3255 & 3256 [296];  $C_f/Zr-Ti-B-C$  (e) composite densified by RMI: reprinted with permission from Author, *Nat. Commun.*, 8[15836], Fig.4a in p.4 [297].

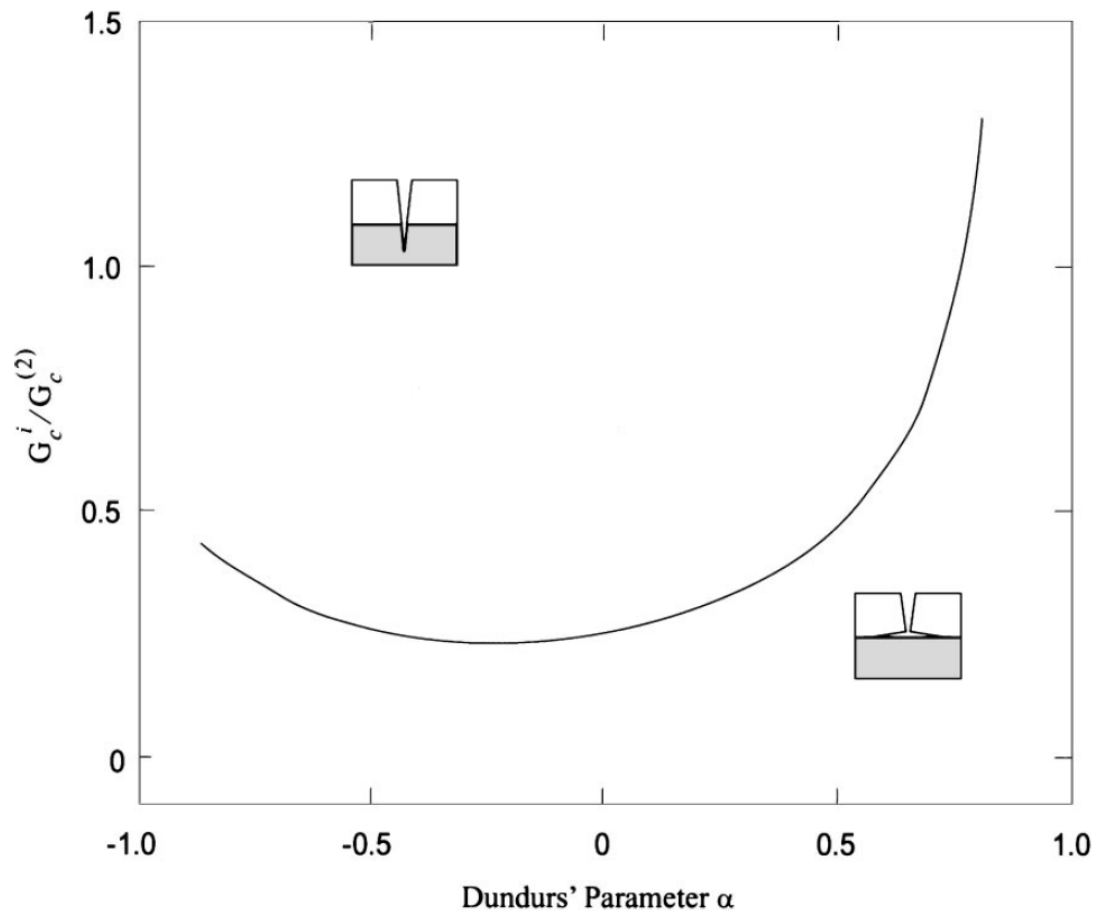


**Fig. 23 Debonding map showing crack penetration and crack deflection regimes as a function of Dundurs's parameter [124].**

# Selection, Processing, Properties and Applications of Ultra-High Temperature Ceramic Matrix Composites, UHTCMCs - A Review

**Total 13 tables**

**Table 1 UHTCMCs reinforced with Chopped fibre / whisker / CNT / graphene reinforcement.**

Sr. No.	Matrix	Reinforcement phase	Processing method and conditions	Density / %TD	Hardness / GPa	Fracture toughness / MPa m <sup>1/2</sup>	Strength / MPa	Reference
1	ZrB <sub>2</sub>	Multi-walled carbon nanotubes, CNT (10 vol%)	Aqueous hetero-coagulation followed by SPS at 1700°C	97.0	-	-	-	[84]
2	ZrB <sub>2</sub> -SiC (20 vol%)	Multi-walled CNTs (2 wt%)	Hot press 1900°C, 1h, 30 MPa	~96.0	15.5	4.6	616	[91], [116]
3	ZrB <sub>2</sub> -SiC (20 vol%)	Multi-walled CNTs (10 vol%)	Hot press 1850°C, 1h, 20 MPa	93.9	8.6	5.1	-	[102]
4	ZrB <sub>2</sub> -SiC	Multi-walled CNTs (2.5 wt%)	Hot press 2000°C, 1h, 30 MPa	>99.0	21.7	6.0	542	[91], [103]
5	ZrB <sub>2</sub> -SiC (20 vol%)	Multi-walled CNTs (5 wt% & 15 vol%)	SPS 1600-1800°C, 5-10 min, 25-40 MPa	94.6-99.1	11.5-23.1	4.9-8.0	214-565	[91], [104]
6	ZrB <sub>2</sub>	Multi-walled CNTs (2-6 vol%)	SPS 1900°C, 15 min, 70 MPa	95.0-99.0	14.1-16.4	1.5-3.5	150-315	[91], [105]

7	ZrC-TiC	Multi-walled CNTs (0.25-1 wt%)	SPS 1750°C, 5 min, 40 MPa	98.5	20.0-21.0	4.2-5.0	-	[91], [107]
8	ZrC-SiC	Multi-walled CNTs (0.25-1 wt%)	SPS 1750°C , 5 min, 40 MPa	99.0	21.6-20.2	5.8-5.2	-	[91], [108]
9	HfB <sub>2</sub>	Multi-walled CNTs (10 vol%)	SPS, 1800°C, 8 min, 30 MPa	99.3	21.8	7.8	894	[87]
10	TaC	Multi-walled CNTs (4 wt%)	SPS, 1850°C, 10 min, 100-363 MPa	>94.0	10.6-22.9	1.1-1.6	-	[99]
11	ZrB <sub>2</sub> - Si <sub>3</sub> N <sub>4</sub> (8 vol% )	Chopped pitch-derived C fibres (46 vol%)	Hot Press, 1800°C, 30 MPa	85.0	-	2.4	103	[109]
12	ZrB <sub>2</sub> - Si <sub>3</sub> N <sub>4</sub> (8 vol%) - SiC (3 vol%)	Chopped high modulus pitch-derived C fibres (45 vol%)	SPS, 1900°C, 60 MPa	>96.7	-	-	200	[110]
13	ZrB <sub>2</sub> & ZrB <sub>2</sub> -ZrSi <sub>2</sub> (20 vol%)	Short carbon fibres with/without heat treated (20 vol%)	Hot Press, 1600°C, 30 min, 30 MPa	98.9 & 97.9	-	7.6 & 6.9	481 & 437	[111], [112]
14	ZrB <sub>2</sub> -Si <sub>3</sub> N <sub>4</sub> (5 vol )	Chopped C fibres (10-20 vol%)	Hot press 1700°C, 10 min, 40 MPa	95.1-98.3	-	3.6-4.0	270	[113]
15	ZrB <sub>2</sub> -SiC (20 vol%)	Short C fibres (10-20 vol%)	Hot Press 1850°C & 2000°C, 30 & 60 min, 16& 30 MPa	100 & 99.3	19.2	6.4-6.6	397-445	[95], [106], [114]

16	ZrB <sub>2</sub> -SiC (2.5-15 wt%)	C fibres (2.5 – 10 wt%)	PS 2100°C-2150°C, 1h, Ar	87.0-95.0	11.0-15.0	3.0-5.9	-	[117]
17	HfB <sub>2</sub> -SiC (20 vol%)-B <sub>4</sub> C (2 wt%)- C (1 wt%)	Short Pitch-based carbon fibres (20-50 vol%)	Hot press 2100°C, 60 min, 20 MPa	98.1-99.5	-	5.6-6.1	160-250	[118]
18	ZrB <sub>2</sub> -SiC (20 vol%)	Graphite nano-flakes (10 vol%)	Hot Press 1850°C, 60 min, 20 MPa	99.6	16.5	7.1	-	[89]
19	ZrB <sub>2</sub> -SiC (20 vol%)	Graphite flakes (10 & 15 vol%)	Hot Press 1900°C, 60 min, 30 MPa	99.7 - 100	10.7-11.2	4.3-6.1	387-491	[85], [120], [121]
20	ZrB <sub>2</sub>	Graphene nano-platelets (2-6 vol%)	SPS, 1900°C, 15 min, 70 MPa	84.5-96.9	13.5-15.9	2.1-2.8	204-316	[86]
21	ZrB <sub>2</sub> -SiC (20 vol%)	Graphene nano-platelets (10 vol%)	SPS, 1800°C, 6 min, 35 MPa	100	-	-	-	[57]
22	ZrB <sub>2</sub> -SiC (20 vol%)	Graphene oxide (GO) (2 & 5 vol%)	Hot press 1950°C, 60 min, 30 MPa	98.9 & 99.2	22.9 & 22.8	6.1 & 7.3	698 & 1055	[88]
23	ZrC-SiC (25 vol%)	Graphene nano-platelets powder (5 wt%)	Hot press 1850°C, 60 min, 20 MPa	99.1	15.7	6.4	-	[89]
24	ZrC-SiC	Macro porous Graphene	Slurry infiltration followed by SPS	97.6	-	4.3	220	[90]
25	ZrB <sub>2</sub> ZrB <sub>2</sub> -Si <sub>3</sub> N <sub>4</sub> ZrB <sub>2</sub> -ZrSi <sub>2</sub>	SiC chopped fibres (0-30 vol%)	Hot press & SPS, 1400°C-1900°C, 10 & 5 min, 50 MPa	93.0-100	-	3.7-6.2	370-457	[92], [93], [115]

	ZrB <sub>2</sub> -MoSi <sub>2</sub> ZrB <sub>2</sub> -TaSi <sub>2</sub> (5-10 vol%)							
26	ZrB <sub>2</sub> -Si <sub>3</sub> N <sub>4</sub> (5 vol%)	Chopped Hi-Nicalon SiC fibres (15 vol%)	Hot press 1720°C, 10 min, 50 MPa	99.0	13.0	5.2	389	[94]
27	ZrB <sub>2</sub> -Si <sub>3</sub> N <sub>4</sub> (5 vol%)	3rd generation SiC short fibres (3 vol%)	Hot press 1700°C, 15 min, 30 MPa	99.0	-	-	-	[93]
28	ZrB <sub>2</sub> -ZrSi <sub>2</sub> (10 vol%)	SiC chopped fibres (20 vol%)	Hot Press, 1650°C, 10 min, 50 MPa	100	-	6.2	385	[96]
29	HfB <sub>2</sub> -Si <sub>3</sub> N <sub>4</sub> (8 vol%) HfB <sub>2</sub> -ZrSi <sub>2</sub> (10 vol%)	Chopped Hi-Nicalon SiC fibres (20 vol%)	SPS, 1550°C -1800°C, 5 min, 75 MPa	95.0-99.9	25.0-38.0	3.8-5.4	399-680	[97]
30	HfC + TaSi <sub>2</sub> (10 vol%)	Short chopped SiC fibres (15 vol%)	Hot press 1750°C, 14 min, 40 MPa	94.8	15.1	3.82	375	[98]
31	ZrB <sub>2</sub>	SiC whiskers (10- 30 vol%)	Hot press 1750°C, 60 min, 28 MPa	94.0-98.0		5.9-7.6	360-380	[100]
32	ZrB <sub>2</sub> -SiC (20 vol%)	ZrO <sub>2</sub> fibres (15 vol%)	Hot press 1850°C, 60 min, 30 MPa	98.6	18.4	6.8	1085	[101]



**Table 2 Mechanical properties of carbon fibres produced by PAN and Pitch precursor [128], [134]-[141]**

<b>Trade name</b>	<b>Manufacturer</b>	<b>Precursor</b>	<b>Tensile strength /MPa</b>	<b>Tensile modulus /GPa</b>	<b>Elongation %</b>
Torayca T300	Toray	PAN	3530	230	1.5
Torayca T800	Toray	PAN	5340-5490	294	1.9-2.0
Torayca T1100	Toray	PAN	7000	324	2.0
Torayca M60	Toray	PAN	3820	588	0.7
Tenax	Toho (Teijin Group)	PAN	4100-5100	240-265	1.7-2.1
Tenax IMS	Toho (Teijin Group)	PAN	4500-6000	290	1.6-2.1
Tenax UMS	Toho (Teijin Group)	PAN	4000-4700	390-550	0.7-1.2
TR series	Mitsubishi	PAN	5520	255	2.1
MR series	Mitsubishi	PAN	7000	325	2.2
HS40	Mitsubishi	PAN	4610	455	1.0
34 series	Mitsubishi	PAN	4482-4826	234	1.9-2.0
37-800	Mitsubishi	PAN	5585	234	2.1
K13D2U	Mitsubishi	Pitch	3700	935	0.4
K13C2U	Mitsubishi	Pitch	3800	900	0.6
Hextow IM10	Hexcel	PAN	6964	310	2.0

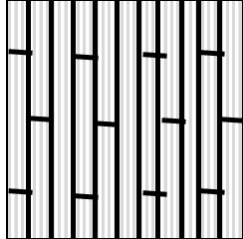
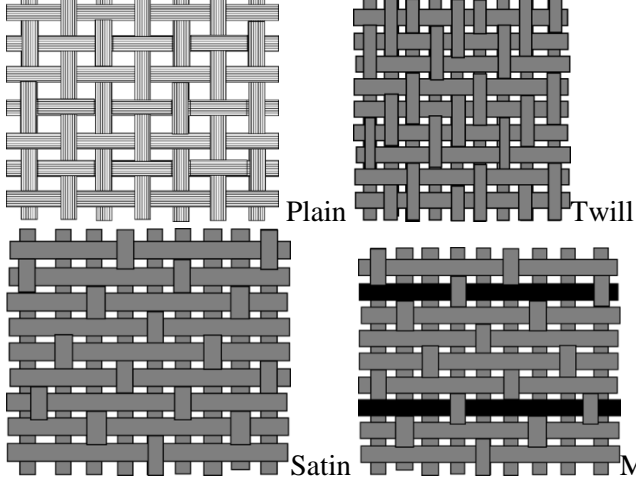

Hextow HM63	Hexcel	PAN	4688	441	1.0
Thornel T650	Solvay	PAN	4280	255	1.7
Thornel P55	Solvay	Pitch	1900	414	0.5
Thornel P100	Solvay	Pitch	2400	830	0.2
Tayrifil TC42S	Formosa plastic Corp.	PAN	5690	290	--
Tayrifil TC55	Formosa plastic Corp.	PAN	4400	380	--
Sigrafil	SGL Carbon	PAN	5000	270	1.9
GRANOC YS90A	Nippon Graphite Fiber Corporation	Pitch	3530	880	0.3
GRANOC YSH50A	Nippon Graphite Fiber Corporation	Pitch	3830	520	0.7

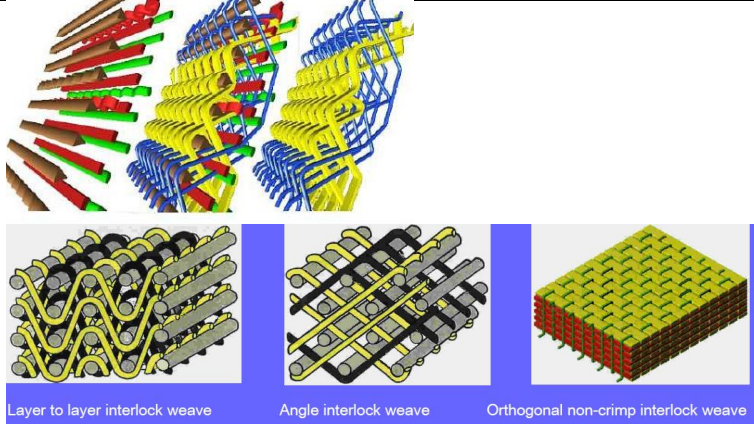
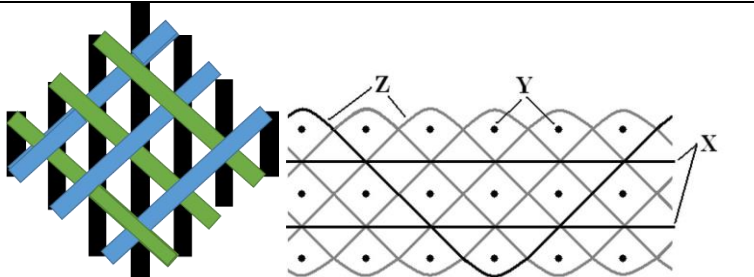
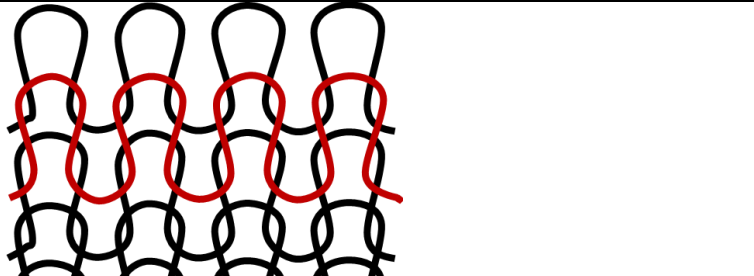
**Table 3 Physical, mechanical and thermal properties of the commercially available SiC fibre [144] - [147].**

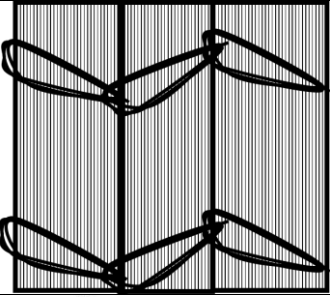
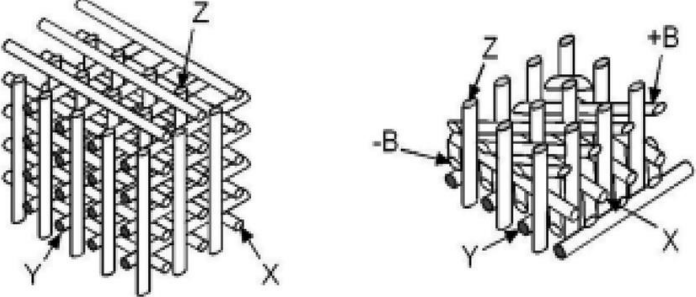
Trade name (manufacturer)	Production method (curing atmosphere)	Temp. production	Composition /wt%	Structure	Fibre diameter / $\mu\text{m}$	Density / $\text{g cm}^{-3}$	Tensile strength /GPa	Tensile Modulus /GPa	Thermal conductivity / $\text{W m}^{-1} \text{K}^{-1}$	Cost /EUR per kg
Nicalon (Nippon carbon)	Polymeric precursor (inert)	1200	56.6 Si+ 37.1 C + 11.7 O	2 nm crystallite in amorphous Si-C-O phase	14	2.55	3.0	220	3.0	1000
Tyranno LOX-M (Ube Industries)	Polymeric precursor (inert)	1200	55.4 Si + 32.4 C + 10.2 O + 2 Ti	1 nm crystallite in amorphous Si-C-O phase	11	2.35	3.3	186	1.4	1200
Hi-Nicalon (Nippon carbon)	Polymeric precursor (inert)	1300	62.4 Si + 37.1 C + 0.5 O	5 nm crystallite in amorphous Si-C-O phase	14	2.74	2.8	270	8.0	3250
Tyranno ZMI (Ube Industries)	Polymeric precursor (inert)	1300	56.1 Si + 34.2 C + 8.7 O + 1 Zr	5-10 nm crystallite in amorphous Si-C-O phase	11	2.48	3.4	193	2.5	1400
Hi-Nicalon Types S (Nippon carbon)	Polymeric precursor (inert)	1600	68.9 Si + 30.9 C + 0.2 O	100 nm crystallites near-stoichiometric	12	3.10	2.6	420	18	7000
Tyranno SA3 (Ube Industries)	Polymeric precursor (inert)	1600	67.8 Si + 31.3 C + 0.3 O + 2 Al	200 nm crystallites near-stoichiometric	7 to 10	3.10	2.8	380	64.5	6500

Sylramic	Polymeric precursor (inert)	>1700	67.0 Si + 29.0 C + 0.8 O + 2.3 B + 0.4 N + 2.1 Ti	100 nm crystallites near-stoichiometric	10	2.95	2.8	310	40-45	8000
Sylramic iBN (ATK-COI)	Polymeric precursor (inert)	>1700	SiC/BN	>100 nm crystallites near-stoichiometric and BN coating	10	3.05	3.2	400	>46	10500
SCS 6 and Ultra (Specialty Materials)	Chemical vapour deposition	1300	70 Si + 30 C + C filament	100 nm columnar SiC on C filament, SiC/C coating	140	3.00	5.9	415	70	8300
Sigma (TISICS)	Chemical vapour deposition	not available	11 W + 86 SiC + 1.3 C + 1.7 TiB <sub>2</sub>	W filament, 80 μm SiC layer and duplex C/TiB <sub>2</sub> layer	100	3.50	4.0	400	not available	7600

**Table 4 Different preform types, manufacturing techniques, advantages and disadvantages.**

Preform	Design	Advantages	Disadvantages
Low crimp, uniweave		High in-plane properties, good tailor ability, highly automated process	Low transverse and out of plane properties, poor fibre stability, labour intensive layup
2D Woven	 <p>Plain Twill Satin Matt</p>	Low crimp, Good in-plane properties, good limited drapability, highly automated process, suited for large covering area and extensive database.	Plain- high crimp, poor mechanical properties, Satin – different fibre orientation so it's good for mechanical properties but the interlace positions are irregular.
2D Braid		Good balance in off-axis, automated process, suitable for complex curved shapes, good drapability	Size limitation, low out of place properties

<p>3D Woven</p>	 <p>The image shows three types of 3D woven structures. The top part is a 3D perspective view of a woven fabric with red, green, and blue threads. Below it are three smaller diagrams: 'Layer to layer interlock weave' showing two layers of threads interlocking, 'Angle interlock weave' showing threads at an angle interlocking, and 'Orthogonal non-crimp interlock weave' showing a flat, orthogonal woven structure.</p>	<p>Moderate in-plane and out of plane properties, automated process,</p>	<p>Poor drapability, limited shapes are possible, limited tailorability for off axis</p>
<p>3D Braid</p>	 <p>The image shows two diagrams of 3D braiding. The left diagram is a 3D perspective view of a braid with black, green, and blue strands. The right diagram is a 2D schematic of a braid with three strands, labeled with X, Y, and Z axes.</p>	<p>Good balance for in-plane and Out of plane properties, Suitable for complex shapes</p>	<p>Slow process, size limitation</p>
<p>Multi axial warp knitting</p>	 <p>The image shows a diagram of multi-axial warp knitting, featuring a grid of black and red loops.</p>	<p>Good tailorability for balanced in plane properties, highly automated process, multilayer high though put, suitable for large covering area Complex shapes can be formed</p>	<p>Low out of plane properties</p>

<p>Stitched Fabrics</p>		<p>Good in plane properties, highly automated process, provides excellent damage tolerance and out of plane strength and excellent assembly aid</p>	<p>Small reduction in in plane properties, poor accessibility to complex curved shapes</p>
<p>Noobed</p>	 <p>reprinted with permission from Journal of the Indian Institute of Science., 95[3] (2015) Fig. 2 in p. 223 [193]</p>	<p>Multi directional delamination ballistic resistance, impact damage tolerance, Un crimped fibres</p>	<p>Yet to develop on large scale and for making complex shapes.</p>

**Table 5 Summary on the advantages and disadvantages of various densification / consolidation methods**

<b>Densification / Consolidation technique</b>	<b>Advantages</b>	<b>Disadvantages</b>
Precursor infiltration and pyrolysis	<ul style="list-style-type: none"> <li>▪ The composition of the ceramic deposit is highly versatile due to chemistry of precursor.</li> <li>▪ A large degree of control of the physical properties of the precursor is obtainable again by tailoring the chemistry of the precursor, allowing significant improvements made to the wettability, viscosity, or thermal properties (i.e. thermally curing) for a given procedure.</li> <li>▪ Precursor can be introduced through vacuum – procedurally simple.</li> <li>▪ As a liquid precursor, penetration into the fibre tow is facile due to the capillary pressure. This area is notoriously hard to penetrate through slurry based processes.</li> </ul>	<ul style="list-style-type: none"> <li>▪ Low yields of ceramic from precursor will require that many cycles of infiltration and pyrolysis are required for densification, increasing time and cost for a given component.</li> <li>▪ The matrix will always be porous and can contain micro-cracks, due to the escape of gaseous by-products and volumetric shrinkage from precursor to ceramic.</li> <li>▪ Reactive chemicals and repeated heat treatments can cause fibre degradation, leading to a loss of mechanical properties</li> </ul>
Reactive Melt Infiltration	<ul style="list-style-type: none"> <li>▪ It produces a near fully dense matrix</li> <li>▪ The processing time is shorter than for most ceramic matrix composite fabrication processes and is subsequently relatively cheap.</li> <li>▪ The closed porosity at the surface can often eliminate the need for a final oxidation resistant coating.</li> <li>▪ A reaction bonded UHTC matrix is effectively produced.</li> </ul>	<ul style="list-style-type: none"> <li>▪ For fibre composites the high temperatures required for reactive metal infiltration exposes the carbon fibres to very aggressive molten metals, often above 1400°C.</li> <li>▪ The exothermic nature of the reaction between constituents can also further increase the temperature locally, causing more damage.</li> <li>▪ The metal in this form is highly reactive and, if infiltration conditions are not strictly controlled, serious degradation of the carbon fibre preform, will occur leading to deleterious consequences on the properties.</li> <li>▪ Residual metallic phases, which have relatively low oxidation resistance and a</li> </ul>



		<p>lower melting point than the ceramic phases present. This metallic phase can lead to accelerated creep, crack propagation and further attack when the material is operating at high temperature.</p>
Chemical Vapour Infiltration	<ul style="list-style-type: none"> <li>▪ The deposited material can have a high purity.</li> <li>▪ It is a low temperature process, thus fibre damage can be avoided.</li> <li>▪ It is a versatile process. Many binary compounds can be deposited, as well as multi-coatings and functional graded materials, without stopping the process.</li> <li>▪ Intricate shapes can be prepared without damaging the continuous fibres used for reinforcement.</li> <li>▪ The morphology and microstructure of the coating can be tailored by changing temperature, pressure and precursor feed rate.</li> <li>▪ High reproducibility</li> <li>▪ High deposition rates are possible.</li> <li>▪ The resulting composites can offer excellent mechanical and anti-ablation properties</li> <li>▪ Deposit has high thermal conductivity and good creep resistance</li> </ul>	<ul style="list-style-type: none"> <li>▪ Processing times of industrial scale CVI is currently very long, on the order of 2-3 months, due to isothermal heating rates and premature surface porosity closure that requires the process to be stopped a number of times.</li> <li>▪ Large energy input is required due to the extended process times.</li> <li>▪ Corrosive by-products require special safety precautions, expensive equipment and maintenance costs are subsequently high, which further increase the cost of the manufacturing process.</li> <li>▪ It is very difficult to obtain fully dense composites; densities of ~90% of theoretical are therefore typical.</li> <li>▪ The cost of some precursors is high, in particular rhenium and hafnium chlorides.</li> <li>▪ Low infiltration depth for large radicals such as Hf, Zr and Ta</li> </ul>
Slurry impregnation process	<ul style="list-style-type: none"> <li>▪ Production of a slurry of ceramic particles is cheap, quick and easy</li> <li>▪ Simple procedure to introduce a slurry to a fibrous substrate</li> <li>▪ Properties of the slurry are easily tuneable based on the chemicals used</li> </ul>	<ul style="list-style-type: none"> <li>▪ Homogeneous penetration of large preforms is difficult</li> <li>▪ Stable suspensions of dense ceramic particles (e.g. HfB<sub>2</sub>) are hard to make; an issue is possible with respect to scalability</li> <li>▪ Issues exist with clogging the surface of preforms with ceramic particles</li> </ul>

	<ul style="list-style-type: none"> <li>▪ Impregnation cycles are easy (requiring only impregnation and drying) to bring the green composite to moderate levels of densification</li> </ul>	<ul style="list-style-type: none"> <li>▪ Low penetration into fibre tows due to large particle sizes relative to tow entrance size</li> <li>▪ Produces a material with a discontinuous porous matrix</li> </ul>
Hot pressing	<ul style="list-style-type: none"> <li>▪ High Fibre volume fraction</li> <li>▪ High density achievable</li> <li>▪ Short manufacturing time</li> <li>▪ Apparatus is the same used for the sintering monolithic ceramics</li> <li>▪ Chemicals involved have minor implications on H&amp;S (if compared to PIP and CVI)</li> </ul>	<ul style="list-style-type: none"> <li>▪ Matrix-fibre interaction due to high temperature and pressure</li> <li>▪ Fibre degradation due to high temperature</li> <li>▪ near-net shape components are not achievable</li> </ul>
Pressureless sintering	<ul style="list-style-type: none"> <li>▪ High Fibre volume fraction</li> <li>▪ Low pressure, theoretically, reduced the matrix-fibre interaction risk and fibre degradation</li> <li>▪ Short manufacturing time</li> <li>▪ Near-net shapes are, in theory, possible</li> <li>▪ Chemicals involved have minor implications on H&amp;S (if compared to PIP and CVI)</li> </ul>	<ul style="list-style-type: none"> <li>▪ Lower density than HP and SPS</li> <li>▪ Low pressures requires higher sintering temperatures and time than HP and SPS</li> </ul>
Spark plasma sintering	<ul style="list-style-type: none"> <li>▪ High Fibre volume fraction</li> <li>▪ High densities achievable</li> <li>▪ Short manufacturing time</li> <li>▪ Reduced sintering temperatures</li> <li>▪ Reduced sintering times</li> <li>▪ Chemicals involved have minor implications on H&amp;S (if compared to PIP and CVI)</li> </ul>	<ul style="list-style-type: none"> <li>▪ Although lower sintering temperature and time, matrix-fibre interaction has been reported</li> <li>▪ Equipment is more expensive than conventional HP and Pressureless furnaces</li> <li>▪ Near-net shape components are not achievable</li> </ul>
Hot isostatic pressing	<ul style="list-style-type: none"> <li>▪ High Fibre volume fraction</li> <li>▪ Near-net shapes are, in theory, possible</li> <li>▪ Chemicals involved have minor implications on H&amp;S (if compared to PIP and CVI)</li> </ul>	<ul style="list-style-type: none"> <li>▪ Equipment is more expensive than conventional HP and Pressureless furnaces</li> <li>▪ Usually works with high pressure</li> </ul>

**Table 6 Literature reported data on RMI of UHTCMCs.**

Matrix	Constituents	Processing conditions	Properties	Reference
ZrC	3D C <sub>f</sub> preforms Pyro. C interface Zr-Si alloy (91.2 at.% Zr & 8.8 at.% Si) Eutectic formed at 1570°C	C deposited by CVI RMI at 1800°C at 8.8x10 <sup>-2</sup> Pa in flowing Ar	Density increased from 1.33 g cm <sup>-3</sup> to 2.46 g cm <sup>-3</sup> 5% porosity Zr <sub>2</sub> Si phase still present Pore size between 20-200 μm Flexural strength 239.5 MPa Linear ablation rate 0.0028 mm s <sup>-1</sup>	[227]
	2D C <sub>f</sub> felts Pyro. C interface and other unspecified interface Zr : Si : C : ZrO <sub>2</sub> powder in a ratio of 3 : 5 : 1 : 0.2	80 h of CVI using CH <sub>4</sub> to deposit carbon at 1050 - 1150°C and 5 - 15 kPa Graphitised at 2500°C in flowing Ar RMI at 2000 - 2300°C, furnace dwell 2h	Mass ablation rates 1.33 μm s <sup>-1</sup> and 0.24 mg s <sup>-1</sup>	[228]
	3D C <sub>f</sub> preform Pyro. carbon interface Zr molten powder	C deposited using CVI Ar atmosphere at 1850°C	No residual Zr detected using XRD	[229]
	C <sub>f</sub> An unspecified interface then a pyro. C interface Molten Zr	Carbon deposited using CVI	Residual α-Zr detected and mechanism for formation proposed	[230]
SiC-ZrB <sub>2</sub> -ZrC	2D C <sub>f</sub> preform SiC interface B <sub>4</sub> C-phenol formaldehyde resin slurry ZrSi <sub>2</sub> alloy powder	Interface produced using CVI of CH <sub>3</sub> SiCl <sub>3</sub> at 1000°C Preform impregnated with resin 4x and pyrolysed at 900°C RMI performed at 1800°C under vacuum Sealed using SiC CVI	ZrSi <sub>2</sub> alloy residual found in microstructure Linear ablation rate 0.002 mm s <sup>-1</sup>	[231]
	3D C <sub>f</sub> / B <sub>4</sub> C - C preform Pyro. C and SiC interface B <sub>4</sub> C - C sol ZrSi <sub>2</sub> alloy	Interfaces produced using CVI Pyrolysis of the sol 900°C Carbothermal reduction 1500°C in Ar RMI performed at 1750 - 1900°C	Higher temperatures resulted in better densification	[232]

ZrC-ZrB <sub>2</sub>	2D C <sub>f</sub> preforms Pyro C interface Eutectic Zr – B alloy (Zr : B = 86 : 14)	Interface produced using CVI of propylene 900°C Alloy was prepared by arc melting Zr and B powder RMI performed at 1800°C	Resulting density 3 g cm <sup>-3</sup> 4% open porosity No residual alloy detected Linear ablation rate 0.0001 mm s <sup>-1</sup>	[224]
	3D C <sub>f</sub> preforms Impregnated with phenolic and resin and B <sub>4</sub> C particles Zr powder	Impregnation process was repeated 4 times before being pyrolysed at 2200°C in Ar RMI performed at 2000°C	Density of 3.07 g cm <sup>-3</sup> Open porosity of 9.1% Flexural strength of 147 MPa Mass ablation rate was 0.0039 g s <sup>-1</sup> Linear ablation rate was 0.01 mm s <sup>-1</sup>	[225]
ZrB <sub>2</sub>	2D C <sub>f</sub> preform TiB <sub>2</sub> interface Zr <sub>2</sub> Cu alloy	Interface produced using CVI at 800°C, at 300 mbar for 4h, resulting in a 4 µm coating RMI performed at 1100 - 1500°C under vacuum	C <sub>f</sub> showed no critical degradation due to TiB <sub>2</sub> coating	[220]
	2D C <sub>f</sub> preform B <sub>2</sub> O <sub>3</sub> phenolic based preforms TiB <sub>2</sub> interface Zr <sub>2</sub> Cu or Zr <sub>2</sub> Cu - 1at.% B or Zr <sub>2</sub> Ag - 1at.% B	Interface produced using CVI at 800°C, at 300 mbar for 2 h, resulting in a 2 µm coating RMI performed at 1500 - 1900°C under vacuum	Addition of B <sub>2</sub> O <sub>3</sub> decreases ceramic yield and causes fibre degradation 2 µm coating insufficient to stop fibre degradation	[226]
HfC	3D C <sub>f</sub> preform Pyro. C and SiC interface Phenol formaldehyde resin HfSi <sub>2</sub> alloy powder	Interfaces produced using CVI at 1000°C Resin pyrolysed three times at 1500°C RMI performed at 1600 - 1700°C under vacuum	Residual HfSi <sub>2</sub> was detected	[207]

**Table 7 Precursors and the conditions needed for the deposition of oxide / non-oxide ceramics [236], [237].**

<b>Matrix deposited</b>	<b>Reactant gases</b>	<b>Temperature / °C</b>
C	CH <sub>4</sub> -H <sub>2</sub>	1000-1200
HfC	HfCl <sub>4</sub> -(CH <sub>4</sub> or C <sub>3</sub> H <sub>6</sub> -H <sub>2</sub> -Ar)	900-1600
ZrC	ZrCl <sub>4</sub> -(CH <sub>4</sub> or C <sub>3</sub> H <sub>6</sub> -H <sub>2</sub> -Ar)	900-1600
TaC	TaCl <sub>5</sub> -(CH <sub>4</sub> or C <sub>3</sub> H <sub>6</sub> -H <sub>2</sub> -Ar)	900-1500
SiC	CH <sub>3</sub> SiCl <sub>3</sub> -H <sub>2</sub>	900-1300
Si <sub>3</sub> N <sub>4</sub>	SiCl-NH <sub>3</sub> -H <sub>2</sub>	1000-1400
TiB <sub>2</sub>	TiCl <sub>4</sub> -BCl <sub>3</sub> -H <sub>2</sub>	800-1200
	TiCl <sub>4</sub> -B <sub>2</sub> H <sub>6</sub> -H <sub>2</sub>	600-1100
ZrB <sub>2</sub>	ZrCl <sub>4</sub> -BCl <sub>3</sub> -H <sub>2</sub> -Ar	900-1200
	ZrCl <sub>4</sub> -B <sub>2</sub> H <sub>6</sub> -H <sub>2</sub>	600-1100
HfB <sub>2</sub>	HfCl <sub>4</sub> -BCl <sub>3</sub> -H <sub>2</sub> -Ar	900-1200
	ZrCl <sub>4</sub> -B <sub>2</sub> H <sub>6</sub> -H <sub>2</sub>	600-1100
	Hf(BH <sub>4</sub> ) <sub>4</sub>	≤300°C
SiO <sub>2</sub>	SiH <sub>4</sub> -O <sub>2</sub> -H <sub>2</sub>	300-750
TiO <sub>2</sub>	TiCl <sub>3</sub> -H <sub>2</sub> O	800-1000
ZrO <sub>2</sub>	ZrCl <sub>4</sub> -CO <sub>2</sub> or O <sub>2</sub> -H <sub>2</sub>	900-1100
Al <sub>2</sub> O <sub>3</sub>	AlCl <sub>3</sub> -CO <sub>2</sub> or O <sub>2</sub> -H <sub>2</sub>	900-1000
HfO <sub>2</sub>	HfCl <sub>4</sub> -CO <sub>2</sub> or O <sub>2</sub> -H <sub>2</sub>	900-1100
Ta <sub>2</sub> O <sub>5</sub>	ZrCl <sub>4</sub> -CO <sub>2</sub> or O <sub>2</sub> -H <sub>2</sub>	900-1100
YSZ	Zr(C <sub>11</sub> H <sub>19</sub> O <sub>2</sub> ) <sub>3</sub> -Y(C <sub>11</sub> H <sub>19</sub> O <sub>2</sub> ) <sub>3</sub>	735

**Table 8 Chemical vapour infiltration variants w.r.t. temperature, pressure, heating [242].**

CVI / CVD Process type	Temperature		Pressure				Heating	
	Uniform	Gradient	Uniform	Gradient	Atmospheric	Low	Radiative	Inductive
Plasma enhanced low pressure	X	X	X	X		X	X	
Thermal gradient, radiantly heated, isobaric		X	X		X	X	X	
Thermal gradient, inductively heated, isobaric		X	X		X	X		X
Liquid immersion, thermal gradient, inductively heated isobaric, atm. pressure		X	X		X	X		X
Isothermal, forced flow	X			X	X	X	X	X
Isothermal, pulsed pressure	X			X	X			
Thermal gradient, forced flow		X		X	X			
Microwave-heated, isobaric or forced-flow		X	X	X	X	X		
Catalyst-enhanced, isothermal, isobaric	X		X		X		X	
Particle-transport enhanced, isothermal, isobaric	X		X		X		X	

**Table 9 Mechanical properties, density achieved and sintering conditions of UHTCMCs processed by hot pressing.**

System	Sintering aids/ non-UHTC phase	Vf / %	T / °C	P / MPa	$\rho_r$ / %	MOR / MPa	$K_{IC}$ / MPa m <sup>1/2</sup>	Ref
C <sub>f</sub> - ZrB <sub>2</sub>	Si <sub>3</sub> N <sub>4</sub>	70	1800	40	78	90	--	[279]
C <sub>f</sub> -ZrB <sub>2</sub>	B <sub>4</sub> C	40	1900	40	-	327	13.8	[275]
C <sub>f</sub> -ZrB <sub>2</sub>	SiC, Si <sub>3</sub> N <sub>4</sub>	20	1900	30	-	310	6.72	[276]
C <sub>f</sub> - ZrB <sub>2</sub>	SiC	40	1800-	30-40	92	235 ± 40	6.4 ± 0.8	[283]
		55	1900		88	125 ± 35	7.3 ± 0.9	
		65			85	140 ± 40	7.5 ± 1.4	
C <sub>f</sub> - ZrB <sub>2</sub>	SiC	55	1800- 1900	30-40	96	152 ± 12	10.6 ± 1.6	
C <sub>f</sub> - ZrB <sub>2</sub>	SiC and Si <sub>3</sub> N <sub>4</sub>	40-45	1800- 1900	30-40	92-95	355 ± 40 500 ± 51 (1200°C) 547 ± 80 (1500°C)	9.6 ± 0.7 8.7 ± 1.2 (1500°C)	[281]
SiC <sub>f</sub> -ZrB <sub>2</sub>	ZrSi <sub>2</sub>	50	1600	40	95	145 ± 10	--	[278]

Abbreviation used: ch=chopped, Vf = fibre volume fraction, T = temperature, P = pressure,  $\rho_r$  = relative density, MOR= Modulus of Rupture,  $K_{IC}$  = fracture toughness

**Table 10 Properties of carbon fibre reinforced ultra-high temperature ceramic matrix composites prepared by different approaches.**

Materials	General characteristic	Detailed Fabrication process	Density / g/cm <sup>3</sup>	Open porosity / %	Flexural strength / MPa	Elastic modulus / GPa	Reference
C <sub>f</sub> / HfB <sub>2</sub> -C	Non-sintered + 2D preform	Injection + infiltration of the HfB <sub>2</sub> -C slurry into the preform + carbon CVI	3.2 ± 0.16	16	121.37 ± 18.30	28.3 ± 3.2	[179]
C <sub>f</sub> / ZrC	Non-sintered PIP + 3D preform	Infiltration of ZrC precursors (ZrO <sub>2</sub> / C sol) into the preform, reduction at 1200°C and further heat treatment at 1600°C.	1.98	12.4	107.6	28.8	[308]
C <sub>f</sub> / ZrC-SiC	Partially sintered + 2D preform	C preform without any treatment; infiltration of ZrC-PCS slurry into the preform plus hot pressing; PIP with PCS + pyrolyzed at 1100°C + final heat treatment at 1800°C	2.47	6.6	178±77	106±13	[294]
C <sub>f</sub> / ZrC-SiC	As above	Preform initially treated by CVI of PyC; others steps same as above	2.18	4.9	748±15	141±12	[294]
C <sub>f</sub> / ZrC-SiC	As above	Preform initially treated by alternated CVI of PyC/SiC; others steps same as above	2.25	7.4	559±121	138±15	[294]
C <sub>f</sub> / ZrC-SiC	RMI + 3D needled preform	(PyC-SiC) <sub>3</sub> deposited in preform by CVI, further infiltrated by ZrC precursors to generate C <sub>f</sub> /ZrC-C; RMI of Si within preform to form dense C <sub>f</sub> /ZrC-SiC-ZrSi <sub>2</sub>	2.52	1.68	380	61	[296]
C <sub>f</sub> / ZrB <sub>2</sub> -ZrC-SiC	RMI + 3D needled preform	(PyC-SiC) deposited in preform by CVI, further infiltrated by B-containing sols to generate Cf/B <sub>4</sub> C-C after heat treatment; RMI of Zr-Si alloy within preform to form dense C <sub>f</sub> /ZrB <sub>2</sub> -ZrC-SiC	2.42 ± 0.01	9.4 ± 0.1	184 ± 9	/	[306]



$C_f / ZrC-SiC$	RMI + 3D braided preform	Preform infiltrated by PCS and PR to form $C_f/SiC-C$ after heat treatment; RMI of Zr-Si alloy with the preform to form dense $C_f/ZrC-SiC$	2.94	5.3	101.5±8.16	35.18±9.58	[191]
$C_f / ZrC-Zr$	RMI + 2D preform	Carbon fibres coated with $ZrO_2 / HfN$ by CVD and then woven into 2D preform. C/C skeleton formed by coating with preform by CVD; RMI of Zr into the preform to form $C_f/ZrC-Zr$	/	/	/	/	[295]
$C_f / ZrC$	RMI + 2D preform	C/C preform infiltrated by RMI of $Zr_2Cu$ alloy at 1200°C to generate $C_f/ZrC$ composites	/	/	172±12	/	[307]
$C_f / C-ZrC$	CVI + MRI + 3D preform	C/C preform infiltrated by RMI of Zr-Si alloy at 1800°C	2.46	5.0	240		[227]
$C_f / ZrB_2$	Vacuum bagging + hot pressing + 1D fabrics	1D fabrics coated with slurry containing $ZrB_2$ powders and additives; fabrics stacked and pressed by vacuum bagging, final densification at 1600-1800°C by hot-pressing	3.3	/	90	/	[279]
$C_f / ZrB_2-SiC-Si_3N_4$	Slurry infiltration + hot pressing + unidirectional fabrics	$ZrB_2 / SiC / Si_3N_4$ slurry infiltrated into C fabrics stacked in 0-0° configuration. Hot pressed at 1800-1900°C under 30-40MPa	/	Very small amount	355 ± 40 (∥) 63 ± 7 (⊥)	239(∥) 188(⊥)	[281]

**Table 11 Thermal properties (melting point, CTE, thermal conductivity, diffusivity, Cp) of UHTCs and UHTCMCs.**

Material	Coefficient of Thermal Expansion, CTE / $\times 10^{-6} \text{ K}^{-1}$	Thermal Conductivity / $\text{W m}^{-1}\text{K}^{-1}$	Thermal Diffusivity / $\text{mm}^2 \text{ s}^{-1}$	Specific Heat Capacity / $\text{J g}^{-1}\text{K}^{-1}$	Reference
C <sub>sf</sub> -HfB <sub>2</sub> -SiC		54.4 - 93.8			[118]
C <sub>f</sub> -HfC	3.36 (1473 K)	4.18 ± 0.14 (473 K – 2073 K)	4.2 - 7.5	0.42 - 0.68	[205]
C <sub>f</sub> -HfC-SiC	2.95 (1473 K)	3.33 ± 0.42 (473 K – 2073 K)	1.9 - 6.1	0.49 - 0.78	[205]
C <sub>f</sub> /C-3.5wt%HfC	1.20 - 3.25	16.5 (⊥) - 19.8 (∥) (298 K); 24.5 (⊥) - 27.5 (∥) (673 K); 23.0 (⊥) - 26.5 (∥) (1073 K)	8.7 - 22.0	0.57 - 1.50 (298 K – 1073 K)	[340]
C <sub>f</sub> /C-6.5wt%HfC	1.60 - 4.00	18.5 (⊥) - 24.8 (∥) (298 K); 25.5 (⊥) - 32.0 (∥) (673 K); 24.0 (⊥) - 30.5 (∥) (1073 K)	16.0 - 24.4	0.60 - 1.55 (298 K – 1073 K)	[340]
C <sub>f</sub> /C-9.5wt%HfC	2.00 - 4.70	14.0 (⊥) - 17.0 (∥) (298 K); 18.5 (⊥) - 26.0 (∥) (673 K); 18.0 (⊥) - 25.0 (∥) (1073 K)	6.5 - 21.5	0.61 - 1.75 (298 K – 1073 K)	[340]
C <sub>f</sub> /C-SiC/HfC coating	3.5 - 4.6				[341]
C <sub>f</sub> /C-SiC/HfC coating-HfC nanowires	4.9 - 6.6				[341]
C <sub>f</sub> /C-SiC		14.5 25 - 53			[342], [343]
C <sub>f</sub> /C-SiC-ZrB <sub>2</sub>	3.05 - 3.45				[326]
C <sub>f</sub> /C-SiC-ZrB <sub>2</sub> -SiC nanowires	2.95 - 3.3				[326]
C <sub>f</sub> /C-SiC-ZrB <sub>2</sub> -SiC nanowires Pre-oxidation	2.75 - 3.15				[326]
C <sub>f</sub> /C-SiC-ZrB <sub>2</sub> -ZrC		37.4 - 45			[210]
C <sub>f</sub> /SiC		9.4 6.2 - 8.4		0.85 - 1.35	[221], [327]
C <sub>f</sub> /ZrB <sub>2</sub> -ZrC		8.1 - 11.7		0.8 - 1.33 <sup>1</sup>	[327]
C <sub>sf</sub> -ZrB <sub>2</sub> -20vol%SiC		48.3 - 104.7			[328]
C <sub>f</sub> /C-ZrB <sub>2</sub> -SiC(compact) & C <sub>f</sub> /C-ZrB <sub>2</sub> -SiC(porous) & C <sub>f</sub> /C-SiC(compact)		3.29			[329]

$C_{pw}$ -ZrB <sub>2</sub> -ZrC		8 - 12			[330]
$C_{sf}$ -ZrB <sub>2</sub> -ZrC		45 - 70			[330]
HfB <sub>2</sub>	6.3	72 - 105		0.25	[221]
HfC	6.8 7.7 (298 K – 885 K) 7.66 ± 0.11 (298 K – 2273 K)	21 - 27		0.182	[205], [221], [331], [332]
HfC <sub>0.98</sub>	7.7 (1773 K)	21 - 28			[38]
HfC <sub>0.67</sub>	7.7 (1773 K) <sup>1</sup>	14 - 24			[38]
HfC+15vol%MoSi <sub>2</sub>	7.26 (298 K – 1573 K)	22.0 - 36.3			[333]
HfC+15vol%TaSi <sub>2</sub>	9.99 (298 K – 1573 K)				[333]
HfC+15vol%TaSi <sub>2</sub> -SiC fibres	7.01 (298 K – 1573 K)	20.7 - 26.5			[98]
HfN <sub>0.92</sub>	7.7 (1773 K)	8 - 14			[38]
HfB <sub>2</sub> -SiC-TaSi <sub>2</sub>	8.0 (298 K – 1523 K)	28 - 34			[342]
HfB <sub>2</sub> -20vol%SiC	7.77 (293 K – 1273 K)				[349]
TaC	6.6 7.08 ± 0.33 (298 K – 2273 K)	22		0.19 <sup>9</sup>	[221], [332]
TaC+15vol%MoSi <sub>2</sub>	6.51 (298 K – 1573 K)	24.1 - 47.3			[333]
TaC+15vol%TaSi <sub>2</sub>	7.63 (298 K – 1573 K)				[98]
TaC+15vol%TaSi <sub>2</sub> -SiC fibres	6.66 (298 K – 1573 K)	27.8 - 37.2			[98]
MoSi <sub>2</sub>	Ave. 9.32 (298 K – 1573 K) 7.3 - 10.5 (298 K – 1273 K)				[335], [336]
TaSi <sub>2</sub>	Ave. 9.78 (298 K – 1573 K)				[335]
SiC	4.3			0.58	[221]
ZrB <sub>2</sub>	6.8 (300 K – 1300 K) & 8.4 (1300 K – 1675 K) 5.9	53 56.4		0.43	[221], [322], [337]
ZrC	7.3	18 - 44		0.37	[221], [338]
ZrB <sub>2</sub> -(10-40)vol%MoSi <sub>2</sub>		76.60 - 87.95		~0.53	[339]
ZrB <sub>2</sub> -20vol%MoSi <sub>2</sub> -(5-30) vol%SiC		82.09 - 97.55		0.53 - 0.60	[339]

ZrB <sub>2</sub> -40vol% MoSi <sub>2</sub> -(5-30) vol% SiC		80.83 - 95.15		0.52 - 0.59	[339]
ZrB <sub>2</sub> -(10-40)vol% ZrSi <sub>2</sub>		74.20 - 98.30			[339]
ZrB <sub>2</sub> -20vol% SiC	7.85 (293 K – 1273 K)	76.2 - 103.8		0.514	[349], [337], [116]
ZrB <sub>2</sub> -30vol% SiC	6.8 (300 K – 1300 K) & 7.8 (1300 K – 1675 K)	56 - 63.5			[322], [337]
ZrB <sub>2</sub> -20vol% SiC-5vol% Si <sub>3</sub> N <sub>4</sub>	7.59 (293 K – 1273 K)				[349]
ZrB <sub>2</sub> -20vol% ZrC-20vol% SiC-5vol% Si <sub>3</sub> N <sub>4</sub>	8.20 (293 K – 1273 K)				[349]
ZrB <sub>2</sub> -SiC-TaSi <sub>2</sub>	7.4 (298 K – 1523 K)	33 - 41			[342]
ZrB <sub>2</sub> -20vol% SiC-0.2wt% CNTs		90.9		0.511	[116]
ZrB <sub>2</sub> -ZrC-SiC		65 - 85			[58]
ZrB <sub>2</sub> -33.3mol% ZrC-33.3mol% SiC		72.6			[337]
ZrB <sub>2</sub> -15mol% ZrC-15mol% SiC		85.6			[337]
ZrB <sub>2</sub> -55mol% ZrC-30mol% SiC		51.8			[337]
ZrB <sub>2</sub> -15mol% ZrC-30mol% SiC		89.0			[337]

**Table 12 Electrical properties of UHTCMCs reported in the literature.**

Materials	Electrical Conductivity $\times 10^4$ / $\Omega^{-1} \text{cm}^{-1}$	Electrical Resistivity $\times 10^{-5}$ / $\Omega \text{cm}$	Reference
ZrB <sub>2</sub> -(10-40)vol% MoSi <sub>2</sub>	8.11 - 7.22	1.23 - 1.34	[339]
ZrB <sub>2</sub> -40vol% MoSi <sub>2</sub> -(5-30)vol% SiC	7.35 - 4.07	1.36 - 2.46	[339]
ZrB <sub>2</sub> -(0-40)vol% SiC	-	1.025 - 8.793	[349]
ZrB <sub>2</sub> -(5-30)vol% SiC	1.989 - 1.199	-	[350]
ZrB <sub>2</sub> -20vol% SiC	-	1.60 - 3.10 (298 K – 700 K)	[348]

ZrB <sub>2</sub>	-	0.80 - 1.60 (298 K – 650 K)	[348]
HfB <sub>2</sub> -(5-30)vol% SiC	2.229 - 1.342	-	[350]
HfB <sub>2</sub> -5vol% SiC	-	0.70 - 1.90 (298 K – 650 K)	[348]
HfB <sub>2</sub>	-	0.25 - 1.25 (298 K – 650 K)	[348]

**Table 13 Thermal ablative methods and properties of various UHTCMCs.**

Material	Fabrication method	Density / g cm <sup>-3</sup>	Ablation method	Temperature / °C		Time / s	Heat flux / MW m <sup>-2</sup>	Ablation rate	Ref
				Flame	Surface				
C <sub>f</sub> /ZrB <sub>2</sub> -ZrC-SiC	PIP	2.44	Plasma wind tunnel	-	2027	300	-	0.010 g s <sup>-1</sup>	[209]
C/SiC-HfC	RMI	2.60	Plasma wind tunnel		1650 - 2500	60 - 600	3.5 - 5	-	[357]
C <sub>f</sub> /SiC-ZrC	CVI-PIP	-	Plasma wind tunnel	2227	-	60	-	-	[358]
C/C-ZrC-SiC	PIP	2.03-2.14	Plasma flame	-	2300	60	-	3.51 mg s <sup>-1</sup> - 1.88 μm s <sup>-1</sup> 1.57 mg s <sup>-1</sup> - 0.37 μm s <sup>-1</sup>	[359]
C/C-ZrC-SiC	PIP	1.98	Plasma flame	-	2342	180	-	1.73x10 <sup>-3</sup> g s <sup>-1</sup> 1.94x10 <sup>-4</sup> mm s <sup>-1</sup>	[360]

50 vol% C <sub>f</sub> - 50 vol% ZrB <sub>2</sub>	HP	3.4	HVOF	2713	1277	30	3.7	Negligible	[109]
C/C-ZrC	CVI-RMI	2.46	Pulse laser	-	3000	20	1000	0.028 mm s <sup>-1</sup>	[227]
C/C-ZrC	CVI-RMI	-	Laser beam-CO <sub>2</sub>	-	3000	-	1000-2000 W	-	[229]
C/C-ZrC	CVI-RMI	-	OAT	-	3000	20	4.2	0.002 mm s <sup>-1</sup>	[229]
C/ZrB <sub>2</sub> -SiC	CVI-SP	2.10	OAT	-	2800 - 3300	20	4.2	0.66 mm s <sup>-1</sup>	[181]
C <sub>f</sub> /HfB <sub>2</sub>	VI-CVI	2.17-2.87	OAT	-	2600	60	17	4.1x10 <sup>-3</sup> g s <sup>-1</sup> - 8.3x10 <sup>-3</sup> g s <sup>-1</sup> 0 mm s <sup>-1</sup>	[187]
C/ZrC	PIP	-	OAT	>3000	2000 - 2300	300	4.2	0.006 g s <sup>-1</sup> 0.004 mm <sup>-1</sup>	[361]
C/C-ZrC-SiC	PIP	2.22	OAT	3000	2400	120	-	3.75x10 <sup>-4</sup> g s <sup>-1</sup> 2.48x10 <sup>-3</sup> mm s <sup>-1</sup>	[182]
C/C-SiC-ZrB <sub>2</sub>	RMI	-	OAT	3000	2050	60	2.4	0.013 g s <sup>-1</sup> 0.0014 mm s <sup>-1</sup>	[362]
C/C-ZrC-SiC	PIP	2.1	OAT	-	1823-1612 2402-2013	60	2.4 4.2	1.33-0.27 mg s <sup>-1</sup> ; 0.585 mg s <sup>-1</sup> cm <sup>-2</sup> 6.16-3.67 mg s <sup>-1</sup> ; 18.092 mg s <sup>-1</sup> cm <sup>-2</sup>	[363]
C/C-SiC-ZrC-HfC	TCVI-PIP	2.3-2.6	OAT	3000	2400	120	2.4	0.151 mg s <sup>-1</sup> cm <sup>-2</sup> 0.225 μm s <sup>-1</sup>	[364]
C/C-ZrB <sub>2</sub> -ZrC-SiC	TCVI-PIP	2.1	OAT	-	1800 2400	60	2.4 - 4.2	15.7 μm s <sup>-1</sup> 22.8 g s <sup>-1</sup> cm <sup>-2</sup> - 36.5 μm s <sup>-1</sup>	[210]
C/SiC-HfC	CVI-RMI	2.61	OAT	3000	2500-3200	20	4.2	2.9x10 <sup>-3</sup> g s <sup>-1</sup> - 2.2x10 <sup>-2</sup> mm s <sup>-1</sup>	[207]
C/SiC-HfC	CVI-PIP	3.19	OAT	3000	2500-3200	20	4.2	1.5x10 <sup>-3</sup> g s <sup>-1</sup> - (-0.4)x10 <sup>-2</sup> mm s <sup>-1</sup>	[207]
C/C-SiC-ZrC	PIP	2.24	OAT	3000	2400	120	-	0.0019 g s <sup>-1</sup> - 0.012 mm s <sup>-1</sup>	[365]
C/C-ZrC-SiC	PIP	2.22	OAT	3000	2550	120	4.2	(-0.30) mg s <sup>-1</sup> - 1.5 μm s <sup>-1</sup>	[366]
C/C-ZrC-ZrB <sub>2</sub> -SiC	LPCVI-PIP	2.1	OAT	-	2077	120	2.4	0.36x10 <sup>-4</sup> g s <sup>-1</sup> cm <sup>-2</sup> - 2.04x10 <sup>-4</sup> mm s <sup>-1</sup>	[197]
C/C-SiC-ZrB <sub>2</sub>	LPCVI-RMI	-	OAT	3000	-	60	2.4	0.0014 g s <sup>-1</sup> - 0.013 mm s <sup>-1</sup>	[222]
C <sub>f</sub> /HfC-SiC	PIP	2.48	OAT	3000	-	60	-	0.51 mg cm <sup>-2</sup> s <sup>-1</sup> - 0.006 mm s <sup>-1</sup>	[367]
C/SiC-ZrB <sub>2</sub>	CVI-PIP	2.56	OAT	-	-	20	4.2	(-0.04) g s <sup>-1</sup> - (-0.074) mm s <sup>-1</sup>	[198]
C/ZrC-SiC	CVI-RMI	3.09	OAT	-	2000	30	-	0.0071 g s <sup>-1</sup> - 0.0047 mm s <sup>-1</sup>	[368]
C/C-HfB <sub>2</sub> -SiC	PIP-RMI	1.85	OAT	-	-	90	2.4	0.129 mg cm <sup>-2</sup> s <sup>-1</sup> - 2.06 μm s <sup>-1</sup>	[369]

C/SiC-ZrB <sub>2</sub> -TaC	CVI-SP	2.35	OAT	-	3000	20	4.2	0.026 mm s <sup>-1</sup>	[370]
C/ZrB <sub>2</sub> -SiC	CVI-SP	2.1	OAT	-	3000	20	4.3	0.066 mm s <sup>-1</sup>	[181]
C/C-SiC-ZrB <sub>2</sub>	ICVI-RMI	2.25	OAT	3000	-	60	2.4	0.61 · 10 <sup>-3</sup> g s <sup>-1</sup> - 6.72 · 10 <sup>-3</sup> mm s <sup>-1</sup>	[371]
C <sub>f</sub> /ZrB <sub>2</sub>	VI-CVI	2.11	OAT	3000	2590	60	17	0.011 g s <sup>-1</sup> - 0.08 mm s <sup>-1</sup>	[18]
C <sub>f</sub> /ZrB <sub>2</sub> -SiC	VI-CVI	2.01	OAT	3000	2550	60	17	0.010 g s <sup>-1</sup> - 0.09 mm s <sup>-1</sup>	[18]
C <sub>f</sub> /ZrB <sub>2</sub> -SiC- LaB <sub>6</sub>	VI-CVI	1.91	OAT	3000	2525	60	17	0.012 g s <sup>-1</sup> - 0.10 mm s <sup>-1</sup>	[18]
C <sub>f</sub> /HfB <sub>2</sub>	VI-CVI	1.93	OAT	3000	2640	60	17	9.5 · 10 <sup>-3</sup> g s <sup>-1</sup> - 0.03 mm s <sup>-1</sup>	[18]
C <sub>f</sub> /HfC	VI-CVI	2.07	OAT	3000	2530	60	17	0.03 g s <sup>-1</sup> (surface layer fell off)	[18]

